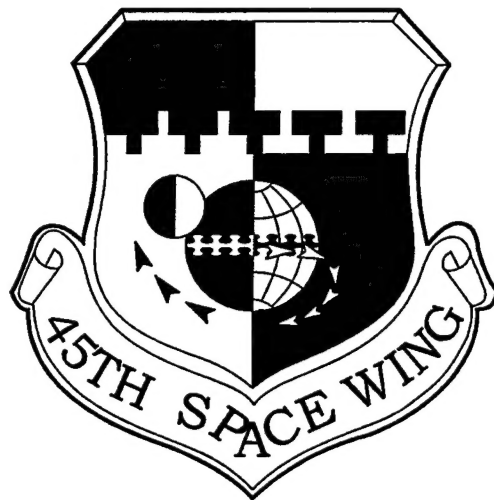# PRESSURE VESSEL
BURST TEST STUDY

November 1996

19970307 042

General Physics Corporation
5095 S. Washington Ave., Suite 201
Titusville, Florida 32783

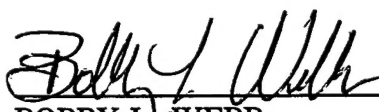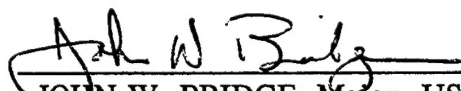**45th Space Wing**
Patrick Air Force Base, Florida

NOTICE

When the government specifications, or other data are used for any purpose other than in connection with a definitely related government procurement operation, the United States Government thereby incurs no responsibility nor any obligation whatsoever; and the fact that the government may have formulated, furnished, or in any way supplied the said specifications, or other data, is not to be regarded by implication or otherwise as in any manner licensing the holder or any other person or corporation, or conveying any right or permission to manufacture use, or sell any patented invention that may in any way be related thereto.
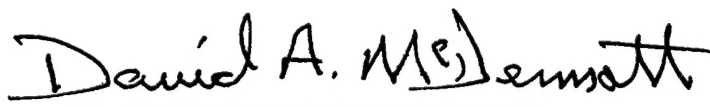
This report has been reviewed by the Office of Public Affairs (45 SW/PA) and is releasable to the National Technical Information Service (NTIS). At NTIS, it will be available to the general public, including foreign nations.

This technical report has been reviewed and is approved for publication.

BOBBY L. WEBB
Project Engineer

JOHN W. BRIDGE, Major, USAF
Chief, Systems Safety Section

FOR THE CHIEF:

DAVID A. MCDERMOTT
Colonel, USAF
Chief, Wing Safety

PRESSURE VESSEL
BURST TEST STUDY

Prepared by

Maurice R. Cain
General Physics Corporation
5095 S. Washington Ave., Suite 201
Titusville, Florida 32783

for

45th Space Wing
Patrick Air Force Base, Florida

November 1996

REPORT DOCUMENTATION PAGE

1. AGENCY USE ONLY (Leave blank)	2. REPORT DATE November 1996	3. REPORT TYPE AND DATES COVERED Final

4. TITLE AND SUBTITLE

Pressure Vessel Burst Test Study

5. FUNDING NUMBERS

FO 8606-86-0030

6. AUTHOR(S)

Maurice R. Cain

7. PERFORMING ORGANIZATION NAME(S) AND ADDRESS(ES)

General Physics Corporation
5095 S. Washington Avenue
Suite 201
Titusville, FL 32780

8. PERFORMING ORGANIZATION REPORT NUMBER

9. SPONSORING/MONITORING AGENCY NAME(S) AND ADDRESS(ES)

Department of the Air Force (AFSPC)
45th Space Wing
Safety Office
Patrick AFB, FL 32925

10. SPONSORING/MONITORING AGENCY REPORT NUMBER

45 SW 96-1

11. SUPPLEMENTARY NOTES

12a. DISTRIBUTION/AVAILABILITY STATEMENT

12b. DISTRIBUTION CODE

13. ABSTRACT (Maximum 200 words)

Pressure vessels are used extensively in both ground and spacecraft applications. Explosive failures of vessels are rare due to precautions normally taken including adherence to consensus design, fabrication and test codes and standards. Yet pressure vessels do occasionally fail, releasing significant energy and possible hazardous commodities into the surroundings. In addition, blastwaves and high velocity fragments can result from a failure and damage structures or cause injuries. This report describes pneumatic burst testing performed to augment an inadequate pressure vessel burst database. The program studied the blastwave and fragmentation of bursting gas filled pressure vessels. This study permits a greater understanding of the differences between well documented high explosive detonations and pressure vessel bursts.

14. SUBJECT TERMS

pressure vessel, blastwave, overpressure, impulse, fragment velocity, fragment range, pneumatic burst, burst testing, mechanical failure

15. NUMBER OF PAGES

163

16. PRICE CODE

17. SECURITY CLASSIFICATION OF REPORT	18. SECURITY CLASSIFICATION OF THIS PAGE	19. SECURITY CLASSIFICATION OF ABSTRACT	20. LIMITATION OF ABSTRACT
Unclassified	Unclassified	Unclassified	SAR

TABLE OF CONTENTS

TABLE OF CONTENTS (continued)

Appendices

LIST OF FIGURES

LIST OF FIGURES (continued)

1.0 INTRODUCTION

Pressure vessels are used extensively in both ground and spacecraft applications. Explosive failures of vessels are rare due to precautions normally taken including adherence to consensus design, fabrication and test codes and standards. Inservice integrity is maintained through monitoring of vessel service conditions and cyclic history. Yet pressure vessels do occasionally fail, releasing significant energy and possible hazardous commodities into the surroundings. Often it is prudent to assess the damage that could result from explosive failure when locating pressure vessels, designing nearby structures and equipment, performing pressure tests, or considering other safety precautions.

A considerable body of data exist on damage and injury due to blast wave and fragmentation, much of it from research using TNT or similar high explosives. However substantially less is known about blast and fragmentation of bursting pressure vessels than of chemical explosions such as TNT. Further, current methods documented in standards, handbooks and other references used to quantify expected energy release, blast waves, and fragmentation are inconsistent and vary in results[1]. Accordingly, a pressure vessel burst test program was conducted for the USAF -45th Space Wing and NASA Headquarters. The program studied the blast wave and fragmentation of bursting gas filled pressure vessels.

1.1 Background

An explosive rupture of a pressure vessel, where the stored energy is released instantaneously, creates a blast wave (i.e., shockwave) in the surrounding air and propels fragments. The shockwave and fragment characteristics depend on such things as vessel contents, pressure, vessel geometry and mode of vessel failure.

As the blast wave advances, the energy is spread over the wave's frontal area, which increases with the square of the distance from the point of rupture. Overpressure, blast wave velocity and therefore blast effect, decrease rapidly with distance. After passage of the shockwave, the pressure decreases until a suction phase follows in which pressure drops below normal atmospheric pressure. The negative pressure is a result of the outrush of gases from the center of the rupture causing an overexpansion. The pressure above atmospheric at the shockwave front is the peak overpressure and is used with impulse to establish the relative hazard (i.e., shockwave intensity and energy in the shockwave, the impulse being the area under the positive portion of the pressure versus time curve) associated with ruptures and explosions at a given distance. The blast wave emanating from a bursting pressure vessel is somewhat similar to that caused by a high explosive detonation. The pressure close in (0 to 10 ft in vessels tested) due to vessel burst is generally lower than high explosive detonation and is a function of burst pressure. This is because the pressure at the vessel surface is less than that of a high explosive blast at the same distance from the explosion center. Other variations are caused by vessel and failure geometry and distance from a firm reflecting surface. Blast wave overpressures for vessel failures with very large ratios of vent area to vessel volume may be estimated using methods of Baker[2] or Held and Jager[3].

1

The explosive failure of a pressure vessel not only generates a blast wave but produces fragments, with very high velocities possible. Fragments constitute a significant hazard to personnel, systems, components and structures in the vicinity. Primary fragments are portions of the vessel or its attachments that are accelerated due to the internal pressure of the vessel. Secondary fragments may also be produced due to the action of the blast wave or primary fragments on nearby objects.

Studies[2,3,4] of the characteristics of vessel fragments have addressed the velocities of fragments produced, their trajectories and, as a result, their ranges and their impact velocities. Determination of the initial velocities of fragments has been undertaken by several researchers. Most such studies are based upon work by Taylor and Price[5] which predicted the velocities of two spherical vessel fragments accelerated by an expanding adiabatic ideal gas. Wiedermann[6] has shown that real gas effects can be expected to reduce the fragment velocity from the ideal gas prediction.

Once the initial velocity of a fragment has been determined, its range may be found through ballistic calculations, generally done through the use of a computer code, a number of which are available. Code considerations are drag coefficient, lift coefficient (if any), initial trajectory angle and reference area - either fixed or varying (tumbling or gradually changing).

The reader is also referred to work by Pittman[7] for velocities of fragments burst from flight weight vessels at 600 and 8000 psig. Baum[4,8] compiles data from his own work and other researchers on fragments from vessels burst at 70 to 4400 psig, mostly at 750 psig or less.

1.2   Test Program

A test program matrix was developed that included a series of test plans each with multiple pneumatic vessel bursts. The objective of the program matrix was to force vessel bursts in such a way as to generate worst case blast waves and fragmentation, such that a model could be developed that would envelop generally expected vessel failures. The latter test plans of the matrix would include such representative vessel failures. Worst case however is a function of several variables, including location and orientation of failure, pressure, vessel shape, fragment type and number, and height above ground. The plans and tests comprising the program matrix have been developed to minimize the number of vessel bursts yet meet the stated objective with valid data.

In the development of a test matrix, it was also recognized that a pressure vessel burst may not produce a spherical shockwave as does a TNT explosion. The blast wave from a pressure vessel burst may be much stronger in one direction than another based on how the vessel shell comes apart. To provide a direct experimental comparison with pressure vessel bursts, approximately spherical high explosive detonations have been conducted as part of the test program.

Accordingly, a test program matrix was developed which incorporated varied failure locations and mechanisms. Seven test plans were envisioned with each test plan consisting of several vessel bursts. The final and truncated test matrix includes 5 pneumatic burst series and is provided in the Test Summary section, see Figure 2.1. Parameters varied in the matrix are burst pressure, height of burst (HOB), split location, number of fragments and vessel geometry.

2.0 TEST SUMMARY

This summary is presented early in this report because it will be referred to by other sections. The section summarizes the tests and associated data which describes the vessels and the test conduction. Primary test output data are deferred to other sections, i.e.: Section 5 for blast overpressures and Section 6 for fragment velocities.

2.1 High Explosive Tests

The high explosive tests initially (PHE-1 and PHE-2) had a twofold purpose: 1.) as a checkout device to ensure all pressure data channels were operating and 2.) as a calibrating tool for comparing high explosive overpressure to pressure vessel burst overpressure when both vessel and high explosive had approximately the same TNT equivalence. (See Section 4.1 for vessel TNT equivalence.) All the high explosive shots are summarized in Table 2.1. Shot PHE-2 was detonated first because pressure vessel P-2 was to be burst first. The charge weight was intended to be approximately 60 lbs TNT equivalent to match the energy of vessel P-2 at its intended burst pressure of 6000 psig. However, 65 pounds of Composition C-4 was furnished (instead of 50) which is very energetic and has a TNT equivalence of 85.5 lbs. Similarly the charge weight for shot PHE-1 is an approximation to the TNT equivalence of vessel P-1. All the high explosive TNT equivalence conversions were made using the equivalent weight in relation to TNT for the average pressure at the mid-arena distance of 30′ using Swisdak's[9] report.

For Test Plan #1, high explosive shots HE1-1 through HE1-3, charge weights of pentolite were used which would provide an overpressure variation but would not exceed the calibrated range of the pressure transducers at the ten foot distance. The use of high explosive shots as a calibration check tool had been abandoned because of the greater output at close distances for high explosives. Resetting gains defeated the purpose and using calibrations for high explosives provided resolution problems for vessel burst. The TNT equivalence of shot HE1-2 was expected to be 10 lbs instead of 14.6 and caused all outputs at 10 ft distance to be off scale.

The geometry of the high explosive shots is as follows: pentolite - all 1:1 diameter to length cylinders, composition B - 1:1 diameter to length cylinder, C-4-close to 1:1:1 square (small blocks stacked together).

3

Table 2.1
Summary of High Explosive Shots

Shot #	Date	NSWC Shot #	lbs. Pent (other)	Offset, ft.	TNT Equiv., lbs.	HOB ft
PHE-2	6-21-90	3201	65, (C-4)	0.0	85.5	3.5
PHE-1	6-26-90	3249	33.3, (Comp B)	0.0	40.0	3.5
HE1-1	1-28-91	3250	.66	0.0	.89	3.5
HE1-2	1-28-91	3256	9.9	0.0	14.6	3.5
HE2-3	7-16-91	3399	4.5	1.0	6.6	14.0
HE2-1	7-18-91	3401	4.5	0.0	6.6	3.5
HE1-3	7-20-91	3526	4.5	0.0	6.6	3.5
HE2-2	7-20-91	3404	4.5	1.0	6.6	8.7

For TP #2 (HE2-1 through HE2-3) all the high explosive shots had the same equivalent weight and provided an opportunity to compare reflection factors for high explosives with that for center split pressure vessel bursts at a single pressure level.

Initially pressure vessels were located in the arena with the edge of the vessel above ground zero, creating a one foot offset for the two foot diameter vessels (see "offset" in Table 2.3). The elevated height of burst shots, HE2-2 and HE2-3, were rigged with wooden supports on the vessel support stand and were thus at the same one foot offset. Other shots followed NSWC usual procedures.

After July 1991 no high explosive shots were detonated. The high explosive shots needed to be detonated before the pressure vessel bursts because of ground zero soil erosion which frequently accompanied the vessel bursts. Detonating high explosive shots first prevented simultaneous preparations of the arena field/transducer recording setup by instrumentation and vessel setup by riggers, explosive technicians and General Physics Corporation personnel. Since a quantity of high explosive data had been recorded using the vessel instrument setup and since the data were of lesser importance, its collection was abandoned.

2.2   Pneumatic Vessel Bursts and LSC Detonations

Test events included LSC detonations and vessel bursts, sometimes separately and sometimes as a combined event. The detonation of 17 linear shaped charges during preliminary testing are listed in Table 2.2. Field overpressure data without a vessel burst were recorded for the first 13 detonations, through 2-2. Number 2-3 (vessel burst P-1) resulted in the recording of

combined LSC and vessel burst overpressure. No data were recorded for the latter three LSC detonations, 3-1 through 3-3. All the LSCs were wrapped around a two-foot diameter pressure vessel with a six inch double pigtail extending to the ungaged side of the arena. These vessels were also offset one foot toward the ungaged side of the arena. Events are discussed under Section 3.1.2, Preliminary Pneumatic Test.

Figure 2.1 is a test matrix of all the bursts, hydraulic and pneumatic.

Table 2.2
Shaped Charges Detonated During Preliminary Testing

Prelim. Test Segment	LSC Charge Number	Vessel Burst Number	Vessel Pressure, psig	LSC charge wt., gr/ft. (lead/RDX)	TNT eqiv., lbs	Overpressure data
1	1A-1	---	0	25	.03	yes
1	1A-2	---	0	10	.01	yes
1	1A-3	---	0	10	.01	yes
1	1A-4	---	0	25	.03	yes
1	1A-5	---	0	15	.02	yes
1	1A-6	---	0	15	.02	yes
1	1A-7	---	0	25	.03	yes
1	1B-1	---	3200[1]	200	.27	yes
1	1B-2	---	3200	50	.07	yes
1	1B-3	---	0	50	.07	yes
1	1B-4	---	3200	200	.27	yes
2	2-1	---	2850	25	.03	yes
2	2-2	---	2950	25	.03	yes
2	2-3	P-1	3250	50	.07	with vessel burst
3	3-1	---	0	50	.07	no
3	3-2	---	0	50	.07	no
3	3-3	---	2700[2]	200	.27	no

[1]Planned pressure = 6000
[2]Planned pressure = 6000, 2700 occurred on depressuring from 5800

5

Description	Hydroburst	Prelim. Bursts: S.C. Test Plan	Test Plan #1	Test Plan #2	Test Plan #5* Preliminary TP #4	Test Plan #6A*
Vessel: Material / Volumes, ft³ / Diameters, in / L/Ds	steel / 53 / 24 / 11	steel / 53 / 24 / 11	steel / 53 / 24 / 11	steel / 53 / 24 / 11	steel, composite / 53,53,2.7 / 24,22 / 11,11,1	composite, steel / 53.2,7,53,53 / 36,22,36,24 / 4,1,4,11
Burst Pressure	varies	varies	varies	3500 nominal	varies	varies
Burst Media	water	nitrogen	nitrogen	nitrogen	nitrogen	nitrogen
Number of bursts	1	2	4	3	5	4
Para. Varied	test techniques	pressure (& test techniques)	burst pressure	burst height	split location	vessel, orientation, # of fragments, L/D
Configurations:	#1:P = 7500 no burst #2:P = 6500 burst without shaped charge	P-2: P = 4700 no shaped charge P-1: P = 3250 with shaped charge, vary groove depth also: shaped charges, with vessels not pressurized	1-1: P = 1475 1-2: P = 3450 1-3: P = 5425 1-4: P = 7125	2-1: h_1 = 3.5 2-2: h_1 = 8.7 2-3: h_1 = 14	5-1,5-2 5-3,5-4 2 each: P = 3600 PC 1 @ 22": P = 4000	6A-1 1 @ 36" P=3280 6A-2 1 @ 22": P =4000 6A-3 1 @ 36": P = 3300 6A-4 1 @ 24": P = 3500
Status:	Completed Aug 89	Completed July 90	Completed Jan 91	Completed July 91	Completed June 92	Completed Nov 93
Vessel #s	H1, H2	P2, P1	1-1 through 1-4	2-1 through 2-3	5-1 through 5-4, PC	6A-1 through 6A-4

*TP #3, 4, 6 deleted

FIGURE 2.1
TEST MATRIX SHOWING ACTUAL BURST

Table 2.3 lists all the pneumatic vessel bursts and the LSC detonations which occurred as a combined event. The TNT equivalence of both the vessel and the LSC are provided. For vessel TNT equivalence see Section 4.1. LSC TNT equivalence was obtained using Table I of Kinney and Graham[10].

Table 2.3
Summary of Vessel Burst Events

Date	NSWC Shot #	Vessel # (WP#)	Vess Pres psig	Vess Vol,* ft³	Type LSC	LSC		TNT Equiv., lbs.		Offset, ft	HOB ft
						Length, ft	Grain /foot	Vess	LSC		
1-25-92	3573	PC	3975	2.7	Lead/RDX	6.5	100	2.0	.125	1.0	3.5
6-26-90	3248	P-1	3250	53	Lead/RDX	7	50	31.7	.07	1.0	3.5
6-25-90	3245	P-2	4700	53	Lead/RDX	0	0	47.0	0.0	1.0	3.5
1-25-91	3251	1-1	1475	53	Lead/RDX	7	200	13.5	.27	1.0	3.5
1-29-91	3252	1-2	3450	53	Lead/RDX	7	50	33.8	.07	1.0	3.5
1-26-91	3253	1-3	5425	53	Lead/RDX	7	25	54.8	.03	1.0	3.5
7-19-91	3402	1-4	7125	53	Lead/RDX	7	100	73.4	.13	1.0	3.5
7-20-91	3403	2-1	3450	53	Lead/RDX	7	25	33.8	.03	1.0	3.5
7-17-91	3400	2-2	3450	53	Lead/RDX	7	25	33.8	.03	1.0	8.7
7-15-91	3398	2-3	3475	53	Lead/RDX	7	25	34.1	.03	1.0	14.0
6-16-92	3574	5-1 (5)	3600	53	AL/RDX	7	50	35.3	.07	0.0	3.5
6-17-92	3575	5-2 (6)	3600	53	AL/RDX	7	50	35.3	.07	0.0	3.5
6-19-92	3577	5-3 (7)	3600	53	AL/RDX	7	50	35.3	.07	0.0	3.5
6-18-92	3576	5-4 (8)	3600	53	AL/RDX	7	50	35.3	.07	0.0	3.5
11-2-93	4053	6A-1 (13)	3280	53	AL/RDX	4 x 8	400	32.2	3.41	0.0	3.5
						3 x 8	200				
11-3-93	4054	6A-2	4000	2.7	AL/RDX	6.5	75	2.0	.07	0.0	3.5
11-3-93	4055	6A-3 (4)	3300	53	AL/RDX	10	200	32.3	.29	0.0	3.5
11-4-93	4056	6A-4 (10)	3500	53	AL/RDX	20 x 4	100	34.3	2.18	0.0	3.5
						2 x 8	200				

* nominal (mfg. guarantee volume) except PC, 6A-2 (measured)

Table 2.4 contains data needed to compute fragment velocities: pressure, pressurant and ambient temperatures, vessel dimensions and fragment weights.

Table 2.4
Data for Computing Fragment Velocities

Vessel #/ Fragment	Vessel Pressure psig	Temperature, °F		Inner Radius,[4] ft	Outer Radius ft	Length of frags[7], ft (cyl. sect.)	Vessel or Fragment Wt[10,11], lbs
		Vessel gas	Ambient Air				
P-2	4700	124	85	.93[8]	1.0	19[8]	5775
P-1	3250	NR[6]	NR	.93[8]	1.0	19[8]	5800
1-1	1475	65	31	.929	1.0	19[8]	5525
1-3	5425	75	38	.93[8]	1.0	19[8]	5825
1-2	3450	109	55	.93[8]	1.0	19[8]	5900
2-3[9]	3475	142	85	.93[8]	1.0	19[8]	5400
2-2[9]	3450	132	90	.924	1.0	19[8]	5300
1-4	7125	133[5]	93[5]	.93[8]	1.0	19[8]	5250
2-1	3450	135	88	.93[8]	1.0	19[8]	5025
PC[1]	3975[4]	125	42	.86	.88	0/0	43.6
5-1/Lg	3600	130	80	.93[8]	1.0	14.0	3500
5-1/sm					1.0	5.0	1425
5-2/lg	3600	140	84	.93[8]	1.0	14.2	3600
5-2/sm					1.0	4.6	1500
5-4/lg	3600	123	78	.93[8]	1.0	19.2	4675
5-4/sm					1.0	.1	300
5-3/lg	3600	126	80	.93[8]	1.0	18.9	4675
5-3/sm					1.0	.1	300
6A-1[3]	3280	106	50	1.352	1.5	7.0[8]	2x800
6A-2[2]	4000[2]	169	44	.86	.88	0/0	43.6
6A-3	3300	97	47	1.348	1.5	7.0[8]	6100
6A-4 sidewall	3500	108	60	.929	1.0	18.7	12x362
6A-4 endcap							2x352

[1] Preliminary composite overwrapped pressure vessel (COPV)
[2] Vessel volume = 2.7 cubic feet, all others 53 ft³
[3] TP #6 Deleted
[4] At groove
[5] Data not recorded. This is from previous day's pressurization to 7200 psig (similar pumpup time and ambient temperature).
[6] Not recorded
[7] of cylindrical sections, of vessel 6A-4 length is point of curvature (PC) to PC
[8] Nominal
[9] Height of burst of V2-2 and V2-3 is 8.7' and 14.0'. All others is 3.5'
[10] See Table 6-2 for individual fragment weights
[11] Weighed, not calculated

Of the 18 vessels burst using pneumatic pressure (gaseous nitrogen) 16 were cylindrical steel vessels and two were composite spheres. Further information on the vessels is provided in Figure 2.1. All vessels were 53 cubic feet volume except for the 2.7 cubic feet spheres. The vessel materials and pressure ratings are listed in Table 2.5.

Table 2.5
Test Vessel Ratings

Size	Ratings, Materials
24″ cylinders:	SA-372, 2450 psi (ASME Section VIII, Div 1, App. 22) (14 were burst)
36″ cylinders:	SA-516, 1770 psi (ASME Section VIII, Div. 1) (2 were burst)
spheres:	cryostretched 301 stainless steel liner with Kevlar-epoxy overwrap, 4000 psi (MIL-STD-1522A)

Since the ground surface conditions in the center of the arena may have affected blast output, these conditions are tabulated in Table 2.6.

Table 2.6
Ground Zero Surface Conditions

Test Series	Date	Vessel Test	Ground Surface	Remarks
1	Jun 90	P-1	soft earth	some erosion
1	Jun 90	P-2	soft earth	some erosion
2	Jan 91	1-1	steel plate	no erosion
2	Jan 91	1-2	steel plate	no erosion
2	Jan 91	1-3	steel plate	no erosion
3	July 91	1-4	soft earth	considerable erosion
3	July 91	2-1	soft earth	considerable erosion
3	July 91	2-2	soft earth	8.7' HOB, min. erosion
3	July 91	2-3	soft earth	14' HOB, no erosion
4	Jan 92	PC	steel plate	no erosion
4	Jun 92	5-1	steel plate	plate blew off, min. erosion
4	Jun 92	5-2	steel plate	no erosion
4	Jun 92	5-3	steel plate	no erosion
4	Jun 92	5-4	steel plate	no erosion
5	Nov 93	6A-1	steel plate	no erosion
5	Nov 93	6A-2	steel plate	no erosion
5	Nov 93	6A-3	steel plate	no erosion
5	Nov 93	6A-4	steel plate	no erosion

3.0   TEST TECHNIQUES

Test techniques include all the activities surrounding the tests, including burst initiation, vessels, pumping and other hardware, instrumentation and observations.

3.1   Establishment of Techniques

Two preliminary burst test series were used to establish basic techniques. However techniques continued to evolve throughout the program. The first burst test series used water as a pressurant and was conducted at Cape Canaveral Air Station, FL. For the second test series a gaseous nitrogen pressurization system was assembled at the Naval Surface Warfare Center at Dahlgren, VA and testing was conducted at that facility.

3.1.1   Hydroburst Test

Planned burst initiation for pneumatic burst tests consisted of detonating a shaped charge in a premachined groove with the vessel at the desired burst pressure. This permits selection of the failure geometry, burst pressure and time of burst. The latter is important because of the limited time available with high speed video tapes (30 minutes), instrumentation tapes (30 to 60 minutes) and high speed photography (as little as 9 seconds).
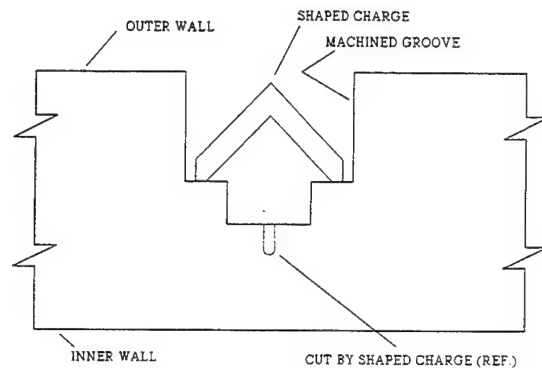
Figure 3.1, Typical Vessel Cross Section Showing Groove and Shaped Charge

The object of the test was to check out failure stress levels for burst initiation purposes. The use of a linear shaped charge (LSC) detonated in a premachined groove was considered essential for utilizing a small shaped charge. A small LSC was necessary to minimize the undesirable explosive blast wave overpressure. Undesirable because the overpressure would later be measured and if possible attributed to the vessel burst. Figure 3.1 is a drawing of the vessel groove geometry.

The desired stress level was to be less than yield by some safety margin on pressurization and achieve ultimate on shaped charge detonation. It was felt that with a narrow circumferential groove the longitudinal stress alone would determine failure. It was expected that local yielding would maintain the tangential stress to a value near the yield strength at a pressure condition and groove geometry which would give a calculated tangential stress at the groove outer diameter above ultimate. Additionally, the longitudinally short groove section was expected to be reinforced by the continuous moment into the adjacent heavy section thus preventing large deflections with resultant high stresses. A preliminary finite element stress analysis by a consultant[11] could not confirm these expectations. It was suggested[12] that tradeoffs in cost versus accurate, positive results were in favor of testing rather than more detailed modeling and that failure could be expected beyond a maximum effective stress of $(S_y+S_u)/2$.

10

A two vessel test was planned, using groove depths which would be useful for a future preliminary pneumatic burst test. The vessel wall thickness was drawing listed as 0.817" minimum with no roundness or wall thickness tolerance provided. Measurements showed vessel H1 to be 0.190" (indicator reading) out of round and vessel H2 to be 0.245" out of round. The wall thickness (ultrasonic thickness gage) varied from .874" to .926" on vessel 1 and from .847" to .929" on vessel 2. A search was initiated for a suitable computer numerically controlled (CNC) milling machine because of the dimensional variations. However none was found and jury-rig procedures were used to permit using a lathe to machine the vessels in Central Florida. General Physics Corporation supported one of the procedures with software[13] to facilitate offsetting the vessel and machining eight slightly larger radii at the groove location. The as-machined grooves are shown in Table 3.1.

Table 3.1
Hydroburst Vessel Dimensions at Circumferential Groove

Vessel	Average O.D., in.	Original Wall, in. (avg. of 16)	Groove width, in.	Groove wall, in. (avg. of 26-31)
H1	24.012	.928	.420	.392
H2	24.192	.914	.200	.320

Each vessel in turn was filled with non-deaerated water and air was bled using a valve on the upper surface. The maximum pressure was held to 7500 psig due to limitations of the 1/2" stainless steel supply tubing. Vessel H1 was held at the maximum pressure for five minutes and depressurized when it did not fail. Vessel H2 failed at 6500 psig. Pressurization schedule after 6000 psig was achieved was to increase pressure in 100 psi increments and hold briefly. A fairly loud report could be heard 950 feet away when the vessel burst.

Upon vessel H2 burst a high response transducer, Endevco model 8511A, recorded a pressure drop to ambient in 2 milliseconds (ms). A 48 frame/second motion picture camera recorded the event and film records later showed that each vessel half was accelerated to 73 feet per second. One frame from the camera is presented as Figure 3.5 in Photo Section, Section 3.7. Accelerometers produced no useful data due to a failure of cement bond mounting. Each half vessel stopped in about 57 feet with its nose partly buried in sand.

Longitudinal stress analyses results for both vessels is provided in Table 3.2. Lab tests[14] on a section cut from one of the fragments provided material strengths as also shown in Table 3.2. The calculated average stress in vessel H2 was less than ultimate at failure. Failure is deemed to have occurred by the groove section stretching to failure as the value of $(S_y+S_u)/2 = 114$ ksi was approached. A later test, (vessel 5-1) Section 5.3, with a 13 ms delay to failure confirms this belief. Note that tangential stresses in a cylinder are twice longitudinal and that these high stresses, well beyond failure, never occurred.

11

Table 3.2
Calculated Stresses and Measured Strengths

	Vessel Stress (ksi)		Measured Strength (ksi)	
	H1	H2	S_y	S_u
Longitudinal	104.1	112.0	98	130.3
Tangential	---	---	97	113.7

The knowledge gained from these tests confirmed initial expectations and permitted simplifying the following preliminary pneumatic burst test.

3.1.2 Preliminary Pneumatic Test

A preliminary pneumatic test was conducted at the Naval Surface Warfare Center at Dahlgren, VA. The test site is described in Section 3.5.

3.1.2.1 Purpose

The purpose of the preliminary test series was fourfold: 1) measure the cutting action of various linear shaped charges (LSC) proposed for use on test vessels, 2) collect data on the overpressure in air due to the detonation of LSCs of various explosive weights (so that LSC overpressure effects can be deleted from real vessel overpressure data as one would delete a tare), 3) explore the combined LSC/internal pressure interaction in causing vessel failure and 4) checkout a gaseous nitrogen (GN2) pressurization system and obtain experience with the joint NSWC/explosive and General Physics Corporation/pressure testing environment. Some background on purpose No. 3 is appropriate. If the LSC cut penetration is about 60% or more of the total section thickness, the effect of shock loading will cause the section to break at the cut line. Then for a section initially under stress, a larger section thickness might break than the cut thickness. This was to be addressed in the preliminary test by providing different stress levels at 3 grooves on each of two pressurized vessels and detonating shaped charges. Vessels are described in Section 3.3.

3.1.2.2 Description of Test Plan

The preliminary test was performed in 4 segments (1A, 1B, 2 & 3) as shown in Table 3.3. With the first vessel, seven shaped charges around the circumference of the unpressurized vessel were to be detonated sequentially. An array of pressure transducers would record pressure as a function of time at different locations in the adjacent arena. Next, four larger shaped charges were to be detonated sequentially while the vessel was pressurized to a planned 6000 psig. The vessel was not expected to burst following any of these shaped charge detonations as the shaped charge cut would not remove enough wall metal to raise the axial stress above the steel's ultimate tensile strength.

12

Table 3.3
Preliminary Pneumatic Test Summary

Test Segment	Vessel Number	Pressure (psig)	Number of Shaped Charges	Purpose
1A	---	0	7	Measure shaped charge overpressures
1B	---	6000	4	Measure shaped charge overpressures, avoid surprise failure in later vessels
2	P-1	3000	3	Study shaped charge/internal pressure interaction in causing vessel failure
3	P-2	6000	3	Study shaped charge/internal pressure interaction in causing vessel failure

The third segment of the test was to utilize a similar pressure vessel which had three grooves machined around the circumference. Shaped charges were to be placed inside the grooves and the vessel would be pressurized to approximately 3000 psig. The shaped charges were to be detonated sequentially at either a deeper groove or with a larger core load such that the axial stress developed at the groove would increase with each detonation.

The fourth segment of the test was to utilize a similar vessel with three different grooves and pressurized to a planned 6000 psig. Larger core loads of shaped charges were to be used but the test would otherwise proceed in the same manner as the second test.

Both the third and fourth segments of the test were designed such that the axial stress was high enough to cause failure when the third charge detonated but failure was not assured when the first or second charge detonated.

3.1.2.3 Summary of Results

Table 2.2 in the summary section, Section 2.2, tabulates all the shaped charges and accompanying vessel burst for this test series. One vessel burst (pressurized until burst), vessel P2, occurred the day following the initiating LSC (No. 3-3) failure to cause a burst due to premature depressurization. Measured shape charge overpressures are discussed in Section 5.3. Vessel burst overpressures are included in Sections 5.4 through 5.15. Fragment flight and velocities are included in Section 6.

The cutting action of various LSCs on SA-372 steel was measured and is shown in Figure 3.2. Data were recorded with and without standoffs. (Standoffs used were rated as optimum for C1018 steel.) The figure shows only the data recorded with standoffs which was typically a 25% to 44% deeper cut than without standoffs. These data were not available from the shaped charge

manufacturer. It was also found that there was no shock interaction to assist failure in a heavy section of a pressurized vessel. The cut penetration must cause a suitable increase in stress due to pressurization to effect failure.

In addition to measuring shaped charge cuts and overpressures, vessel overpressure and film/video data for fragment velocities, experience with the pressurization system and with explosives personnel was gained. Problems with the pressurization system were documented but were not fully resolved this trip to NSWC. Measurements of shaped charge cross-section dimensions became a regular procedure in lieu of following the catalog. The method for preventing damage to the pumping systems by a fragment jerking the line was changed to using the safety anchor block as a primary device. The prior method of explosively cutting the fill line caused operational problems including the premature depressurization of a vessel.
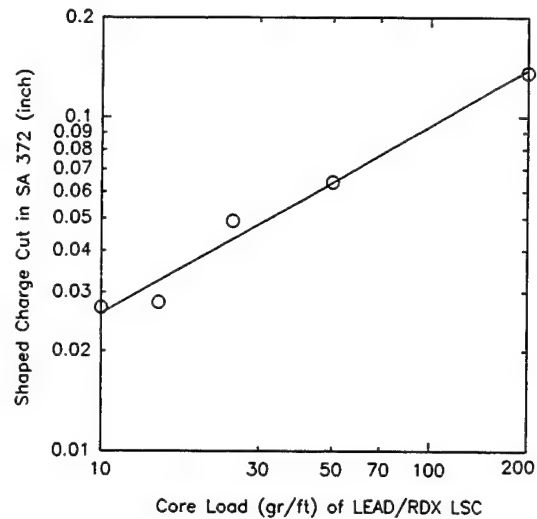
Figure 3.2, Shaped Charge Performance

Average dimensions and longitudinal stresses for the two vessels that burst are shown in Table 3.4. Like vessel H1, vessel P1 appeared to have burst because the average of $(S_y+S_u)/2$ = 114 ksi was approached. The failure mechanism for vessel P2 could not be explained. The groove appeared to be fairly uniformly machined based on 32 measurements more or less equally spaced about the circumference although the maximum LSC cut was .035 inches greater than average (measured since detonation was the day prior). This caused us to modify techniques to use pre-LSC cut stresses generally less than 90 ksi and to start recorders early when that value was exceeded. Recorders and high speed video were also started early for some of the other tests.

Table 3.4
Vessel Dimensions & Longitudinal Stresses

Vessel	Average O.D. (in.)	Average orig. WT (in.)	Groove WT as machined (in)	LSC cut, (in.)	Average stress (ksi)
P1	23.992	.941	.240	.066[1]	112.2
P2	24.032	.959	.576[2]	NA[3]	90.3
[1]From Fig. 3.2 [2]Includes measured LSC cut				[3]Not applicable, cut the day prior	

3.2   Test Plans and Test Reports

Eight test plans[15-22] were prepared. This includes a test plan for each of the six test series shown in Figure 2.1 plus two additional test plans which were not conducted for lack of funds. The deleted test series are for Test Plan 3 and Test Plan 4. Test Plan 3 was to have been the center split burst of four cylindrical vessels at 3.5' HOB. The vessels were: two at 53 cubic feet volume with diameters of 24 inches and 36 inches and two of 22 cubic feet volume with diameter of 16 inches and 36 inches. One of these vessels was burst in Test Plan 6A when TP#3 was canceled. Test Plan 4 was to have been the test of four composite spheres, 2 with vertical split and 2 with horizontal split. One of these was also burst in TP #6A testing.

Each test plan included items typical of the following:

- ▲   Vessels - stresses, inspection, testing, machining
- ▲   Schedule - grooves, pressures, shape charges, other explosives.
- ▲   Site preparation
- ▲   Instrumentation
    - •   Expected values
    - •   Transducers - vessel & arena
    - •   Make/break wire instrumentation
    - •   Data recording
    - •   Calibration
- ▲   Support equipment
- ▲   Photo support
- ▲   Safety
    - •   Explosives
    - •   High Pressure Gas
    - •   Vessel Fragments: blockhouse penetration and range
    - •   Blast and test stand
- ▲   Post Test
- ▲   Procedures/checklists
- ▲   Drawings

Five test reports[23-27] cover testing and provide much the same kind of information found herein for the entire test program.

3.3   Test Vessels

At program initiation a telephone search was conducted of NASA, Air Force and Navy installations for vessels that could be contributed for testing. Many vessels were offered but were never used because they would represent one of a kind vessels to the test program. Repeat tests or the variation of some parameters which were actually varied would be impossible. The largest collection of similar vessels was found at Cape Canaveral Air Station. Fifteen of these vessels, 2' diameter and 53 cubic feet, were used in the test program. A typical modification drawing for these vessels is provided in Appendix A.

In addition two composite vessels, obtained from Lewis Research Center, were burst. These were stainless steel lined spheres, overwrapped with Kevlar/epoxy that were rejected for space shuttle use. Two additional 53 cubic feet vessels were fabricated for testing so that a variation of diameter with the same internal volume would be available for testing. A specification drawing for these vessels is included in Appendix A.

Data on all three vessels are provided in Table 2.5 in the Summary Section, Section 2. The section also contains tabulations of some of the most pertinent data relative to burst conditions.

3.3.1 Preparation for Testing

Two penetrations were added to the cylindrical vessel: pressure transducers at 1/4 length from supply end (1/4 length or more to split) and for a thermocouple. One or more grooves were cut in the circumferential direction in all cylinders and four axial grooves were cut in vessels 6A-1 and 6A-4 of Test Plan 6A. For TP #5, machining of vessels was switched from a central Florida shop where a lathe was used for groove cutting to Wright Patterson Air Force Base where a computer numerically controlled (CNC) six axis milling machine was recently installed. This provided better accuracy and made it possible to cut the longitudinal grooves.

Prior to cutting grooves, an ultrasonic volumetric inspection was made of the groove area to ensure against defects in the area to be machined.

On site but away from the arena, one of the Preliminary Pneumatic Test vessels had standoffs built up on the vessel surface using tape. These were for the LSCs detonated to measure penetration depth. Heavier pieces, to locate the LSCs laterally, were also applied. Measurements of the LSCs showed a smaller cross-section than the catalog and this necessitated adding thicknesses of tape to the sides of grooves for proper LSC alignment.

3.3.2 Groove designs/dimensions/stresses

Stress analyses used the remaining area available to resist tensile stress after reduction in area by machining and detonation of a shaped charge. These equations reduce to:

$$S_L = \frac{P}{\left(\dfrac{R_o}{R_i}\right)^2 - 1} \qquad \text{(eq. 3.1)}$$

$$S_C = P \left(\frac{R_o^2 + R_i^2}{R_o^2 - R_i^2}\right) \qquad \text{(eq. 3.2)}$$

16

where:

S_L = longitudinal stress
S_C = circumferential stress
P = vessel pressure, psig
R_o = outer radius remaining at groove, inches
R_i = inner radius, inches

It was desired to hold the stress level below yield at pressurization conditions, prior to the cut or penetration caused by the LSC detonation (Section 3.1.2.3). In one instance, vessel 1-1, pre-detonation stress was held quite low to increase the safety factor for handling and machining, Table 3.5. Of course this required a larger LSC.

On 24 January 92 a burst of vessel 5-2 was attempted at 3500 psig internal pressure by detonating a 25 gr/ft lead/RDX LSC. The vessel failed to burst at a calculated average stress of 116 ksi using .050" typical penetration. After depressurization, measurements confirmed that the typical penetration had been realized. Yet the vessel failed to burst at a calculated average stress that was higher than that of every vessel burst except vessel 1-4. This was also the first attempted burst of a vessel whose groove had been machined at WPAFB using a six axis CNC milling machine. It was concluded that since the vessel was machined to a greater accuracy with less local variability that one of the following was true:

1.) the average wall thickness using 32 measurements more or less equally spaced on the lathe machined vessels was not accurately enough known or
2.) on vessels burst previously the weak spots transferred the load to the strong spots to a greater degree than was thought, causing burst at a lower average stress level.

The test of Test Plan 5 vessels was abandoned for January 92 and only vessel PC was burst. Changes to burst initiation for TP #5 vessels included:

1.) increasing the pressure to 3600 psig
2.) switching LSCs from 25 gr/ft lead/RDX to 50 gr/ft Al/RDX.

The aluminum LSC's are physically smaller than 50 gr/ft lead/RDX and with .005 inches filed from each edge of the LSCs by the manufacturer, Explosive Technology, they fit in the grooves. This avoided the cost of sending the vessels back for additional machining.

The first vessel to be burst in the continuation of Test Plan #5 in June 1992 was vessel 5-1. Since the aluminum/RDX shaped charges require a greater standoff distance, layered "gaffer's" tape was used to build up the surface and allow the LSC to cut through the tape and into the steel. Tape was placed intermittently with two inch strips and two inch open areas. On LSC detonation there was a delay of 13 ms until vessel burst. Later inspection of fragments revealed that there was no LSC penetration through the two inch lengths of tape. For succeeding TP5 bursts the standoff tape was changed to 3/4 inch lengths spaced two inches apart and the delays were reduced to near nothing (Table 5.2).

17

Table 3.5
Steel Vessel Groove, Stress Data

Vessel #	Groove[1]	Avg. O.D, in.	Avg. orig. WT, in.	WT_1[7], in.	LSC, gr/ft.	Typ. avg. LSC cut, in	WT_2[8], in.	Pressure, psig	Pressure stress, ksi @ WT_1	Pressure stress, ksi @ WT_2	Fails
H1	C	24.012	.928	.397	---	---	---	7500	103	---	no
H2	C	24.192	.914	.335	---	---	---	6500	107	---	yes
P1	C	23.992	.941	.240	50	.066	.174	3250	74	102	yes
P2	C	24.032	.959	.430	200	.146[3]	.284	4700[3]	---	90	yes
1-1	C	24.032	.903	.222	200	.136	.08[5]	1475	36.5	95	yes
1-2	C	23.992	.960	.250	50	.066	.184	3450	75	103	yes
1-3	C	23.992	.938	.313	25	.050	.263	5425	94.5	113	yes
1-4	C	24.012	.928	.397	100[3]	.080	.317	7125	98	123[2]	yes
2-1	C	24.032	.951	.232	25	.050	.182	3450	85	109	yes
2-2	C	24.012	.956	.232	25	.050	.182	3450	81	104	yes
2-3	C	24.022	.940	.230	25	.050	.180	3475	83	106	yes
5-1	C	24.350	.919	.217	50	.071	.167	3600	92.5	111.3[5]	yes
5-2	C	24.022	.951	.215	50	.071	.144	3600	91.7	119.7[6]	yes
5-3	C	24.016	.940	.213	50	.071	.142	3600	92.6	119.9[6]	yes
5-4	C	24.012	.950	.216	50	.071	.145	3600	91.2	119.5[6]	yes
6A-1	C	35.970	1.765	.541	200	.270	.271	3280	48.3	97.3	yes
6A-1	L			1.036	400	.450	---[9]		53.0	---[9]	no
6A-3	C	35.890	1.771	.565	200	.270	.295	3300	52.4	80.2	yes
6A-4	C	24.152[4]	.924[4]	.223	100	.123	.100	3500	86.6	130+	yes
6A-4	L			.430	200	.196	.234		92.5	130+	yes

[1] Circumferential (Longitudinal Stress) or Longitudinal (Circumferential Stress)
[2] Did not burst with earlier 25 gr/ft LSC at lower stress
[3] Measured after LSC detonation since no burst occurred, pressure applies to WT_2
[4] In center
[5] Cut intermittently
[6] Cut intermittently by LSC, 73% of circumference
[7] WT_1 = as machined groove wall thickness, in.
[8] WT_2 = as cut by LSC at groove, in
[9] Only one of 4 grooves cut to depth

Knowledge gained from Test Plan 5 provided additional confidence in using a pre-detonation stress that was very close to yield. However the practice of starting tape recorders and high speed video 15 minutes prior to estimated burst pressure being achieved was continued.

Stress analyses for Test Plan 6A required a knowledge of the penetration of Al/RDX LSCs into both SA516 and SA372. Samples from vessel materials were sent to Explosive Technology who provided data[28] for Table 3.6. Samples of SA516 were also furnished to the Materials Lab at Wright Patterson Air Force Base for material properties. The new data[29] are combined with data from Table 3.2 to form Table 3.7.

Table 3.6
Penetration of AL/RDX LSC at Optimum Standoff

Charge wt. grain/ft.	Penetration	
	into SA516, in.	into SA372, in.
50	.098	.069
75	.127	.101
100	.160	.123
200	.270	.196
325	.365	.315
400	.450	.336

Table 3.7
Measured Strengths of Steels in TP #6A

	Measured Strength, ksi				
	SA516			SA372	
	Sy		Su	Sy	Su
	P[1]	RP[2]			
Longitudinal	48.6	52.4	76.4	76.5	98	130.3
Tangential	48.7	53.7	76.6	77.3	97	113.7
[1]Plate	[2]Rolled Plate				

For the multi-fragment vessels in TP6A no delay between detonation and failure could be tolerated because the delay at one groove would exceed another, thereby altering breakup. To avoid a burst delay and use minimum LSC core loads a pre-detonation stress slightly below yield and post-detonation stress slightly above ultimate tensile was desired. This determined LSC sizes which are shown in Table 3.5 along with all the steel vessel stresses. The post-detonation stress in the longitudinal groove of vessel 6A-1 is for one groove only. The LSCs failed to cut adequately in the other grooves as discussed in Section 3.7. The stresses in the circumferential grooves of vessel 6A-1 and 6A-4 were not continuous. The circumferential grooves were interrupted so that the axial grooves could be continuous. A firing scheme using 8 detonators was used for these vessels. Two LSCs in longitudinal grooves were extended 6" beyond grooves for detonators at angles 180 degrees apart at both the east and west end. In between 2 each 1/4 circumference length LSCs were extended beyond their grooves and one detonator used for both shaped charge segments.

3.4   Nitrogen Pressurization System

System design requirements included 7500 psig output, capability of protecting expensive components and operation remotely from the blockhouse. The pressurization system[30] which evolved is designed to free flow/pump nitrogen from a 6000 psig, 240 cubic feet storage vessel into the test vessel. An Arnold Engineering Development Center (AEDC) vessel was recertified[31] and shipped to the test site to provide gas storage. The storage vessel is semi-buried and protected. Commercially available repressurization used a transporter which pumped liquid nitrogen through a vaporizer and into the systems. Two Haskel gas boosters in parallel provide pressures to 9000 psig in the presence of zero leaks. Booster drive gas was initially bootstrapped from the storage volume. Modifications[25,26] made to the system include provisions for a high flow, low pressure compressor to furnish drive air, and was thereafter always used. A system diagram is furnished in Appendix B.

In operation, equalization flow is used until the test vessel achieves storage vessel pressure at which time the boosters are started. After starting, the boosters draw supply air from the high flow compressor, located behind the blockhouse from the arena, which has been idling. Test vessel pressure is read with a transducer and on a gage at the pumping system. Closure of a valve at the pumping system shuts off the flow and permits both items to be exposed to the same pressure. The valve is operated to get a 2 to 3 point calibration within a few hundred psi of test pressure. This calibration thus includes zero and sensitivity shift effects due to solar and compression heating and provides an accurate final pressure.

Pressurization of the 2450 psi rated vessel to an attempted 7500 psi was more difficult than expected due to leaks at the 2-3/4 nozzle plug weld at one end. The leak was found at low pressure and an unsuccessful repair attempted. Test pressure of 7125 psig, where inflow matched leaks, was accepted. Approximate pressurization rates for this pump up at different pressures are given in Table 3.8. For equalization flow, the 240 ft³ storage vessel was initially at 5430 psig.

Table 3.8
Pressurization Rates for Vessel 1-4

Vessel Pressure (psig)	Pressurization Rate (psi/min)	Flow Type	Storage Vessel Pressure (psig)
1000	250	Equalization	4860
2000	170		4480
3000	115		4210
4000	40	Booster	4070
5000	40		3930
6000	30		3760
7000	10		3520

Photos of the installation are included in the photo section, Section 3.7. Figure 3.6 shows the storage vessel in a partial excavation with output plumbing attached. In Figure 3.7 the vessel has been covered with approximately 12" of earth and surplus pressure vessels having 1.2 inch wall thickness. Two more feet of earth completes the installation. Figure 3.8 shows the free flow/booster pumping system that is controlled by an operator in the blockhouse. The system is skid mounted for removal when not in use for pressure vessel testing. Figure 3.9 shows the storage vessel being pressurized.

3.5   Site for Pneumatic Burst Tests

The Preliminary Pneumatic Test and all pneumatic burst tests were conducted at the Naval Surface Warfare Center's (NSWC) experimental test area at Dahlgren, VA. The Center has personnel experienced in explosive detonation and blast data recording from small up to very large charges of high explosive. High speed motion picture coverage is available with multiple cameras and hardened camera shelters. Heavy duty handling equipment is available such as cranes, fork lifts, payloaders, etc. A variety of transducers, tape recorders and timing controls are available for testing. A hardened blockhouse and instrumentation room plus the capability of tape recorder control from a remote site is available. This site provides an already wired arena in close proximity to a blockhouse which can prevent penetration of high kinetic energy fragments. Figure 3.3 is a sketch of the test area. An isometric drawing of a pressure vessel installed in a blast field arena at NSWC is shown in Figure 3.4. (Drawing pertains to Test Plan 2 vessels.)

3.6   Test Hardware

The 24" diameter vessels were initially found to be out of round with a 12.050" radius template and feeler gages.
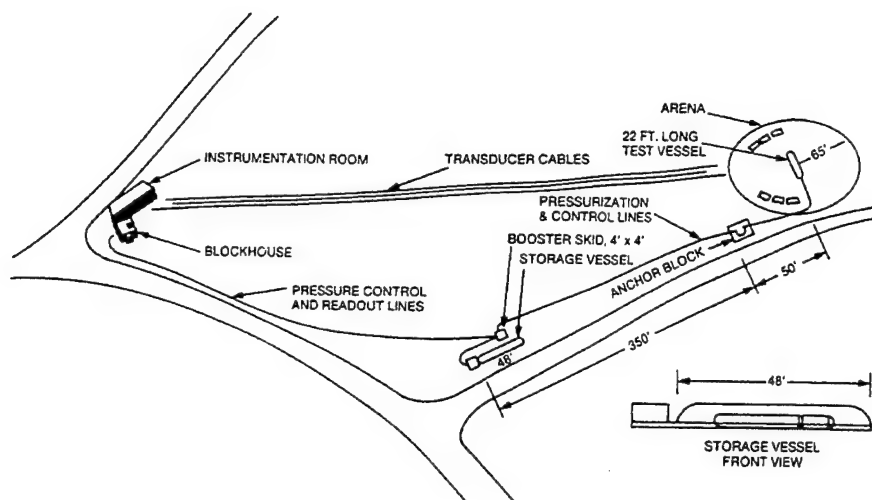
Figure 3.3, NSWC Test Arena
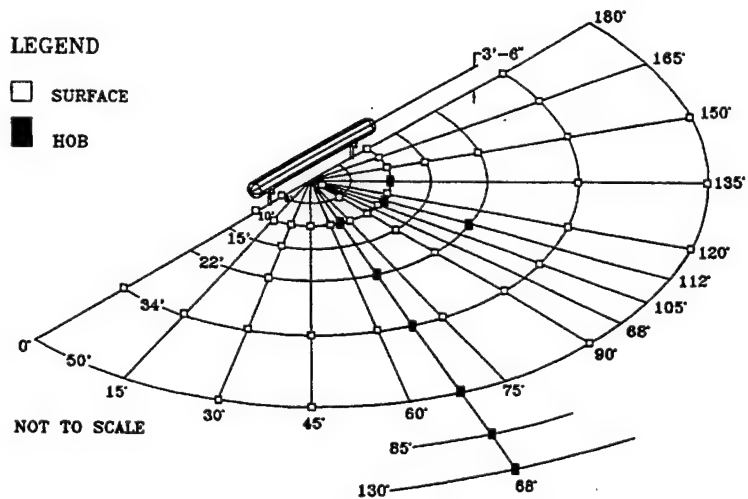
Figure 3.4
Pressure Vessel Installed in NSWC Arena

22

Two roller assemblies were fabricated for mounting and turning the vessels at Dahlgren. These facilitated cleaning preservative from grooves, making groove measurements and modifying standoffs in the field.

Four vessel support stands were fabricated and one was jury-rigged. The fabricated stands were used for:

1. Center split, 1/4 length and end cap split vessels.
2. Composite vessel with vertically launched fragments.
3. Composite vessel with horizontally launched fragments.
4. Multi-fragment vessels.

NSWC supplied height of burst instrument stands for 3.5' HOB. These were a standard type fabrication they used frequently. A HOB instrument stand was designed by General Physics Corporation and built by an NSWC welder because of the size. This was used for HOB measurements at 8.7' and 14' height and 10 ft. to 22 ft. distances.

Two make/break wire stands were fabricated and one was jury rigged. The fabricated stands are:

1. Wooden stands with adjustable height and center line wires.
2. Metal stand with multiple crisscross wires.

A deflector stand was fabricated for use with end caps of vessels 5-3 and 5-4. The requirements for the metal make/break wire stand and the deflector stand emanated from the inability to predict, a priori, the angle that the preliminary composite vessel fragment and the end cap fragment would depart. The metal wire stand was made wide and square to avoid contact and to assure a wire strike. Computations showed that the end cap fragment would travel too great a distance if it departed at an angle greater than 7° up elevation. The deflector stand was to absorb energy and thus reduce the fragment range if it was struck. It turned out that both fragments appeared to have flown a straight and true path compared to their original orientation.

3.7 Photos/Burst Observations/Site Rework

Figures 3.5 through 3.9 were discussed earlier. Figure 3.10 shows vessel 1-1 ready for testing. The legs to the test stands are both aligned with and normal to the vessel axis. The blast typically blows both stands off of their 1" thick round plate bases and may invert one of them. For vessel 1-2 the stands were inadvertently placed at 45° angles to the vessel axis. The aftermath of such a placement is shown in blast Figure 3.11 where both stands were inverted by the blast. There was some concern that the blast asymmetry may have been increased but a close screening of the data[25] didn't seem to show it.

Figure 3.12 shows a 12" diameter tree trunk broken off by the 1/2 vessel 1-4 fragment and displaced 4' from the stump. This is one of 10 trees of 4" to 12" diameter which were broken off in woods approximately 850 feet from the arena center.

Figures 3.13 through 3.16 are all Test Plan 2 vessel shots. For this test plan the legs to the vessel stand were buried flush with the ground surface to preserve alignment and minimize blockage to the gas outflow. Figure 3.13 is a shot of the 14' HOB vessel 2-3. Figure 3.14 is a post-test shot of the 8.7' HOB vessel 2-2. Figures 3.15 and 3.16 are pre and post-test shots of the 3.5' HOB vessel 2-1. The latter figure shows scouring of the earth in the center of the arena. This occurred frequently in warm weather until light steel plate was used in the center of the arena.

Figure 3.17 is vessel 5-1 prior to test. A steel plate under the split region was blown out of the arena on burst. The contact wire frame (used earlier in vessel PC test, Figure 3.25) was also blown over as shown in Figure 3.18.

The steel plate length was increased at each end in the east-west direction and the ends bent 90° and buried 9" in the ground for vessel 5-2 test, Figure 3.19. At burst the east edge of the plate was scooted about 3" to the west with the center of the plate bulged. The makewire stand was moved about a foot by the blast and rotated a few degrees to the south, Figure 3.20.

Vessel 5-4, shown in Figure 3.21, was tested before vessel 5-3. The makewire stand was changed to a breakwire stand by cutting sections of steel (bolted in a modification on June 15). Reinforcement was added to the top of the makewire stand to slow down the end cap fragment in case of penetration. The deflection stand was added and welded to the makewire stand braces added for vessel 5-2. At burst the makewire stand was destroyed as the blast compressed the eastern part of the entire stand, straight areas being compressed more than corner areas, Figure 3.22. Total compression was approximately 1-1/2 feet. The stand was also pushed by the blast about 40 feet which required overcoming 8 trailer stakes and 3/16" cables. Some were yanked out and some cables pulled through the clamps. The end-cap fragment appeared (by its location in the woods) to depart on a line which would be an extension of the vessel axis.

For vessel 5-3, Figure 3.23, the makewire (now breakwire) stand was cut loose and the barely damaged deflection stand was located to its original position. Locally available steel pipe was added to form a holding device for a single row of four breakwires using the music wire. This was placed 6" below center so that another device could be used on centerline. A pipe, supported in two places, was added to the centerline of the vessel to break graphite pencil leads at a location (greater than 6 feet from ground zero) where the pipe would arrive before the blast wave. The graphite leads were supported in a wood framework by modifying the wood makewire stand. Pre-test calculations had shown that a pole attached to this fragment could be a difficult design problem due to potential bending due to acceleration. However, the effort was minimal and NSWC favored pencil leads where useable due to the sharp break obtained. The devices can be seen in the photo.

Upon burst the structure added to the front of the stand was destroyed, Figure 3.24, by being bent outward from fragment flight path. The blast also scooted the structure about 10' to the west and rotated the eastern edge about 20° to the north. The wooden legs of the support for the pencil leads were broken and the east end of the base was rotated about 50° to the north. Sharp break data were obtained from the graphite leads. However the graphite lead data showed a considerably lower velocity than the wire data. The lower velocity can only be explained by a bending of the pole as the endcap accelerated. The graphite lead data were not included in Section 6.

Figure 3.25 is a pre-burst shot of the preliminary composite sphere, vessel PC. Fragments were launched vertically. The bottom portion fragmented into very small pieces upon striking the steel plate. The upper fragment was launched through a wire grid with crossing contact wires spaced a foot apart. Figure 3.26 is the second composite sphere, vessel 6A-2. Fragments were launched horizontally. The left hemisphere carried the support with it, which broke off at the bottom steel plate. Figures 3.27 and 3.28 are both fragments from vessel 6A-2. The latter is the largest liner fragment found.

Figure 3.29 is vessel 6A-1 ready for test. No shaped charge was used in the center circumferential groove. The axial grooves were supplied with angle iron for lateral positioning of the shaped charges. Shaped charge standoff was multiple strips of "gaffers" tape to build up to .221 inches (to nearest .010" tape thickness). The tape was used in 1" widths with the angle iron on top (screwed through tape gaps). Vessel 6A-1 was supposed to be a multi-fragment test, however at burst only the two end caps separated, Figure 3.30. The center section remained in place and shifted about a foot. The blast broke the shear pins at the frame to support and the frame was driven to the ground. The frame was distorted beyond on-site repair.

The axial grooves were examined closely in vessel 6A-1 after the edges failed to part. Some of the grooves were not adequately cut by the LSC with the jet impingence on the side of some grooves. Apparently the LSCs, which were very stiff, could not be adequately held in place by the duct seal which was pressed on top of it as a holding device. At least one groove was adequately cut with the LSC cut located along the groove center. The reason this groove did not split is unclear.

Figure 3.31 is an end cap fragment from vessel 6A-1.

Figure 3.32 is the center-split 3' diameter vessel 6A-3 ready for test. Vessel support was jury-rigged because 1.) economics and time did not permit building 3 frames, 2.) vessel 6A-1 seemed unsteady on the inadequately strengthened frame and 3.) it was important to reserve a good frame for vessel 6A-4. The support blocked the gas outflow to the extent that one of the lower 12 x 12s was found half way to the woods, about 400' away. This could have affected data asymmetry but no affect is apparent, Section 5.9. The center (cut edge) of each of the two fragments was seen to tip up on the video monitor. This never occurred on other center-split tests.

After the unsuccessful multi-fragment burst of vessel 6A-1 the second multi-fragment vessel, 6A-4 was painstakingly prepared for test, Figure 3.33. Steel bars, under angle iron positioning devices, had been prepared for precise stand-offs. However the duct seal would not hold the stiff LSCs in the bottom of the space between the angles. The angles sloped away from each other due to the vessel curvature. A combination of duct seal and clamping the angles against the LSCs as each mounting screw was tightened was finally successful. Four circumferential grooves were cut but no LSCs were placed in the two center grooves because the fragment velocity program[32] did not anticipate a split circumferentially except at end caps when side fragment are considered. However 14 fragments were found at separate locations. Figure 3.34 is taken from high speed film of the vessel burst. The film appears to show two axial fragments that landed separately flying together as an integral unit.

The support for vessel 6A-4 incorporated shear pins at the vertical supports to permit the frame to be driven to the ground, Figure 3.35. This design minimized damage to the vertical supports and permitted acceleration of the lower fragments with a possible result of a stronger blast wave. The side fragments in Figure 3.33 were intended to depart horizontally and clear the instrumented arena.

Figure 3.36 is a lineup of vessel 6A-4 fragments (rotated 90°).

3.8 Instrumentation

Most of the following is repeated from the Test Plan 5 test report[26] and is typical for all tests. The following parameters were measured and recorded during the two test series:

- vessel pre-burst pressure
- vessel pre-burst gas (and wall) temperatures
- vessel fragment location versus time
- nitrogen pressurization line pressure
- time of shaped charge detonation
- time of each contact wire signal
- field pressure at each transducer location

Instrumentation used to measure the above parameters is listed in Table 3.9.

Table 3.9
Instrumentation

pressure transducer (vessel)	Endevco 8511A
pressure transducer (field)	PCB 137A11/21 (HOB) PCB 102A02 (ground) PCB 102A (ground)
thermocouple	Omega TJ36-CPSS-18U-12 Omega TJ36-CPSS-116U-18
pressure gage (line)	Ashcroft 45-1377SS-04B
pressure transducer (line)	Omega PX303-10KG-5V
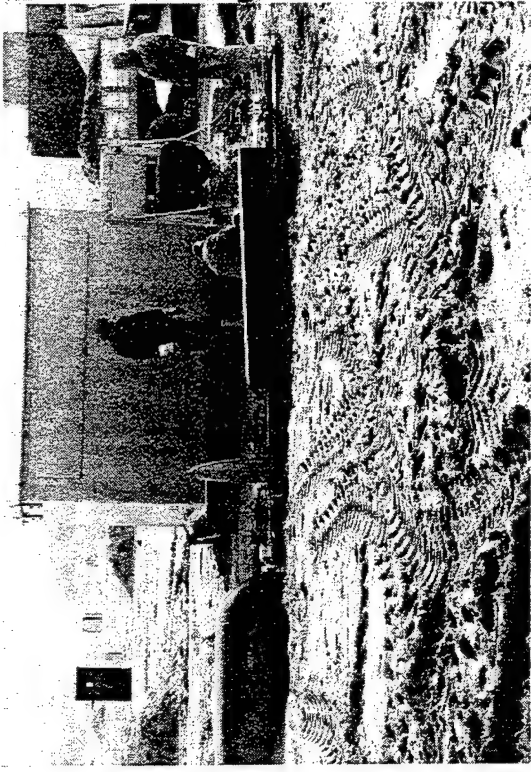
Figure 3.6, Storage Vessel Installation

Figure 3.8, Remote Pumping Skid

Figure 3.5, Hydroburst

Figure 3.7, Storage Vessel Protection

27

Figure 3.10, Above Ground Use of Vessel Stands

Figure 3.12, Broken Trunk Displaced From Stump
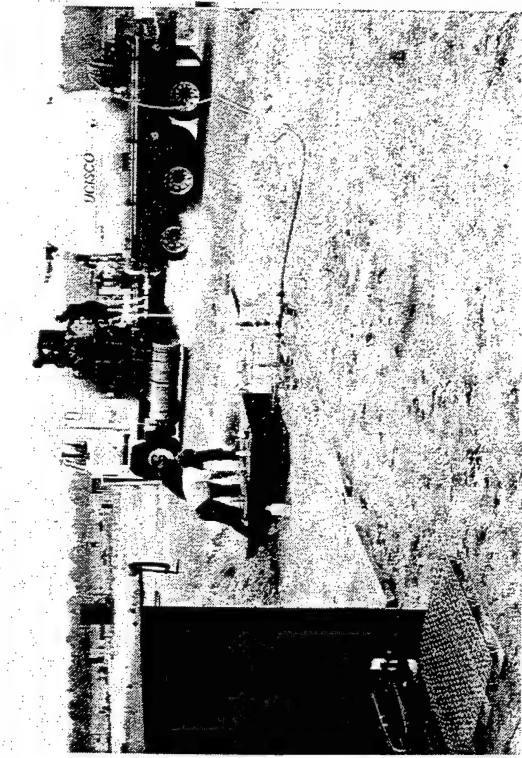
Figure 3.9, Pressurizing Storage Vessel
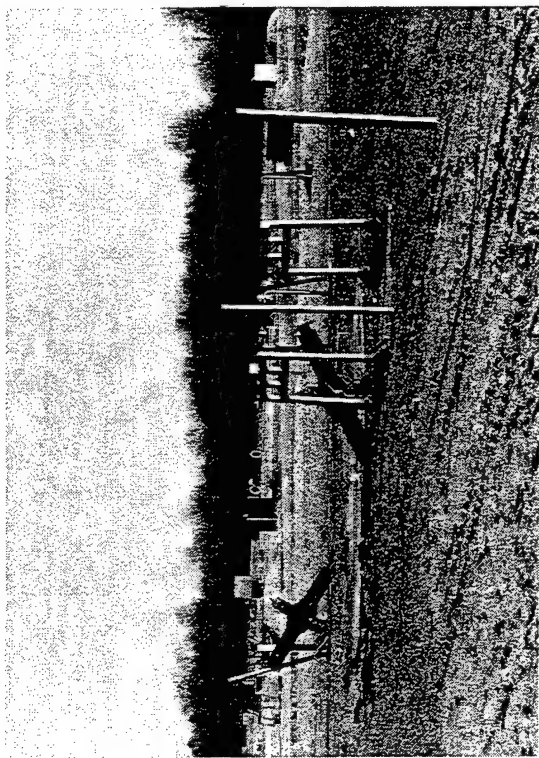
Figure 3.11, Stands Inverted During Test

28

Figure 3.14, 8.7' HOB Vessel 2-2 After Test

Figure 3.16, Ground Scoured by Vessel 2-1

Figure 3.13, 14' HOB Vessel 2-3 Before Test
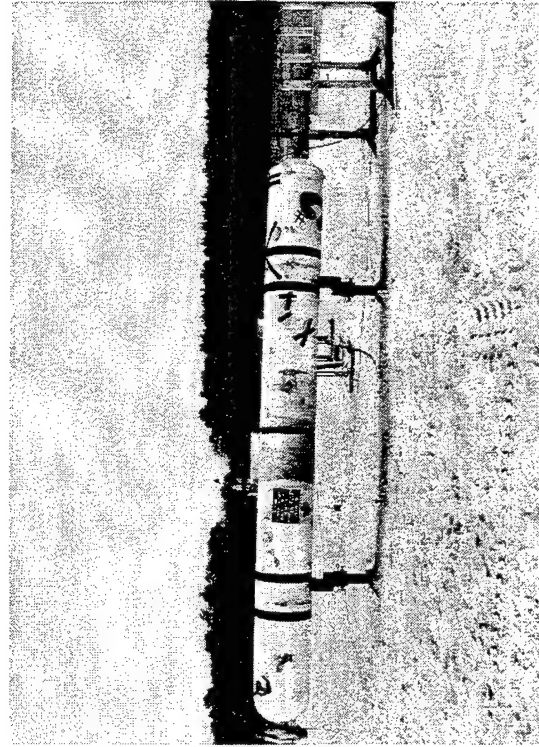
Figure 3.15, 3.5' HOB Vessel 2-1 Before Test

29

Figure 3.18, Wire Frame After Vessel 5-1 Test

Figure 3.20, Arena After Vessel 5-2 Test

Figure 3.17, Vessel 5-1 Before Test
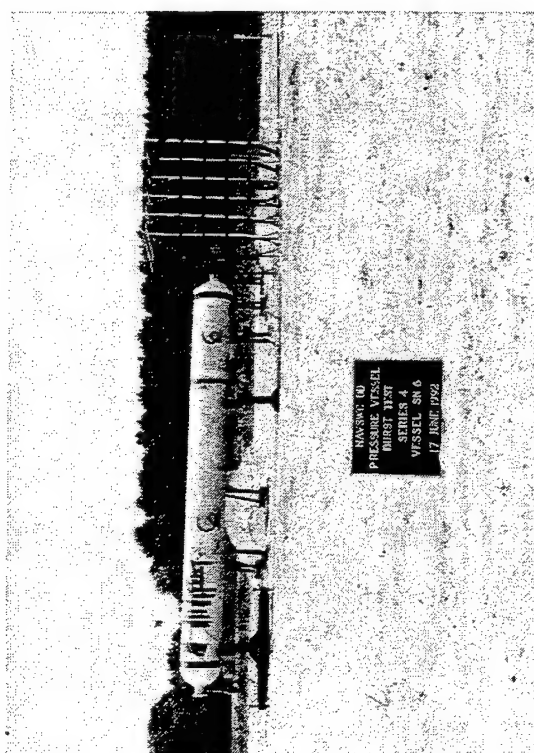
Figure 3.19, Vessel 5-2 Before Test

30
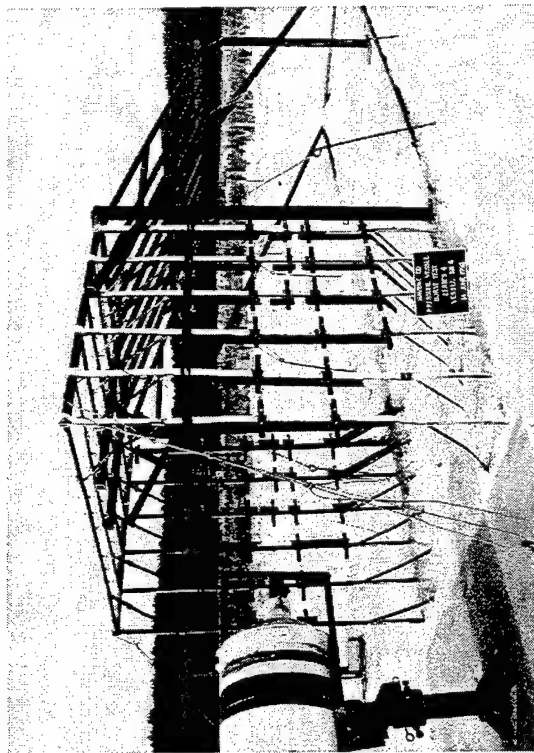
Figure 3.21, Vessel 5-4 Before Test
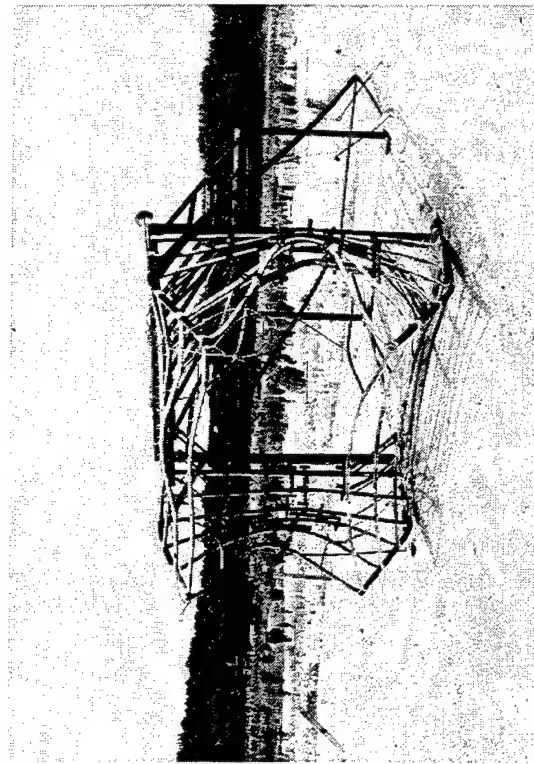
Figure 3.22, Aftermath of Vessel 5-4 Test
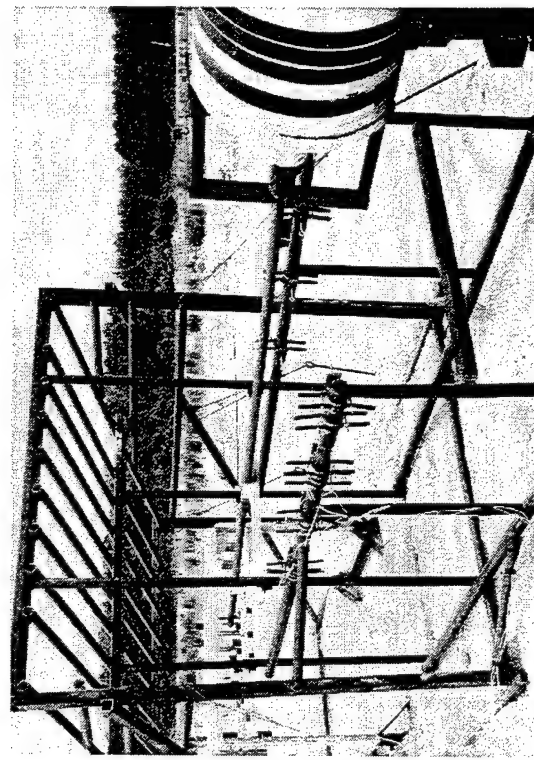
Figure 3.23, Vessel 5-3 Before Test
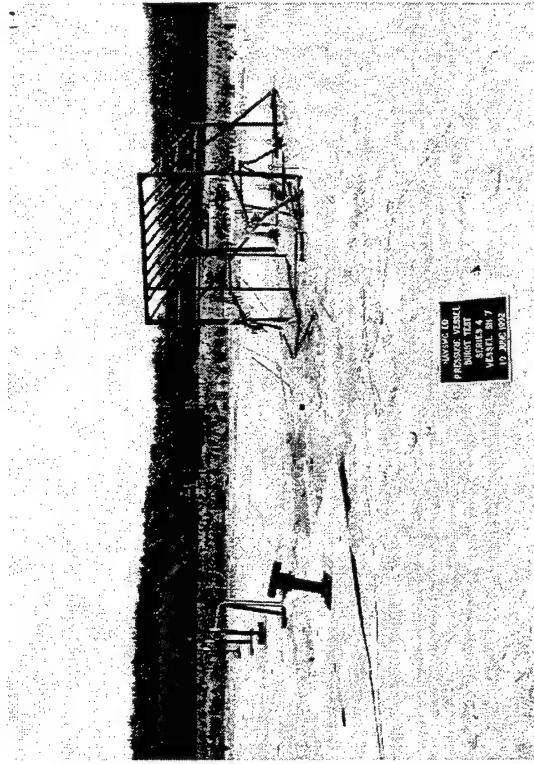
Figure 3.24, Arena After 5-3 Test

31

Figure 3.26, Vessel 6A-2 Before Test
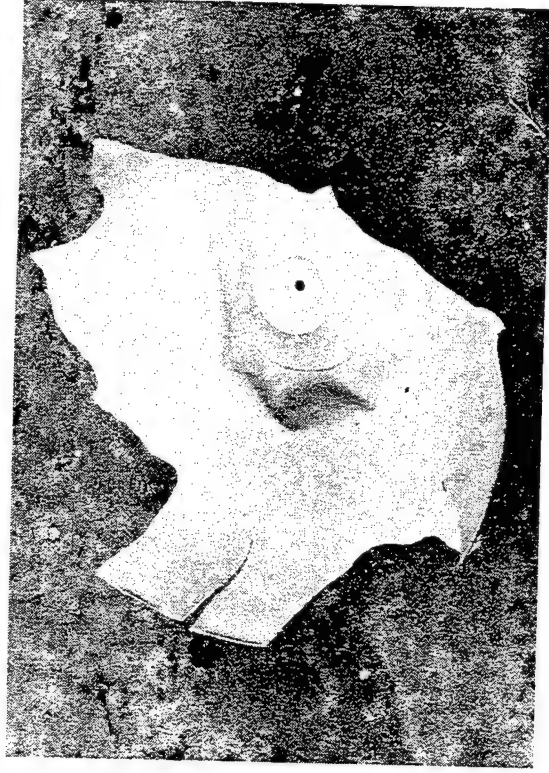
Figure 3.28, Vessel 6A-2 Fragment
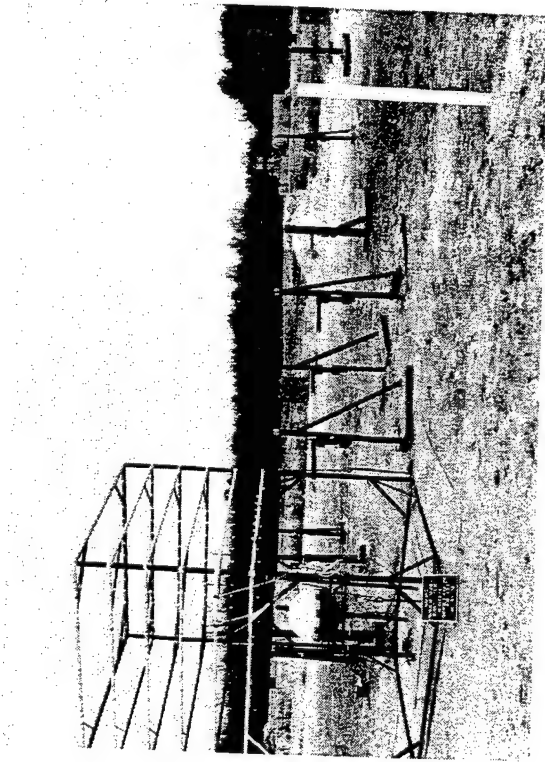
Figure 3.25, Vessel PC Before Test
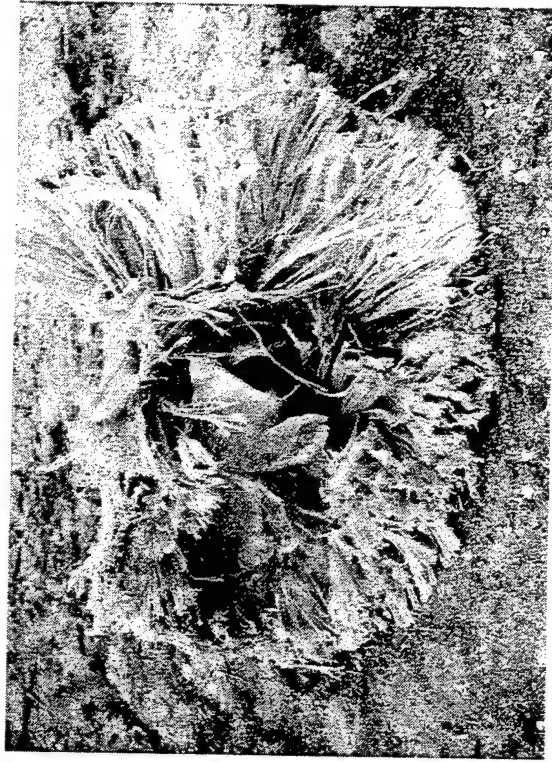
Figure 3.27, Vessel 6A-2 Fragment

32

Figure 3.30, Vessel 6A-1 After Test

Figure 3.32, Vessel 6A-3 Before Test

Figure 3.29, Vessel 6A-1 Before Test

Figure 3.31, Vessel 6A-1 Fragment

33

Figure 3.34, Vessel 6A-4 Burst

Figure 3.36, Vessel 6A-4 Fragments

Figure 3.33, Vessel 6A-4 Being Readied

Figure 3.35, Vessel 6A-4 Support After Test

34

The field pressure transducers were calibrated by NSWC prior to the test program. Many of the transducers were to be used to measure expected pressures well below their full scale ranges, as piezoelectric transducers are not normally available at pressures below 50 to 100 psig. As a result, a special calibration stratagem was devised to ensure the accuracy of transducer measurements. Rather than selecting one sensitivity for the full scale range (industry practice for transducers used to measure pressures near full scale rating), the transducers were calibrated at a range of pressures with a different sensitivity determined at each pressure. This stratagem permitted the selection of a sensitivity for the actual pressure anticipated and for which the recorder was ranged. Calibrating to full scale rather than the expected value could produce many results with poor signal to noise ratio on the FM tape recorder.

A line pressure gage was used for calibrating each test vessel pressure transducer and for accuracy checks during pressurization. The gage connection was 450 feet away from the test vessel in a 1/2" O.D. pressurization line. At low flow rates and high pressures (booster operation) there is a negligible pressure drop in the line. At low test vessel pressures and appreciable mass flow rates (equalization flow) there was a measurable pressure drop in the line. A spot check on the transducer calibration (needed due to potential thermal drifts) was generally obtained when flow was stopped as maximum pressure was reached. This gage was calibrated by the Johns Hopkins Applied Physics Laboratory after testing in July 1991. It was recalibrated by High Purity Systems, Titusville, Florida in October 1993.

Vessel work instruments were also used. General Physics Corporation used a combination of ultrasonic wall thickness (UT) measurements and depth micrometer to determine remaining groove thickness of the SA372 vessels. The UT device used was a Panametrics model 22 with a Microscan number M112-RM transducer having a range of .035" to 3". WPAFB used a similar device. Two gage blocks of SA372 from vessel material were furnished by WPAFB to General Physics Corporation. For measuring LSC detonation cuts in vessels General Physics Corporation used a Starrett model 449AZ-3R depth micrometer with the non-rotating narrow blade ground thinner as required to fit in slots cut by the smaller LSCs.

3.8.1 Instrumentation Channels

Approximately 45 instrumentation channels were used in each test for field pressure transducers plus a vessel pressure transducer, a pressurization line pressure transducer, vessel and fragment make/break wires. Some strain gage channels were recorded during multi-fragment testing, but since the vessels did not burst prematurely the data were not analyzed. Field and vessel pressures and timing data were all recorded on Fairchild Model 9 FM tape recorders at a speed of 60 inches/s for a frequency response of 40 khz.

Figure 3.37 is a block diagram illustrating the sequence by which data are measured, recorded, filtered and prepared for output display and analysis. The block diagram is from an NSWC paper[33] on the pressure vessel burst testing.
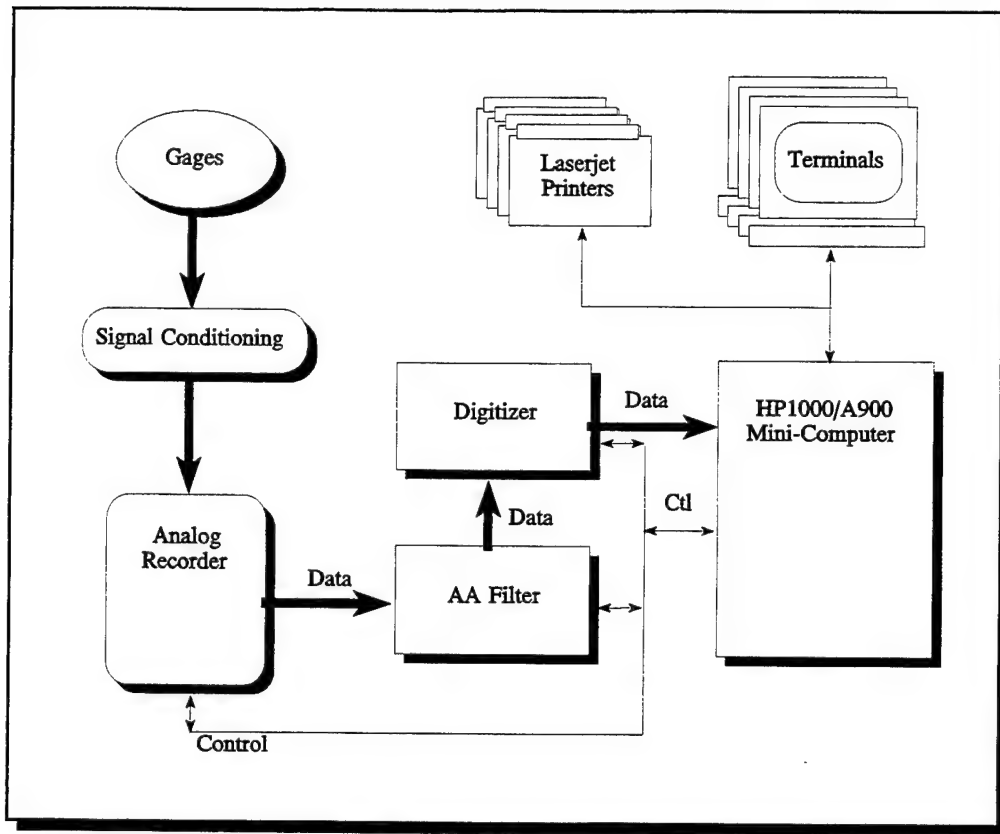
Figure 3.37, NSWC Data Conditioning Block Diagram [Courtesy NSWC]

3.9   Photography

Typical photographic support requirements requested of NSWC are as follows:

▲   2 to 5 high speed film cameras. Typically 2 were used for dual fragment tests and 5 for the multi-fragment tests. Camera placement for dual fragment tests varied and was unsatisfactory for TP #5 endcap vessels. Desired camera placement for TP #6A is shown in Figure 3.38. (However no film was furnished from the two cameras at position A). Frame rates of 1000 to 2000 frames per second (FPS) were typically used.

▲   400 and 200 FPS video cameras were used except in TP #6A. The 400 FPS camera used a field of view of about 60 feet and the 200 FPS camera approximately 300 feet at the vessel distance. These cameras were mounted in a tower above the blockhouse and were not used for TP #6A because fragments would be launched in the blockhouse direction.

▲   2 - 4 standard video cameras for an overall view

▲   Still photos before and after vessel bursts

▲   Photo data reduction for fragment velocity

▲   Composite video tapes, selected still photos and viewgraphs

36
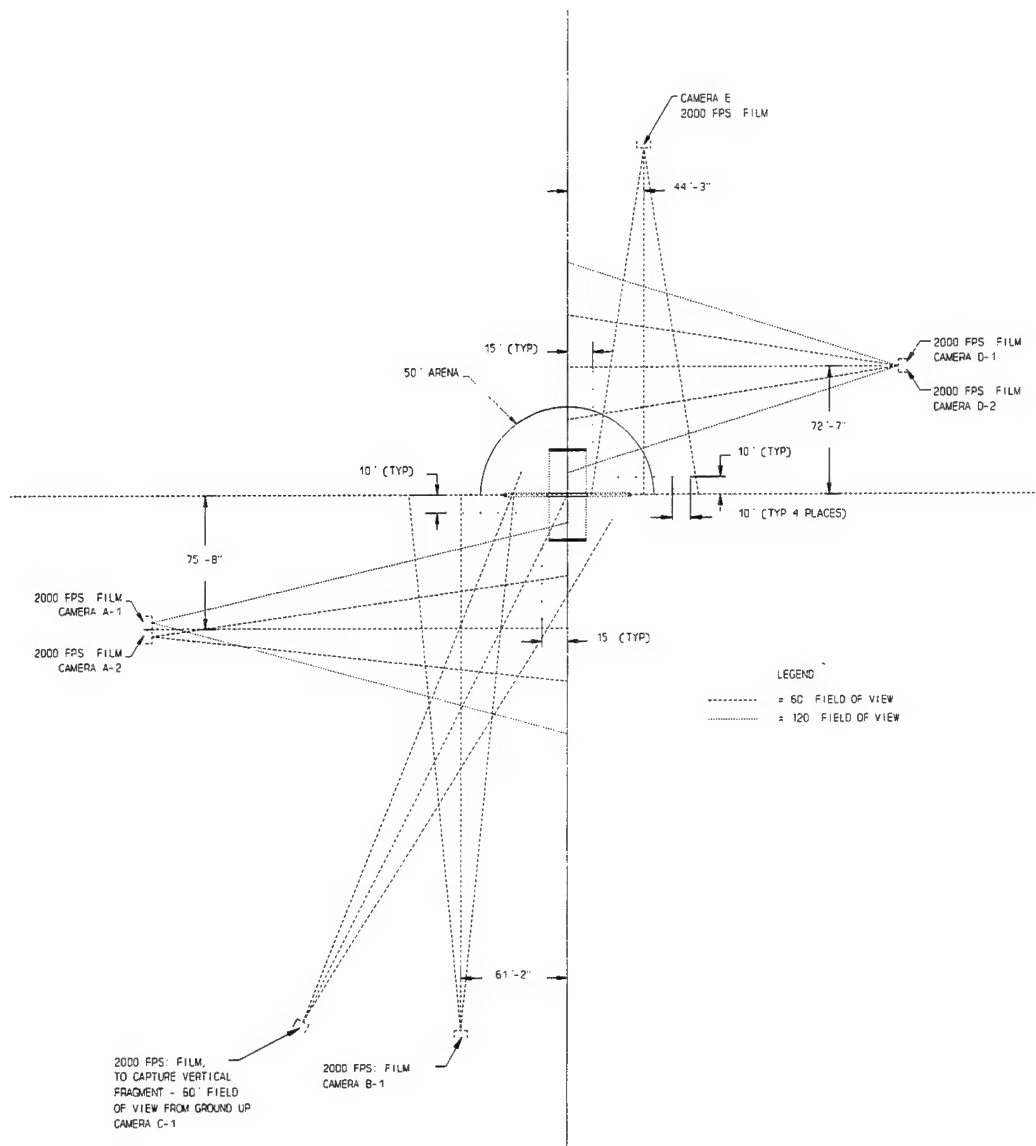
Figure 3.38, TP #6A Camera Setup

3.10 Computer Software

Over 90 different computer programs were used or written as part of the Burst Test Study. This includes the following programs written by others: Burst, Fortran compiler, Lotus 123©, Pvsafe-d, Sigma-plot©, Traj, WordPerfect©, WP Presentations©, Microsoft Excel©, Wordscan©. It also includes over 80 Fortran programs and more than 35 variations of the 80+ Fortran programs that were written for use and a scientific subroutine package, written in Fortran, that was purchased for use. Several programs were often used in preparing files for input to the plotting program as shown in the block diagram of Figure 3.39 prepared for Test Plan 5 report.

TP5 BURST SOFTWARE/FILES
FOR BLAST OVERPRESSURE

REGRESSION

PLOTTING

```
............... KB ...............
                                  │
                                  ▼
KB                         ┌──────────────┐
 │                         │   CONTOUR    │
 ▼                         └──────────────┘
┌──────────────┐  ┌──────────────┐        │
│   REGCK7     │  │  3577.RG7    │        ▼
│     OR       │──│     OR       │  ┌──────────────┐
│   REGCK8     │  │  3577.RG8    │  │  P3577.CON   │        ┌──────────────┐
│  (If offset)*│  └──────────────┘  └──────────────┘        │  PC3577.SPG  │
└──────────────┘                           │                └──────────────┘
      │                                    ▼
┌──────────────┐                   ┌──────────────┐
│  3577.DAT    │                   │  SIGMA PLOT  │
│ (  = shot #) │                   └──────────────┘        ┌──────────────┐
└──────────────┘                                           │  PT3577.SPG  │
      │                                                    └──────────────┘
┌──────────────┐
│ 3577_B.DAT   │
│(version 8    │
│   only)*     │
└──────────────┘
```

FILES F1, F2, F3 IN SIGMAPLOT:
F1 - Col 1-22 to plot measured test (symbol) data
F2 - Col 23-30 to plot measured test (symbol) data
F2 - Col 31, 32 not plotted, for reference only
F3 - Col 33-45 to plot calculated data on angles from strongest array
F3 - Col 46, 47 to plot calculated P or I for high explosive

* Some vessels offset 1 foot from 0°-180°

```
┌──────────────┐  ┌──────────────┐  ┌──────────────┐
│  P3577.F1    │  │  P3577.F2    │  │  P3577.F3    │
│  col 1-22    │  │  col 23-32   │  │  col 33-47   │
└──────────────┘  └──────────────┘  └──────────────┘

        KB ........▶  ┌──────────────┐
                      │   TP5PLOT    │
                      └──────────────┘
```

PT3577.F1

P or I - Pr or Imp ⎫
T or P - Source ID ⎬
Shot #   ⎭

File # of TP5PLOT ⎰

Figure 3.39

38

4.0 BLAST OVERPRESSURE MODELING

Equations and techniques used for estimating burst pressures or for comparing to TNT are included in this section. The equations and techniques have also been incorporated into a computer program, BLAST (discussed in more detail in a workbook[49] written for the Air Force and Navy).

4.1 Vessel Stored Energy

The following equation gives the isentropic energy released by the failure of a vessel containing a volume of ideal gas, V_1, at a pressure of P_1. P_2 is the surrounding atmospheric pressure. γ is the specific heat ratio:

$$W = \frac{P_1 V_1}{\gamma - 1}\left[1 - \left(\frac{P_2}{P_1}\right)^{\frac{\gamma-1}{\gamma}}\right]$$

(eq. 4.1)

Multiplying the above energy in foot pounds by a conversion factor yields the TNT equivalence in pounds TNT. All the TNT equivalence calculations in this report use the ideal gas energy equation and a conversion factor of 1.545×10^6 ft lbs per lb TNT as used by Kinney and Graham[10]. A literature survey[1] as part of the Burst Test Study found values in use from 1.4×10^6 (by Baker[2]) to 1.6×10^6 (by the U.S. Air Force[34]).

Ideal gas behavior is considered adequate for most low pressure applications (1500 psi or less). The ideal gas assumption for high pressure ruptures gives expansion energies that can be unrealistically high due to compressibility effects. For example, using Figure 4.1, the real gas energy for the highest pressure burst at 7125 psi and 133°F is less than the ideal gas energy by 15% to 20%. Figure 4.1 was published as Figure 4 by Wiedermann[6] who used van der Waal's equation of state for evaluating the energy of the integral of PdV. (Wiedermann uses 1.426×10^6 ft. lbs per lb. TNT as a conversion factor.)
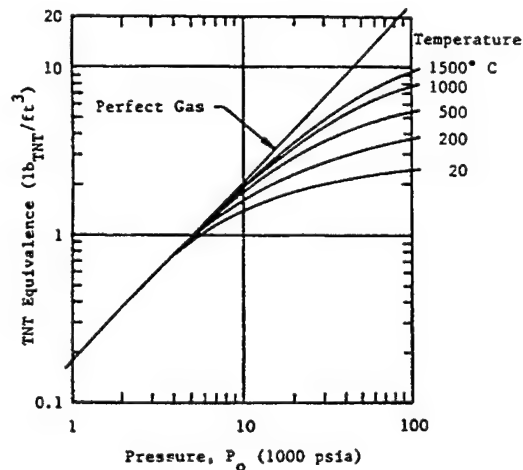
Figure 4.1, TNT Equivalency for Pressurized Vessels Filled with Nitrogen

The kinetic energy imparted to the fragments reduces the energy available to create a blast wave and should be subtracted. This energy is not subtracted in this report. The kinetic energy is computed and is presented in Table 6.3 in Section 6.3 as a percentage of the isentropic expansion energy.

39

4.2   Blast Overpressure Equations

Some authors use the one-dimensional shock tube equation for computing the blast wave initial shock overpressure at the vessel surface. This equation is provided as equation 4.2 and may be obtained from Liepman and Roshko[35] by renaming variables. Efforts to measure pressures close to the vessel to approach the initial shock overpressure were unsuccessful due to side loading as the venting fragment departed. No measurements taken in the test program show the shock tube equation to be inappropriate.

$$P_{so} = P_1 \left[1 - \frac{(\gamma_{ves}-1)\left(\dfrac{a_o}{a_1}\right)\left(\dfrac{P_{so}}{P_o}-1\right)}{\sqrt{2\gamma_o}\sqrt{2\gamma_o+(\gamma_o+1)\left(\dfrac{P_{so}}{P_o}-1\right)}} \right]^{\frac{2\gamma_{ves}}{\gamma_{ves}-1}}$$

(eq. 4.2)

where P_1 =   initial vessel pressure, psia

P_{so} =   initial shock pressure, psia

a_o =   ambient sound velocity

a_1 =   sound velocity in vessel gas

P_o =   ambient pressure

γ =   specific heat ratio, either ambient (γ_o) or vessel gas (γ_{ves})

The shock velocity may also be found in Liepman & Roshko and, by renaming variables, becomes:

$$\mu_{so} = a_o \left(\frac{P_{so}}{P_o}-1\right) \sqrt{\frac{2/\gamma_o}{(\gamma_1+1)\dfrac{P_{so}}{P_o}+(\gamma_1-1)}}$$

(eq. 4.3)

One data point was obtained for checking the actual versus computed shock velocity. On 1/26/91 a 2450 psi rated pressure vessel was burst at 5425 psig. One gage was mounted on a stand 8" from the vessel surface and axially at the groove. Another gage was located on the ground at 6.1' from the groove and edge of the vessel. The 8" gage was destroyed when the stand was carried away, however shock arrival time was recorded. The difference in arrival times provides an average shock velocity between the two points of 1900 ft/sec compared to a calculated velocity of 2230 ft/sec at the vessel which then slows as the shock wave advances.

A graph of initial overpressure and velocity versus vessel pressure using the equations cited is provided as Figure 4.2. The values were computed for air in the vessel with both vessel gas and ambient air at 60°F.

Kinney and Graham[10] provide Bode type equations (their 6-2 and 6-12) for the incident shock overpressure and positive impulse. These equations are used to compute the TNT equivalence overpressures in the plots which are furnished, Section 5.1. The equations, after conversion to English units as used in the Burst Test Data Reports furnished by NSWC, are provided as equations 4.4 and 4.5. Both equations are based on chemical explosions.

$$\frac{P^{\circ}}{P_a} = \frac{808\left[1+\left(\frac{Z}{11.344}\right)^2\right]}{\left(\left[1+\left(\frac{Z}{.121}\right)^2\right]\left[1+\left(\frac{Z}{.807}\right)^2\right]\left[1+\left(\frac{Z}{3.403}\right)^2\right]\right)} \quad \text{(eq. 4.4)}$$

Figure 4.2, Initial Shock Overpressure and Velocity vs. Vessel Pressure

$$\frac{I}{A} = \frac{4.756\left[1+\left(\frac{Z}{.580}\right)^4\right]^{\frac{1}{2}}}{Z^2\left[1+\left(\frac{Z}{3.907}\right)^3\right]^{\frac{1}{3}}}(TNT)^{\frac{1}{3}} \quad \text{(eq. 4.5)}$$

Where:

P°/P_a = ratio of shock overpressure to ambient pressure

I/A = impulse per unit area, psi-ms (Ref. 10 considers impulse to have units of force x time rather than pressure x times)

and:

Z = scaled distance
= $D/(TNT)^{1/3}$
D = distance, ft
TNT = TNT equivalency, lbs.

The term $(TNT)^{1/3}$ is factored into the Kinney & Graham equation to produce equation 4.5 so that the result will not be a scaled value. Hopkinson's scaling law[36] permits the comparison of overpressures of large and small blasts (by comparison to one pound TNT) by dividing distance by the cube root of TNT equivalence. Impulse may also be compared if the impulse is also scaled. Scaled values are used in Sections 5.2 and 5.13.

41

4.3   Methods from references

Baker[2] uses P_{so}, Section 4.2, as a starting point in calculating the overpressure due to a bursting pressure vessel. Baker's curves (based on one-dimensional hydrocode calculations), assume sudden vessel wall disappearance, hence the theoretical predictions are typically higher than can be achieved in a real vessel burst since a finite time is required for the gas to exhaust. Baker's curves were used for estimating some of the overpressures for test planning and are used to compare test results for two type bursts with calculated values, Section 5.15.

Held[3] presents a method for estimating shock overpressure using a TNT explosion located at a greater distant than the bursting pressure vessel. Held's method is based on the fact that the impulse from a bursting vessel is the same as that from a TNT detonation and is based on equations reduced from Baker's curves. Like Baker's curves, a spherical vessel with walls that suddenly disappear is assumed. This approach was not used for burst calculations.

4.4   Reflected Shocks

It is characteristic of an explosive shock front that amplification of the overpressure occurs when a nearby reflecting surface exists. The amplification is typically termed a reflection factor or reflection coefficient. Kinney and Graham[10] develop equations for reflection coefficients and provide limiting values of 2.0 for very weak shocks and 8.0 for very strong, normal (head on) shocks. They also provide data for oblique shocks and reflection factors due to Mach stem formation (grazing incident shock and reflected shock joined at the reflective surface). Figure 5.8 of Kinney and Graham is reproduced here as Figure 4.3 (shock angle sketch was added to the figure). The Mach number (ratio of shock velocity to sound velocity) is related to blast overpressure by equation 4.6, thus strong blast waves are propagated at high velocity.

Swisdak[9] provides curves for reflection factor based on overpressure. Baker's workbook[2] (paragraph 2.3.4) provides some approximate reflection factors for pressure vessel bursts. Reed[37] presents a curve (his Figure 2) of HOB yield factor versus scaled burst height and is reproduced here as Figure 4.4 (English units added). Reed's software also computes an overpressure-distance function.

Shock wave overpressures close to an explosion can be very high as shown by Swisdak's[9] Figure 3A which is reproduced here as Figure 4.5. Shock waves emanating from pressure vessels are typically much less at the source as shown in Figure 4.2 and thus can be expected to generate low reflection factors.

42
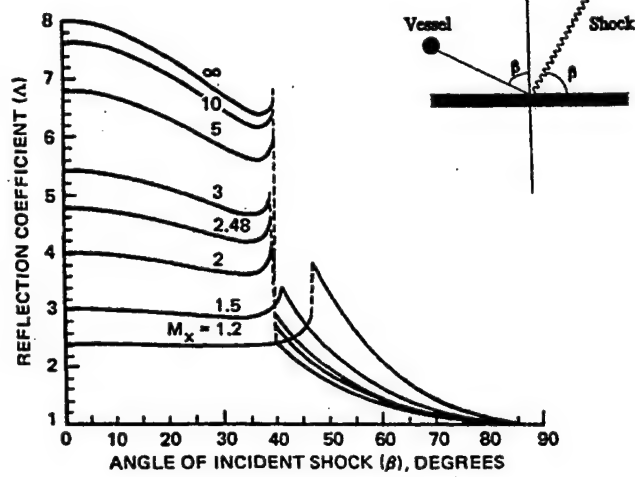
Figure 4.3, Reflection coefficient versus angle of the incident shock front. (For ideal gases at lower pressure and with k = 1.4.)
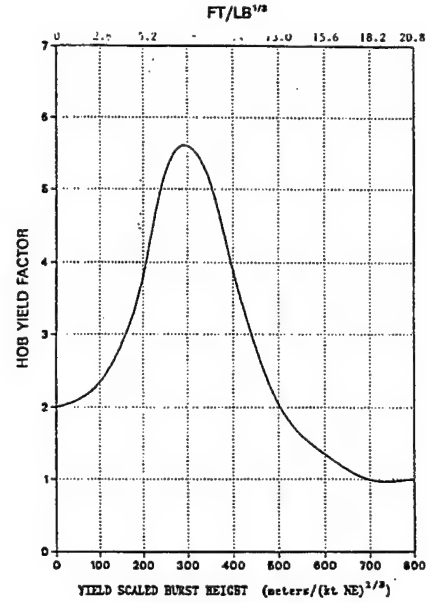
Figure 4.4
Airblast Height-of-Burst Effect on Apparent Yield
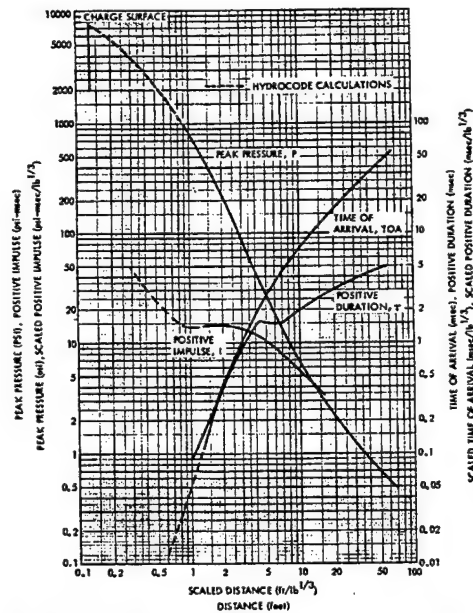
Figure 4.5, Shock Wave Parameters for a one pound spherical TNT explosion in air

43

4.5   Pretest Calculation of Burst Overpressures

For the initial vessel burst, vessel P-2, TNT equivalence was used to estimate overpressures. The data results were a fraction of the recorder scale and rescaling was accomplished for the following burst which was to occur at a lower burst pressure. To prepare for Test Plan #1, the overpressures from vessels P-2 and P-1, 4700 psig and 3250 psig burst pressure, were plotted versus distance and extended toward the vessel to the nominal vessel pressure. Starting at new vessel burst pressures, new overpressure versus distance lines were drawn parallel to the original lines. This resulted in good recorder scaling for the following test series.

New estimates for 3.5 ft HOB burst for the following test series #3 were based on normalizing overpressure data by converting measurements from gage to absolute and dividing by the calculated initial shock overpressure, P_{so} from equation 4.2. An average was obtained for each distance in the arena for normalized overpressures from 5 vessel bursts. A log-log plot of these averages was used to establish a base-line for converting to the expected results from 3500 psi and 7500 psi testing. With some scatter the normalized overpressures ranged from 0.24 at 10' to 0.153 at 50'.

Elevated height of burst tests were also to be conducted as part of test series 3 (Test Plan #5 and completion of Test Plan #2). To determine the necessary variation in height of burst, the optimum heights of burst for the 10 to 50 foot range of the arena were found using four techniques. The results are plotted in Figure 4.6. The methods used were: (1) Swisdak's[9] Figures 5B and 5C, (2) Figure 8-8 of Kinney and Graham[10], and (4) a HOB curve by Reed[37]. Input data were the TNT equivalent as computed using the overpressure at each distance from the 3250 psi burst of the preliminary test[24]. It was decided to use an optimum height for the mid-range of the arena of 22 feet. This required a height of 14 feet to cover the requirement of 3 of the 4 techniques and 19 feet to cover technique number 3. For practical reasons it was decided to limit the height to 14 feet.
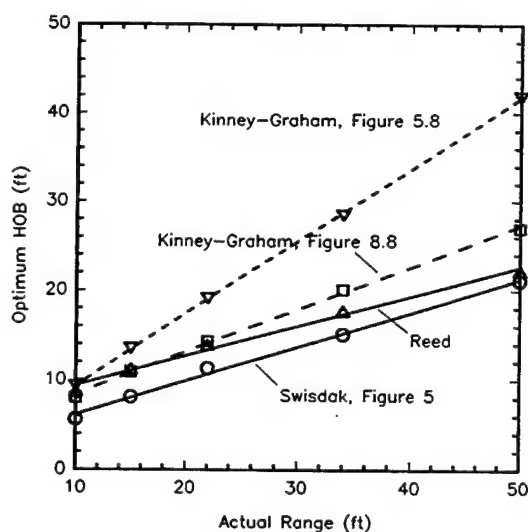
Figure 4.6, Peak Overpressure Versus Distance Comparison

44

Two methods were used to estimate overpressure variation with HOB in order to determine if the overpressure variation would be large enough to measure. One used the shock overpressure ratio and the other used the shock Mach number. These two methods are not necessarily independent because both use a shock incident angle and the shock Mach number and overpressure ratio are related by an equation[9] given below (equation 4.6). Figure 4.7 is a plot of the equation and pressure vessel burst overpressure data versus average shock velocity between two stations prior to the pressure measuring point. It shows reasonable correlation, with the better scaled data for vessel P-1 showing better correlation than P-2 data.
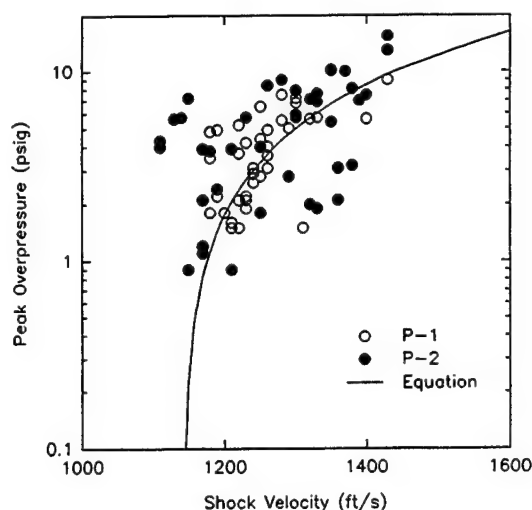
Figure 4.7, Peak Overpressure Versus Shock Velocity for 3250 psi Vessel P-1 and 4700 psi Vessel P-2

$$\mu = a_0 \left(1 + \frac{\gamma+1}{2\gamma}\frac{P}{P_0}\right)^{\frac{1}{2}}$$

(eq. 4.6)

where μ = shock velocity (ft/s)
a_0 = sonic velocity ahead of shock front for air at ambient temperature
γ = ratio of specific heats
P = peak overpressure
P_0 = ambient pressure (atmospheric)

The shock Mach number was estimated from Preliminary Pneumatic Burst Test data[24]. These data were obtained by time of arrival differences between two distances in the array. An estimate of Mach 1.2 was used at 5' to 10' from the vessel and Mach 1.1 at 50'.

Incident overpressure data were estimated using incident angles, based on 3.5' HOB. Figure 4.3 (Figure 5-8 of Kinney & Graham[10]) and the 3500 psi burst data found earlier. The resultant overpressures ranged from 10.5 psi at 10 feet to 3.9 psi at 50 feet on a log-log plot with slight scatter.

Overpressure data were then computed by the reverse of the procedure in the preceding paragraph with incident angles for 3.5', 8.7' and 14' HOBs.

45
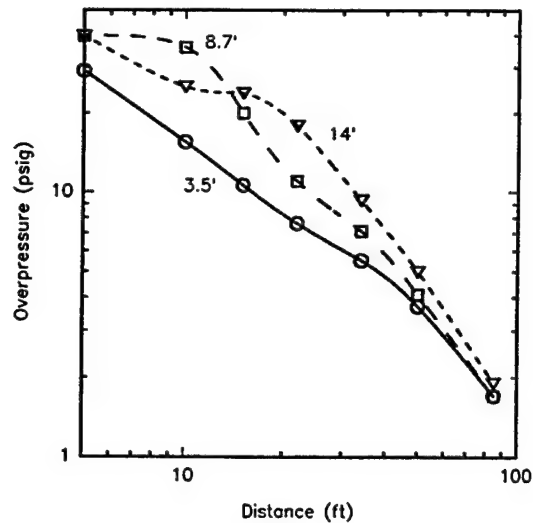
Figure 4.8
Estimated Overpressures for Height of Burst Testing.

Overpressure data were then computed using the same incident overpressures, the overpressure ratios (to ambient) and the incident angle using Figure 13a of Swisdak's[9] report. The results are plotted in Figure 4.8. The two methods yielded similar results. The expected difference in overpressures from 3.5' to 14' were deemed to be adequately measurable at 22' distance and less so for lesser or greater distances.

Overpressures for the preliminary composite sphere, vessel PC, and the multi-fragment bursts, vessels 6A-1 and 6A-4, were estimated using the methods of Baker, Section 4.3 for spheres with a volume factor of 2. The closest distance to the cylindrical vessels was used. Baker's cylinder correction factors were not used but a safety factor of 2.5 was used to allow for ground reflection to avoid saturation recorder conditions.

46

5.0 BLAST OVERPRESSURE TEST RESULTS

Graphs are provided to show blast strength and patterns. Most of the graphs will be provided in Appendix E except where specific references are made. NSWC data sheets which led to the graphs are included as Appendix C.

5.1 Data Reduction and Presentation

The following equation is used wholely or in part for all data reduction of blast overpressures:

$$\log_e P = B_n + B_1 \log_e D + B_2 A + B_3 (\log_e D)^2 \qquad \text{(eq. 5.1)}$$

where:
- $P =$ pressure, psig (or I= impulse, psi-ms)
- $D =$ distance (slant height except for height of burst measurements) from vessel center (and burst point)
- $A =$ absolute value of angle from reference blast angle (reference angle found by selecting one of 36 overpressure curve fits, $0°$ to $180°$ using $5°$ increments, having least sum square errors)
- $B_i =$ coefficients, B_3 is zero unless 2nd order provides an accuracy improvement (vessels 2-2 and 2-3 only)

The terms involving B_n and B_1 are always used. This provides a regression of overpressure or impulse (the area under the positive portion of the overpressure curve) versus distance without consideration of arena angle. The addition of the $B_2 A$ term permits a consideration of asymmetry. Note that the angle is taken from a reference angle as defined above. The second order term in $\log_e D$ was used only for 8.7' and 14' height of burst data reductions where a non-linear relationship between $\log_e P$ and $\log_e D$ was anticipated from the test plan. All data were reduced twice, with and without the asymmetry term.

A typical curve fit, using burst of vessel P-1, is shown in Figure 5.1. The asymmetric curve fit which calculates an angle term $B_2 A$ is provided. This vessel burst had a calculated peak overpressure at about 80°, or almost normal to the vessel. The same best fit array angle is assigned to the impulse curve fit and in this case it fits very well as can be seen by the impulse error deviation being nearly the same as that for pressure. None of the height of burst data were used for the regression. Pressures were measured beyond 50' but these data are also not used. Errors are provided in percent of reading instead of full scale in order to weigh all errors equally. Data shown were collected at ground distances of 10', 15', 22', 34' and 50'. The curve fit computes slant height after correcting for the vessel edge rather than centerline lying on the origin.

47

DATA PROGRAM VERSION = REGCK10.FOR, JAN 94
CENTER SPLIT VESSEL P-1 @ 3250 PSIG   (FILE=3248.R10)
TP:PRELIM, TEST DATE: 6-26-90, ORD=1, OFFSET=1., NSWC SHOT#: 3248
PHI= 80.=BEST FIT CENTER ARRAY & ANGLE REFERENCE,   HOB= 3.5 FT
REGRESSION MODEL: LN(V)=B(N)+B(1)*LN(SL)+B(2)*A+B(3)*(LN(SL))**2+...

ARENA	A	D		V(1)=PRESSURE			V(2)=IMPULSE		
ANGLE	ANGLE	SLANT	MS	MEAS	CALC	ERROR	MEAS	CALC	ERROR
DEG	DEG	FT	HT	PSIG	PSIG	%RDG	PSI-MS	PSI-MS	%RDG
30.	55.	11.10	G	9.90	10.52	6.3	31.0	36.7	18.3
60.	23.	11.43	G	9.00	12.78	42.0	40.0	58.8	47.0
75.	6.	11.51	G	14.30	14.21	-.6	60.0	75.1	25.2
90.	10.	11.54	G	13.10	13.82	5.5	60.0	70.9	18.1
105.	26.	11.51	G	10.00	12.36	23.6	50.0	55.2	10.4
120.	43.	11.43	G	13.60	11.11	-18.3	38.0	43.2	13.6
150.	75.	11.10	G	7.50	9.15	22.0	28.0	26.9	-3.9
0.	84.	15.44	G	6.70	6.09	-9.1	18.0	18.0	-.1
30.	53.	15.91	G	7.50	7.31	-2.6	27.0	28.2	4.3
60.	22.	16.26	G	9.00	8.90	-1.1	53.0	45.0	-15.2
90.	10.	16.38	G	10.10	9.59	-5.0	64.0	53.6	-16.2
0.	83.	22.30	G	4.90	4.18	-14.6	17.0	13.7	-19.6
15.	67.	22.55	G	5.20	4.60	-11.6	19.0	17.1	-10.0
30.	52.	22.79	G	6.50	5.06	-22.2	20.0	21.5	7.4
60.	21.	23.14	G	5.60	6.18	10.4	38.0	34.2	-10.0
98.	18.	23.26	G	6.80	6.28	-7.7	58.0	35.6	-38.6
105.	26.	23.23	G	5.70	5.97	4.8	44.0	31.9	-27.6
120.	41.	23.14	G	5.60	5.38	-4.0	28.0	25.1	-10.3
150.	72.	22.79	G	4.00	4.40	10.0	19.0	15.8	-17.0
0.	82.	34.19	G	3.70	2.70	-27.1	12.0	9.9	-17.9
15.	67.	34.45	G	3.10	2.97	-4.1	10.0	12.4	23.6
30.	51.	34.69	G	4.40	3.28	-25.4	16.0	15.5	-2.9
45.	36.	34.89	G	3.60	3.63	.8	19.0	19.6	3.1
60.	21.	35.04	G	4.90	4.02	-17.9	27.0	24.7	-8.4
75.	5.	35.14	G	5.50	4.47	-18.8	38.0	31.3	-17.6
90.	10.	35.17	G	5.00	4.32	-13.5	37.0	29.1	-21.2
0.	81.	50.13	G	1.80	1.82	.9	8.0	7.3	-8.5
15.	66.	50.39	G	1.50	2.01	33.8	8.0	9.2	15.0
30.	51.	50.63	G	1.60	2.22	38.7	9.0	11.6	28.6
45.	36.	50.83	G	2.20	2.46	11.7	11.0	14.6	32.6
60.	21.	50.99	G	2.60	2.73	4.8	16.0	18.4	15.0
75.	5.	51.09	G	2.80	3.03	8.1	18.0	23.3	29.3
98.	18.	51.11	G	3.10	2.77	-10.8	22.0	19.1	-13.3
105.	25.	51.09	G	2.90	2.63	-9.2	16.0	17.1	6.8
120.	41.	50.99	G	1.90	2.37	24.7	13.0	13.5	4.0
150.	71.	50.63	G	1.50	1.93	28.6	7.0	8.5	21.4

ERROR STD DEV IN % READING OF MEAS.:   17.9   19.5
PRESSURE COEFS: B(N)=   5.24688   IMPULSE COEFS: C(N)=   6.36686
                B(1)= -1.04286   C(1)=   -.79778
                B(2)=   -.00700   C(2)=   -.01544

Figure 5.1, Typical Blast Curve Fit

48

Copies of the regression analyses are typically not furnished. Plots are furnished that together with the furnished error deviation provide a clear picture of the accuracy and distribution of errors. Table of coefficients from the regression analyses may be found in Appendix D. Table D-1 provides overpressure curve fit coefficients for all the LSC detonations. Table D-2 and D-4 provide overpressure coefficients for all the vessel burst data and Tables D-3 and D-5 provide impulse coefficients for all the vessel burst data.

Three types of individual burst plots will be used for overpressure herein and will be demonstrated using vessel burst P-1. These are pressure (or impulse) versus angle, pressure (or impulse) versus distance and a contour plot.

Pressure versus angle and impulse versus angle plots for vessel P-1 are shown in Figure 5.2 and 5.3 respectively. The data points are connected by a cubic spline for clarity. The lines are labeled 10′ through 50′ for convenience. Only points where measurements were made on the ground are shown. No measurements were made beyond 50′ for this test. The graphs of impulse versus angle are only furnished for a limited number of cases such as vessel bursts 5-3 and 5-4, Section 5.7, where overpressure and impulse asymmetry differ.

The dashed line shown on the plots were computed with the regression coefficients. The lines are truncated to the maximum angle at each horizontal distance from ground zero where measurements were made. The distances shown are nominal, ground based arena measurements. The computations corrected the distances shown for vessel offset and slant height. This would provide a one to one graphical correspondence of measured to computed pressures if there was a perfect fit of coefficients to all data.

Pressure versus distance and impulse versus distance plots for vessel P-1 are shown in Figures 5.4 and 5.5 respectively. Two regression lines are shown. The solid line is an "average", obtained without an angle coefficient. This line is shown solid from 10′ to 50′ where data were typically recorded, and dotted at closer or farther distances. A dashed line above (for negative B_2 coefficient) the solid line and labeled "asymmetric" in the legend is for values computed with angle "A" (equation 5.1) set equal to zero, i.e. values computed for the best fit array angle which is 80° for vessel P-1. Two dotted lines are shown. The upper line represents the vessel TNT equivalent as computed using ideal gas isentropic expansion, equation 4.1. The lower TNT equivalence line represents the TNT equivalence of the LSC(s) detonated to initiate vessel burst (see Section 5.12).

Measurements made at the vessel height of burst are not used for coefficient computation. These values are shown in Figures 5.4 and 5.5 with open circles. Values beyond 50′ distance are not shown and are discussed in Section 5.8. Measurements made on the ground closer than 10′ are shown with filled circles. These were included in coefficient computation if the data were a reasonable extension of the regression line with scatter typical of the main body of data. Some measurements were a considerable departure from the regression line as shown in Section 5.5.

49
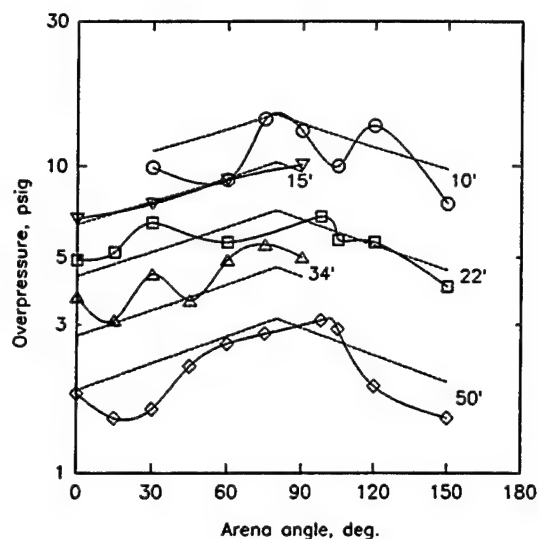
Figure 5.2
Overpressure versus angle for Vessel P-1
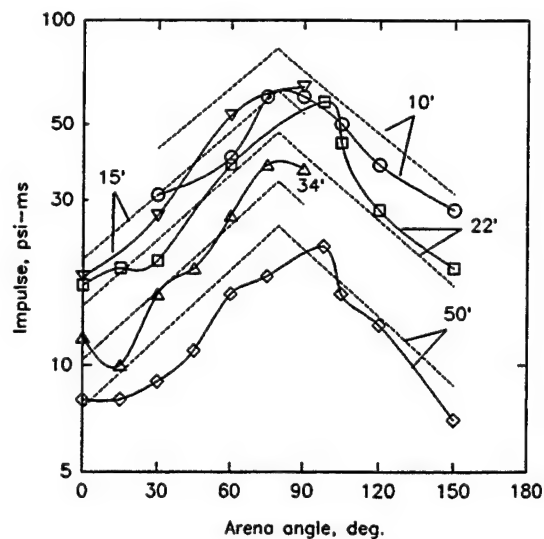
Figure 5.3
Impulse versus Angle for Vessel P-1
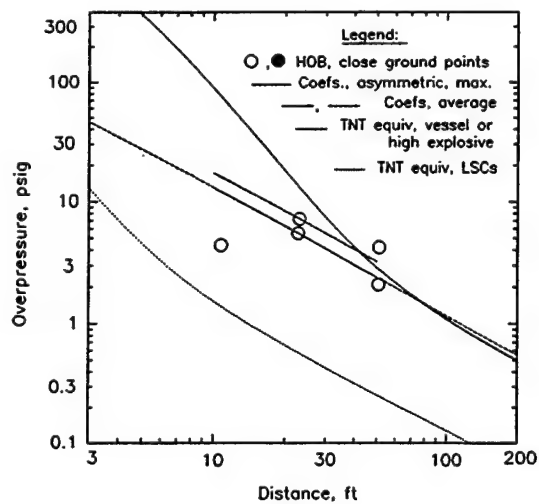
Figure 5.4
Overpressure versus Distance for Vessel P-1
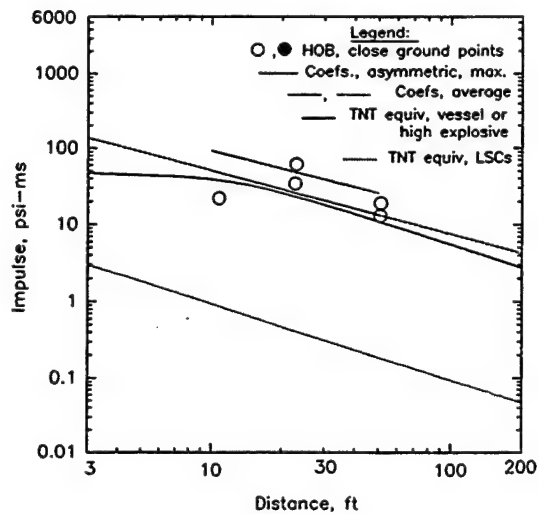
Figure 5.5
Impulse versus Distance for Vessel P-1

50
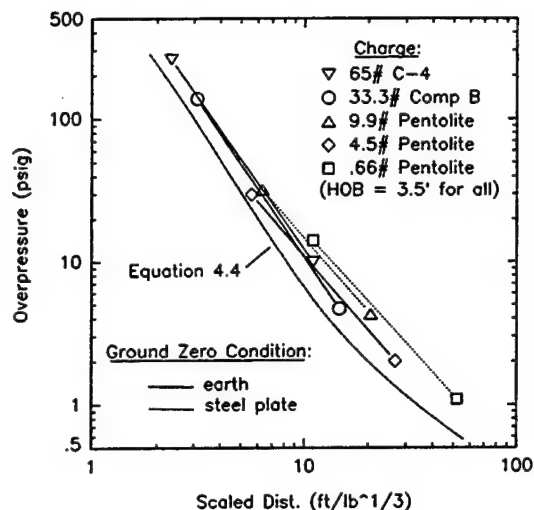
Figure 5.6, Explosive Blast Overpressures
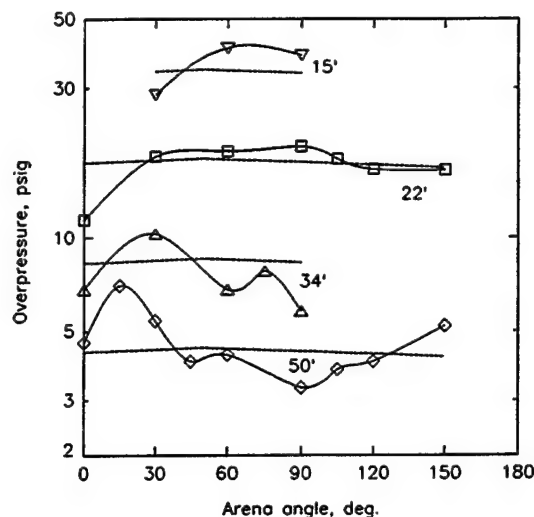
Figure 5.7, Overpressures from Detonation of High Explosive PHE-1

The overpressure (impulse) versus angle plots graphically present the asymmetry, irregularities and data scatter. The overpressure (impulse) versus distance plots permit comparison of blast strength versus distance and permit comparing vessel bursts versus each other and with TNT equivalence.

A special regression analysis for vessel 6A-4 is discussed in Section 5.10.1.

5.2 High Explosive Detonations

High explosives were detonated as discussed in Section 2.1. Since it was not the purpose of the test program to evaluate high explosives, these are only discussed in Section 5.6 where vessel HOB tests are compared to high explosive tests. However data plots are included in Appendix E and a combined plot of several explosive blasts is provided as Figure 5.6. The TNT equivalence line was computed using equation 4.4 with $Z = D$ (i.e., $(TNT)^{1/3} = 1$) to compare all explosions to one pound of TNT. Table 5.1 compares measured data in Figure 5.6 to equation 4.4. The ratio of measured overpressure to TNT equivalence should be the reflection factor (see Section 4.4). An overpressure angle plot is provided here as Figure 5.7. The figure shows the overpressure resulting from detonating 33.3 pounds of composition B (TNT equivalency 40.0 lbs). As expected the asymmetry in the high explosive data is minimal compared to vessel burst data. This is evidenced by the nearly horizontal regression lines in Figure 5.7. Considerable data scatter exist in the results from this detonation as it does in all the data, including the pressure vessel burst tests.

51

Table 5.1
High Explosive Overpressures versus Equation 4.4

Charge	TNT Equiv.	Measured/Calculated - Eq. 4.4		Ground zero surface condition
		Near (10')	Far (50')	
65 lbs. C-4	94.0	1.50	1.82	earth
33.3 lbs. Comp B	40.0	1.48	1.44	earth
9.9 lbs. Pentolite	14.6	1.79	2.23	steel plate
4.5 lbs. Pentolite	6.6	1.28	1.50	earth
.66 lbs. Pentolite	.89	2.58	1.77	steel plate

5.3 Linear Shaped Charge Overpressures

Linear shaped charge overpressures were measured without attendant vessel bursts during preliminary testing, Section 3.1.2. LSCs from 10 grains/foot to 200 grains/foot were detonated. Coefficients from the regression analyses are provided in Table D-1 in Appendix D. Overpressures from the regression analyses are plotted in Figure 5.8.

The purpose in making the measurements was to quantify the LSC overpressure output to get an idea of how much of the vessel burst output might have to be attributed to the initiating LSC. Note that 1/2 of the LSC is on the far side of an unburst vessel. It was also desired to subtract the LSC output from the vessel burst output as a tare if that was practical. (It seems not to be.)

The LSC overpressure for many of the vessel bursts can be completely ignored. Delays were observed on the overpressure versus time graphs furnished by NSWC. These are delays between LSC overpressure peak and the sudden rise to the vessel peak overpressure at burst. The delay is caused by a lower than ultimate stress level after LSC detonation. A sample delay of 9.8 ms from LSC peak to vessel burst peak is shown in Figure 5.9. The delay includes a gradual rise in pressure after initial vessel overpressure rise. The delays at sample angles and given distances are listed in Table 5.2. For those delays that show a superscript of 5 or 6 the LSC overpressure is not a consideration because either an LSC was not used or the LSC overpressure has returned to zero prior to the vessel burst response. Consideration may also be ruled out for superscript of 1, 2 and 3 because the peak vessel pressure did not occur at initial vessel pressure rise.

Comparison of the LSCs in Figure 5.8 that were actually used for vessel bursts (25, 50 and 200 gr/ft) shows that measurements were 35% to 40% more than the LSC TNT equivalent at 10' range and 30% to 60% more at 50' range. The TNT equivalence is computed using an equation (equation 4.4) from Kinney and Graham[10] and is for side-on overpressures.

Table 5.2
Peak Overpressure Delays
LSC Peak to Vessel Burst Peak

Vessel Burst	NSWC Shot #	Delay, (ms) at Arena Range		
		10 ft	22 ft	50 ft
P-2	3245	NA[5]	NA[5]	NA[5]
P-1	3248	2.1[6]	4.0[3,6]	1.8[6]
1-1	3251	9.4[1]	5.5[1]	3[1]
1-3	3253	6.8[3,6]	5.9[3,6]	1.2[4,6]
1-2	3252	2.0[6]	.9[6]	.6[4,6]
2-3	3398	2.1[6]	.8[6]	.6[4]
2-2	3400	7.4[3,6]	3.5[6]	3.8[6]
1-4	3402	0(2.4)[2]	0	0
2-1	3403	5.0[3,6]	.8[6]	1.1[4,6]
PC	3573	0	0	0
5-1	3474	15.5[3,6]	12.3[6]	9.5[6]
5-2	3475	1.7	0(3.4)[2]	0
5-4	3476	2.2	0	0
5-3	3577	0(2.1)[2]	0	0
6A-1	4053	0	0	0
6A-2	4054	0	0	0
6A-3	4055	6.0[3,6]	4.8[3]	0.5[4]
6A-4	4056	0	0	0

[1] gradual rise
[2] no discernible delay, but time to peak in parenthesis
[3] delay plus gradual rise
[4] at 34′ (too small to read at 50′)
[5] LSC not used
[6] returned to zero before rise

53
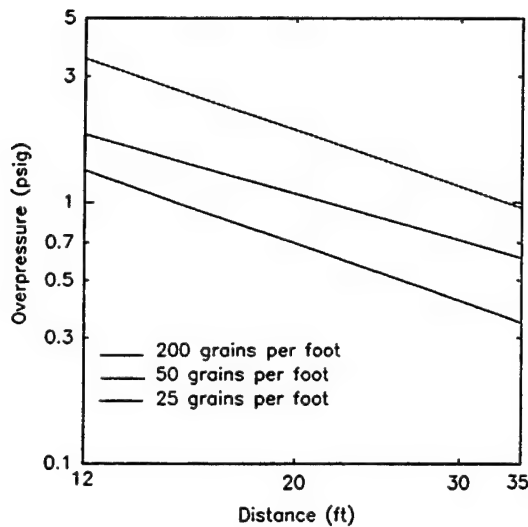
*Figure 5.8, Overpressures from
LSC Detonation on 2' Diameter Steel vessel*
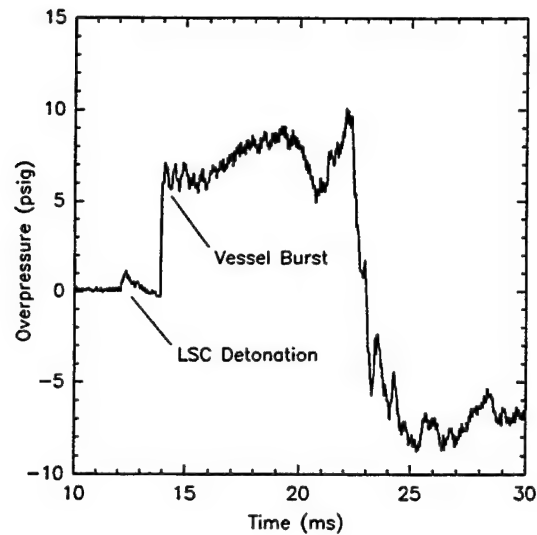
*Figure 5.9, Overpressure vs Time for
3250 psig Vessel P-1 at 90° and 15 ft*

5.4   Composite Spheres

Burst overpressures for the composite sphere vessels are shown in Figure 5.10 for vessel PC and Figure 5.11 for vessel 6A-2. The angle plots for both bursts show a high degree of symmetry about the origin (regression lines almost horizontal). Vessel PC was split in the horizontal plane with 1/2 of the vessel flying up and 1/2 driven to the ground. The reason for the dip in data at 10′ distance for vessel PC are unknown. The slanted regression lines for the vessel 6A-2 angle plot can be explained. This vessel was cantilever supported from the 90°-180° side with the split in the vertical plane along the 90° axis. The 90°-180° side fragment accelerated more slowly than the 0°-90° side because it carried the support structure with it, after breaking it off at the base. This shielded the 90°-180° side slightly and caused the highest burst pressures on the 0°-90° side.

5.5   Burst Pressure Variation

Vessel burst pressure was intentionally varied in four vessel bursts of TP #1: 1-1 through 1-4. These were all center-split 2′ diameter steel cylinders burst at a center line height of 3.5 feet. In addition vessel bursts P-1, P-2 and 2-1 were conducted at 3.5′ height of burst (HOB) and may be compared to TP #1 vessels. The comparison is made in Figure 5.12 where pressures at 10′ and 50′ nominal ranges are computed from the peak value with symmetric regression analyses using all the appropriate bursts and then are plotted in the figure. The dashed lines are a further regression of the 10′ and 50′ computed points.

54
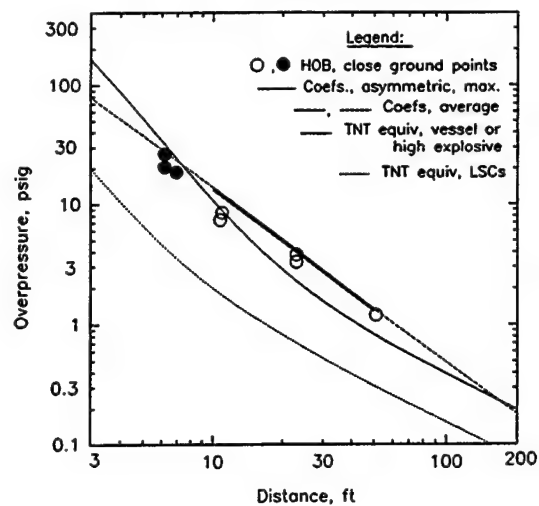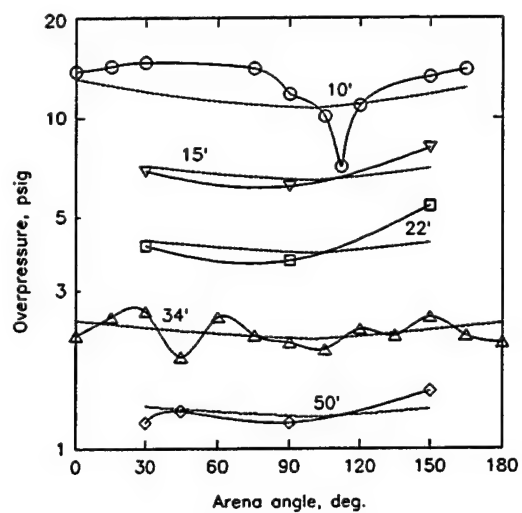
Figure 5.10, Burst Overpressures for Composite Sphere Vessel PC
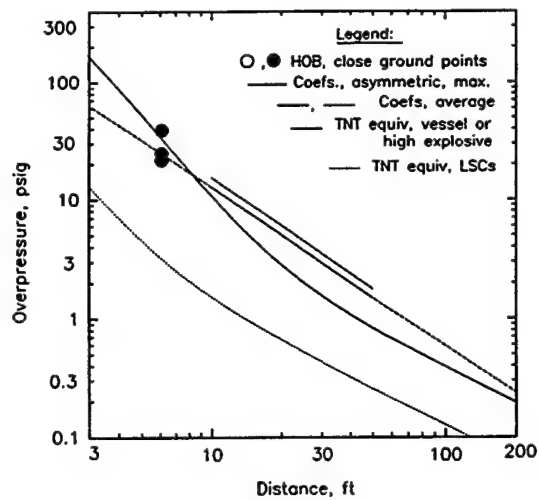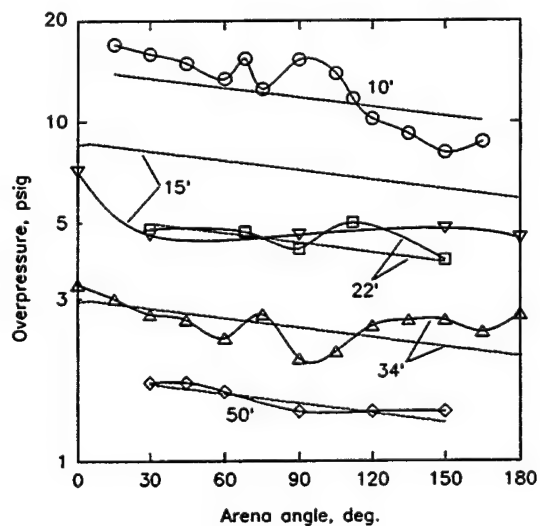
Figure 5.11, Burst Overpressures for Composite Sphere Vessel 6A-2

55

Figure 5.13 and Figure 5.14 each show a data point at a slant height of 3.5 feet (the vessel centerline height). These bursts, conducted at 1475 psig and 5425 psig, respectively, show an overpressure directly under the vessel that is quite high, higher than would be computed with the regression coefficients or by the methods of Baker[2] or with weak shock reflection coefficient. The pressure rise was gradual instead of a step rise as shown in Section 5.14. (A similar measurement was also attempted with the 3450 psig vessel 1-2 but no data were collected). This shows that the limited flow escape area under the vessel causes a pressure rise which would not be predicted.

One of the purposes of the pressure variation Test Plan, TP #1, was to evaluate real gas effects. However data scatter, see Figure 5.12, was too great for an evaluation. The overpressure caused by the vessel burst is comparable to its TNT equivalency overpressure at 50' distance. Using equation 4.4 with a 50' distance and a 17% energy decrease (from the value computed with 7125 psig and equation 4.1), the overpressure decrease is 11%. The overpressure at 50' distance from the three vessels burst at 3.5' HOB and 3250 to 3475 psig varied more than 11% and in a random fashion. The 7125 psig vessel burst overpressure decrease from the regression lines in Figure 5.12 must include real gas effects but of unknown magnitude.

5.6   Height of Burst Variation

Three steel vessels of 2 ft. diameter, center split, were burst at centerline heights of 3.5', 8.7' and 14'. (The 3.5' HOB was included in Section 5.5.) Preparations for these tests included special pressure probe mounts to obtain side on peak overpressure, prior to ground reflection if possible. These were used for the 8.7' and 14' HOB. The vessels were burst at the same nominal pressure, 3450 to 3475 psig. Data from both 8.7' and 14' HOB were combined and are shown in Table 5.3. Three probes were provided under the vessel (90° in the table) and three at HOB (75° in the table). The closest probes at locations both under the vessel and at height of burst broke off due to side loading and only one is included. A regression analysis for the pressure values yielded the coefficients $B_n = 4.36426$ and $B_1 = -.95341$.

Two regression analyses were performed for all the ground based data at all three HOBs: 1.) 1st order in $\log_e$ (distance) with no angle (or asymmetry) coefficient and 2.) 1st or 2nd order with an angle coefficient. Both are used for pressure versus distance plots but the asymmetric coefficients are used in this discussion. First order was used for 3.5' HOB but 2nd order for 8.7' and 14' HOB because a non-linearity with $\log_e$ of distance was anticipated from pre-test calculations. The data in Figure 5.15 resulted from division of the pressures versus distance at each height of burst by the probe pressure data. Coefficients were used to compute the pressure values. The results are plotted in the figure.
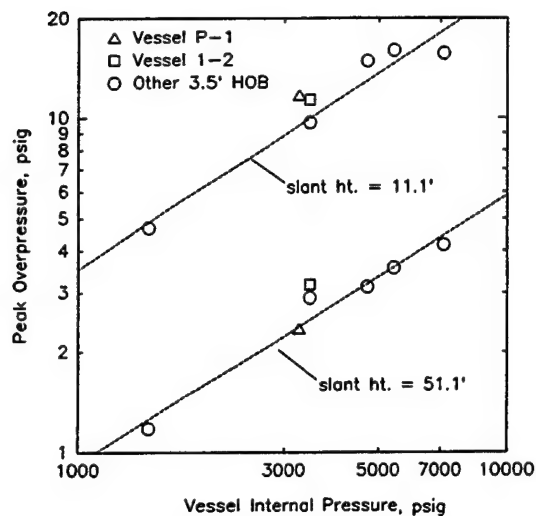
Figure 5.12, Overpressure Comparison from Mid-Length Split
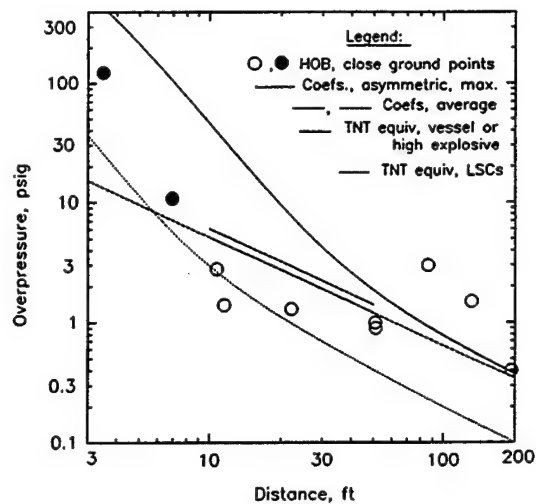
Figure 5.13, Vessel Burst 1-1 at 1475 psig
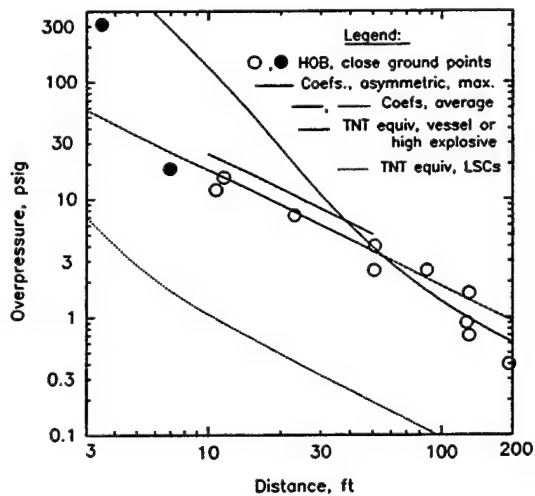
Figure 5.14, Vessel Burst 1-3 at 5425 psig
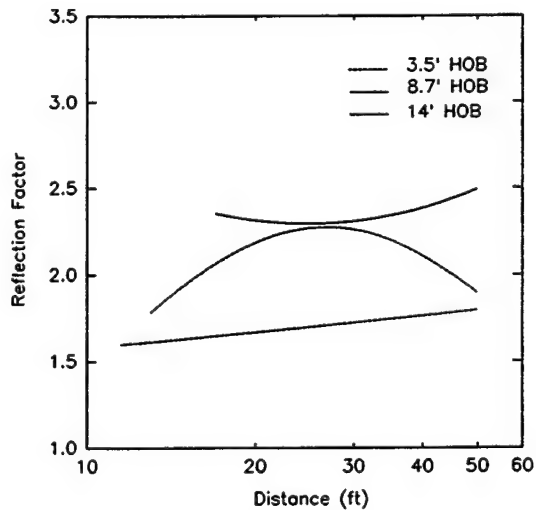
Figure 5.15, Reflection Factors for Vessel Burst

57

Table 5.3
Pressure Probe Measurements for Pressure Vessel Bursts

Vessel Burst	Angle, deg.	Distance, ft. Vessel Center to transducer	Pressure, psig	Impulse, psi-ms
2-2	90	1.83	56.3	Bad*
2-2	90	4.25	26.00	35.0
2-2	90	6.67	6.50	19.0
2-2	75	15.97	5.80	38.0
2-2	75	22.97	3.70	25.0
2-3	90	7.50	9.00	17.0
2-3	90	13.17	8.00	25.0
2-3	75	15.97	4.70	32.0
2-3	75	22.97	6.20	42.0

*Probe broke after initial response complete

Three high explosive (HE) shots of 4.5 lbs pentolite were also detonated as part of height of burst testing. The HE shots were sized to yield approximately the same overpressure at the 10' range as the pressure vessel burst. The HE shots for 8.7' and 14' were mounted from the vessel support and used the same 1' offset. No probes were used under the shots because gain changes were not desired and the pressure values would have been off scale. The probe data that were collected is shown in Table 5.4. The resulting coefficients from regression analyses are $B_n = 6.72653$ and $B_1 = -1.81578$.

Reflection factors were computed in a manner similar to that for the pressure vessels. Dividing by the overpressure for TNT equivalent of the pentolite charge should produce reflection factors that compare to the probe based factors. The comparison is poor. The factors and pressures used for computation are shown in Table 5.5. Coefficients for 14' HOB are valid for 17' distance (slant height to the ground) and beyond.

The poor comparison between probe-based and TNT equivalence based reflection factors for high explosive may be partly caused by the small number of pressure points which also appear to be low in pressure. This also makes the reflection factor for pressure vessels suspect. It can be shown however that quantitatively the reflection factors for pressure vessels do change with distance and pressure in a manner similar to that for high explosives but not necessarily the same magnitude. In Table 5.6 the computed pressures at 8.7' and 14' HOB for both pressure vessels and high explosives is divided by the 3.5' HOB values to show trends.

58

This test would have been much improved if many more height of burst pressure measurements were made. However these measurements are expensive to make for a one time application to the support structure required.

Table 5.4
Pressure Probe Measurements for High Explosive Detonations

HE shot	angle	Distance, to transducers, ft.	Pressure, psig	Impulse, psi-ms
HE 2-2	75°	10.97	10.60	13.0
HE 2-2	75°	15.97	5.30	13.0
HE 2-2	75°	22.97	2.60	9.0
HE 2-3	75°	15.97	5.80	13.0
HE 2-3	75°	22.97	3.00	6.0

Table 5.5
High Explosive Overpressures and Reflection Factors

Dist., ft.	side-on overpressure		HOB, ft	pressure @ ground	Reflection factor based on	
	probe, (coefs.) psig	TNT equiv.* (equa.), psig			probe	TNT equiv.
17	4.865	7.30	3.5	13.109	2.69	1.79
			8.7	16.256	3.34	2.23
			14	20.572	4.28	2.82
50	.686	1.26	3.5	2.021	2.95	1.60
			8.7	2.684	3.91	2.13
			14	3.754	5.47	2.98

* 5.7 lbs. used based on average probe pressure and Figure 2F of Swisdak[9].

59

Table 5.6
Reflection Factor Trends for High
Explosive (HE) and Pressure Vessels (PV)

Distance, ft.	Ratio of pressure to 3.5' HOB test			
	8.7' HOB		14' HOB	
	HE	PV	HE	PV
17'	1.24	1.34	1.57	1.51
50'	1.33	1.23	1.86	1.53

5.7 Split Location Variation with 2' Diameter Cylinders

Prior to Test Plan 5 several center split bursts were conducted. The purpose of TP#5 was to compare results using a different split location with the same 2 ft. diameter, 53 cubic feet steel cylinders. Locations used for the split were 3/4 - 1/4 length and full-endcap length. Two bursts were conducted for each location. For each burst the split location was placed at the arena origin with the vessel along the 0° - 180° axis and the short fragment end toward 0°.

The 3/4 - 1/4 bursts, vessels 5-1 and 5-2, provided a variation in fragment velocity but very little change in blast results from center split vessels. Blast strength was reduced slightly but symmetry was approximately the same as center split. Table D-4, Appendix D shows that all the center split vessels plus vessels 5-1 and 5-2 had an angle of blast symmetry within 15° of normal to the vessel axis. There was also a close correlation between bursts of vessels 5-1 and 5-2. Vessel 5-1 had a line of symmetry of 75° (using overpressure) with a deviation of 16.9% of reading whereas 5-2 symmetry angle was 80° with a deviation of 16.6%.

The endcap failures had a greater degree of asymmetry. Again both bursts correlated well with each other, vessel 5-3 having an angle of symmetry of 55° (using overpressure) with a deviation of 15.9% versus 50° and 15.8% for vessel 5-4. The impulse data also correlated well from burst of 5-3 to burst of 5-4. The impulse regression errors are high due to apparent data scatter, however the appearance of impulse versus arena angle graphs of bursts 5-3 and 5-4 are similar as shown in Figure 5.16 and 5.17.

A strong flow along the 0° array is expected from the endcap vessels and high impulse measurements and high pressure along 0° might also be expected. However the distribution of overpressure versus angle does not correlate with impulse versus angle for either endcap vessel 5-3 or 5-4. This can be seen by comparing the impulse versus angle for vessel 5-3, Figure 5.16, with the overpressure versus angle for vessel 5-3, Figure 5.18. The best fit angle using pressure is 55°; but the best fit angle using impulse appears to be 0°. This was confirmed with a temporary program change which picked the best fit angle due to impulse. The selected angle was 0° with coefficients C_n, C_1, C_2 of 6.41162, -.75905 and -.01516 respectively. However the deviation was only slightly improved, from 44.3% to 37.4%.
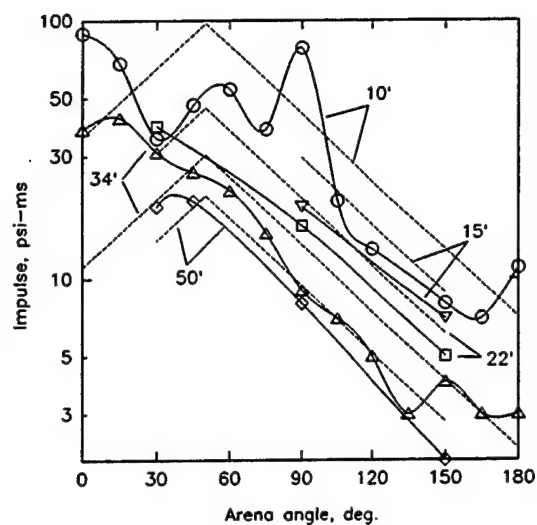
Figure 5.16, Impulse for Vessel Burst 5-3
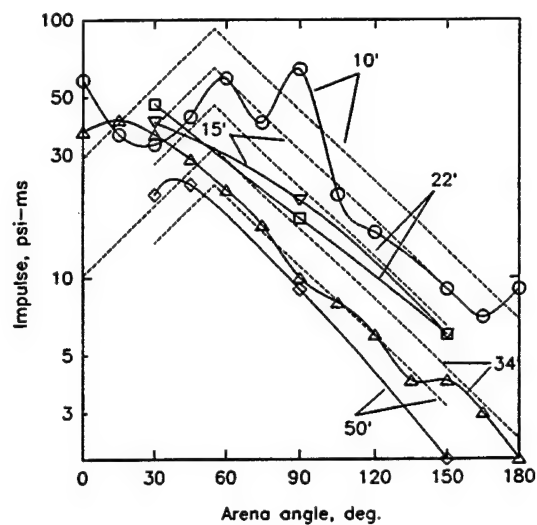
Figure 5.17, Impulse for Vessel Burst 5-4
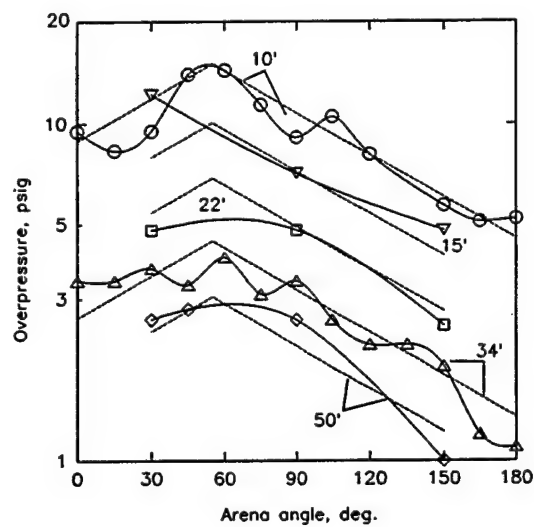
Figure 5.18, Overpressure for Vessel Burst 5-3

Figure 5.19 shows the overpressure and impulse versus time at 15° and 10 ft distance. The measurement dipped below atmospheric pressure and then experienced a second positive pressure phase. This occurred to several transducers in the vicinity. Most of the waveform included in the impulse occurred in about 7 milliseconds. But at 15° and 34 ft, Figure 5.20, the pressure gradually dropped to ambient over a period of about 21 milliseconds. This seems to explain high impulses occurring at not so high pressures.

A contour plot of all four of Test Plan 5 vessels is included as Figure 5.21. The contours are computed from the coefficients and indicate where in the field the maximum overpressure at 50' and the strongest blast angle would appear.

5.8   Far Field Overpressure Measurements

Far field measurements were made for all but the first (preliminary) and last (TP#6A) test series to see how far away window breakage (approximately 1/2 psig but is a function of thickness and size) would occur. These measurements were made at the typical HOB of 3.5 ft due to uneven terrain beyond the 50' arena. Measurements used side-on pressure probes typically used for measurements without a reflection factor. No HOB measurements were made for the last test series due to expected fragment flight toward the arena transducer field.

Far field can be loosely defined as the distance at which amplification due to ground reflection is reduced to a factor of approximately one. Baker[2] provides a reflection factor of 1.1 for $\overline{R} = 1$ and 1.0 for $\overline{R}$ greater than 1. With a reflection factor of 1, then measurements made on the ground or at HOB should be the same. The distance for $\overline{R} = 1$ can be found using equation 5.2 (Baker's $\overline{R} = 1$ equation solved for r).

$$r = \overline{R} \left[\frac{(\frac{P_1}{P_a}-1)(2V_i)}{\gamma_1-1} \right]^{\frac{1}{3}}$$

(eq. 5.2)

where: P_1 = initial vessel pressure

P_a = atmospheric pressure

2   is for burst at ground level

V_i = initial vessel volume

γ_1 = ratio of specific heats for the pressurant

$\overline{R}$ = a normalized distance

r = distance

62
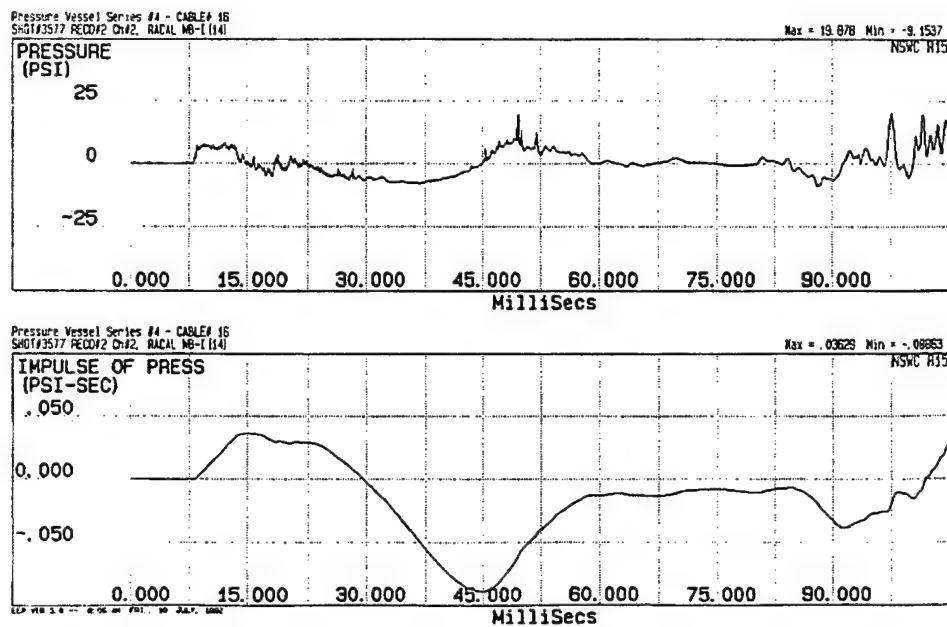
Figure 5.19, Pressure and Impulse versus Time for Vessel Burst 5-3 at 15° and 10 ft
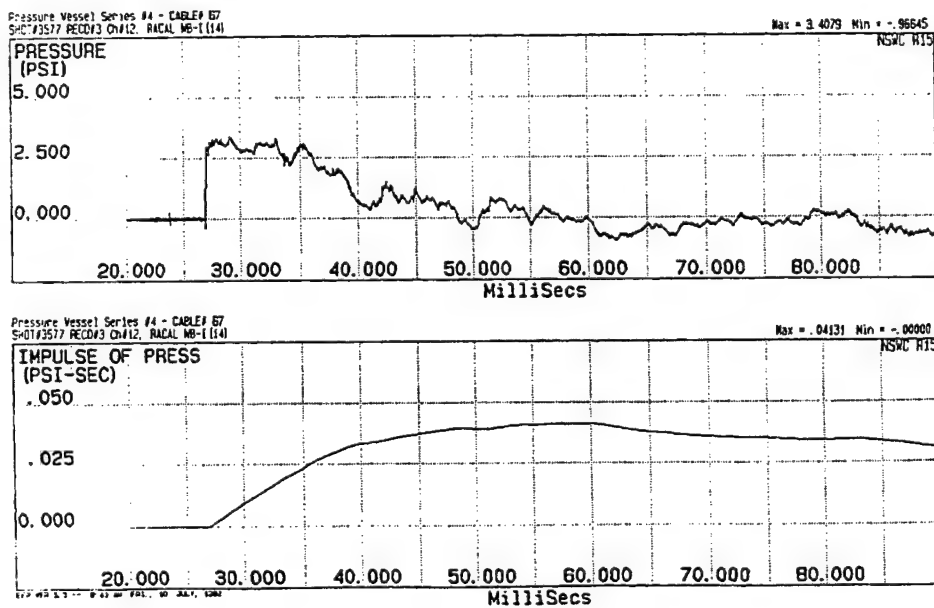
Figure 5.20, Pressure and Impulse versus Time for Vessel Burst 5-3 at 15° and 34 ft

63

Table 5.7
Distance to R bar = 1

Vessel		Distance, ft
volume, cubic feet	pressure, psig	
53	1475	27.8
53	7125	50.4
2.7	3975	15.4
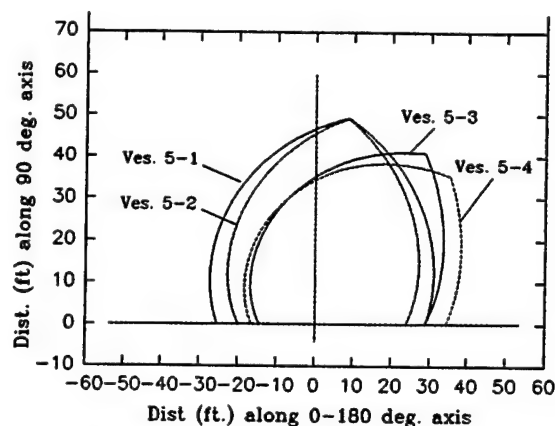
Figure 5.21, Lines of equal overpressure for 1/4 length and end cap vessels.

Table 5.7 provides distances for $\overline{R} = 1$ for vessels tested.

The trend for HOB overpressure and impulse is to be less than the average regression line at 10 ft. distance and increase as the far field is approached. At distances of 85 ft. to 200 ft. the TNT equivalent line for the vessel energy sometimes appears to be a better predictor than the average regression line as shown in Figure 5.22 for overpressure of vessel 5-1 and in Figure 5.23 for impulse from vessel 1-3. However, the overpressure for the composite spheres is above the TNT equivalence line for much of the distance. See Figure 5.10 for vessel PC and Appendix E, Figure E24 for vessel 6A-2. Reflection does not account for the higher pressures since the reflection factor should be approximately one for 15 to 50 feet. (See also Section 5.15).

5.9   Diameter Variation with Center Split

Three 2′ diameter center split vessels were burst at a pressure range of 3250 to 3450 psig at 3.5′ HOB: P-1, 1-2 and 2-1. P-1 will be used to compare to the center split 3′ diameter vessel, 6A-3, because its burst pressure of 3250 most closely matches the 6A-3 burst pressure of 3300 psig. Based on the inner diameters, the 3′ vessel has 2.1 times the flow area of the 2′ vessel and was expected to develop higher blast overpressures. Since impulse should be a function of total energy rather than release rate, a higher impulse for the 3′ diameter vessel was not expected. Due to scatter it is difficult to compare overpressures in Figures 5.2 and 5.24 or impulses in Figures 5.3 and 5.25. Using symmetric coefficients the overpressure and impulse for both vessels is compared at distances of 10' and 50' in Table 5.8. Based on the table it is unclear if expectations were realized.

Table 5.8
Comparison of Vessels P-1 and 6A-3

Distance, ft.	Pressure, psig		Impulse, psi-ms	
	P-1	6A-3	P-1	6A-3
10'	13.079	14.082	50.6	37.2
50'	3.22	2.39	19.45	19.52

64
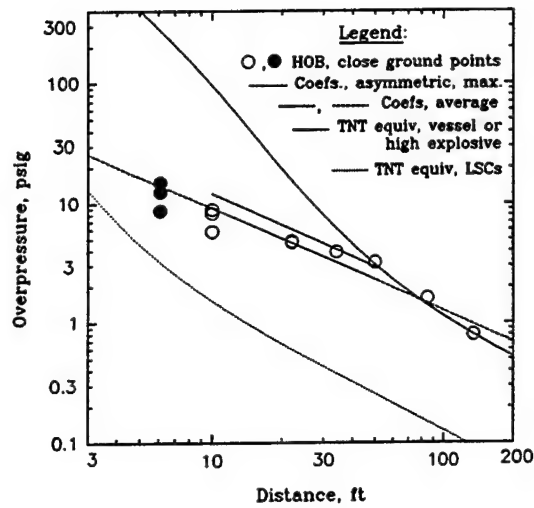
Figure 5.22, Overpressure from Vessel 5-1
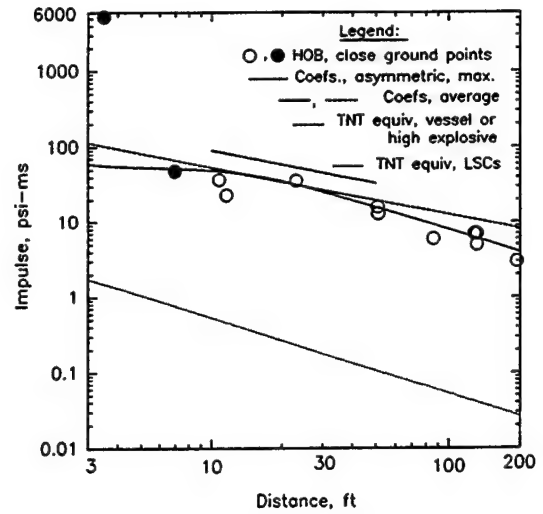
Figure 5.23, Impulse from Vessel 1-3
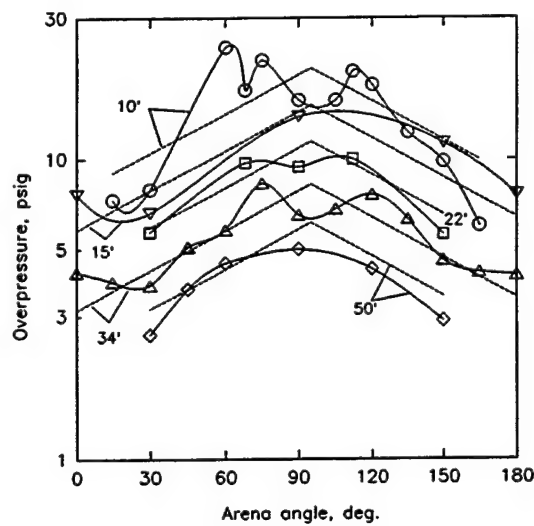
Figure 5.24, Overpressure from Vessel 6A-3
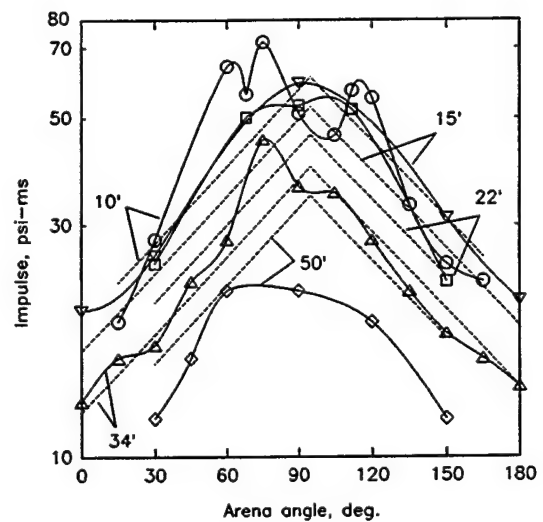
Figure 5.25, Impulse from Vessel 6A-3

65

5.10 Dual versus Multi-fragment in 2′ Cylinders

The multi-fragment vessel was expected to produce a high blast overpressure due to the sudden release of energy, however the distribution of overpressure with respect to geometry was uncertain. For center split vessels the distance to the vessel from the semi-circular field of overpressure transducers may be taken as the distance to the split. An overpressure plot with symmetry about the origin might be expected. However the exhausts from each section impinge at the center and a strong blast field normal (or nearly normal) to the vessel axis is produced. Typical plots are shown in Figure 5.26. The closest distance to choose for the multi-fragment burst, with the sudden disintegration of the whole vessel, is not so clear. Figure 5.26 indicates that the end points of the 10 ft and 15 ft semicircles experienced high pressures due to proximity to the ends of the vessel. This trend is even displayed to a lesser extent at the 34 ft distance. There is also a tendency for a strong blast field normal to the vessel centerline, showing that the confined jet impingement as in the center-split is not necessary to cause that type of asymmetry. A special regression analysis of test data for a hazard assessment workbook[49] is repeated as Section 5.10.1.

Overpressures and impulses were also considerable higher for the 3500 psi multi-fragment vessel than any other due to the more sudden release of energy. This is even true when considering the 7125 psi center split vessel.

5.10.1 Special Regression Analysis, Vessel 6A-4

Figure 5.26 contains an angle plot of overpressure from the multi-fragment vessel, 6A-4. The distances are measured radially from the center of the arena, and center of the vessel. (The distances are all nominal and refer to distances along the ground. Data reduction used slant height distances.) Data at 10′, 15°; 15′, 0° and 15′, 180° (points labeled 1, 2 and 3) showed a trend in opposition to the balance of the arena which showed high overpressures near 90° and low near 0° and 180°. For this reason the distance (slant height) for all the points was computed at 90° to the vessel axis. The data are replotted in Figure 5.27.

In Figure 5.27 the three points are again labeled and it is seen that these points are not high but are either average (point 1) or quite low (points 2 and 3) compared to the regression line, "average 90° distance". Thus it is seen that the overpressure is high along a line normal to the center of the vessel and is low at more remote distances from the normal line. (See also Appendix F.)

Four regression lines are shown in Figure 5.27. The two dashed lines, " maximum radial distance" and "average radial distance" are the average and maximum pressure from the type of data reduction described in Section 5.1, with radial distances. The line "average 90° distance" results from a regression of the Figure 5.27 data with the solid symbols excluded. These were beyond the vessel length and appeared to be sufficiently low for both pressure and impulse to discard. The "maximum 90° distance" line results from a regression using points at or above "average 90° distance" line and replaces "maximum radial distance". The effect of the new regression lines is to lower the "measured" pressure for vessel 6A-4 for close distances.

66
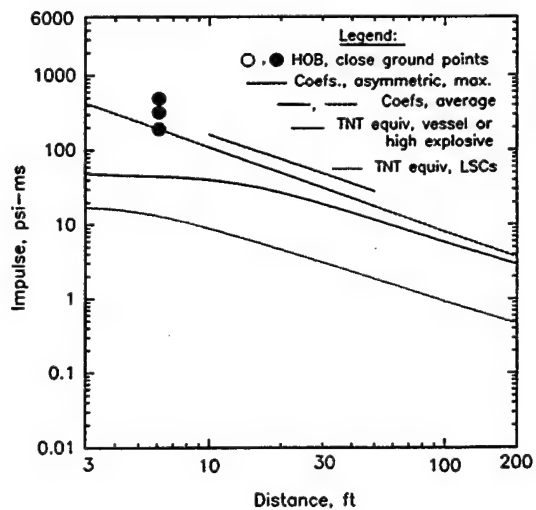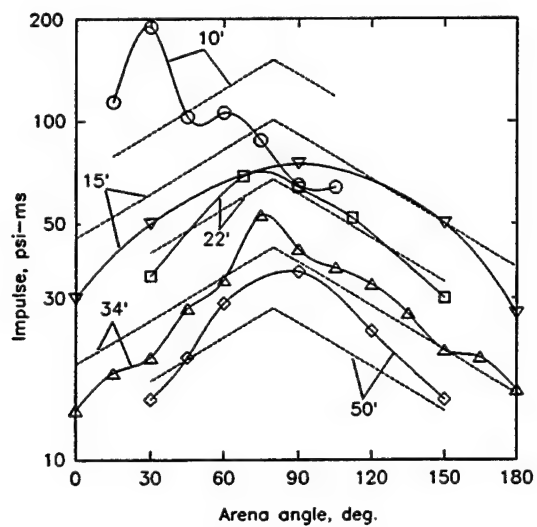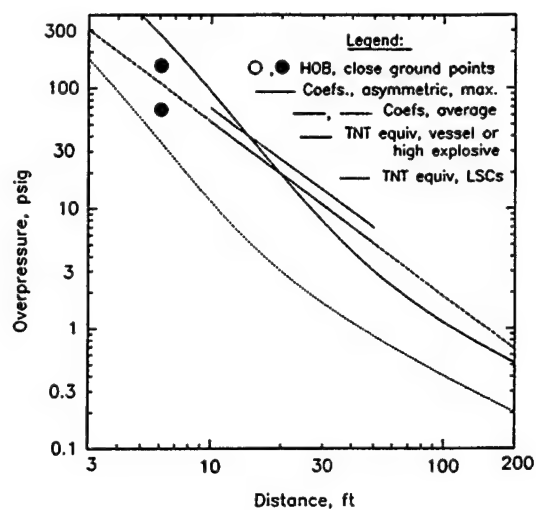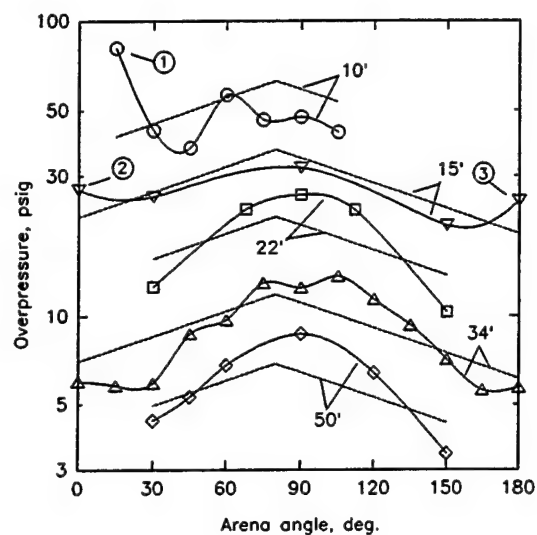
Figure 5.26, Overpressure (top) and Impulse (bottom) from Vessel Burst 6A-4
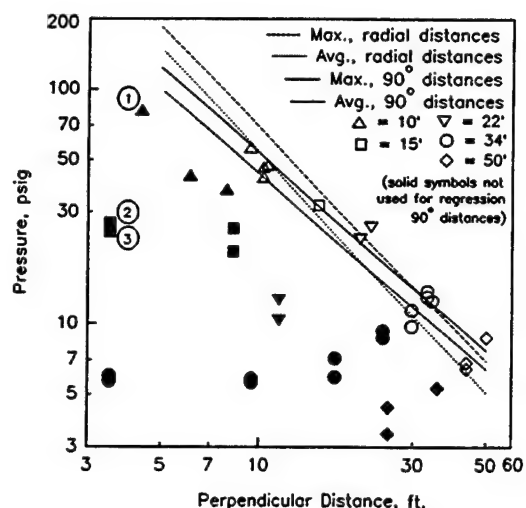
Figure 5.27, Overpressure of Vessel 6A-4
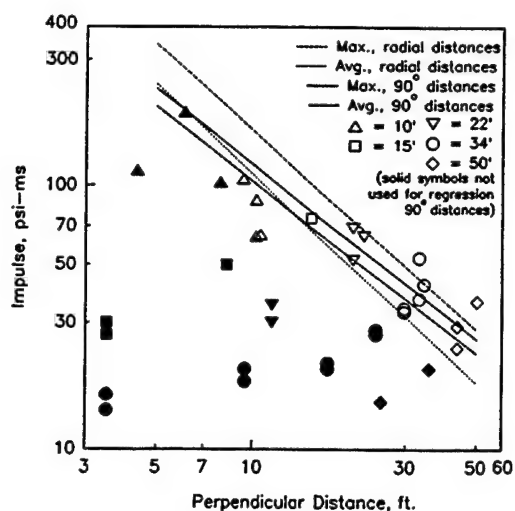
Figure 5.28, Impulse of Vessel 6A-4

The overall appearance of the impulse data is very similar to the pressure data and is shown in Figure 5.28. Coefficients based on the special regression analyses are shown on the last line of Tables D-2 through D-5 of Appendix D.

5.11 Dual versus Multi-fragment in 3' Cylinders

Vessel 6A-1 was expected to burst along horizontal grooves as well as at the two end cap grooves. This did not happen and a double end cap failure resulted with the center section remaining in place (shifted a foot).

The double end cap failure results in twice the pressurant exhaust area than the center split and can be expected to result in higher overpressures. This did occur as shown in Figure 5.24 versus Figure 5.29. In Figure 5.29 three peaks can be seen in the overpressure pattern at 10 ft distance. The side peaks represent the outrush of gas at each end and the center peak is evidently due to the intersection of the flow from each end. The high pressure tendency at the center of the field remains out to the 50' distance. This burst also exhibited a greater impulse field than the center split 3' diameter or the 2' diameter center split vessels at any pressure range.

5.12 Bursts compared to TNT equivalence

TNT Equivalence lines in the pressure (or impulse) versus distance plots were identified in Section 5.1. The TNT equivalence for the upper line, vessel TNT equivalence, was computed using the isentropic expansion energy of the vessel, with a factor of 1.545×10^6 applied to convert from foot pounds of energy to lbs TNT. The conversion factor is within a range of 1.4 to 1.6 presented by various authors[1]. The factor selected is from Kinney and Graham[10]. No corrections are made for energy expended in propelling fragments rather than creating a blast

wave. Once the TNT equivalence is known, the overpressure (or impulse) is computed using equation 4.4 (or 4.5 for impulse) from Kinney and Graham[10]. The overpressure (or impulse) equations are for side-on overpressures and do not consider reflection (amplification) factors other than 1.0. No corrections are applied for ground reflection factors. Some experimentation was conducted, Section 5.6, but insufficient data is available for quantifying vessel burst reflection factors.

A constant TNT equivalence is used in the high explosive plots and was taken from the mid range (34 ft) distance overpressure using Swisdak's[9] report. The report shows that the conversion factor for pounds of an arbitrary explosive to pounds of TNT is not a constant.
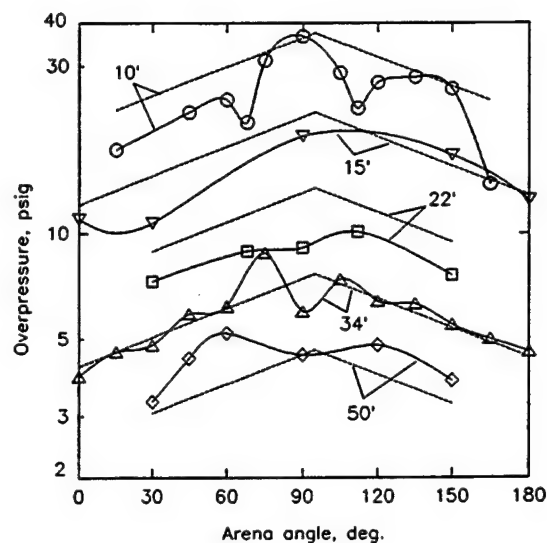
Figure 5.29, Overpressure from Vessel 6A-1

Most vessel bursts used a linear shaped charge, typically in a machined groove, to initiate a vessel burst. Overpressures due to LSCs detonated on a steel vessel surface are presented in Section 5.3. These are not used for the LSC overpressure (or impulse) versus distance lines in the plots. Rather the conversion factor for RDX to TNT was obtained from Kinney and Graham[10] and the values for the lines determined as discussed above. Neither the TNT equivalent overpressure for the initiating LSC from reference 10 nor the overpressure from Figure 5.8 is added to the vessel TNT equivalence to compare to actual data in the data overpressure versus distance plots. This might be convenient to have, but how and whether to add it is unclear. Timing eliminates some LSCs from consideration. For others the rated conversion to TNT from reference 10 may not be a constant but may vary with overpressure per reference 9. Additionally reflection factor is not a constant but varies with distance.

From Table 5.2, the contribution of LSC overpressure for vessel burst overpressure can probably be ignored for the following bursts: P-1, P-2, 1-1, 1-2, 1-3, 2-1, 2-1, 2-3, 5-1, 6A-3 and possibly 5-3.

5.13   All 3.5 ft HOB bursts compared

It is convenient to borrow the Hopkinson or "cube root scaling" law for high explosives[36] and apply it to vessel bursts. This requires dividing the actual distance by the cube root of the vessel TNT equivalence. In this way large and small vessel bursts (or explosions) may be compared to each other and to the overpressure (which is not scaled) for one pound TNT. Similarly if the impulse is divided by the cube root of the vessel TNT equivalence, then the impulse for large and small vessel bursts may be compared.

69
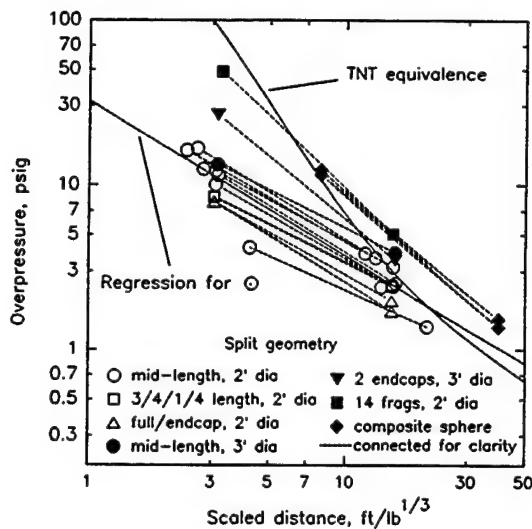
Figure 5.30, Overpressure Comparison at 10', 50' for all 3.5' HOB Bursts
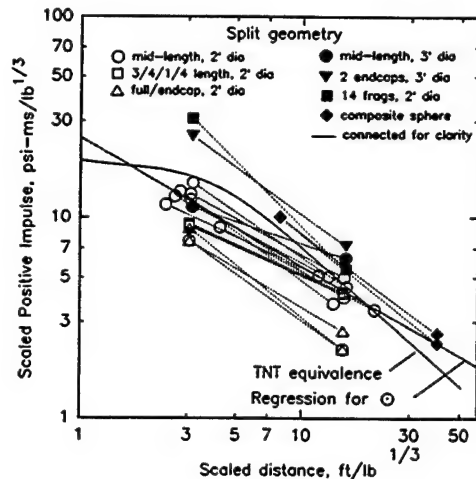
Figure 5.31, Impulse Comparison at 10', 50' for all 3.5' HOB bursts

Figure 5.30 is a plot of peak overpressure versus scaled distance for all vessels burst at a centerline height of 3.5 ft. All the points are evaluations from coefficients (no angle term) at either 10 ft or 50 ft distance and are connected by a dashed line. The distances represent distance extremes for the regression analysis (actually 10.6 or 11.5 to 50.1 or 51.1 when corrections for offset and slant height are applied). The open circles are all replotted from Figure 5.12, of overpressure versus vessel pressure (i.e., coefficients used to compute overpressure at 10' and 50' distances). A regression line is plotted for the open circled points (cylinders burst at mid-length). The two points considerably below the line are for vessel 1-1. No explanation for the low pressures can be offered. The filled points, all at or above the regression line, have a vessel and/or burst geometry which permits a faster venting of the pressurized gas. The open squares and triangles have a burst geometry which increases the exhaust time.

Also plotted in Figure 5.30 is an equation showing the overpressure versus scaled distance for the TNT equivalence of the vessel (or for overpressure versus distance for a one pound TNT explosion). It is apparent that increasing the exhaust rate increases the overpressure towards the TNT equivalence line. Some of the points appear to be greater than the TNT equivalence pressure. This can be explained (except for the spheres at 15' and 50') by the fact that the TNT pressures are incident pressures, not amplified by ground reflections, whereas the vessel overpressures are reflected pressures. See height of burst variation, Section 5.6.

Regression coefficients were also obtained for $\log_e$ (impulse) versus $\log_e$ (distance) with no angle term. As before the coefficients were used to compute the impulse at the 10' and 50' range. The distances were then converted to scaled distance by dividing by the TNT equivalence of the vessel energy. The data is plotted in Figure 5.31 where again the points are connected by

70

a dashed line and a regression line is found for the mid-length split vessels with 2′ diameter. The TNT equivalence impulse equation is also plotted. The ordinates are now scaled values as are the abscissas.

The measured impulse values tend to be close to the TNT equivalence for any distance. The fact that some points appear to be greater than TNT equivalence can again be explained by the fact that the TNT equivalence uses incident overpressure and the measured values are reflected.

5.14   Pressure versus Time Waveform

Ideal high explosive waveform characteristics include a sharp rise followed by an exponential decay. Two of the traces in Figure 5.32 are similar to high explosive response. All recordings shown were made from transducers located in the same general location: at a range of 10 feet to 15 feet and within 30° of normal to center of the long vessel axis.

Figure 5.32 presents data from vessel bursts P-1, 6A-2 and 6A-4. P-1 is a cylinder burst about its mid-length. The square wave (also shown in Figure 5.9 in Section 5.3) was seen at distances of 22 feet and closer. At greater distances the waveform transitioned to an exponential decay. The pre-burst pressure rise is the LSC detonation. Vessel 6A-2 is the latter composite sphere. The equatorial split presented a large ratio of exhaust area to vessel volume compared to the cylinder. Additionally the lightweight fragments accelerate rapidly and minimally reduce the vent area at the beginning of launch. The sphere waveform has the sharp peak, semi-exponential decay and second shock similar to a high explosive blast. Vessel 6A-4 was burst

Figure 5.32, Vessel Burst Overpressure Time Response

into 14 fragments, providing a large vent area for a cylindrical burst. The waveform has a sharp peak, a generally, although somewhat ragged, exponential decay and second shock. The overpressure measured was greater than with any other cylindrical burst.

Figure 5.33 shows the 13 millisecond delay between LSC detonation and burst of vessel 5-1 as mentioned in Section 3.1.1.

Figures 5.34 and 5.35 show the pressure on the ground directly under the burst of vessels 1-1 and 1-3 as mentioned in Section 5.5. In each case the transducer experienced a gradual pressure rise rather than a step rise as expected for a shock passing. This characteristic was not observed anywhere else in the arena.

71
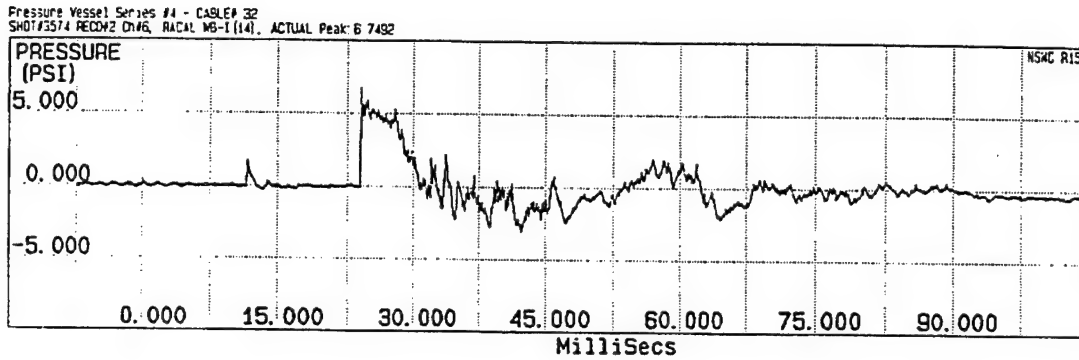
Figure 5.33, Burst Delayed 13 ms after LSC Detonation, Vessel 5-1
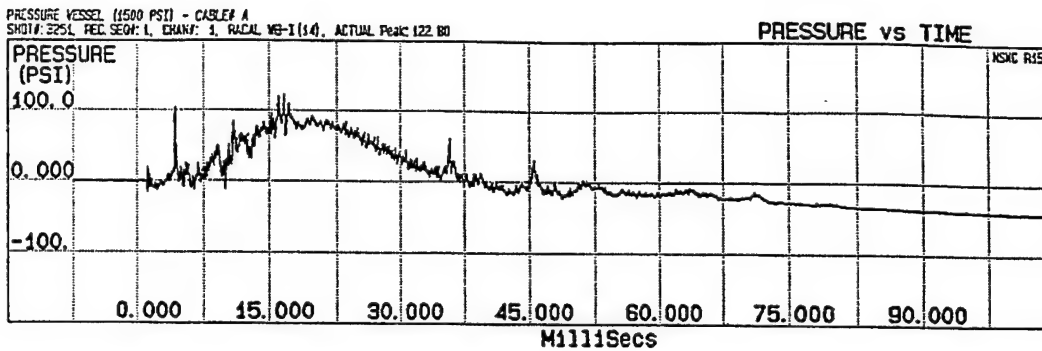
Figure 5.34, Pressure Measured on the Ground Under Vessel 1-1
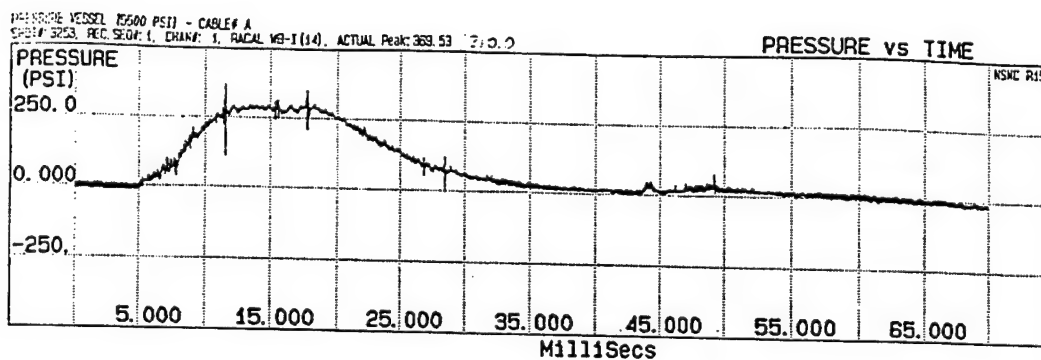
Figure 5.35, Pressure Measured on the Ground Under Vessel 1-3

72
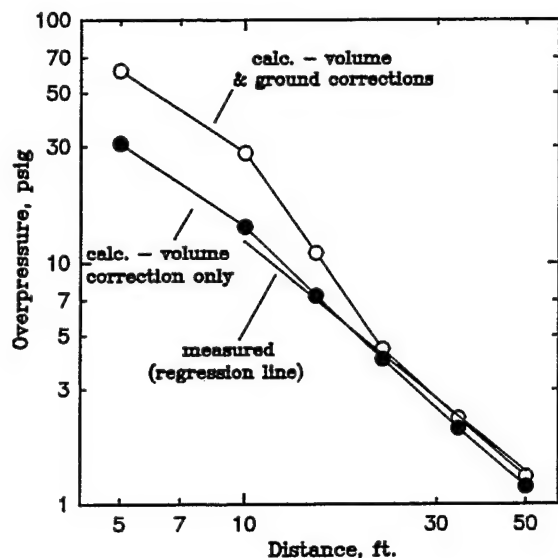
Figure 5.36
Comparison of Composite Sphere Overpressures
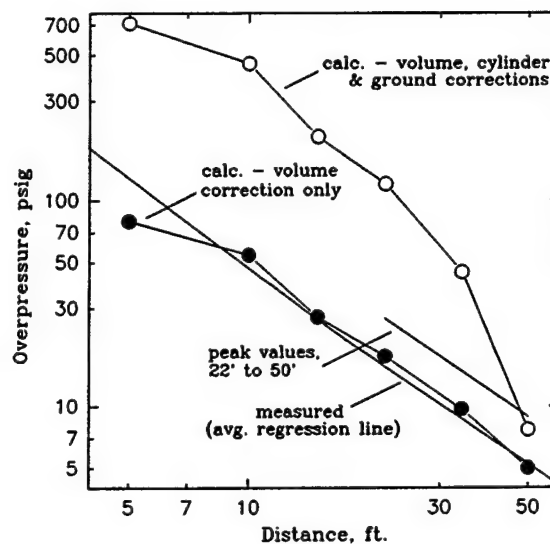
Figure 5.37
Comparison of Multi-fragment Cylinder Overpressures

5.15   Selected Data Compared to Literature

Curves published by Baker[2] assume sudden vessel wall disappearance. Two types of bursts conducted under the Burst Study approach that assumption and can be compared. One is the composite spheres which have a large vent area to volume ratio and fragments which rapidly accelerate to high velocity. The other is the multi-fragment vessel that, with 14 fragments, also has a very large vent area to volume ratio. Figure 5.36 presents data for the initial composite sphere burst, vessel PC. The measured data was recorded at ground level and hence is reflected data. The calculated line using "volume correction" uses a volume of twice actual as a partial reflection correction. This decreases the distance by 20% and increases the pressure by about 40% in the near field and 90% in the far field. The curve having additional ground corrections includes a factor of 2 times the "volume" curve at near field and 1.1 at far field. (Calculated data procedure includes picking points from curves of normalized values, hence the lack of smooth curves.)

Figure 5.37 presents data for cylinder burst 6A-4. This cylinder broke into 14 fragments of approximately equal weight, which also approximates the disappearing wall assumption. The figure presents curves for measured, calculated with volume correction and a curve which contains both cylinder correction factors and ground reflection factors. The cylinder correction factors (which Baker et al stated are "very crude") varied from 4.5 in the near field to 1.4 in the far field. The reflection correction factors varied from 2.0 in the near field to 1.1 in the far field.

It is doubtful that much greater overpressures from these two vessels would ever occur accidentally since this would require a greater number of fragments with attendant faster venting. The corrections to the cylinder calculations which are required by the reference appear to be excessive except at the 50 ft. distance.

73

6.0 FRAGMENT MODELING AND TEST RESULTS

The explosive failure of a pressure vessel not only may generate a blast wave but may also propel fragments. The fragments may be massive and the velocities quite high, presenting a significant hazard. The lethality and damage potential of a fragment propelled by a bursting pressure vessel depends on the impact velocity and mass of the fragment. Both the impact velocity and distance a fragment may travel depend on the initial velocity. The Burst Test Study used a two pronged approach to the study of fragments. The initial velocity of fragments was measured and a computer program for the prediction of initial velocities was rewritten and improved. Maximum distance travelled by fragments was also measured and for initial tests the ricochet points were also obtained.

6.1 Measurement of Initial Velocities

This section is concerned with fragment initial velocity. Initial velocity will mean the maximum velocity the fragment achieves after vessel breakup prior to a decay in velocity due to aerodynamic drag. During the acceleration phase the fragment is acted upon by the expanding containment gas and by drag. Initial velocity is the resulting velocity at the end of that phase. Drag can almost be ignored in the calculation of initial velocity of fragments from high pressure vessels, but greater accuracy is obtained by considering drag.

6.1.1 Methods

Two methods were used to capture fragment displacement versus time. The primary method was high speed photography or in some instances high speed video or both. For instance only high speed video was available for the burst of vessel P-2 since the time of burst was unknown: the shaped charge was detonated the day before in a failed test. The running time of the high speed cameras is dependent on the frame speed in use but is typically less than 15 seconds. The second method was the use of contact wires. Sometimes the wires were contact making and sometimes contact breaking.

High speed photography was the preferred method and was useable for all of the fragments for most of the tests. It has the disadvantage that the fragment may be obscured from the camera for a period of time by the cloud of dust and condensation caused by the vessel burst. For most fragments this was not a problem, the fragments would be visible for a sufficient period of time to track them for several distance measurements. However the endcaps from vessels 5-3 and 5-4 were never seen with the high speed cameras. The field of view was limited to get adequate resolution for a high velocity fragment. They were seen with standard video cameras having a wider field of view, however the camera angles were not good and the frame rate was slow.

Contact wires were used for backup and as an attempt to obtain acceleration data immediately after rupture when the vessel may be obscured by the dust/condensation cloud. Contact break wires were initially used. These are preferred by the NSWC instrument personnel

when brittle wires, such as pencil leads that break cleanly, can be used. However since the exact fragment launch direction was unknown, long wires were used that would be broken by the leading surface of the fragment, hopefully with the wire framework undamaged. This caused some concern about accuracy because the copper wires in use (Test Plans 1 and 2) could stretch before breaking. Additionally the possibility existed for shock loading to deflect the wires and effect the data.

For vessel PC a new contact wire arrangement was used that utilized pretensioned piano wire in a more rigid frame and a change of the signal sense from contact breaking to contact making. Crossing grids of wires one inch apart was used to ensure continuity in the face of high acceleration loads (a common wire was previously attached to the vessel) and to allow for a slightly angled fragment motion. Six sets of grids were used at one foot intervals. For the next vessel test, 5-3, the makewire contact sensing was changed to breakwire due to readability problems and the frame was turned on its side . Damage during testing and modifications to the stand are discussed in Section 3.7.

Distances to contact wires for three vessels are shown in Table 6.1. For these vessels; PC, 5-3 and 5-4; the fragment velocities are listed in Table 6.2 using the wire data rather than photography data.

Table 6.1
Distances to wires, ft.

Wire #	Vessel		
	PC[1]	5-3[2]	5-4[2]
1	.68	.69	.70
2	1.68	2.07	1.65
3	2.68	3.40	2.66
4	3.68	5.10	3.64
5	4.68	---	4.63
6	5.68	---	5.64

[1]Makewire
[2]Breakwire
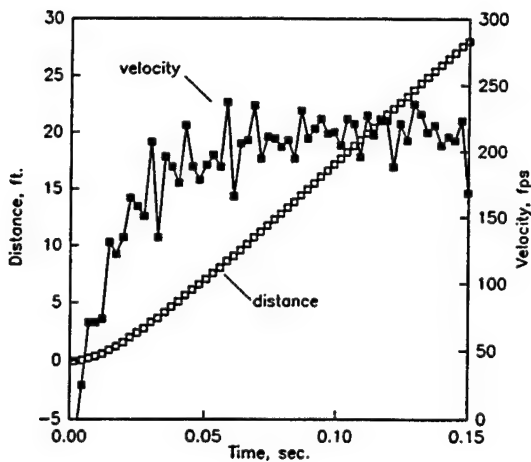
Figure 6.1, Typical Type of
Distance/Velocity Plots from NSWC
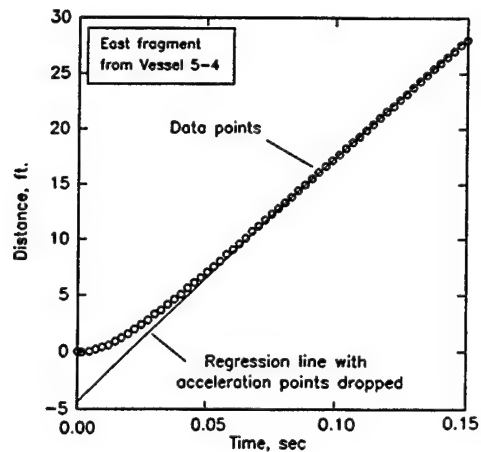
Figure 6.2, Regression Line Omitting
Acceleration Distance Points

6.1.2   Data Reduction

Typically each camera was placed normal to the expected fragment track and aimed at a location where the fragment would be after motion commenced. Frequently the unburst vessel was at the edge of the field of view. A series of 2" by 4" lumber placed slightly off the fragment track provided data for a length calibration and for angle corrections when the fragment was not exactly normal to the camera view. High speed motion pictures were digitized to distance versus time data by NSWC using a special projection/digitizing table and computer system. Light bursts on the edge of the film provided the actual frame rate which was used in place of the nominal value. Spread-sheet software was then used for calculations.

Data furnished by NSWC included point to point velocity versus time as well as distance versus time. Figure 6.1, plotted by GP, shows the type of typical velocity data and plots furnished by NSWC.

GP then used the distance versus time data and a computer program to obtain the velocity. The program provided a slope-intercept regression analysis, a slope printout from the intercept to each point and the option to exclude points from the regression analysis. The data printout made it obvious which points were part of the initial acceleration and which points were part of the deceleration due to drag. By discarding only these points an accurate and maximum velocity was obtained. Usually two to four trips through the routine yielded a final value. Figure 6.2 is a plot of the data and the regression line for the east fragment from vessel 5-4.

76

6.1.3 Accuracy of photo-based data

Accuracy in obtaining velocities from high speed photography probably varied with each vessel burst. The accuracy achieved with vessel 5-4 was examined and is probably typical for fragments that travelled in a predictable direction, normal to the camera field of view as noted in Table 6.2. Figure 6.1 shows that some data scatter exists, resulting from inaccuracies in reading the vessel position. However 65 points were used in the regression analysis for slope (velocity) and intercept, providing an error variance for computed distance of a small fraction of an inch. There is still a potential calibration error of scale distance versus actual distance. This calibration scale was established using 2" X 4" lumber at known distances that could be accurately measured, and this error is also expected to be small, less than 0.5%

In spite of the inherent high accuracy to be expected from photo data recorded in the manner described, certain things can affect the data and render a result outside of expectations. These cases are:

- Due to a high pressure area between supports, fragments of vessel 6A-3 may have been pivoting during acceleration, resulting in a lower actual velocity than might otherwise have been recorded.

- One sidewall fragment from vessel burst 6A-4 was tracked at 500 ft/second. Others that were tracked (over half of the 12 could not be seen) at considerably lower velocities used cameras with less than optimum angles.

- The lightweight spherical vessels PC and 6A-2 were composite overwrapped pressure vessels having stainless steel liners and Kevlar overwrap. It is believed that the overwrap was tracked for vessel fragments PC top and 6A-2 west, resulting in a lower velocity than would otherwise have been measured. These two fragments will be discussed in Section 6.1.4.

6.1.4 Lightweight sphere fragment velocities

Two lightweight spherical vessels were burst, resulting in very high fragment velocities. Considering both vessel bursts together, the correct velocity for fragments from both vessels may be between 978 fps and 1252 fps. The uncertainty lies in the wire framework used for vessel PC and in the condition of overwrap shedding for both vessels. The Kevlar/epoxy overwrap from these vessels appeared to be shedding at the start of photo tracking. The overwrap had been painted white and being light in color and having the tendency to fluff out, it was not only easier than the stainless steel liner to track but it also decelerated faster. This can be seen in the high speed film for vessel PC. It is believed to have also occurred for fragment 6A-2 west since the liner was found at a greater distance than the overwrap.

77

The velocity of the top fragment of vessel PC was measured using both contact times through a wire grid and photo tracking at the exit to the wire framework. The data from both types of measurements is plotted in Figure 6.3. The photo data shows a lower velocity than the wire data and shows a much more rapid deceleration due to drag than would be computed for the intact vessel half. The wire data shows no deceleration within the wire grid framework, however there might have been an effect on the maximum velocity attained, during the acceleration phase.

The contact wire data for vessel PC appeared to be very erratic. Negative voltages were measured where none were applied (a possible capacitance effect as the shock passed
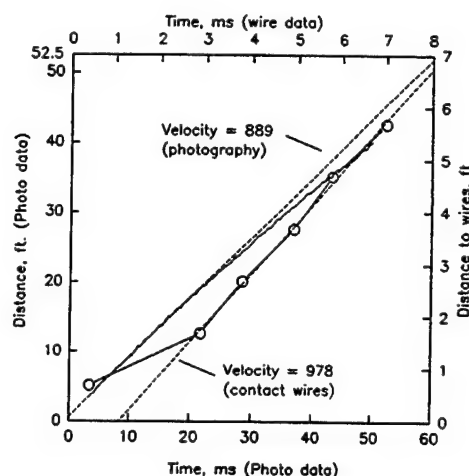
Figure 6.3, Contact Wire and Photo-Based Velocity Data for Vessel PC

through the framework) and these were seen prior to fragment contact. However, by taking the initial sharp positive break, as shown in Figures 6.4a and 6.4b, consistent data was achieved.

The west fragment from vessel 6A-2 showed an initial velocity, for three points, of 1252 fps. The velocity then dropped suddenly to 889 fps, Figure 6.5, and decayed rapidly to 705 fps at .090 seconds. The initial three points tracked may be the correct value. The velocity is at least 889 fps and may be as high as 1252 fps. The east fragment carried additional weight of part of the vessel support and had a lower velocity.

6.1.5   Endcap velocities of vessels 5-3 and 5-4

The velocities for the west (end cap) fragments of vessel bursts 5-3 and 5-4 were measured with contact wire instrumentation that was itself being pushed by the blast and must be considered minimum velocities. The velocities may actually be fairly accurate based on repeatability, differences in acceleration capability of wire frame versus end cap and direction of initial exhaust during fragment acceleration. Planned three dimensional hydrocode modeling will include this case as a check. The displacement versus time data for both of these fragments is plotted in Figure 6.6.

78
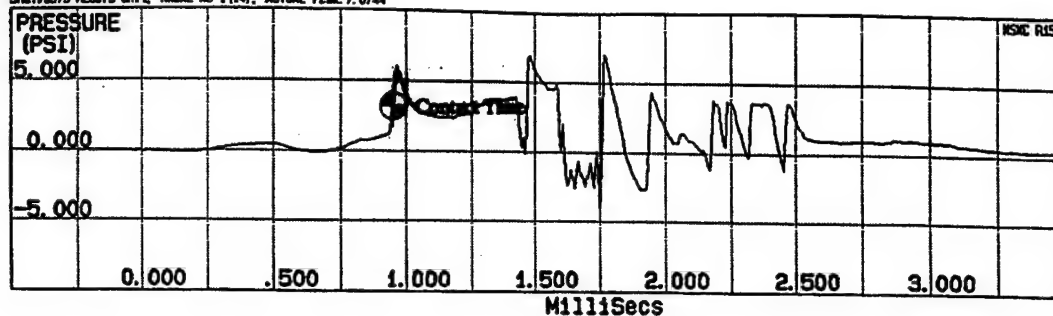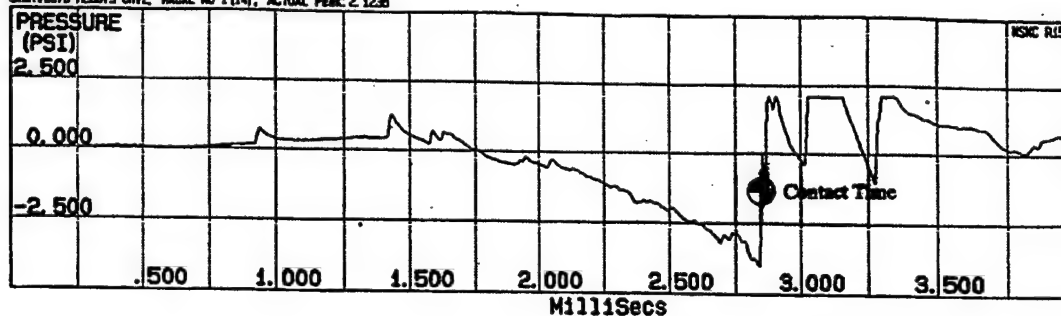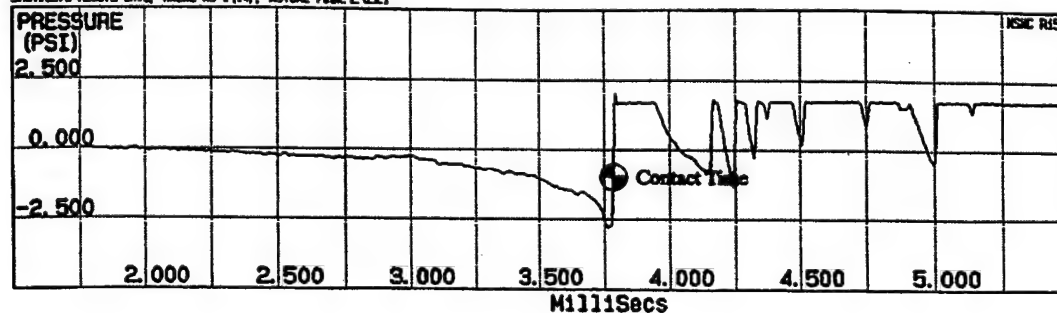
Figure 6.4a Contact Times for Vessel PC, Wires 1 through 3
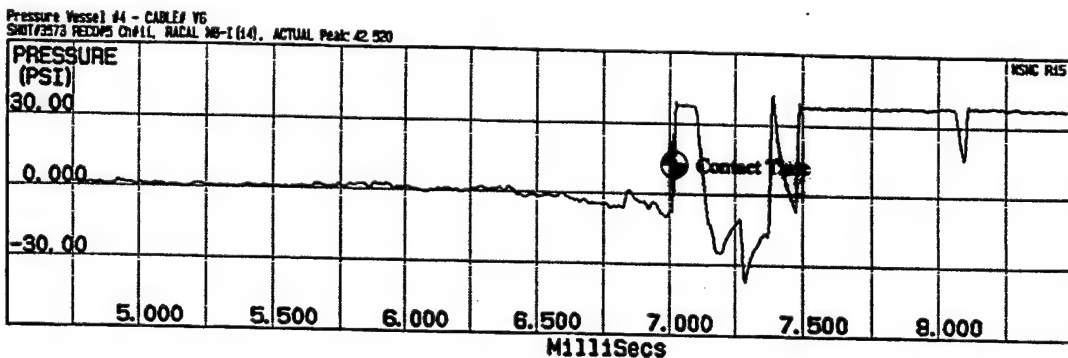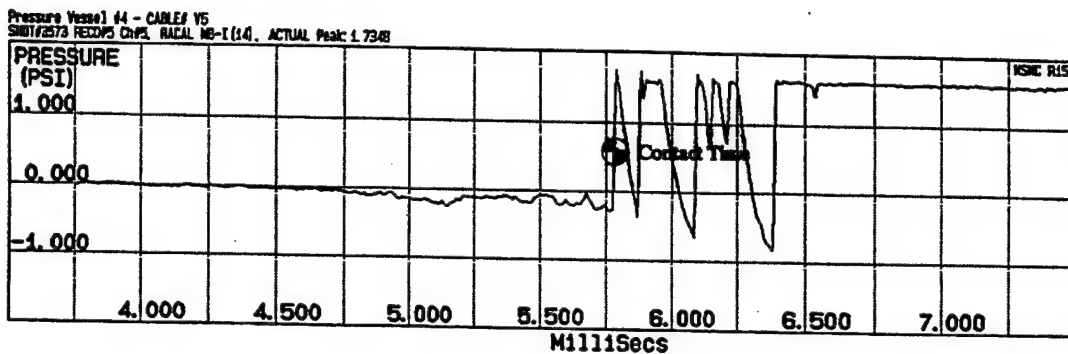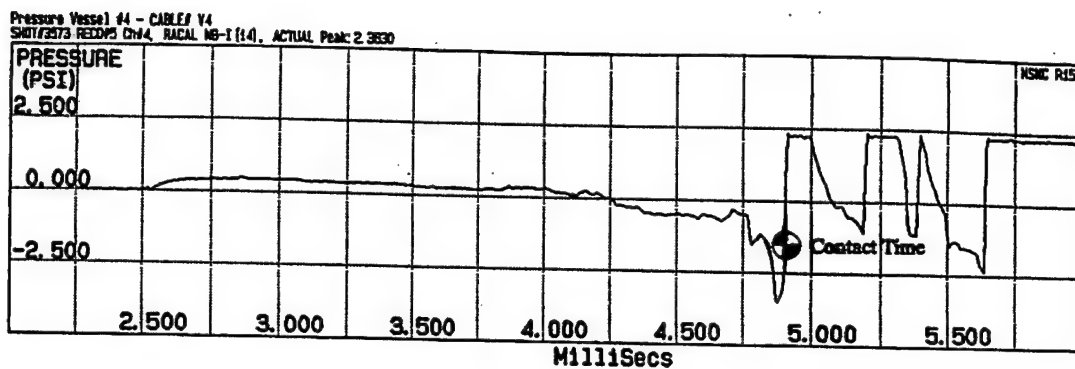
Figure 6.4b Contact Times for Vessel PC, Wires 4 through 6
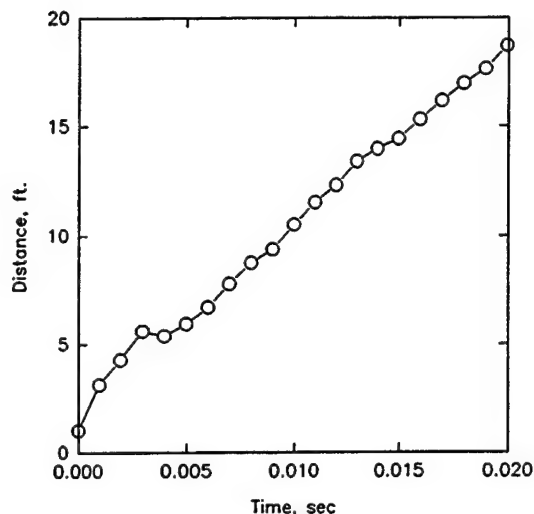
Figure 6.5, Initial Distance versus Time for Vessel 6A-2 West Fragment
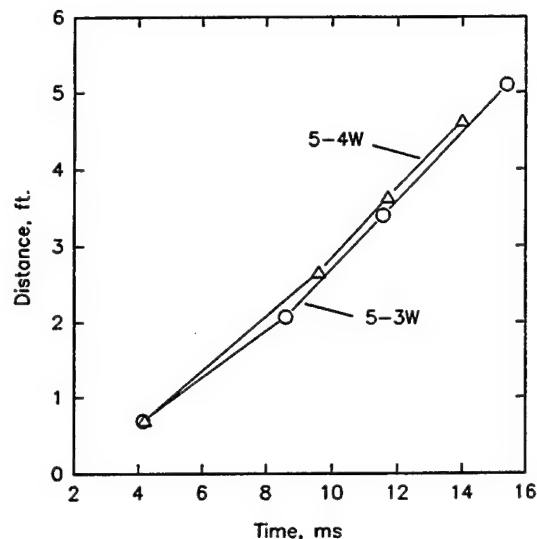
Figure 6.6, Contact Wire Distances Versus Time for West Fragment of Vessel 5-3 and 5-4

6.2   Calculation of initial velocities/program BURST

As fragment velocities were measured during the Burst Test Study, improvements were made to a computer program for estimating the velocities.

6.2.1   Background

Taylor and Price[5] in 1971 presented a technique for calculating the velocity of fragments resulting from a bursting gas reservoir. The technique, based on an original work by Grodzovskii, et al[38], removed two important restrictions: acceleration with small displacements and velocity not too large. The technique analyzed the displacement of two fragments from a bursting sphere and derived a differential equation for the motion. Specific cases, to compare to empirical data, were solved using numerical integration on a digital computer.

In 1972, R. A. Lorenz, in an appendix to Pittman's[7] report, presented computer program FRAG for calculating the velocities of bursting spheres and cylinders. The work was part of test planning for those pneumatic bursts. In 1975 Baker[2] included in his workbook SPHER and CYLIN, computer codes for calculating the initial velocity of two fragments from either spherical or cylindrical vessels respectively.

Program BURST is based on a Pascal version of the Taylor and Price code as written and modified by Baicher[39]. Ambrosio[40] has rewritten the program, made a number of improvements to the program from 1990 through 1994, and documented the velocity model in 1993. These improvements removed the original assumptions of perfect gas law and fragments propelled into a vacuum. The improvements were made as a cooperative effort on the Burst Test Study to better predict the fragment velocities that were being measured. The latter program is called BURST and is the program that will be discussed herein.

For additional background material the reader is referred to other authors whose work will not be covered in this report. Moore[41] presents equations, based on experiments with explosives by Gurney[42] and Sterne[43] for estimating initial fragment velocity by assuming that 60% of the initial energy is converted into kinetic energy. Baum[44] presents data from his own research and that of others for examining the accuracy of the Moore equations. Bessey and Kulesz[45] discuss an analytical model and based on modeling results show that fragment velocities increase with the number of fragments until ten is reached. They also provide curves to show the effect of pressurant to fragment mass ratio for spheres and cylinders. Baker[2] presents two computer programs, SPHER for spheres and CYLIN for cylinders, for estimating initial fragment velocities. Wiedermann[6] shows through analysis that fragment velocities are significantly reduced by real gas effects. Held and Jager[3] present equations for estimating the initial velocity of fragments based on gas discharge time constants. Brown[46] and Baker[47] have both written summaries of the then current (1984) state of the art in fragmentation.

6.2.2 Program BURST Characteristics[48]

The Burst program assumes a variable length cylinder capped at each end with hemispherical domes. The latest version of the program, 9.0, contains four rupture geometry models:

- Multi-fragment burst: The cylindrical portion ruptures along longitudinal lines and fragments are propelled radially. The domes are propelled longitudinally.

- Fractional split burst: The cylinder ruptures across the diameter at a specified location. The cylindrical portion remains intact and attached to its respective dome.

- Dual end cap split: Each dome separates from the cylinder and is propelled longitudinally. The cylindrical section remains intact.

- The dual end cap split model will calculate the initial velocity of a sphere by inserting a zero length cylindrical section.

The following gas expansion and fragment motion modeling considerations/assumptions are incorporated in the program:

- Real gas properties are used (air, N2, H2, and CO2 are available)

- Expansion of gas is assumed to be adiabatic (isentropic)

- Gas temperature, speed of sound and gas compressibility computed from gas expansion

- Gas expansion is computed independently for each fragment

- Amount of gas escaping into gaps between fragments proportioned according to the square of the critical velocities

- Flow coefficients (which determine transition from choked to unrestricted flow) are functions of ratio of gap to outer radius

- Atmospheric drag is accounted for in acceleration computation

- Fragment tumbling is not considered

- Velocity of fragments is taken into account in computing pressure exerted on the fragment

- Computations for a section are stopped when critical pressure drops below atmospheric pressure

6.3 Measured velocities compared to BURST

A comparison of measured initial velocities and initial velocities as computed with program BURST are provided in Table 6.2. Also included are measurements of displacement and time to maximum (initial) velocity. Most of the initial displacement and time data were not available because reference locations in use on the fragments were not visible at the start of acceleration due to the dust and condensation cloud. Displacement and time of maximum velocity from the BURST model, however, were also calculated and are included in the table.

Various investigators have estimated the percentage of total energy that appears as kinetic energy in the velocity and mass of the fragments. This value has been computed for each burst and is provided as Table 6.3. The table includes an "effective fragment velocity". This velocity, when used with the total mass of the fragments, produces the kinetic energy, i. e. $w_{tot}v^2_{eff} = \Sigma w_i v_i^2$. A value of 500 ft/sec is used for the sidewall fragments from vessel 6A-4. This is not an average velocity of the sidewall fragments but is rather the maximum velocity. It is used for an average because it is the only fragment that was measured on a track almost normal to the camera field of view. The actual average may be less but is considered to be unknown because of camera angles. The fragment tracked at 500 ft/sec is a south side panel that was launched horizontally and struck a dirt mound just outside the arena. Four other fragments were tracked. These originated from the top or north side of the vessel. Their velocities and angles from the horizon are 228 @ 30, 314 @ 33, 314 @ 81 and 338 ft/sec @ 69°. For reasons yet unknown these were not measured with the camera having the best angle. In fact two cameras are probably needed to determine the velocity if the track was not normal to the field of view. A total of 7 cameras were in use as shown in Figure 3.38.

Table 6.2
Burst Comparisons with Fragment Test Data

Test ID	Fail Mode	Press (psig)	Burst Temp (°F)	Frag Weight (lb)	TEST Max Frag Ves (fps)	Displ @ Max Vel (ft)	Time @ Max Vel (m-sec)	BURST MODEL[1] Max Frag Vel (fps)	Displ @ Max Vel (ft)	Time @ Max Vel (m-sec)
1-1	CL split	1475	65	2825 2700	148 148	2.1 2.5	26 27	134 140	2.78 2.91	30.31 30.33
1-2	CL	3450	109	3050 2850	244 250	--- ---	--- ---	202 215	3.73 3.97	25.18 25.20
1-3	CL	5425	75	3000 2825	315 315	2.3 3.8	12 17	267 282	4.61 4.88	22.81 22.84
1-4	CL	7125	133	2700 2550	379 ---	2.3 ---	13 ---	370 390	5.48 5.78	19.92 19.95
2-1	CL	3450	135	2575 2450	251 ---	--- ---	--- ---	224 234	3.90 4.08	23.72 23.73
2-2	CL	3450	132	2700 2600	253 259	--- ---	--- ---	217 225	3.83 3.97	24.21 24.22
2-3	CL	3475	142	2750 2650	262 268	--- ---	--- ---	216 223	3.83 3.97	--- ---
P-1	CL	3250	124	3075 2725	239 ---	2.4 ---	24 ---	192 215	3.54 3.96	25.25 25.30
P-2	CL	4700	124	3085 2715	295 318	--- ---	--- ---	233 263	4.07 4.59	23.24 23.28
PC	Sphere	3975	125	2x21.8	978	1.5	3	1050	2.84	3.07
5-1	3/4, 1/4	3600	130	3500 1425	251 284	4.7 ---	43(?) ---	258 312	2.64-3.50 4.45	19.2-22.5 19.20
5-2	3/4, 1/4	3600	140	3600 1500	242 281	2.2 ---	19 ---	223 302	2.58-3.33 4.34	19.4-22.7 19.40
5-3	single endcap	3600	126	4675 300	220 395	--- ---	--- ---	183 380	1.85 2.73	18.65 8.86
5-4	single endcap	3600	123	4675 300	218 400	--- ---	--- ---	178 380	1.80 2.73	18.44 8.86
6A-1	dual endcap	3280	106	800 800	479 408	--- ---	--- ---	---[3] ---	---[3] ---	---[3] ---
6A-2	Sphere	4000	169	90.1[2] 21.8	598 889-1252	--- <6	--- ---	576 1050	1.84 2.84	3.94 3.07
6A-3	CL	3300	97	3050 3050	238 ---	--- ---	--- ---	294 294	4.03 4.03	18.57 18.57
6A-4	Multi-Frag	3500	108	12x362 frags	~500	--- ---	--- ---	516	3.50	7.90
				352 352 endcaps	263 271	--- ---	--- ---	278 278	1.40 1.40	6.36 6.36

[1]Computed by Chrostowski
[2]Weight includes part of support structure
[3]Program revised to compute dual endcap but data not available at time of writing

Table 6.3
Kinetic Energy of Fragments as a Percent
of Isentropic Expansion Energy

Vessel	Weight, lbs	Effective Velocity, fps	KE/IE, %
P-1	5800	239	10.5
P-2	5800	306	11.6
1-1	5525	148	9.0
1-2	2900	247	10.7
1-3	5825	315	10.7
1-4	5250	379	10.4
2-1	5025	251	9.4
2-2	5300	256	10.4
2-3	5400	265	11.2
PC	44	978	21.0
5-1	4925	261	9.6
5-2	5100	253	9.3
5-3	4975	234	7.8
5-4	4975	233	7.7
6A-1	1600*	445	10.0
6A-2	112	770	33.2
6A-3	6100	238	10.8
6A-4	5048	474	33.3

*Excluding center section that remained in place.

6.4   Further Velocity Correlation

Although improvements were made to the BURST program for computing fragment velocities, there are still some limitations to the code, namely there are failure cases not addressed by the program. In his 1988 paper, Baum[4] enumerated eleven failure cases for either spheres or cylinders. Seven failure cases for pressurized gas vessels were treated in the paper. Five equations covered the seven cases. These equations determine the failure type in a computer program LIMITV, written for a hazard assessment workbook[49]. Three of the cases are appropriate for correlation of Burst Test Study data and are included herein.

Baum's equations provide guidelines on fragment velocity that are realistic upper limit values derived from experimental data. The data were either correlated by parameters indicated by dimensional analysis or for a limited number of cases as a function of the total energy available. In some cases a simple experimental model was used. Pertinent graphs from Baum's paper are included in this section. New graphs, showing correlation with experimental data gathered for this report are also included. His equations used in LIMITV are provided in Table 6.4.

The term F, equation 6.4, is a dimensionless initial acceleration. The term E, equation 6.5 is the maximum expansion work available from the pressurized contents. This is an additional equation, beyond equation 4.1 to describe the energy. Note that equation 6.5 using only the first term from 6.6 is the same as equation 4.1. The second term of equation 6.6 is a negative correction term, making 6.5 less than 4.1.

All of the models used herein assume an ideal gas. Section 6.4.2 will show that, for certain burst geometries, the results are also applicable for a real gas but are more conservative.

Some of the burst tests conducted under this study are appropriate to compute with either the BURST model or the LIMITV model. These are shown in Table 6.5 along with the test data. Typically BURST calculated velocities that were slightly lower than test data although some are high. Since the LIMITV velocities are limiting velocities they can be expected to be high.

6.4.1 End cap fragment

Figure 6.7 is Baum's[4] Figure 1, for endcap data, with an average velocity for the endcaps of Test 5.3 and 5.4 from Table 6.5 added. Also included is the velocity computed by the BURST model, (5% less than measured). (See Section 6.1.5: the test velocities must be considered to be minimum velocities although the results appear to accurate.)

SYMBOL	P_o/P_e	Y	L/R	SOURCE
x	30-40	1.4	8.33	BNL DATA
•	5-40	1.4	8.33	BNL DATA
•	5-20	1.66	8.33	BNL DATA
▲	5-20	1.4	16.66	BNL DATA
□	10-20	1.4	5.0	BNL DATA
■	10-20	1.66	5.0	BNL DATA
○	20	1.4	10.0	BNL DATA
•	20	1.66	10.0	BNL DATA
+	100-285	1.4	13.5	HELD & JAGER (1982)
•	25.6	1.4	5.3	HERZOG et al (1981)
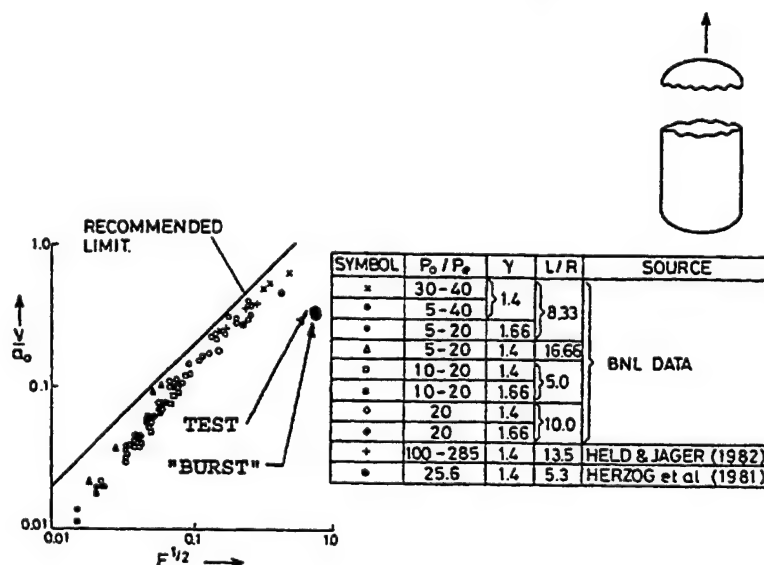
Figure 6.7, Test 5.3 and 5.4 endcaps added to Baum's endcap data

86

Table 6.4
Equations used in LIMITV

LIMITV Type	Equation	Equation number
1	$$\frac{V}{a_o} = 2F^{1/2}$$	6.1
2	$$\frac{V}{a_o} = 2.18\left(F\left(\frac{L}{R}\right)^{1/2}\right)^{2/3}$$	6.2
5*	$$\frac{V}{a_o} = .88F^{.55}$$	6.3
Where: $$F = P_o AR/Ma_o^2$$ $$E = \frac{P_o \phi_o k}{\gamma - 1}$$ where: $$k = \left[1 - \left(\frac{P_e}{P_o}\right)^{\frac{\gamma-1}{\gamma}}\right] + (\gamma - 1)\frac{P_e}{P_o}\left[1 - \left(\frac{P_e}{P_o}\right)^{-\frac{1}{\gamma}}\right]$$ and: V = peak fragment velocity a_o = velocity of sound in undisturbed high pressure gas L = length of cylindrical vessel (LIMITV will use length of fragment) R = vessel inner radius M P_o = rupture pressure P_e = atmospheric pressure ϕ_o = volume of high pressure gas γ = ratio of specific heats (1.4 was used in LIMITV) A = projected area on which pressure acts (exhaust area for rocketing fragments)		6.4 6.5 6.6

* See the workbook[49] for types 3 and 4

Table 6.5
Comparison of Test and Model Velocities
(Rocket and end cap fragments)

Vessel	Pressure psig	Frag.	Weight, lbs	Cyl. length, ft.	I.D., ft.	Gas temp. °F	Test, fps	Calc. Model, BURST	Limit Model[1], LIMITV
1-1	1475	West	2700	9.5	.93	65	148	140	156
		East	2825				148	134	152
1-2	3450	West	2850	9.5	.93	109	250	215	262
		East	3050				244	202	251
P-2	4700	West	2715	9.5	.93	124	318	263	331
		East	3085				295	233	304
1-3	5425	West	2825	9.5	.93	75	315	282	360
		East	3000				315	267	346
1-4	7125	West	2550	9.5	.93	133	---	390	455
		East	2700				379	370	438
5-1	3600	West	1425	5.0	.93	130	284	312	344
		East	3500	14.0			251	258	333
5-2	3600	West	1500	4.6	.93	140	281	302	322
		East	3600	14.2			241	223	262
5-3	3600	West	300	0.1	.93	126	395[6]	380	748[2]
		East	4675	18.9			220	183	243
5-4	3600	West	300	0.1	.93	123	400[6]	380	748[2]
		East	4675	19.2			218	178	244
6A-3	3300	West	3050	3.5	1.348	97	---	294	325
		East	3050				238	294	325
6A-4	3500	End Caps	2@352	---	.929	108	267[4]	278	493[3]
		Side Frags	12@362	18.7			500[5]	516	

[1]Rocket model unless shown otherwise
[2]End cap model
[3]Cylinder disintegration model
[4]Average of both caps
[5]Max. - 1 frag. others may be less
[6]A minimum, to be checked with hydrocode

6.4.2 Rocketing Fragment

Most of the Burst Test Study data falls into this category and data comparisons are shown in two graphs.

Baum's plot for rocketing fragments (his Figure 2) is presented as Figure 6.8. Baum used the vessel length in the $F(L/R)^{1/2}$ expression. In Figure 6.9 the Held and Jager[3] data is plotted using L both as a vessel length and as a fragment length (some unavailable ancillary data was estimated). This has no change on the ordinate for each point but the increase in abscissa with a longer L places the points lower with respect to the line. For this plot the use of the fragment length was a slightly under-conservative estimate. The BURST computed velocity for each test is also plotted at the fragment length abscissas.

For the Burst Test Study data shown in Figure 6.10, L was taken as the fragment length. The recommended limit appears to be a conservative estimator of the test data (filled symbols), typically more accurate than the BURST computations (open symbols) except at higher pressures. The sonic velocity, a_o, in Figure 6.10 was computed for air as an ideal gas. Sonic velocity for the actual test gas, nitrogen, as a real gas, was used in Figure 6.11 to replot the data from Figure 6.10. The sound velocity values are available from BURST output. In the new plot the recommended limit is no longer a good conservative estimator but the BURST computed values are still typically low. The percentage difference is not large as can be seen in Tables 6.2 and 6.5.
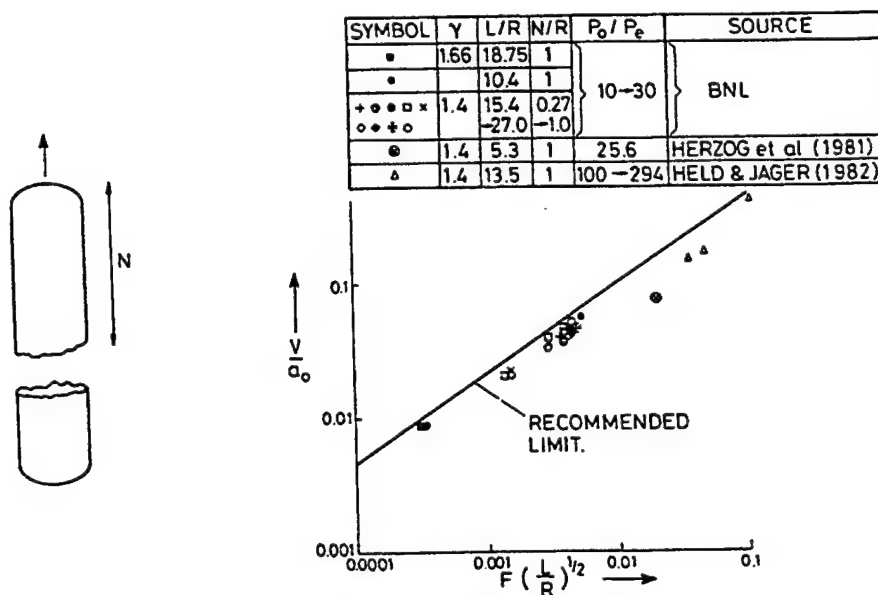
Figure 6.8, Rocketing Fragments (from Ref. 4)
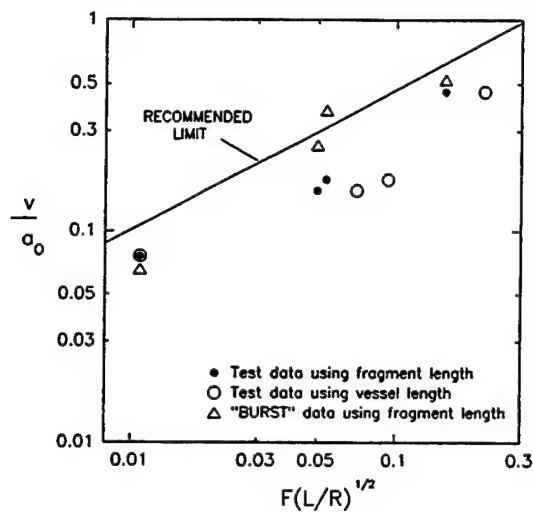
Figure 6.9, Held and Jager[3] rocketing fragments using L for both vessel length and fragment length
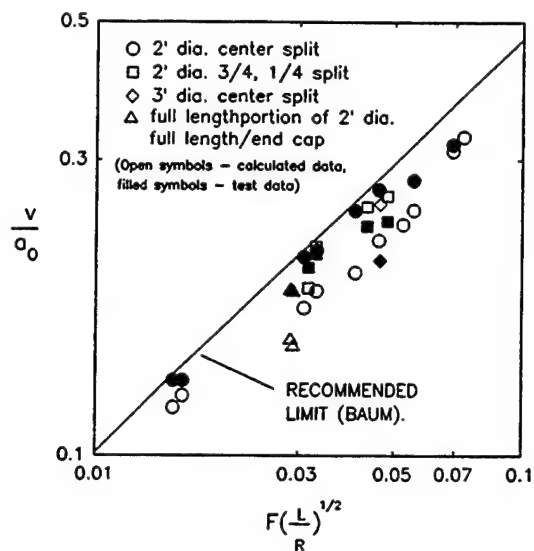
Figure 6.10, Burst Test Study Rocketing Fragments using a_o for ideal gas
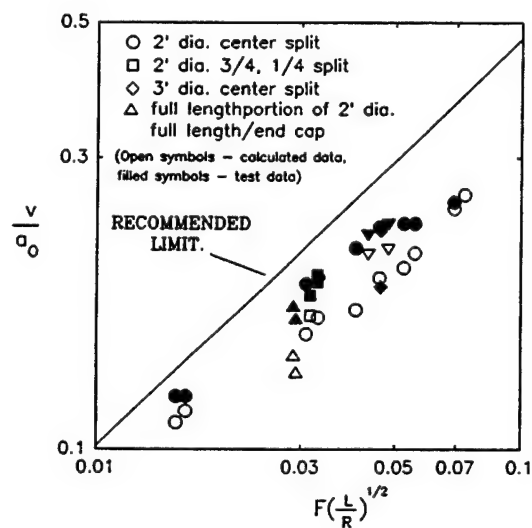
Figure 6.11, Burst Test Study Rocketing Fragments using a_o for real gas

6.4.3 Disintegration of sphere or cylinder

Disintegration of a cylinder is modeled by BURST providing the endcaps remain intact and sidewall fragments are full length strips of selected quantity. One such test case was conducted, vessel 6A-4. Disintegration of a sphere is not modeled by BURST. If BURST is needed to predict fragment velocities then velocities from the centerline split of a sphere could be used. The predicted velocities would be lower than expected since there would be only two fragments and the fragment velocity increases as the number of fragments increases until approximately ten is reached.[45]

Baum presented a separate graph for cylinders, reproduced here as Figure 6.12, and for spheres, reproduced here as Figure 6.13. Two new plots are presented that include both cylinders and spheres. (The recommended limit velocity equation does not differentiate between these two configurations.) Figure 6.14 plots the data for the function F versus V/a_0 where a_0 is the sonic velocity using the ideal gas assumption.

SYMBOL	Y	P_0/P_e	L/R	SOURCE
◦	1.4	11.2–28.3	8	BNL
×	1.4	9–24	2	COLLINS (1960)
♦	1.4	3.3	8	MOSKOWITZ (1965)
▲	1.4	4.3	2	PITTMAN (1972)
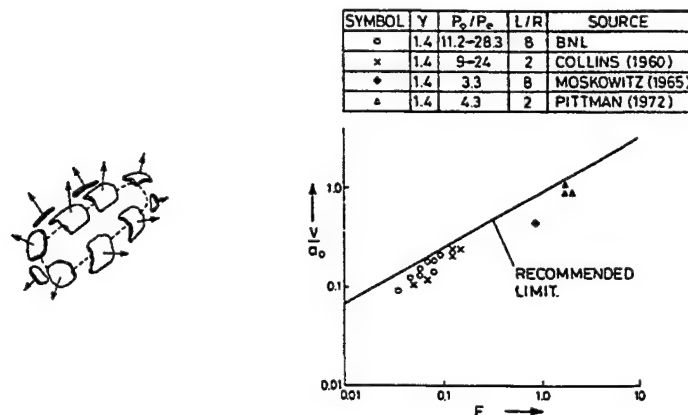
Figure 6.12, Disintegrating cylinders (from ref.4)

SYMBOL	Y	P_0/P_e	SOURCE
◦	1.4	7–12	BNL
▲	1.4	15–52	ESPARZA & BAKER(1977)
▲	1.66	14–52	ESPARZA & BAKER(1977)
×	1.4	21–28	BOYER (1959)
+	1.66	22	BOYER (1959)
●	1.3	5	GLASS (1960)
●	1.4	4–3	MOORE (1967)
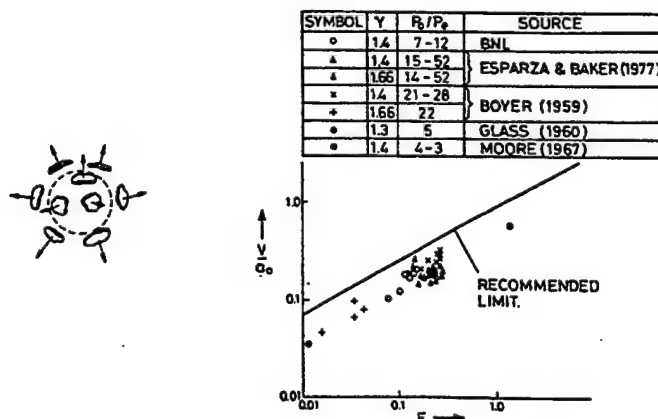
Figure 6.13, Disintegrating Spheres (from Ref. 4)

91

Figure 6.14 includes comparisons to test cases, to Baum's recommended limit and to BURST calculated velocity. BURST can model only one of the cases, vessel 6A-4 - a multi-fragment burst. However, BURST computations were made for comparison purposes with other test configurations in spite of the fact that the technique does not strictly apply. Baum's limit velocity technique does not apply to vessel burst 6A-4, since the end caps remained intact, and burst 6A-2 that resulted in only 2 fragments. BURST computed velocities higher than measured for the Esparza and Baker[50] data shown in Table 6.6. BURST computed velocities less than measured for the Pittman[7] bursts, some of which occurred at pressures around 8000 psig. One point, the 625 psig Pittman cylinder burst was slightly above

Figure 6.14, Disintegrating spheres and cylinders from Burst Test Study and the literature

Baum's recommended limit for the V/a_0 used. Burst gas temperatures of 60°F were assumed for both the Esparza and Baker bursts and the Pittman bursts. The actual sidewall fragment velocity was also above the recommended limit while the end cap velocities were considerably below. The greatest error, measured versus BURST, occurs at the highest pressure Pittman burst for which BURST is 36% low and Baum's recommended limit is 26% high.

Table 6.6
Esparza & Baker Fragment Data

Test	Vol, Ft³	Uncorrected Burst Pres. psig	Inner Radius, Ft[1]	Vessel Weight, lbs	Measured Velocity, FPS
4	.0023	300	.082	.044	233.9
5	.0200	200	.168	.258	205.4
8	.0028	750	.088	.180	249.0
17	.0027	401	.086	.066	216.2

[1]Calculated from volume, added .001 ft for outer radius

92

Baum did not present a case for two sphere halves propelled by a pressurized gas burst (only a liquid, not covered herein). It can be seen by Figure 6.16 that BURST did a good job of estimating fragment velocity for both the heavy side (includes support hardware) and the light side of 6A-2. The velocities of fragments from vessel 6A-4 were also closely estimated.

6.5 Fragment Recovery Distances

A fragment from a pressure vessel that bursts at high pressure can be massive and yet travel a considerable distance, presenting a significant hazard. The distance a fragment may travel is of safety interest both for a pressure vessel installation and for test planning for the Burst Test Study (Section 3.2). With a known breakup geometry and an estimated initial fragment velocity using the method of Section 6.2, the fragment range can be estimated by assigning a launch angle and using a ballistic trajectory computer program, a number of which are available. Baker published computer programs FRISB for lifting type fragments and TRAJE for drag type fragments in his workbook[2]. TRAJE was keyed from the literature and modified (it was written to produce a family of solutions). It appeared to work reasonably well using a test case of a vertically launched, light weight fragment, vessel PC. However in preparation for end cap bursts in the Burst Test Study a better known program was desired. Program TRAJ was offered for use by the Naval Surface Warfare Center. TRAJ is a two dimensional drag trajectory computer program that will run on any IBM compatible machine using DOS 3.1 or higher operating system. This program is easier to use, also corrects for drag and will calculate ricochets using an empirical ricochet model. The ricochet model is described by Chrostowski and Collins[51]. The program was documented by Montanaro[52].

The only known fragment launch angles during Burst Test Study were horizontal. Thus only the ricochet model is relevant in comparing calculated distances with actual distances travelled by fragments. Table 6.7 shows distances travelled by fragments from vessels ruptured during the Burst Test Study and includes comments on damage inflicted to trees by fragments. All of these fragments from the study, except for two vessels, were launched horizontally and reached their final location by a variety of means such as cartwheeling, bouncing, skidding or rolling. The type of ricochet depended on such things as ground condition, fragment length and mass. A half vessel fragment that buried its nose in soft clay such that the aft end was flipped over, began to cartwheel. A horizontal launch was confirmed by measuring the location of the first ground strike position where it could be identified and comparing that distance to a computed distance using the initial velocity and the acceleration due to gravity. The final distance where the fragment was found was therefore achieved by bouncing for most fragments. For some tests a video camera recorded the action of the fragments. The west fragments of vessel bursts P-1 and P-2 were seen to cartwheel many times and the ricochets are recorded in Tables 6.8 and 6.9. The west fragment of vessel 1-4 was observed to bounce only three times in reaching the woods approximately 800 feet away. The east fragment of vessel 1-4 spun in the horizontal plane as it bounced. This was typical of the east fragments. The pressurant tubing, attached to that end was pulled in two by the motion of the fragment and the restraining action of an anchor block approximately 80 feet from the arena center. Since there was no plan to improve a ricochet model the ground strike depressions were not filled so that each fragment

93

would have a unique and identifiable pattern. The east half fragment typically went a lesser distance because of the restraining force necessary to break the supply tubing. A half vessel striking frozen ground would skid and/or bounce. It is likely that some of the fragments would have travelled a greater distance had they been launched at an upwards angle, especially a 45° angle for maximum range.

TRAJ provided a reasonable and conservative range estimate through the ricochet model for the horizontally launched fragments, even though the correlation with number of ricochets is poor. The ricochet depends in part on the "soil constant". A soil constant of 0.5 is reasonable for the Dahlgren test area. Table 6.10 provides ricochets and distances for the west fragment of vessel P-2 for various values of the soil constant as calculated by the program.

In vessel test PC one fragment was launched vertically up and the other down. After vessel 6A-4 was prepared for testing the vessel grooves were measured with respect to the vessel support to determine if the top fragments would be launched straight up. A small angle of 1.7° toward the north was discovered. This angle and an initial velocity of 500 ft/sec would not produce the distance travelled by some of the top fragments, 892' to 1640', using a ballistic trajectory. An initial velocity of 8500 ft/sec would be required (program TRAJ). Therefore the trajectory was not ballistic, the shape of each quarter-circular section affected its travel by aerodynamics: lift and variation of angle of attack. Recovery distances for vessel 6A-4 are shown in Table 6.7.

Table 6.7
Fragment Distances
from Burst Test Study

Vessel #/Fragment		Vessel Pressure, psig	Vessel or Fragment Wt, lbs	Distance Recovered, feet	Comments
P-1	E	3250	3075	870	
	W		2725	822	
P-2	E	4700	3085	723	
	W		2715	1047	Hit tree at 1060'
1-1	E	1475	2825	409	
	W		2700	404	
1-2	E	3450	3050	not	
	W		2850	recorded	
1-3	E	5425	3000	783	West fragment cut tree at 40'
	W		2825	1347	height on final bounce (1327')
1-4	E	7125	2700	1027	West fragment broke off 10 trees
	W		2550	1271	with diameters between 4" & 12"
2-1	E	3450	2575	702	Short supply tube
	W		2450	873	Stopped by embankment
2-2	E	3450	2700	767	
	W		2600	732	
2-3	E	3750	2750	666	
	W		2650	614	
5-1	E[1]	3600	4925	1160	
	W[2]		1425	1176	
5-2	E[1]	3600	5100	916	
	W[2]		1500	800	
5-3	E[4]	3600	4075	1130	
	W[3]		300	1508	
5-4	E[4]	3600	4975	1079	
	W[3]		300	1303	
6A-1	E	3280	2 X 800	1644	East fragment was ballistic last
	W			1176	757' (bounced off camera shelter)
6A-2	E	4000	43.6	213	overwrap = 186E, 243W
	W			390	
6A-3	E	3300	3050	1156	
	W			3050	1176	
6A-4 sidewall		3500	12 X 362	10 to 1640 (563 avg)	3 pieces driven down and bounced, average of others = 740'
6A-4 endcap			2 X 352	194E, 163W	East endcap struck dirt mount

[1] 3/4 length
[2] 1/4 length
[3] end cap
[4] full vessel length

Table 6.8
Ground Strike Distances
for Vessel P-1

Ground Strike #	Distance, ft.	
	East Half	West Half
1	160	171
2	283	421
3	448	447
4	467	432
5	577	615
6	702[1]	635
7		667
8		698
9		727
10		756
11		769
12		785
13		810
14		820
15		826
16		822[2]

[1] starts rolling
[2] at rest

Table 6.9
Ground Strike Distances
for Vessel P-2

Ground Strike #	Distance	
	East Half	West Half
1	114	143
2	467	192
3	509	423
4	603	443
5	621	584
6	676	601
7	710	617
8	723[1]	648
9		697
10		712
11		728
12		743
13		807
14		822
15		838
16		927
17		1031
18		1060[2]
19		1047[3]

[1] at rest [2] tree [3] at rest

Table 6.10
Range Variation with
Soil Constant for P-2W

Soil constant	Number of ricochets & final distance, ft.	
	No.	Dist.
0	0	148
.25	6[2]	1095
.5[1]	6[2]	1326
.75	*	*
1.00	4[3]	1557
1.25	4[3]	1595
1.50	4[3]	1596
1.75	4[4]	1572
2.00	*	*
2.25	5[4]	1593
2.50	5[4]	1594
2.75	*	*
3.00	*	*
3.25	5[4]	1621
3.50	5[4]	1643
3.75	5[4]	1665
4.00	5[4]	1689

* overflow - no results
[1] Reasonable soil constant for the area
[2] 1st ricochet is greatest height
[3] last ricochet is greatest height
[4] 2nd ricochet is greatest height

7.0 CONCLUSIONS AND RECOMMENDATIONS

The test program fulfilled its purpose of augmenting the available pneumatically pressurized vessel burst test data. Both overpressure and fragment data were collected on a variety of vessels and burst scenarios and both types of data were compared to existing models. An existing model for fragment velocity was rewritten and improved as a cooperative effort with Acta Inc. Damage/injury data developed during explosives testing can now find greater application to pressure vessel bursts.

For vessels that exhaust rapidly on bursting it was found that the overpressure and impulse could be approximated using Baker's workbook for spheres but not for cylinders. With regard to his workbook, slow exhaust vessels produced less overpressure and cylinder corrections are much less than shown. The Pressure Vessel Hazard Assessment Workbook provides models for computing overpressure and impulse for Burst Test Study tested vessels. (For lack of available information, reflected impulses were assumed to have the same reflection factors as their attendant overpressures.) If there is a very close reflecting surface then reflected overpressures and impulses may be produced that exceed computations by either workbook.

It is felt that height of burst (HOB) testing might have produced more meaningful results if rapid exhaust vessel bursts were conducted and at more than three heights. The use of reflection factors based on incidence angle and incident overpressure from testing with high explosives is recommended until data are available from additional testing or hydrocode simulation. (See Section 5.6.)

Pressure vessel burst overpressures cannot be computed using TNT equivalence except in the far field (Section 5.8). In the near field TNT equivalence result is higher than actual. In the far field measured overpressures approached TNT results for most vessels. Even in the far field the two spheres produced overpressures that exceeded TNT equivalence results.

The initial velocities of fragments were computed with BURST software that was improved during the course of the effort. Close results were obtained with computations being typically slightly lower than actual velocity. Baum's limit models were found to provide useful limiting velocities for the cases not appropriate for BURST (Section 6.4).

Additional testing and/or hydrocode solutions to bursting vessels would be very useful. Efforts should be directed toward obtaining additional data in the areas of lower pressures, larger vessels, reflection factors for both overpressures and impulses, cylinder corrections to overpressure and impulse and bursts with other fluids such as argon, helium or a propellant.

References

[1]Coleman, M. et al, "A Review of Energy Release Processes From the Failure of Pneumatic Pressure Vessels," ESMC-TR-88-03, Eastern Space and Missile Center, August 1988, pages 7, 32, 35, 38, 40, 53.

[2]Baker, W. et al, "Workbook for Predicting Pressure Wave and Fragment Effects of Exploding Propellant Tanks and Gas Storage Vessels", NASA CR-134906, November, 1975.

[3]Held and Jager, "Assessment of Gas Pressure Vessel Burst Hazard", ASME PVP, Volume 62, 1982.

[4]Baum, "Disruptive Failure of Pressure Vessels: Preliminary Design Guidelines for Fragment Velocity and the Extent of the Hazard Zone", Transaction of the ASME -Journal of Pressure Vessel Technology, May, 1988.

[5]Taylor, T.D. and Price, C.S., "Velocities of Fragments from Bursting Gas Reservoirs", Journal of Engineering for Industry, November, 1971.

[6]Wiedermann, A.H., "Air Blast & Fragment Environments Produced by the Bursting of Vessels Filled with Very High Pressure Gases", ASME-PVP Vol 106, January 1986.

[7]Pittman, "Blast and Fragment Hazards from Bursting High Pressure Tanks", Naval Ordnance Laboratory, May, 1972.

[8]Baum, "The Velocity of Missiles Generated by the Disintegration of Gas-Pressurized Vessels and Pipes", American Society of Mechanical Engineers Journal of Pressure Vessel Technology, November 1984.

[9]Swisdak, "Explosion Effects and Properties Part I - Explosion Effects in Air", NSWC/WOL/TR 75-116.30, 1975.

[10]Kinney and Graham, Explosive Shocks in Air, 2nd ed, Springer Verlag, 1985.

[11]Stoneking, J.E., Landes, J.D., Pressure Vessel Burst Test Analysis submitted to General Physics Corp., Structural Mechanics Consultants, April 89.

[12]Stoneking, J.E., private communication, May 89.

[13]General Physics Corporation: Groove Machining Report of the Pressure Vessel Burst Test Program, June 1990.

References (continued)

[14]WL/MLSE, Wright-Patterson AFB, OH, Tensile Test of SA372 Class IV Steel, MLS 92-012, Feb 92.

[15]General Physics Corporation: Hydroburst Test Plan of the Pressure Vessel Burst Test program, July 1989.

[16]General Physics Corporation: Preliminary Shaped Charge Test Plan of the Pressure Vessel Burst Test Program, December 1989.

[17]General Physics Corporation: Test Plan #1 of the Pressure Vessel Burst Test Program, November 1990.

[18]General Physics Corporation: Test Plan for Series #3 of the Pressure Vessel Burst Test Program, Comprising the Completion of Test Plan #1 & Conduction of Test Plan #2, May 1991.

[19]General Physics Corporation: Test Plan for Series #4 of the Pressure Vessel Burst Test Program, Comprising the Conduction of Test Plan #5 & Preliminary Test Plan #4, December 1991.

[20]General Physics Services Corporation: Test Plan for Series #5 of the Pressure Vessel Burst Test Program, Comprising the Conduction of Test Plan #4, August 1992.

[21]General Physics Services Corporation: Test Plan for Series #6 of the Pressure Vessel Burst Test Program, Comprising the Conduction of Test Plan #3, September 1992.

[22]GPS Technologies: Test Plan for Conduction of Test Plan #6A of the Pressure Vessel Burst Test Program, Revision B, September 1993.

[23]General Physics Corporation: Hydroburst Test Report of the Pressure Vessel Burst Test Program, August 1989.

[24]General Physics Corporation: Report of Preliminary Pneumatic Burst Testing for the Pressure Vessel Burst Test Program, July 1990.

[25]General Physics Services Corporation: Test Report on Burst Test Plans 1 & 2 of the Pressure Vessel Burst Test Program, January 1992.

[26] GPS Technologies: Report of Testing of Test Plan #5 Vessels and Preliminary Composite Vessel of the Pressure Vessel Burst Test Study, October 1993.

References (continued)

[27]GPS Technologies: Report of Testing of Test Plan #6A Vessel of the Pressure Vessel Burst Test Program, (in preparation).

[28]Private communications, D.T. Coolidge, Explosive Technology, April 1992 and August 1992.

[29]WL/MLSE, Wright Patterson AFB, OH, Tensile Test of SA516 Grade 70 Steel, MLS92-038, April 92.

[30]General Physics Corporation: Nitrogen Pressurization System Report of the Pressure Vessel Burst Test Program, December 1990.

[31]General Physics Corporation: Storage Vessel Report of the Pressure Vessel Burst Test Program, June 1990.

[32]ACTA Inc., BURST, An Adiabatic Cylinder Burst Program, modifications in progress, May 94.

[33]Rye, K., NSWC, Pressure Vessel Burst Test Program (Test Series 1, 2 and 3), Presented at 4th Tri-Service Symposium on Explosive Testing, November 91.

[34]U.S. Air Force, "Air Force System Command Design Handbook 1-6, December 1982.

[35]Leipman and Roshko, "Elements of Gas Dynamics", Wiley, 1967, pages 80, 81.

[36]ASME/ANSI, Estimating Airblast Characteristics for Single Point Explosions in Air, With a Guide to Evaluation of Atmospheric Propagation and Effects, ANSI S2.20, 1983.

[37]Reed, Explosion Airblast Predictions on a Personal Computer and Application to the Henderson, Nevada Incident, Sandia National Laboratory SAND 88-0681C, August 1988.

[38]Grodzovskii, G.L. and Kukanov, F. A.,"Motion of Fragments of a Vessel Bursting in a Vacuum...", Inzhenernyi Zhurnal, v 5, No 2, March 1965.

[39]Baicher, V., LMSC, Sunnyvale, CA, Private communication to Lou Ullian, Patrick AFB, FL, April 1987.

[40]Ambrosio, A. Vessel Burst Velocity Model, Nov. 1993

[41]Moore, C.V., The Design of Barricades for hazardous Pressure Systems, North-Holland Publishing Co. Nuclear Engineering & Design.

References (continued)

[42]Gurney, R.W., Initial velocites of fragments from bombs, shells and grenades, BRL Report 405, 1943.

[43]Sterne, T.E., A note on the initial velocities of fragments from workbook, BRL Report 648, 1947.

[44]Baum, "The Velocity of Missiles Generated by the Disintegration of Gas-Pressurized Vessels and Pipes", American Society of Mechanical Engineers Journal of Pressure Vessel Technology, November 1984.

[45]Bessey and Kulesz, Fragment Velocities from Bursting Cylindrical & Spherical Pressure Vessels, Southwest Research Institute, 1976.

[46]Brown, S.J., Pressure Systems Energy Release Protection (Gas Pressurized Systems) NASA Contract Report 178090, Quest Engr. Development Corp, May 1986.

[47]Baker, W.E., Blast & Fragments from Bursting Pressure Vessels, 83-PVP-61, ASME/Southwest Research Institute, May 1983. (also in 84-PVP-82)

[48]Chrostowski, J., private communication, August 1994.

[49] Cain, M.R., Pressure Vessel Hazard Assessment Workbook, GP-R-741016, March 1995.

[50]Esparza, E.D. and Baker, W.E., Measurements of Blast Waves from Bursting Pressurized Frangible Spheres, NASA Contract Report 2843, Southwest Research Institute, May 1977.

[51]Chrostowski, J. and Collins, J., Pressure Vessel Hazard Model Development, ACTA Report No. 94-297/54-01, September 1994.

[52]Montanaro, P.E., TRAJ--A Two Dimensonal Trajectory Program For Personal Computers, March 1992.

APPENDIX A

Drawings and Sketches of Test Vessels

Penetration Locations
End on view from "Detail B" end

Groove Schedule -- 1 Groove per Vessel				
Vessel	Dim. A	Dim. B	Dim. C	Dim. D
1	.250	.100	.195	.045
2	.250	.100	.195	.045
3	.250	.100	.195	.045
Tolerance	±.015	±.015	+.005 −.000	+.000 −.000

GENERAL NOTES:

1. Location of groove may vary as per noted instruction

2. All dimensions are in inches.

Detail C

Detail B

Detail A

Detail D

Detail E

Accelerometer Mounting Block
Orientation to match Detail B

VESSEL PENETRATIONS

① THERMOCOUPLE PENETRATION — Drill and tap 1/8" NPTF thru vall.

② PRESSURE TRANSDUCER PENETRATION — Spot bore to obtain full 1/2" diameter flat, drill and tap thru 3/8-24-UNF-2A thread, tap 1/2" deep, counterbore .375/.380 dia. x .050/.060 deep.

③ ACCELEROMETER — (Smooth surface Ls) 84 dista, V required

④ WIRE TIE HOLE — Cross in location of grooved penetration, x-2 and tap 10-32 1/8" deep.

.015 ±.015 R

.050 ±.015 R

General Physics
Corporation
ENGINEERING & INSPECTION SERVICES

BURST TEST PROGRAM

TP-2 Vessel Modifications
Drg. No. 810001

A-1

PART NO.	NUMBER REQUIRED	DESCRIPTION	MATERIAL	REMARKS
1	2	SHELL	SA 516 GR. 70	W/O SKIRT
2	4	HEMISPHERICAL HEAD	SA 516 GR. 70	
3	4	1 1/2" 1500# CL ANSI WELD NECK RING JOINT BLANK FLANGE	SA 105	W/ 4" LENGTH 1.50"XXS PIPE
4	4	1.50" RING JOINT GASKET GROOVE #R20	RED RUBBER	
5	16	7/8" STUD BOLTS	SA 193 GR. B5	
6	4	1 1/2" 1500# CL ANSI BLIND FLANGE	SA 105	
7	2	NAME PLATE		

SHELL WELDS L-1

BACK GOUGE ROOT AND WELD BOTH SIDES

60°

1.75"

1.75"

NOZZLE N-1, N-2

TAP 0.50"-14 ANPT ON CENTER LINE

1.50" 1500# CL ANSI WELDNECK BLANK FLANGE

60°

.50"

1.50" XXS PIPE

HEAD TO SHELL WELDS C-1, C-2

30°

2.25"

1.75"

BUILD UP WITH WELD METAL

1"

42.75"±0.50"

18"± 0.00" 0.25"

85.50"±1"

18"

C-2

N-2

L-1

C-1

N-1

NOTES:

1. CONSTRUCTION IN ACCORDANCE WITH GENERAL PHYSICS SPECIFICATION ETR-SPEC-141001 AND ASME BOILER AND PRESSURE VESSEL CODE SECTION VIII, DIVISION 1.

2. GRIND ENTIRE LENGTH OF LONGITUDINAL WELD L-1 FLUSH INTERNALLY.

3. ALL WELDS (EXCEPT FILLET WELDS) ARE FULL PENETRATION.

4. ACTUAL VESSEL CAPACITY TO BE MEASURED AND STAMPED ON NAME PLATE.

NOT TO SCALE

GENERAL PHYSICS CORPORATION
ENGINEERING SERVICES
CAPE CANAVERAL AIR FORCE STATION

TWO (2) EACH 53 CUBIC FOOT NITROGEN STORAGE VESSELS
ASME CODE SECTION VIII, DIVISION 1, MAWP 1770 PSIG
DESIGN TEMPERATURE RANGE -20° F TO 200° F

DRAWN: J. D. SCHNEIDOTFIGER	
CHECKED: MIKE COLEMAN	
APPROVED: JIM PFEFFERLE	
DATE: 7-25-91	REVISION:

DRAWING NUMBER: 91B003

SHEET 1 OF 1

A-2

APPENDIX B

Pressurization System Diagram

NOTE A: External pilot modification. (Typical two places.)

NOTE B: Break apart tubing is anchored to concrete slab such that it breaks apart upon vessel burst.

NOTE C: Revision Two Changes. See Nitrogen Pressurization System Report Addendum for description.

B-1

APPENDIX C

NSWC Data Sheets

High Explosives

Vessels

PHE-1, 33.3# COMP B, SHOT 3249

GAGE #	POSITION	Pmax (psi)	MAX IMPULSE(psi-sec)
6799 (B3)	150 @ 10'	133.6	0.072
262 (B4) *	135 @10'	47.4	0.034
6800 (B5)	120 @10'	96.6	0.065
5175 (B7)	105 @ 10'	125.6	0.056
6803 (B9)	90 @10'	302.5	0.090
6391 (B11)	75 @10'	191.1	0.085
5187 (B13)	60 @ 10'	78.4	0.048
6796 (B15)	30 @ 10'	131.7	0.080
4718 (B26)	90 @ 15'	57.7	0.054
6797 (B30)	60 @ 15'	51.9	0.051
5257 (B32)	30 @ 15'	80.0	0.069
5176 (B34)	0 @ 15'	73.0	0.060
6801 (B37)	150 @ 22'	22.6	0.031
261 (B38) *	135 @ 22'	35.4	0.056
4792 (B39)	120 @ 22'	30.6	0.037
6802 (B41)	105 @ 22'	32.6	0.042
514 (B42)	98 @ 22'	21.0	0.040
6798 (B43) *	90 @ 22'	37.4	0.045
4572 (B47)	60 @ 22'	26.7	0.039
6395 (B49)	30 @ 22'	33.9	0.054
5256 (B50)	15 @ 22'	24.8	0.046
5215 (B51)	0 @ 22'	11.5	0.014
5254 (B60)	90 @ 34'	10.3	0.024
5194 (B62)	75 @ 34'	12.1	0.024
5269 (B64)	60 @ 34'	10.6	0.025
6795 (B65)	45 @ 34'	15.3	0.027
4727 (B66)	30 @ 34'	17.5	0.033
5236 (B67)	15 @ 34'	11.4	0.022
6394 (B68)	0 @ 34'	12.0	0.020
5255 (B71)	150 @ 50'	4.3	0.014
512 (B72) *	135 @ 50'	5.4	0.021
5076 (B73)	120 @ 50'	5.8	0.018
6385 (B75)	105 @ 50'	7.5	0.019
527 (B76)	98 @ 50'	4.6	0.021
6392 (B77) *	90 @ 50'	6.6	0.017
6162 (B79)	75 @ 50'	1.7	0.008
4555 (B81)	60 @ 50'	DATA NOT AVALIABLE	DATA NOT AVALIABLE
5085 (B82)	45 @ 50'	DATA NOT AVALIABLE	DATA NOT AVALIABLE
5277 (B83)	30 @ 50'	DATA NOT AVALIABLE	DATA NOT AVALIABLE
5078 (B84)	15 @ 50'	DATA NOT AVALIABLE	DATA NOT AVALIABLE
5245 (B85)	0 @ 50'	DATA NOT AVALIABLE	DATA NOT AVALIABLE

PHE-2, 65# C-4, SHOT 3201

GAGE #	POSITION	Pmax (psi)	MAX IMPULSE(psi-sec)
5175 (B1)	180 @ 10'	NOGAGE	NOGAGE
6799 (B3)	150 @ 10'	176.5	0.090
262 (B4) *	135 @10'	BAD	BAD
6800 (B5)	120 @10'	197.6	0.090
584 (B9)	90 @10'	371.6	0.400
6577 (B13)	60 @ 10'	232.5	~ 0
6796 (B15)	30 @ 10'	201.2	0.101
6391 (B17)	0 @10'	195.0	0.110
6570 (B26)	90 @ 15'	278.4	0.156
6797 (B30)	60 @ 15'	129.0	0.065
5257 (B32)	30 @ 15'	106.6	0.081
5176 (B34)	0 @ 15'	BAD (OVERLOADED)	OVERLOADED
6801 (B37)	150 @ 22'	45.5	0.068
261 (B38) *	135 @ 22'	68.2	0.085
4792 (B39)	120 @ 22'	36.6	0.060
6802 (B41)	105 @ 22'	75.8	0.061
514 (B42)	98 @ 22'	BAD	BAD
6798 (B43) *	90 @ 22'	90.9	0.079
4572 (B47)	60 @ 22'	50.4	0.060
6395 (B49)	30 @ 22'	66.5	0.076
5256 (B50)	15 @ 22'	OVERLOADED	OVERLOADED
5215 (B51)	0 @ 22'	OVERLOADED	OVERLOADED
5254 (B60)	90 @ 34'	54.9	0.091
5194 (B62)	75 @ 34'	18.9	0.047
5269 (B64)	60 @ 34'	23.4	0.048
6795 (B65)	45 @ 34'	29.3	0.048
4727 (B66)	30 @ 34'	23.2	0.051
5236 (B67)	15 @ 34'	OVERLOADED	OVERLOADED
6394 (B68)	0 @ 34'	OVERLOADED	OVERLOADED
5255 (B71)	150 @ 50'	10.3	
512 (B72) *	135 @ 50'	10.1	
5076 (B73)	120 @ 50'	10.4	0.029
6385 (B75)	105 @ 50'	7.5	0.026
527 (B76)	98 @ 50'	7.0	0.035
6392 (B77) *	90 @ 50'	7.6	0.030
6162 (B79)	75 @ 50'	7.4	0.028
4555 (B81)	60 @ 50'	13.7	0.030
5085 (B82)	45 @ 50'	9.2	0.027
5277 (B83)	30 @ 50'	8.9	0.026
5078 (B84)	15 @ 50'	7.9	0.024
5245 (B85)	0 @ 50'	OVERLOADED	OVERLOADED
525 (B96) *	75 @ 85'	6.7	0.029
258 (B98) *	60 @ 85'	8.4	0.036
250 (B99) *	45 @ 85'	6.2	0.029
520 (B109) *	105 @130'	1.6	0.008
515 (B113) *	75 @ 130'	2.1	0.015
517 (B115) *	60 @ 130'	2.5	0.013
255 (B130) *	75 @ 200'	2.9	0.025

* HOB GAGES

HE1-1 .66#, SHOT 3250

GAGE POSITION	ORIENTATION/RANGE	Pmax (psi)	MAX IMPULSE(psi-sec)
A	270° @ 1'	~~160.0~~ 242.4	0.033
B*	270° @ 3'	NO DATA	NO DATA
C	90° @ 5'	18.0	0.010
D*	270° @ 3'	NO DATA	NO DATA
B3	150° @ 10'	12.7	0.009
B4*	135° @ 10'	5.8	0.008
B5	120° @ 10'	14.0	0.008
B7	105° @ 10'	11.2	0.009
B9	90° @ 10'	11.6	0.007
B13	60° @ 10'	14.8	0.009
B15	30° @ 10'	21.2	0.011
B16	15° @ 10'	13.8	0.009
B26	90° @ 15'	5.5	0.0057
B30	60° @ 15'	9.0	0.0061
B32	30° @ 15'	6.4	0.0072
B34*	0° @ 11.5'	1.7	0.0008
B37	150° @ 22'	4.9	0.0041
B38*	135° @ 22'	1.6	0.0019
B39	120° @ 22'	3.4	0.0047
B41	105° @ 22'	2.9	0.0043
B43	90° @ 22'	2.9	0.0043
B45*	75° @ 22'	2.8	0.0041
B47	60° @ 22'	4.5	0.0050
B49	30° @ 22'	3.6	0.0043
B51	0° @ 22'	3.0	0.0041
B60	90° @ 34'	2.0	0.0027
B62	75° @ 34'	3.0	0.0040
B64	60° @ 34'	1.7	0.0025
B66	30° @ 34'	2.0	0.0029
B68	0° @ 34'	2.1	0.0030
B71	150° @ 50'	1.3	0.0021
B72*	135° @ 50'	0.8	0.0017
B73	120° @ 50'	1.0	0.0019
B75	105° @ 50'	1.3	0.0022
B77	90° @ 50'	1.2	0.0019
B79*	75° @ 50'	1.2	0.0015
B81	60° @ 50'	1.1	0.0020
B82	45° @ 50'	1.0	0.0018
B83	30° @ 50'	1.2	0.0020
B84	15° @ 50'	1.6	0.0023
B85	0° @ 50'	1.3	0.0021
B96*	75° @ 85'	1.3	0.0010
B109*	105° @127' 2"	0.2	0.0005
B113*	75° @ 130' 2"	0.2	0.0004
B115*	60° @ 130' 4"	0.2	0.0004
B130*	75° @ 192' 5"	0.1	0.0002

* HOB GAGES

HE1-2, 9.9#, SHOT 3256

GAGE POSITION	ORIENTATION/RANGE	Pmax (psi)	MAX IMPULSE(psi-sec)
A	270° @ 1'	NO DATA	NO DATA
B*	270° @ 3'	NO DATA	NO DATA
C	90° @ 5'	307.0	0.088
D*	270° @ 3'	NO DATA	NO DATA
B3	150° @ 10'	overloaded	overloaded
B4*	135° @ 10'	overloaded	overloaded
B5	120° @ 10'	overloaded	overloaded
B7	105° @ 10'	overloaded	overloaded
B9	90° @ 10'	overloaded	overloaded
B13	60° @ 10'	overloaded	overloaded
B15	30° @ 10'	overloaded	overloaded
B16	15° @ 10'	overloaded	overloaded
B26	90° @ 15'	38.3	0.023
B30	60° @ 15'	40.4	0.031
B32	30° @ 15'	28.6	0.037
B34*	0° @ 11.5'	bad	bad
B37	150° @ 22'	16.5	0.021
B38*	135° @ 22'	15.6	0.026
B39	120° @ 22'	16.6	0.020
B41	105° @ 22'	17.9	0.017
B43	90° @ 22'	19.6	0.015
B45*	75° @ 22'	10.7	0.019
B47	60° @ 22'	18.9	0.024
B49	30° @ 22'	18.2	0.024
B51	0° @ 22'	11.4	0.018
B60	90° @ 34'	5.8	0.013
B62	75° @ 34'	7.8	0.015
B64	60° @ 34'	6.8	0.010
B66	30° @ 34'	10.3	0.015
B68	0° @ 34'	6.8	0.016
B71	150° @ 50'	5.2	0.012
B72*	135° @ 50'	3.7	0.012
B73	120° @ 50'	4.0	0.010
B75	105° @ 50'	3.7	0.012
B77	90° @ 50'	3.3	0.010
B79*	75° @ 50'	3.5	0.007
B81	60° @ 50'	4.2	0.010
B82	45° @ 50'	4.0	0.010
B83	30° @ 50'	5.4	0.010
B84	15° @ 50'	7.0	0.012
B85	0° @ 50'	4.6	0.010
B96*	75° @ 85'	0.3	0.0003
B109*	105° @127' 2"	bad	bad
B113*	75° @ 130' 2"	bad	bad
B115*	60° @ 130' 4"	bad	bad
B130*	75° @ 192' 5"	0.4	0.0022

* HOB GAGES

HE2-1, 4.5#, SHOT 3401

GAGE #	POSITION	Pmax (psi)	MAX IMPULSE(psi-sec)
(A)	under vessel 10"	No Gage	No Gage
(B)	under vessel 78"	No Gage	No Gage
(C)	under vessel 146"	No Gage	No Gage
(D)	90° @ 1'	261.5	No Gage
(E)	90° @ 5'	93.1	0.039
6156 (B3)	150° @ 10'	31.7	0.018
528 (B4) *	135° @ 10'	13.4	0.014
5193 (B5)	120° @ 10'	32.1	0.016
6158 (B7)	105° @ 10'	BAD	BAD
4727 (B9)	90° @ 10'	26.1	0.019
5221 (B13)	60° @ 10'	33.9	0.018
6160 (B15)	30° @ 10'	31.6	0.024
5203 (B16)	15° @ 10'	34.1	0.021
5075 (B25)	98° @ 15'	BAD	BAD
5266 (B30)	60° @ 15'	14.7	0.015
6391 (B32)	30° @ 15'	23.1	0.017
517 (B34)*	0° @ 15'	17.6	0.020
6390 (B37)	150° @ 22'	7.0	0.010
264 (B38) *	135° @ 22'	26.0	0.014
7247 (B39)	120° @ 22'	9.0	0.012
5239 (B41)	105° @ 22'	7.6	0.010
6400 (B43)	90° @ 22'	8.2	0.012
250 (B45) *	75° @ 22'	4.7	0.009
4799 (B47)	60° @ 22'	7.2	0.010
5252 (B49)	30° @ 22'	6.3	0.010
5205 (B51)	0° @ 22'	6.6	0.010
6384 (B60)	90° @ 34'	4.9	0.006
5250 (B62)	75° @ 34'	3.4	0.006
5274 (B64)	60° @ 34'	3.3	0.006
5215 (B66)	30° @ 34'	4.3	0.008
6389 (B68)	0° @ 34'	5.6	0.007
5222 (B71)	150° @ 50'	2.2	0.004
262 (B72) *	135° @ 50'	1.8	0.006
7253 (B73)	120° @ 50'	2.3	0.005
6386 (B75)	105° @ 50'	2.3	0.004
5211 (B77)	90° @ 50'	2.0	0.005
516 (B79) *	75° @ 50'	1.6	0.005
4730 (B81)	60° @ 50'	2.1	0.004
5194 (B82)	45° @ 50'	2.2	0.005
6385 (B83)	30° @ 50'	2.0	0.005
6387 (B84)	15° @ 50'	2.0	0.005
5265 (B85)	0° @ 50'	2.3	0.005
520 (B96)*	75° @ 85'	0.6	0.002
5256(B109)*	105° @ 130'	0.5	0.002
261 (B113)*	75° @ 130'	0.5	0.002
5078(115)*	60° @ 130'		
524 (B130) *	75° @ 200'	0.4	0.002

* HOB GAGES

HE2-3, 4.5#, SHOT 3399

GAGE #	POSITION	Pmax (psi)	MAX IMPULSE(psi-sec)
(A)	under vessel 10"	No Gage	No Gage
(B)	under vessel 78"	No Gage	No Gage
(C)	under vessel 146"	No Gage	No Gage
(D)	90° @ 1'	29.0	0.024
(E)	90° @ 5'	20.0	0.042
6156 (B3)	150° @ 10'	15.7	0.018
5269 (B4)	135° @ 10'	16.3	0.018
5193 (B5)	120° @ 10'	17.0	0.018
6158 (B7)	105° @ 10'	19.4	0.022
4727 (B9)	90° @ 10'	16.3	0.020
262 (B11) *	75° @ 10'	BAD	BAD
5221 (B13)	60° @ 10'	17.7	0.018
6160 (B15)	30° @ 10'	18.8	0.023
5203 (B16)	15° @ 10'	16.8	0.019
5075 (B25)	98° @ 15'	15.1	0.014
516 (B27) *	75° @ 15'	5.8	0.013
5266 (B30)	60° @ 15'	15.0	0.012
6391 (B32)	30° @ 15'	24.1	0.013
517 (B34)*	0° @ 15'	12.9	0.013
6390 (B37)	150° @ 22'	10.6	0.011
5256 (B38)	135° @ 22'	10.8	0.009
7247 (B39)	120° @ 22'	12.0	0.011
5239 (B41)	105° @ 22'	10.7	0.008
6400 (B43)	90° @ 22'	10.9	0.009
250 (B45) *	75° @ 22'	3.0	0.006
4799 (B47)	60° @ 22'	12.5	0.009
5252 (B49)	30° @ 22'	11.0	0.008
4024 (B51)	0° @ 22'	BAD	BAD
6384 (B60)	90° @ 34'	8.9	0.006
5250 (B62)	75° @ 34'	4.9	0.006
5274 (B64)	60° @ 34'	5.2	0.006
5215 (B66)	30° @ 34'	6.8	0.008
6389 (B68)	0° @ 34'	8.5	0.008
5222 (B71)	150° @ 50'	3.0	0.005
5233 (B72)	135° @ 50'	3.9	0.006
7253 (B73)	120° @ 50'	3.1	0.006
6386 (B75)	105° @ 50'	3.3	0.005
5211 (B77)	90° @ 50'	2.8	0.005
5078 (B79)	75° @ 50'	3.5	0.006
4730 (B81)	60° @ 50'	3.1	0.003
5194 (B82)	45° @ 50'	3.3	0.006
6385 (B83)	30° @ 50'	3.2	0.005
6387 (B84)	15° @ 50'	3.4	0.005
5265 (B85)	0° @ 50'	3.2	0.005
520 (B96)*	75° @ 85'	0.8	0.003
523 (B113) *	75° @ 130'	0.4	0.002
524 (B130) *	75° @ 200'	No Gage	No Gage

* HOB GAGES

HE2-2, 4.5#, SHOT 3404

GAGE #	POSITION	Pmax (psi)	MAX IMPULSE(psi-sec)
(A)	under vessel 10"	No Gage	No Gage
(B)	under vessel 78"	No Gage	No Gage
(C)	under vessel 146"	No Gage	No Gage
(D)	90° @ 1'	No Gage	No Gage
(E)	90° @ 5'	No Gage	No Gage
6156 (B3)	150° @ 10'	29.1	0.021
5269 (B4)	135° @ 10'	29.3	0.021
5193 (B5)	120° @ 10'	25.6	0.021
6158 (B7)	105° @10'	23.2	0.024
4727 (B9)	90° @10'	23.4	0.023
516 (B11)*	75° @10'	10.6	0.013
5221 (B13)	60° @ 10'	31.2	0.021
6160 (B15)	30° @ 10'	28.4	0.021
5203 (B16)	15° @ 10'	34.6	0.021
5075 (B25)	98° @ 15'	36.4	0.018
528 (B27)*	75° @15'	5.3	0.013
5266 (B30)	60° @ 15'	18.1	0.015
6391 (B32)	30° @ 15'	32.6	0.021
517 (B34)*	0° @ 15'	BAD	BAD
6390 (B37)	150° @ 22'	9.0	0.011
6154 (B38)	135° @ 22'	10.2	0.011
7247 (B39)	120° @ 22'	12.3	0.013
5239 (B41)	105° @ 22'	9.9	0.009
6400 (B43)	90° @ 22'	11.5	0.013
250 (B45)*	75° @ 22'	2.6	0.009
4799 (B47)	60° @ 22'	10.8	0.010
5252 (B49)	30° @ 22'	9.0	0.009
4024 (B51)	0° @ 22'	10.0	0.011
6384 (B60)	90° @ 34'	5.1	0.006
5250 (B62)	75° @ 34'	4.0	0.007
5274 (B64)	60° @ 34'	4.4	0.007
5215 (B66)	30° @ 34'	5.5	0.010
6389 (B68)	0° @ 34'	4.6	0.010
5222 (B71)	150° @ 50'	2.5	0.006
5233 (B72)	135° @ 50'	3.3	0.007
7253 (B73)	120° @ 50'	2.4	0.006
6386 (B75)	105° @ 50'	2.8	0.006
5211 (B77)	90° @ 50'	2.2	0.006
5258 (B79)	75° @ 50'	2.5	0.005
4730 (B81)	60° @ 50'	2.3	0.004
5194 (B82)	45° @ 50'	2.7	0.006
6385 (B83)	30° @ 50'	2.4	0.005
6387 (B84)	15° @ 50'	2.5	0.005
5265 (B85)	0° @ 50'	2.5	0.005
520 (B96)*	75° @ 85'	0.7	0.003
261 (B113)*	75° @ 130'	0.5	0.003
524 (B130)*	75° @ 200'	No Gage	No Gage

* HOB GAGES

HE1-3, 4.5#, SHOT 3526

GAGE #	POSITION	Pmax (psi)	MAX IMPULSE(psi-sec)
(A)	under vessel 10"	No Gage	No Gage
(B)	under vessel 78"	No Gage	No Gage
(C)	under vessel 146"	No Gage	No Gage
(D)	90° @ 1'	No Gage	No Gage
(E)	90° @ 5'	No Gage	No Gage
6156 (B3)	150° @ 10'	31.2	0.019
5269 (B4)	135° @ 10'	28.2	0.019
5193 (B5)	120° @ 10'	27.5	0.017
6158 (B7)	105° @10'	20.1	0.018
4727 (B9)	90° @10'	26.4	0.020
516 (B11)*	75° @10'	10.5	0.015
5221 (B13)	60° @ 10'	31.4	0.017
6160 (B15)	30° @ 10'	27.8	0.024
5203 (B16)	15° @ 10'	30.9	0.016
5075 (B25)	98° @ 15'	30.9	0.014
528 (B27)*	75° @15'	11.6	0.014
5266 (B30)	60° @ 15'	17.9	0.014
6391 (B32)	30° @ 15'	21.4	0.019
517 (B34)*	0° @ 15'	BAD	BAD
6390 (B37)	150° @ 22'	6.7	0.010
6154 (B38)	135° @ 22'	7.6	0.010
7247 (B39)	120° @ 22'	9.1	0.011
5239 (B41)	105° @ 22'	7.6	0.009
6400 (B43)	90° @ 22'	8.8	0.013
250 (B45)*	75° @ 22'	4.7	0.009
4799 (B47)	60° @ 22'	7.9	0.009
5252 (B49)	30° @ 22'	6.5	
4024 (B51)	0° @ 22'	7.3	0.010
6384 (B60)	90° @ 34'	3.7	0.005
5250 (B62)	75° @ 34'	3.6	0.006
5274 (B64)	60° @ 34'	3.5	0.006
5215 (B66)	30° @ 34'	4.5	0.009
6389 (B68)	0° @ 34'	3.8	0.008
5222 (B71)	150° @ 50'	2.2	0.005
5233 (B72)	135° @ 50'	2.7	0.006
7253 (B73)	120° @ 50'	2.0	0.006
6386 (B75)	105° @ 50'	2.3	0.005
5211 (B77)	90° @ 50'	1.9	0.005
5258 (B79)	75° @ 50'	2.1	0.004
4730 (B81)	60° @ 50'	1.9	0.003
5194 (B82)	45° @ 50'	2.3	0.005
6385 (B83)	30° @ 50'	2.0	0.004
6387 (B84)	15° @ 50'	2.2	0.004
5265 (B85)	0° @ 50'	2.1	0.004
520 (B96)*	75° @ 85'	0.6	0.002
261 (B113)*	75° @ 130'	0.5	0.002
524 (B130)*	75° @ 200'	No Gage	No Gage

* HOB GAGES

GAGE POSITION	ORIENTATION/RANGE	Pmax (psi)	MAX IMPULSE(psi-sec)
A	270° @ 1'	122.8	1.569
B*	270° @ 3'	NO DATA	NO DATA
C	90° @ 5'	10.8	0.033
D*	270° @ 3'	NO DATA	NO DATA
B3	150° @ 10'	5.2	0.032
B4*	135° @ 10'	2.8	0.015
B5	120° @ 10'	6.6	0.030
B7	105° @ 10'	7.9	0.041
B9	90° @ 10'	8.8	0.054
B13	60° @ 10'	6.8	0.035
B15	30° @ 10'	7.2	0.032
B16	15° @ 10'	5.2	0.014
B26	90° @ 15'	3.8	0.025
B30	60° @ 15'	2.4	0.018
B32	30° @ 15'	1.7	0.010
B34*	0° @ 11.5'	1.4	0.005
B37	150° @ 22'	1.0	0.006
B38*	135° @ 22'	BAD	BAD
B39	120° @ 22'	1.5	0.011
B41	105° @ 22'	1.7	0.015
B43	90° @ 22'	BAD	BAD
B45*	75° @ 22'	1.3	0.011
B47	60° @ 22'	1.8	0.013
B49	30° @ 22'	1.1	0.006
B51	0° @ 22'	2.3	0.009
B60	90° @ 34'	2.3	0.021
B62	75° @ 34'	2.1	0.017
B64	60° @ 34'	1.7	0.014
B66	30° @ 34'	2.9	0.010
B68	0° @ 34'	1.9	0.008
B71	150° @ 50'	1.2	0.008
B72*	135° @ 50'	1.0	0.007
B73	120° @ 50'	1.2	0.009
B75	105° @ 50'	1.8	0.013
B77	90° @ 50'	1.5	0.011
B79*	75° @ 50'	0.9	0.006
B81	60° @ 50'	1.2	0.010
B82	45° @ 50'	1.1	0.008
B83	30° @ 50'	1.3	0.007
B84	15° @ 50'	1.3	0.007
B85	0° @ 50'	1.1	0.006
B96*	75° @ 85'	3.0	0.009
B109*	105° @127' 2"	BAD	BAD
B113*	75° @ 130' 2"	BAD	BAD
B115*	60° @ 130' 4"	1.5	0.013
B130*	75° @ 192' 5"	0.4	0.004
* HOB GAGES			

GAGE #	POSITION	Pmax (psi)	Pmax (psi) Filtered	MAX IMPULSE(psi-sec)
A	90° @ 1'	BAD	BAD	BAD
B	90° @ 5'	18.6	16.5	BAD
C	180° @ 5'	26.5	22.0	BAD
D	0° @ 5'	20.6	18.3	0.016
E*	135° @ 5'	20.8	19.6	0.014
F*	45° @ 5'	32.3	27.1	0.013
B1	180° @ 10'	31.3	29.5	BAD
B2	165° @ 10'	14.0	11.4	0.014
B3	150° @ 10'	13.3	9.5	0.013
B4*	135° @ 10'	7.4	6.4	0.012
B5	120° @ 10'	10.9	8.1	0.013
B6	112° @ 10'	7.1	6.3	0.011
B7	105° @ 10'	10.1	9.5	0.013
B9	90° @ 10'	11.8	9.5	0.011
B11	75° @ 10'	14.1	10.4	0.013
B12*	68° @ 10'	8.5	7.2	0.013
B13	60° @ 10'	21.3	19.2	0.021
B14*	45° @ 10'	7.8	6.7	0.012
B15	30° @ 10'	14.7	12.6	0.013
B16	15° @ 10'	14.3	10.7	0.013
B17	0° @ 10'	13.8	12.6	0.017
B20	150° @ 15'	8.1	7.8	0.012
B26	90° @ 15'	6.2	5.7	0.009
B32	30° @ 15'	6.9	6.7	0.010
B37	150° @ 22'	5.4	4.4	0.006
B40*	112° @ 22'	3.8	3.2	0.006
B43	90° @ 22'	3.7	3.5	0.006
B46*	68° @ 22'	3.3	3.0	0.006
B49	30° @ 22'	4.1	3.7	0.006
B52	180° @ 34'	2.1	2.1	0.004
B53	165° @ 34'	2.2	2.1	0.004
B54	150° @ 34'	2.5	2.4	0.004
B55	135° @ 34'	2.2	2.1	0.004
B56	120° @ 34'	2.3	2.1	0.004
B58	105° @ 34'	2.0	1.9	0.004
B60	90° @ 34'	2.1	2.0	0.004
B62	75° @ 34'	2.2	2.1	0.004
B63*	68° @ 34'	BAD	BAD	BAD
B64	60° @ 34'	2.5	2.4	0.004
B65	45° @ 34'	1.9	1.8	0.004
B66	30° @ 34'	2.6	2.5	0.005
B67	15° @ 34'	2.5	2.4	0.004
B68	0° @ 34'	2.2	2.1	0.004
B71	150° @ 50'	1.5	1.4	0.003
B77	90° @ 50'	1.2	1.2	0.003
B80*	68° @ 50'	1.2	1.0	0.003
B82	45° @ 50'	1.3	1.3	0.003
B83	30° @ 50'	1.2	1.2	0.002

* HOB GAGES
Filter - Low Pass 4000 Hz

P-2, 4700 psi @ 3.5' HOB, SHOT 3245

GAGE #	POSITION	Pmax (psi)	MAX IMPULSE(psi-sec)
5175 (B1)	180 @ 10'	NO GAGE	NO GAGE
6799 (B3)	150 @ 10'	12.6	0.028
262 (B4) *	135 @10'	6.5	0.018
6800 (B5)	120 @10'	13.8	0.044
584 (B9)	90 @10'	126.5	0.100
6577 (B13)	60 @ 10'	15.1	0.051
6796 (B15)	30 @ 10'	12.7	0.036
6391 (B17)	0 @10'	11.8	0.033
6570 (B26)	90 @ 15'	15.5	0.074
6797 (B30)	60 @ 15'	13.0	0.060
5257 (B32)	30 @ 15'	10.0	0.034
5176 (B34)	0 @ 15'	9.0	0.025
6801 (B37)	150 @ 22'	5.4	0.020
261 (B38) *	135 @ 22'	7.6	0.034
4792 (B39)	120 @ 22'	7.0	0.035
6802 (B41)	105 @ 22'	8.4	0.056
514 (B42)	98 @ 22'	8.1	0.050
6798 (B43) *	90 @ 22'	10.2	0.061
4572 (B47)	60 @ 22'	7.5	0.044
6395 (B49)	30 @ 22'	7.9	0.025
5256 (B50)	15 @ 22'	5.9	0.025
5215 (B51)	0 @ 22'	5.7	0.021
5254 (B60)	90 @ 34'	6.9	0.039
5194 (B62)	75 @ 34'	7.1	0.048
5269 (B64)	60 @ 34'	7.2	0.033
6795 (B65)	45 @ 34'	5.7	0.024
4727 (B66)	30 @ 34'	5.6	0.020
5236 (B67)	15 @ 34'	4.3	0.015
6394 (B68)	0 @ 34'	4.0	0.014
5255 (B71)	150 @ 50'	2.1	0.009
512 (B72) *	135 @ 50'	2.4	0.014
5076 (B73)	120 @ 50'	2.8	0.015
6385 (B75)	105 @ 50'	4.0	0.019
527 (B76)	98 @ 50'	3.9	0.023
6392 (B77) *	90 @ 50'	5.7	0.022
6162 (B79)	75 @ 50'	3.9	0.021
4555 (B81)	60 @ 50'	3.2	0.020
5085 (B82)	45 @ 50'	3.1	0.014
5277 (B83)	30 @ 50'	2.1	0.013
5078 (B84)	15 @ 50'	2.0	0.011
5245 (B85)	0 @ 50'	1.9	0.009
525 (B96) *	75 @ 85'	1.8	0.012
258 (B98) *	60 @ 85'	3.8	0.020
250 (B99) *	45 @ 85'	NO DATA	NO DATA
520 (B109) *	105 @130'	0.9	0.006
515 (B113) *	75 @ 130'	1.1	0.010
517 (B115) *	60 @ 130'	1.2	0.008
255 (B130) *	75 @ 200'	0.9	0.007

* HOB GAGES

P-1, 3250 psi @ 3.5' HOB, SHOT 3248

GAGE #	POSITION	Pmax (psi)	MAX IMPULSE(psi-sec)
6799 (B3)	150 @ 10'	7.5	0.028
262 (B4) *	135 @10'	4.4	0.022
6800 (B5)	120 @10'	13.6	0.038
5175 (B7)	105 @ 10'	10.0	0.050
6803 (B9)	90 @ 10'	13.1	0.060
6391 (B11)	75 @ 10'	14.3	0.060
5187 (B13)	60 @ 10'	9.0	0.040
6796 (B15)	30 @ 10'	9.9	0.031
4718 (B26)	90 @ 15'	10.1	0.064
6797 (B30)	60 @ 15'	9.0	0.053
5257 (B32)	30 @ 15'	7.5	0.027
5176 (B34)	0 @ 15'	6.7	0.018
6801 (B37)	150 @ 22'	4.0	0.019
261 (B38) *	135 @ 22'	5.5	0.034
4792 (B39)	120 @ 22'	5.6	0.028
6802 (B41)	105 @ 22'	5.7	0.044
514 (B42)	98 @ 22'	6.8	0.058
6798 (B43) *	90 @ 22'	7.2	0.061
4572 (B47)	60 @ 22'	5.6	0.038
6395 (B49)	30 @ 22'	6.5	0.020
5256 (B50)	15 @ 22'	5.2	0.019
5215 (B51)	0 @ 22'	4.9	0.017
5254 (B60)	90 @ 34'	5.0	0.037
5194 (B62)	75 @ 34'	5.5	0.038
5269 (B64)	60 @ 34'	4.9	0.027
6795 (B65)	45 @ 34'	3.6	0.019
4727 (B66)	30 @ 34'	4.4	0.016
5236 (B67)	15 @ 34'	3.1	0.010
6394 (B68)	0 @ 34'	3.7	0.012
5255 (B71)	150 @ 50'	1.5	0.007
512 (B72) *	135 @ 50'	2.1	0.013
5076 (B73)	120 @ 50'	1.9	0.013
6385 (B75)	105 @ 50'	2.9	0.016
527 (B76)	98 @ 50'	3.1	0.022
6392 (B77) *	90 @ 50'	4.2	0.019
6162 (B79)	75 @ 50'	2.8	0.018
4555 (B81)	60 @ 50'	2.6	0.016
5085 (B82)	45 @ 50'	2.2	0.011
5277 (B83)	30 @ 50'	1.6	0.009
5078 (B84)	15 @ 50'	1.5	0.008
5245 (B85)	0 @ 50'	1.8	0.008
525 (B96) *	75 @ 85'	2.2	0.014
258 (B98) *	60 @ 85'	4.8	0.026
250 (B99) *	45 @ 85'	3.5	0.025
520 (B109) *	105 @130'	1.8	0.014
515 (B113) *	75 @ 130'	2.1	0.019
517 (B115) *	60 @ 130'	2.1	0.017
255 (B130) *	75 @ 200'	1.5	0.013

* HOB GAGES

C-6

GAGE POSITION	ORIENTATION/RANGE	Pmax (psi)	MAX IMPULSE(psi-sec)
A	270° @ 1'	122.8	1.569
B *	270° @ 3'	NO DATA	NO DATA
C	90° @ 5'	10.8	0.033
D *	270° @ 3'	NO DATA	NO DATA
B3	150° @ 10'	5.2	0.032
B4 *	135° @ 10'	2.8	0.015
B5	120° @ 10'	6.6	0.030
B7	105° @ 10'	7.9	0.041
B9	90° @ 10'	8.8	0.054
B13	60° @ 10'	6.8	0.035
B15	30° @ 10'	7.2	0.032
B16	15° @ 10'	5.2	0.014
B26	90° @ 15'	3.8	0.025
B30	60° @ 15'	2.4	0.018
B32	30° @ 15'	1.7	0.010
B34 *	0° @ 11.5'	1.4	0.005
B37	150° @ 22'	1.0	0.006
B38 *	135° @ 22'	BAD	BAD
B39	120° @ 22'	1.5	0.011
B41	105° @ 22'	1.7	0.015
B43	90° @ 22'	BAD	BAD
B45 *	75° @ 22'	1.3	0.011
B47	60° @ 22'	1.8	0.013
B49	30° @ 22'	1.1	0.006
B51	0° @ 22'	2.3	0.009
B60	90° @ 34'	2.3	0.021
B62	75° @ 34'	2.1	0.017
B64	60° @ 34'	1.7	0.014
B66	30° @ 34'	2.9	0.010
B68	0° @ 34'	1.9	0.008
B71	150° @ 50'	1.2	0.008
B72 *	135° @ 50'	1.0	0.007
B73	120° @ 50'	1.2	0.009
B75	105° @ 50'	1.8	0.013
B77	90° @ 50'	1.5	0.011
B79 *	75° @ 50'	0.9	0.006
B81	60° @ 50'	1.2	0.010
B82	45° @ 50'	1.1	0.008
B83	30° @ 50'	1.3	0.007
B84	15° @ 50'	1.3	0.007
B85	0° @ 50'	1.1	0.006
B96 *	75° @ 85'	3.0	0.009
B109 *	105° @127' 2"	BAD	BAD
B113 *	75° @ 130' 2"	BAD	BAD
B115 *	60° @ 130' 4"	1.5	0.013
B130 *	75° @ 192' 5"	0.4	0.004
* HOB GAGES			

1-3, 5425 psi @ 3.5' HOB, SHOT 3253

GAGE POSITION	ORIENTATION/RANGE	Pmax (psi)	MAX IMPULSE(psi-sec)
A	270° @ 1'	310.0	5.261
B*	270° @ 3'	(10 ?)	
C	90° @ 5'	18.2	0.048
D*	270° @ 3'	(12.3 ?)	
B3	150° @ 10'	12.1	0.036
B4*	135° @ 10'	12.0	0.037
B5	120° @ 10'	18.0	0.052
B7	105° @ 10'	16.7	0.060
B9	90° @ 10'	16.7	0.065
B13	60° @ 10'	17.0	0.051
B15	30° @ 10'	18.7	0.024
B16	15° @ 10'	11.6	0.028
B26	90° @ 15'	12.7	0.083
B30	60° @ 15'	17.7	0.051
B32	30° @ 15'	11.3	0.035
B34*	0° @ 11.5'	15.3	0.023
B37	150° @ 22'	5.0	0.025
B38*	135° @ 22'	BAD	BAD
B39	120° @ 22'	7.9	0.051
B41	105° @ 22'	8.0	0.070
B43	90° @ 22'	BAD	BAD
B45*	75° @ 22'	7.3	0.036
B47	60° @ 22'	10.2	0.058
B49	30° @ 22'	7.2	0.024
B51	0° @ 22'	4.6	0.020
B60	90° @ 34'	6.6	0.042
B62	75° @ 34'	5.8	0.028
B64	60° @ 34'	5.3	0.031
B66	30° @ 34'	4.2	0.021
B68	0° @ 34'	4.0	0.017
B71	150° @ 50'	3.0	0.015
B72*	135° @ 50'	2.5	0.016
B73	120° @ 50'	3.8	0.021
B75	105° @ 50'	5.4	0.028
B77	90° @ 50'	4.4	0.022
B79*	75° @ 50'	4.0	0.013
B81	60° @ 50'	3.9	0.021
B82	45° @ 50'	3.0	0.015
B83	30° @ 50'	3.5	0.014
B84	15° @ 50'	3.5	0.015
B85	0° @ 50'	2.7	0.013
B96*	75° @ 85'	2.5	0.006
B109*	105° @127' 2"	0.9	0.007
B113*	75° @ 130' 2"	1.6	0.005
B115*	60° @ 130' 4"	0.7	0.007
B130*	75° @ 192' 5"	0.4	0.003

* HOB GAGES

1-2, 3450 psi @ 3.5' HOB, SHOT 3252

GAGE POSITION	ORIENTATION/RANGE	Pmax (psi)	MAX IMPULSE(psi-sec)
A	270° @ 1'	NO DATA	NO DATA
B*	270° @ 3'	NO DATA	NO DATA
C	90° @ 5'	21.1	0.655
D*	270° @ 3'	NO DATA	NO DATA
B3	150° @ 10'	9.1	0.025
B4*	135° @10'	8.2	0.043
B5	120° @ 10'	12.5	0.046
B7	105° @ 10'	13.4	0.059
B9	90° @10'	13.1	0.060
B13	60° @ 10'	11.2	0.044
B15	30° @ 10'	8.8	0.028
B16	15° @ 10'	7.9	0.019
B26	90° @ 15'	18.0	0.072
B30	60° @ 15'	11.8	0.043
B32	30° @ 15'	6.8	0.027
B34*	0° @ 11.5'	16.8	0.016
B37	150° @ 22'	6.0	0.020
B38*	135° @ 22'	5.1	0.025
B39	120° @ 22'	6.1	0.038
B41	105° @ 22'	8.0	0.058
B43	90° @ 22'	8.7	0.066
B45*	75° @ 22'	6.4	0.038
B47	60° @ 22'	7.7	0.045
B49	30° @ 22'	5.7	0.019
B51	0° @ 22'	4.2	0.013
B60	90° @ 34'	5.1	0.040
B62	75° @ 34'	5.6	0.038
B64	60° @ 34'	4.3	0.027
B66	30° @ 34'	3.3	0.013
B68	0° @ 34'	4.3	0.016
B71	150° @ 50'	2.6	0.012
B72*	135° @ 50'	2.3	0.013
B73	120° @ 50'	3.2	0.017
B75	105° @ 50'	4.6	0.022
B77	90° @ 50'	4.3	0.020
B79*	75° @ 50'	3.4	0.011
B81	60° @ 50'	3.3	0.019
B82	45° @ 50'	2.5	0.013
B83	30° @ 50'	2.9	0.012
B84	15° @ 50'	2.9	0.011
B85	0° @ 50'	2.2	0.010
B96*	75° @ 85'	2.5	0.008
B109*	105° @ 127' 2"	0.8	0.006
B113*	75° @ 130' 2"	BAD	BAD
B115*	60° @ 130' 4"	0.7	0.006
B130*	75° @ 192' 5"	0.7	0.005

* HOB GAGES

1-4, 7125 psi @ 3.5' HOB, SHOT 3402

GAGE #	POSITION	Pmax (psi)	MAX IMPULSE(psi·sec)
(A)	under vessel 10"	No Gage	No Gage
(B)	under vessel 78"	No Gage	No Gage
(C)	under vessel 146"	No Gage	No Gage
(D)	90° @ 1'	No data from tape #4	No data from tape #4
(E)	90° @ 5'	No data from tape #4	No data from tape #4
6156 (B3)	150° @ 10'	11.3	0.030
528 (B4)*	135° @ 10'	8.7	0.027
5193 (B5)	120° @ 10'	14.9	0.039
6158 (B7)	105° @ 10'	15.7	0.052
4727 (B9)	90° @ 10'	15.4	0.048
5221 (B13)	60° @ 10'	16.4	0.044
6160 (B15)	30° @ 10'	13.8	0.037
5203 (B16)	15° @ 10'	11.5	0.030
5075 (B25)	98° @ 15'	15.0	0.043
5266 (B30)	60° @ 15'	12.7	0.051
6391 (B32)	30° @ 15'	16.2	0.039
517 (B34)*	0° @ 15'	9.0	0.033
6390 (B37)	150° @ 22'	6.7	0.030
264 (B38)	135° @ 22'	9.0	0.035
7247 (B39)	120° @ 22'	11.0	0.053
5239 (B41)	105° @ 22'	10.1	0.050
6400 (B43)	90° @ 22'	-23.5	0.160
250 (B45)*	75° @ 22'	6.2	0.033
4799 (B47)	60° @ 22'	8.8	0.046
5252 (B49)	30° @ 22'	6.0	0.040
5205 (B51)	0° @ 22'	4.5	0.021
6384 (B60)	90° @ 34'	9.3	0.032
5250 (B62)	75° @ 34'	6.1	0.036
5274 (B64)	60° @ 34'	5.5	0.028
6389 (B66)	30° @ 34'	5.6	0.025
6389 (B68)	0° @ 34'	5.5	0.018
5222 (B71)	150° @ 50'	3.0	0.015
262 (B72)*	135° @ 50'	2.9	0.017
7253 (B73)	120° @ 50'	4.1	0.024
6386 (B75)	105° @ 50'	4.7	0.023
5211 (B77)	90° @ 50'	4.0	0.024
516 (B79)*	75° @ 50'	3.1	0.021
5194 (B81)	60° @ 50'	3.6	0.018
6385 (B82)	30° @ 50'	3.7	0.018
6387 (B84)	15° @ 50'	No data from tape #4	No data from tape #4
5265 (B85)	0° @ 50'	No data from tape #4	No data from tape #4
520 (B96)*	75° @ 85'	No data from tape #4	No data from tape #4
5256 (B109)*	105° @ 130'	BAD	BAD
261 (B113)*	75° @ 130'	No data from tape #4	No data from tape #4
5078 (B115)*	60° @ 130'	1.0	0.007
524 (B130)*	75° @ 200'	No data from tape #4	No data from tape #4

* HOB GAGES

2-1, 3450 psi @ 3.5' HOB, SHOT 3403

GAGE #	POSITION	Pmax (psi)	MAX IMPULSE(psi·sec)
(AA)		225.0	3.1
(B)	under vessel 78"	No Gage	No Gage
(C)	under vessel 146"	No Gage	No Gage
(D)	90° @ 1'	55.0 (pushback)	1.365
(E)	90° @ 5'	(15 - 20.0)	0.066
6156 (B3)	150° @ 10'	8.2	0.025
5269 (B4)	135° @ 10'	8.1	0.030
5193 (B5)	120° @ 10'	8.5	0.036
6158 (B7)	105° @ 10'	10.6	0.050
4727 (B9)	90° @ 10'	10.1	0.048
516 (B11)*	75° @ 10'	8.5	0.030
5221 (B13)	60° @ 10'	10.0	0.030
6160 (B15)	30° @ 10'	9.5	0.037
5203 (B16)	15° @ 10'	6.7	0.031
5075 (B25)	98° @ 15'	8.5	0.046
528 (B27)*	75° @ 15'	BAD	BAD
5266 (B30)	60° @ 15'	8.5	0.041
6391 (B32)	30° @ 15'	8.4	0.030
517 (B34)*	0° @ 15'	5.0	0.021
6390 (B37)	150° @ 22'	4.7	0.019
6154 (B38)	135° @ 22'	5.1	0.022
7247 (B39)	120° @ 22'	6.4	0.039
5239 (B41)	105° @ 22'	6.1	0.043
6400 (B43)	90° @ 22'	8.7	0.053
250 (B45)*	75° @ 22'	4.0	0.025
4799 (B47)	60° @ 22'	5.5	0.032
5252 (B49)	30° @ 22'	3.8	0.015
4024 (B51)	0° @ 22'	3.5	0.015
6384 (B60)	90° @ 34'	4.5	0.026
5250 (B62)	75° @ 34'	3.9	0.026
5274 (B64)	60° @ 34'	3.5	0.019
5215 (B66)	30° @ 34'	4.1	0.017
6389 (B68)	0° @ 34'	2.7	0.012
5222 (B71)	150° @ 50'	2.3	0.010
5233 (B72)	135° @ 50'	3.2	0.014
7253 (B73)	120° @ 50'	2.8	0.016
6386 (B75)	105° @ 50'	3.3	0.017
5211 (B77)	90° @ 50'	2.8	0.017
5258 (B79)	75° @ 50'	2.9	0.015
4730 (B81)	60° @ 50'	2.3	0.010
5194 (B82)	45° @ 50'	2.4	0.011
6385 (B83)	30° @ 50'	1.9	0.009
6387 (B84)	15° @ 50'	1.8	0.008
5265 (B85)	0° @ 50'	1.7	0.008
520 (B96)*	75° @ 85'	1.0	0.007
261 (B113)*	75° @ 130'	0.8	0.006
524 (B130)*	75° @ 200'	No Gage	No Gage

* HOB GAGES

2-3, 3475 psi @ 14.0' HOB, SHOT 3398

GAGE #	POSITION	Pmax (psi)	MAX IMPULSE(psi-sec)
(A)	under vessel 10"	BAD	BAD
(B)	under vessel 78"	9.0	0.017
(C)	under vessel 146"	8.0	0.025
(D)	90° @ 1'	77.3	0.545
(E)	90° @ 5'	29.4	0.228
6156 (B3)	150° @ 10'	9.6	0.031
5269 (B4)	135° @ 10'	8.8	0.041
5193 (B5)	120° @ 10'	8.4	0.052
6158 (B7)	105° @ 10'	9.3	0.074
4727 (B9)	90° @ 10'	15.7	0.192
262 (B11) *	75° @ 10'	BAD	BAD
5221 (B13)	60° @ 10'	9.6	0.070
6160 (B15)	30° @ 10'	11.2	0.045
5203 (B16)	15° @ 10'	8.6	0.034
5075 (B25)	98° @ 15'	7.9	0.050
516 (B27) *	75° @15'	4.7	0.032
5266 (B30)	60° @ 15'	8.5	0.046
6391 (B32)	30° @ 15'	11.6	0.028
517 (B34) *	0° @ 15'	3.2	0.006
6390 (B37)	150° @ 22'	5.5	0.016
5256 (B38)	135° @ 22'	5.2	0.021
7247 (B39)	120° @ 22'	6.9	0.032
5239 (B41)	105° @ 22'	6.3	0.032
6400 (B43)	90° @ 22'	6.6	0.046
250 (B45) *	75° @22'	6.2	0.042
4799 (B47)	60° @ 22'	6.4	0.030
5252 (B49)	30° @ 22'	5.0	0.019
4024 (B51)	0° @ 22'	5.9	0.010
6384 (B60)	90° @ 34'	8.1	0.021
5250 (B62)	75° @ 34'	4.9	0.023
5274 (B64)	60° @ 34'	5.3	0.018
5215 (B66)	30° @ 34'	5.6	0.015
6389 (B68)	0° @ 34'	6.0	0.011
5222 (B71)	150° @ 50'	3.0	0.008
5233 (B72)	135° @ 50'	4.2	0.013
7253 (B73)	120° @ 50'	4.1	0.015
6386 (B75)	105° @ 50'	4.2	0.015
5211 (B77)	90° @ 50'	4.3	0.015
5078 (B79)	75° @ 50'	5.1	0.015
4730 (B81)	60° @ 50'	4.3	0.022
5194 (B82)	45° @ 50'	3.4	0.012
6385 (B83)	30° @ 50'	3.3	0.009
6387 (B84)	15° @ 50'	2.9	0.008
5265 (B85)	0° @ 50'	2.8	0.009
520 (B96) *	75° @ 85'	1.2	0.006
523 (B113) *	75° @ 130'	0.7	0.005
524 (B130) *	75° @ 200'	No Gage	No Gage

* HOB GAGES

2-2, 3450 psi @ 8.7' HOB, SHOT 3400

GAGE #	POSITION	Pmax (psi)	MAX IMPULSE(psi-sec)
(A)	under vessel 10"	56.3 (Before damaged)	BAD
(B)	under vessel 78"	26.0	0.035
(C)	under vessel 146"	6.5	0.019
(D)	90° @ 1'	134.4	0.295
(E)	90° @ 5'	18.0	0.194
6156 (B3)	150° @ 10'	8.5	0.029
5269 (B4)	135° @ 10'	7.7	0.038
5193 (B5)	120° @ 10'	11.4	0.049
6158 (B7)	105° @ 10'	11.5	0.079
4727 (B9)	90° @10'	9.9	0.132
262 (B11) *	75° @10'	BAD	BAD
5221 (B13)	60° @ 10'	11.6	0.055
6160 (B15)	30° @ 10'	10.7	0.039
5203 (B16)	15° @ 10'	9.0	0.029
5075 (B25)	98° @ 15'	7.9	0.052
516 (B27) *	75° @15'	5.8	0.038
5266 (B30)	60° @ 15'	9.4	0.041
6391 (B32)	30° @ 15'	10.9	0.029
517 (B34) *	0° @ 15'	2.8	0.011
6390 (B37)	150° @ 22'	6.2	0.018
5256 (B38)	135° @ 22'	6.8	0.022
7247 (B39)	120° @ 22'	9.0	0.036
5239 (B41)	105° @ 22'	6.9	0.031
6400 (B43)	90° @ 22'	7.5	0.047
250 (B45) *	75° @22'	3.7	0.025
4799 (B47)	60° @ 22'	8.1	0.026
5252 (B49)	30° @ 22'	5.5	0.016
4024 (B51)	0° @ 22'	5.0	0.014
6384 (B60)	90° @ 34'	8.0	0.019
5250 (B62)	75° @ 34'	4.6	0.020
5274 (B64)	60° @ 34'	4.3	0.018
5215 (B66)	30° @ 34'	5.0	0.017
6389 (B68)	0° @ 34'	5.0	0.012
5222 (B71)	150° @ 50'	2.4	0.010
5233 (B72)	135° @ 50'	3.4	0.014
7253 (B73)	120° @ 50'	3.1	0.015
6386 (B75)	105° @ 50'	3.6	0.014
5211 (B77)	90° @ 50'	2.9	0.014
5078 (B79)	75° @ 50'	3.8	0.014
4730 (B81)	60° @ 50'	2.7	0.007
5194 (B82)	45° @ 50'	2.7	0.012
6385 (B83)	30° @ 50'	2.3	0.009
6387 (B84)	15° @ 50'	2.4	0.009
5265 (B85)	0° @ 50'	2.2	0.008
520 (B96) *	75° @ 85'	1.1	0.006
523 (B113) *	75° @ 130'	0.8	0.005
524 (B130) *	75° @ 200'	No Gage	No Gage

* HOB GAGES

5-2 (6), 3600 psi @ 3.5' HOB, SHOT 3575

GAGE #	POSITION	Pmax (Pmax)	MAX IMPULSE(Psi-sec)
A	90° @ 1'	30.200	0.187
B	90° @ 5'	13.300	0.097
C	180° @ 5'	9.300	0.03
D	0° @ 5'	12.9/51.9	.024/.327
B1	180° @ 10'	7.900	0.030
B2	165° @ 10'	5.4/11.1	0.017
B3	150° @ 10'	6.700	0.022
B4*	135° @ 10'	10.900	0.016
B5	120° @ 10'	10.200	0.037
B6*	112° @ 10'	9.100	0.030
B7	105° @ 10'	11.900	0.047
B9	90° @ 10'	13.300	0.078
B11	75° @ 10'	11.700	0.046
B12*	68° @ 10'	18.500	0.032
B13	60° @ 10'	13.200	0.047
B14	45° @ 10'	10.600	.042/.107
B15	30° @ 10'	7.400	0.022
B16	15° @ 10'	7.700	0.029
B17	0° @ 10'	8.300	0.023
B20	150° @ 15'	5.400	0.017
B26	90° @ 15'	12.500	0.050
B32	30° @ 15'	(5.2?)	BAD
B37	150° @ 22'	4.900	0.013
B40*	112° @ 22'	4.700	0.022
B43	90° @ 22'	6.100	0.039
B46*	68° @22'	5.2/29.2	.035/.190
B49	30° @ 22'	3.800	0.030
B52	180° @ 34'	1.800	0.007
B53	165° @ 34'	1.900	0.008
B54	150° @ 34'	2.900	0.011
B55	135° @ 34'	2.900	0.009
B56	120° @ 34'	2.900	0.015
B58	105° @ 34'	3.800	0.016
B60	90° @ 34'	4.000	0.020
B62	75° @ 34'	4.000	0.028
B63*	68° @ 34'	3.5/10.9	0.024
B64	60° @ 34'	3.300	0.025
B65	45° @ 34'	3.200	0.021
B66	30° @ 34'	3.400	0.019
B67	15° @ 34'	2.700	0.022
B68	0° @ 34'	2.500	0.017
B71	150° @ 50'	1.500	0.006
B77	90° @ 50'	3.900	0.016
B80*	68° @ 50'	2.800	0.016
B82	45° @ 50'	2.700	0.017
B83	30° @ 50'	1.900	0.012
B96*	68° @ 85'	1.700	0.008
B113*	68° @ 135'	0.800	0.005

* HOB GAGES

5-1 (5), 3600 psi @ 3.5' HOB, SHOT 3574

GAGE #	POSITION	Pmax (psi)	MAX IMPULSE(psi-sec)
A	90° @ 1'	BAD	BAD
B	90° @ 5'	12.5	0.092
C	180° @ 5'	8.7	0.018
D	0° @ 5'	15.0/35.8	.025/.363
B1	180° @ 10'	11.6	0.050
B2	165° @ 10'	7.8	0.045
B3	150° @ 10'	6.6	0.020
B4*	135° @ 10'	5.8	0.017
B5	120° @ 10'	8.9	0.030
B6*	112° @ 10'	8.3	0.020
B7	105° @ 10'	9.6	0.038
B9	90° @ 10'	12.1	0.055
B11	75° @ 10'	10.8	0.044
B12*	68° @ 10'	8.9	0.031
B13	60° @ 10'	13.2	0.053
B14	45° @ 10'	11.0	0.033
B15	30° @ 10'	8.3	0.023
B16	15° @ 10'	7.1	0.024
B17	0° @ 10'	6.8	0.022
B20	150° @ 15'	6.2	0.017
B26	90° @ 15'	7.2	0.043
B32	30° @ 15'	6.7	0.026
B37	150° @ 22'	4.9	0.016
B40*	112° @ 22'	4.7	0.023
B43	90° @ 22'	6.8	0.042
B46*	68° @22'	4.8/13.9	.030/.150
B49	30° @ 22'	3.9	0.026
B52	180° @ 34'	2.1	0.007
B53	165° @ 34'	2.1	0.008
B54	150° @ 34'	3.1	0.011
B55	135° @ 34'	2.7	0.009
B56	120° @ 34'	3.3	0.015
B58	105° @ 34'	3.6	0.017
B60	90° @ 34'	3.6	0.020
B62	75° @ 34'	3.9	0.025
B63*	68° @ 34'	3.9/5.3	.023/.078
B64	60° @ 34'	3.5	0.029
B65	45° @ 34'	3.0	0.023
B66	30° @ 34'	3.0	BAD
B67	15° @ 34'	2.9	0.020
B68	0° @ 34'	2.4	0.017
B71	150° @ 50'	1.6	0.007
B77	90° @ 50'	3.9	0.015
B80*	68° @ 50'	3.2	0.016
B82	45° @ 50'	2.9	0.018
B83	30° @ 50'	2.0	0.013
B96*	68° @ 85'	1.6	0.008
B113*	68° @ 135'	0.8	0.005

* HOB GAGES

5-4 (8), 3600 psi @ 3.5' HOB, SHOT 3576

GAGE #	POSITION	Pmax (psi)	MAX IMPULSE(psi-sec)
A	90° @ 1'	94.8	0.666
B	90° @ 5'	16.3	0.034
C	180° @ 5'	9.7	0.014
D	0° @ 5'	13.2/48.0	0.250
B1	180° @ 10'	6.9	0.011
B2	165° @ 10'	4.1	0.007
B3	150° @ 10'	5.2	0.008
B4*	135° @ 10'	4.5	0.009
B5	120° @ 10'	8.5	0.013
B6*	112° @ 10'	5.6	0.012
B7	105° @ 10'	10.6	0.020
B9	90° @ 10'	9.0	0.078
B11	75° @ 10'	11.4	0.038
B12*	68° @ 10'	11.2/34.5	0.061
B13	60° @ 10'	12.9	0.054
B14	45° @ 10'	13.5	0.047
B15	30° @ 10'	10.1	0.035
B16	15° @ 10'	8.7/26.7	0.068
B17	0° @ 10'	8.6/15.8	0.089
B20	150° @ 15'	4.2	0.007
B26	90° @ 15'	6.6	0.019
B32	30° @ 15'	5.7	BAD
B37	150° @ 22'	2.2	0.005
B40*	112° @ 22'	3.0	0.007
B43	90° @ 22'	4.1	0.016
B46*	68° @ 22'	4.4/8.6	0.023
B49	30° @ 22'	5.5	0.039
B52	180° @ 34'	1.1	0.003
B53	165° @ 34'	1.3	0.003
B54	150° @ 34'	1.8	0.004
B55	135° @ 34'	1.7	0.003
B56	120° @ 34'	1.7	0.005
B58	105° @ 34'	2.2	0.007
B60	90° @ 34'	2.7	0.009
B62	75° @ 34'	3.0	0.015
B63*	68° @ 34'	3.0	0.016
B64	60° @ 34'	3.0	0.022
B65	45° @ 34'	3.1	0.026
B66	30° @ 34'	3.6	0.031
B67	15° @ 34'	3.7	0.042
B68	0° @ 34'	3.5	0.038
B71	150° @ 50'	0.9	0.002
B77	90° @ 50'	2.3	0.008
B80*	68° @ 50'	2.2	0.012
B82	45° @ 50'	2.7	0.020
B83	30° @ 50'	2.6	0.019
B96*	68° @ 85'	1.2	0.007
B113*	68° @ 135'	0.6	0.005

* HOB GAGES

5-3 (7), 3600 psi @ 3.5' HOB, SHOT 3577

GAGE #	POSITION	Pmax (psi)	MAX IMPULSE(psi-sec)
A	90° @ 1'	244.7	0.48
B	90° @ 5'	12.9	0.038
C	180° @ 5'	8.2	0.017
D	0° @ 5'	11.8/36.3	0.192
B1	180° @ 10'	5.2	0.009
B2	165° @ 10'	5.1	0.007
B3	150° @ 10'	5.7	0.009
B4*	135° @ 10'	4.9	0.010
B5	120° @ 10'	8.1	0.015
B6*	112° @ 10'	6.4	0.014
B7	105° @ 10'	10.5	0.021
B9	90° @ 10'	9.1	0.064
B11	75° @ 10'	11.4	0.040
B12*	68° @ 10'	11.2	0.046
B13	60° @ 10'	14.4	0.059
B14	45° @ 10'	14.0	0.042
B15	30° @ 10'	9.5	0.033
B16	15° @ 10'	8.3/20.0	0.036
B17	0° @ 10'	9.5/16.3	0.058
B20	150° @ 15'	4.8	0.006
B26	90° @ 15'	7.1	0.020
B32	30° @ 15'	12.2	0.040
B37	150° @ 22'	2.5	0.006
B40*	112° @ 22'	3.1	0.009
B43	90° @ 22'	4.8	0.017
B46*	68° @ 22'	4.9	0.022
B49	30° @ 22'	4.8	0.047
B52	180° @ 34'	1.1	0.002
B53	165° @ 34'	1.2	0.003
B54	150° @ 34'	1.9	0.004
B55	135° @ 34'	2.2	0.004
B56	120° @ 34'	2.2	0.006
B58	105° @ 34'	2.6	0.008
B60	90° @ 34'	3.4	0.010
B62	75° @ 34'	3.1	0.016
B63*	68° @ 34'	3.0	0.016
B64	60° @ 34'	4.0	0.022
B65	45° @ 34'	3.3	0.029
B66	30° @ 34'	3.7	0.036
B67	15° @ 34'	3.4	0.041
B68	0° @ 34'	3.4	0.037
B71	150° @ 50'	1.0	0.002
B77	90° @ 50'	2.6	0.009
B80*	68° @ 50'	2.2	0.013
B82	45° @ 50'	2.8	0.023
B83	30° @ 50'	2.6	0.021
B96*	68° @ 85'	1.2	0.007
B113*	68° @ 135'	0.6	0.005

* HOB GAGES

6A-1 (13), 3280 psi @ 3.5' HOB, SHOT 4053

GAGE#	POSITION	Pmax (psi)	MAX IMPULSE (psi-sec)
A	135° @ 5'	104.0	0.2200
B	90° @ 5'	89.1	0.2400
C	45° @ 5'	119.7	0.2500
B2	165° @ 10'	13.8	0.0493
B3	150° @ 10'	25.8	0.0586
B4	135° @ 10'	27.9	0.0561
B5	120° @ 10'	26.9	0.0781
B6	112° @ 10'	22.7	0.0796
B7	105° @ 10'	28.7	0.0627
B9	90° @ 10'	36.6	0.0638
B11	75° @ 10'	31.2	0.0888
B12	68° @ 10'	20.7	0.0650
B13	60° @ 10'	24.0	0.0745
B14	45° @ 10'	22.1	0.0632
B15	30° @ 10'	bad	bad
B16	15° @ 10'	17.3	0.0620
B18	180° @ 15'	12.4	0.0416
B20	150° @ 15'	16.7	0.0720
B26	90° @ 15'	18.9	0.0602
B32	30° @ 15'	10.7	0.0512
B34	0° @ 15'	11.0	0.0520
B37	150° @ 22'	7.6	0.0451
B40	112° @ 22'	10.1	0.0521
B43	90° @ 22'	9.1	0.0476
B46	68° @ 22'	8.9	0.0597
B49	30° @ 22'	7.3	0.0446
B52	180° @ 34'	4.5	0.0260
B53	165° @ 34'	5.0	0.0314
B54	150° @ 34'	5.5	0.0322
B55	135° @ 34'	6.3	0.0305
B56	120° @ 34'	6.4	0.0362
B58	105° @ 34'	7.4	0.0338
B60	90° @ 34'	6.0	0.0347
B62	75° @ 34'	8.8	0.0472
B64	60° @ 34'	6.2	0.0375
B65	45° @ 34'	5.9	0.0354
B66	30° @ 34'	4.8	0.0291
B67	15° @ 34'	4.6	0.0268
B68	0° @ 34'	3.9	0.0251
B71	150° @ 50'	3.8	0.0206
B72	135° @ 50'	bad	bad
B73	120° @ 50'	4.8	0.0239
B77	90° @ 50'	4.5	0.0252
B81	60° @ 50'	5.2	0.0278
B82	45° @ 50'	4.4	0.0238
B83	30° @ 50'	3.3	0.0195

6A-2, 4000 psi @ 3.5' HOB, SHOT 4054

GAGE#	POSITION	Pmax (psi)	MAX IMPULSE (psi-sec)
A	135° @ 5'	21.7	0.0167
B	90° @ 5'	38.9	0.0245
C	45° @ 5'	24.7	0.0252
B2	165° @ 10'	8.7	0.0113
B3	150° @ 10'	8.1	0.0109
B4	135° @ 10'	9.2	0.0112
B5	120° @ 10'	10.2	0.0131
B6	112° @ 10'	11.7	0.0128
B7	105° @ 10'	13.9	0.0128
B9	90° @ 10'	15.3	0.0135
B11	75° @ 10'	12.5	0.0192
B12	68° @ 10'	15.4	0.0154
B13	60° @ 10'	13.4	0.0182
B14	45° @ 10'	14.9	0.0154
B15	30° @ 10'	15.9	0.0167
B16	15° @ 10'	17.0	0.0167
B18	180° @ 15'	4.5	0.0046
B20	150° @ 15'	4.8	0.0053
B26	90° @ 15'	4.6	0.0054
B32	30° @ 15'	4.6	0.0068
B34	0° @ 15'	7.1	0.0088
B37	150° @ 22'	3.9	0.0057
B40	112° @ 22'	5.0	0.0060
B43	90° @ 22'	4.2	0.0063
B46	68° @ 22'	4.7	0.0074
B49	30° @ 22'	4.8	0.0095
B52	180° @ 34'	2.7	0.0038
B53	165° @ 34'	2.4	0.0041
B54	150° @ 34'	2.6	0.0041
B55	135° @ 34'	2.6	0.0037
B56	120° @ 34'	2.5	0.0039
B58	105° @ 34'	2.1	0.0039
B60	90° @ 34'	2.0	0.0037
B62	75° @ 34'	2.7	0.0055
B64	60° @ 34'	2.3	0.0050
B65	45° @ 34'	2.6	0.0056
B66	30° @ 34'	2.7	0.0056
B67	15° @ 34'	3.0	0.0056
B68	0° @ 34'	3.3	0.0056
B71	150° @ 50'	1.4	0.0027
B72	135° @ 50'	bad	bad
B73	120° @ 50'	1.4	0.0027
B77	90° @ 50'	1.4	0.0027
B81	60° @ 50'	1.6	0.0039
B82	45° @ 50'	1.7	0.0038
B83	30° @ 50'	1.7	0.0036

6A-4 (10), 3500 psi @ 3.5' HOB, SHOT 4056

GAGE#	POSITION	Pmax (psi)	MAX IMPULSE (psi-sec)
A	135° @ 5'	154.5	0.3200
B	90° @ 5'	66.4	0.1914
C	45° @ 5'	152.5	0.4900
B2	165° @ 10'	bad	bad
B3	150° @ 10'	bad	bad
B4	135° @ 10'	bad	bad
B5	120° @ 10'	bad	bad
B6	112° @ 10'	bad	bad
B7	105° @ 10'	42.2	0.0639
B9	90° @ 10'	47.5	0.0655
B11	75° @ 10'	46.5	0.0878
B12	68° @ 10'	bad	bad
B13	60° @ 10'	56.3	0.1061
B14	45° @ 10'	37.4	0.1031
B15	30° @ 10'	42.9	0.1894
B16	15° @ 10'	81.0	0.1140
B18	180° @ 15'	24.6	0.0267
B20	150° @ 15'	20.3	0.0498
B26	90° @ 15'	32.0	0.0747
B32	30° @ 15'	25.5	0.0501
B34	0° @ 15'	27.0	0.0299
B37	150° @ 22'	10.3	0.0297
B40	112° @ 22'	23.0	0.0525
B43	90° @ 22'	25.9	0.0643
B46	68° @ 22'	23.1	0.0694
B49	30° @ 22'	12.6	0.0346
B52	180° @ 34'	5.7	0.0160
B53	165° @ 34'	5.6	0.0197
B54	150° @ 34'	7.1	0.0211
B55	135° @ 34'	9.3	0.0268
B56	120° @ 34'	11.4	0.0330
B58	105° @ 34'	13.7	0.0375
B60	90° @ 34'	12.5	0.0420
B62	75° @ 34'	13.0	0.0527
B64	60° @ 34'	9.7	0.0341
B65	45° @ 34'	8.7	0.0285
B66	30° @ 34'	5.9	0.0203
B67	15° @ 34'	5.8	0.0185
B68	0° @ 34'	6.0	0.0142
B71	150° @ 50'	3.4	0.0150
B72	135° @ 50'	bad	bad
B73	120° @ 50'	6.4	0.0239
B77	90° @ 50'	8.7	0.0358
B81	60° @ 50'	6.8	0.0286
B82	45° @ 50'	5.3	0.0204
B83	30° @ 50'	4.4	0.0149

6A-3 (4), 3300 psi @ 3.5' HOB, SHOT 4055

GAGE#	POSITION	Pmax (psi)	MAX IMPULSE (psi-sec)
A	135° @ 5'	21.7	0.0277
B	90° @ 5'	38.8	0.0300
C	45° @ 5'	13.0	0.0304
B2	165° @ 10'	6.0	0.0232
B3	150° @ 10'	9.8	0.0259
B4	135° @ 10'	12.3	0.0335
B5	120° @ 10'	17.8	0.0549
B6	112° @ 10'	19.8	0.0566
B7	105° @ 10'	15.8	0.0462
B9	90° @ 10'	15.8	0.0514
B11	75° @ 10'	21.6	0.0722
B12	68° @ 10'	17.1	0.0565
B13	60° @ 10'	23.9	0.0642
B14	45° @ 10'	bad	bad
B15	30° @ 10'	7.9	0.0280
B16	15° @ 10'	7.3	0.0195
B18	180° @ 15'	7.6	0.0207
B20	150° @ 15'	11.3	0.0306
B26	90° @ 15'	13.9	0.0589
B32	30° @ 15'	6.6	0.0257
B34	0° @ 15'	7.6	0.0205
B37	150° @ 22'	5.6	0.0233
B40	112° @ 22'	10.0	0.0519
B43	90° @ 22'	9.4	0.0534
B46	68° @ 22'	9.7	0.0502
B49	30° @ 22'	5.7	0.0246
B52	180° @ 34'	4.1	0.0141
B53	165° @ 34'	4.2	0.0162
B54	150° @ 34'	4.6	0.0185
B55	135° @ 34'	6.3	0.0220
B56	120° @ 34'	7.6	0.0279
B58	105° @ 34'	6.8	0.0354
B60	90° @ 34'	6.5	0.0357
B62	75° @ 34'	8.3	0.0447
B64	60° @ 34'	5.8	0.0282
B65	45° @ 34'	5.1	0.0232
B66	30° @ 34'	3.8	0.0172
B67	15° @ 34'	3.9	0.0158
B68	0° @ 34'	4.2	0.0130
B71	150° @ 50'	2.9	0.0123
B72	135° @ 50'	bad	bad
B73	120° @ 50'	4.3	0.0188
B77	90° @ 50'	5.0	0.0223
B81	60° @ 50'	4.5	0.0223
B82	45° @ 50'	3.7	0.0165
B83	30° @ 50'	2.6	0.0122

APPENDIX D

Overpressure/Impulse Coefficients

Index

Table D-1
Pressure Coefficients for LSC Detonations

LSC Charge N+	grains per ft.	Coefficient		Error, std dev., % of reading
		B_n	B_1	
1A-2, 1A-3 combined	10	2.57403	-1.15727	16.9
1A-5, 1A-6 combined	15	3.22303	-1.29661	19.3
1A-1, 1A-4, 1A-7 combined	25	3.38636	-1.24933	19.9
1B-2, 1B-3 combined	50	3.11826	-1.01572	20.5
1B-1, 1B-4 combined	200	4.29318	-1.22225	25.9
2-1	25	3.31845	-1.26838	30.0
2-2	25	not reduced, similar to 2-1		

Table D-2
Symmetric Pressure Coefficients for Vessel Burst

Vessel Burst	Coefficient		Error, Std. dev., % reading
	B_n	B_1	
P-2	5.05345	-.98558	29.6
P-1	5.00237	-1.05581	26.5
1-1	3.71934	-.90354	46.8
1-2	4.44026	-.83577	24.0
1-3	5.14076	-.98428	26.1
1-4	4.83746	-.86672	30.0
2-1	4.39180	-.88109	23.9
2-2	4.92157	-.96390	21.1
2-3	4.75478	-.86476	19.2
PC	5.96755	-1.45037	16.1
5-1	4.20666	-.86358	25.4
5-2	4.43625	-.93645	29.7
5-3	4.32214	-.93868	47.4
5-4	4.48667	-1.01354	44.9
6A-1	6.41996	-1.32488	30.3
6A-2	5.61240	-1.33255	23.7
6A-3	4.51066	-.81016	38.0
6A-4[1]	7.31726	-1.45505	33.2
6A-4[2]	6.47962	-1.18289	38.2

[1]For radial distance
[2]For distances normal to vessel axis

Table D-3
Symmetric Impulse Coefficients for Vessel Burst

Vessel Burst	Coefficient		error, std. dev., % of reading
	B_n	B_1	
P-2	5.44016	-.66163	42.0
P-1	5.82760	-.82635	45.9
1-1	5.07290	-.79185	55.2
1-2	5.32406	-.64697	49.8
1-3	5.42485	-.62706	42.0
1-4	4.95254	-.45454	33.9
2-1	5.41929	-.72406	37.9
2-2	6.84018	-1.12561	37.4
2-3	7.72843	-1.33472	49.0
PC	4.96020	-1.00060	13.3
5-1	4.86168	-.58916	53.3
5-2	5.40752	-.75853	56.4
5-3	5.04190	-.74506	144.7
5-4	5.24812	-.82165	135.4
6A-1	6.33977	-.82148	24.8
6A-2	4.60186	-.87193	27.6
6A-3	4.54099	-.40119	42.5
6A-4[1]	7.30874	-1.13451	48.8
6A-4[2]	6.79787	-.93861	39.7

[1]For radial distances
[2]For distances normal to vessel axis

Table D-4
Asymmetric Pressure Coefficients for Vessel Burst

Vessel Burst	Coefficient				$\phi,^1$ deg	error, std. dev., % of reading
	B_n	B_1	B_2	B_3		
P-2	5.80369	-1.08903	-.00932	---	80	15.1
P-1	5.24688	-1.04286	-.00700	---	80	17.9
1-1	3.90297	-.91138	-.00390	---	80	43.4
1-2	4.67180	-.81933	-.00680	---	90	11.9
1-3	5.45171	-.98185	-.00764	---	80	14.3
1-4	5.22369	-.90703	-.00662	---	95	22.4
2-1	4.63716	-.87346	-.00629	---	95	13.0
2-2	.12293	2.12668	-.00425	-.46848	85	15.2
2-3	6.98762	-2.06836	-.00424	.17331	80	15.9
PC	5.90204	-1.44416	.00092	---	100	15.7
5-1	4.54765	-.88896	-.00542	---	75	16.9
5-2	4.73660	-.91404	-.00798	---	80	16.6
5-3	5.00056	-.99360	-.00960	---	55	15.9
5-4	5.13864	-1.06984	-.00862	---	50	15.8
6A-1	6.60403	-1.29551	-.00640	---	95	22.6
6A-2	5.80860	-1.33704	-.00216	---	5	20.8
6A-3	4.82324	-.76885	-.01018	---	95	20.6
6A-4[2]	7.49824	-1.42274	-.00660	---	80	27.4
6A-4[3]	6.73789	-1.20199	0	0	---	19.8

[1] Best fit center array angle, and strongest blast angle if B_2 less than zero
[2] For radial distances
[3] For distances normal to vessel axis

Table D-5
Asymmetric Impulse Coefficients for Vessel Burst

Vessel Burst	Coefficient				ϕ, deg[1]	error, std. dev., % of reading
	C_n	C_1	C_2	C_3		
P-2	6.62655	-.82523	-.01474	---	80	16.3
P-1	6.36686	-.79778	-.01544	---	80	19.5
1-1	5.65255	-.81658	-.01230	---	80	39.0
1-2	5.80677	-.61270	-.01418	---	90	19.6
1-3	5.94240	-.62301	-.01271	---	80	25.5
1-4	5.44440	-.50587	-.00843	---	95	25.6
2-1	5.84232	-.71089	-.01085	---	95	18.8
2-2	8.56167	-1.88809	-.01127	.11325	85	23.5
2-3	20.38713	-8.41012	-.01482	1.02299	80	19.4
PC	4.98115	-1.00259	-.00030	---	100	13.1
5-1	5.52768	-.63873	-.01059	---	75	27.8
5-2	5.91690	-.72052	-.01354	---	80	26.5
5-3	6.51361	-.86414	-.02082	---	55	44.3
5-4	6.77268	-.95328	-.02015	---	50	48.7
6A-1	6.45241	-.80351	-.00392	---	95	22.2
6A-2	4.90008	-.87874	-.00329	---	5	20.9
6A-3	4.91664	-.35155	-.01223	---	95	29.6
6A-4[2]	7.58337	-1.08548	-.01002	---	80	34.8
6A-4[3]	6.98007	-.95196	0	0	---	36.8

[1] Best fit center array angle, and strongest blast angle if B_2, Table D-4, less than zero (based on pressure measurements)
[2] For radial distances
[3] For distances normal to vessel axis

APPENDIX E

OVERPRESSURE/IMPULSE PLOTS
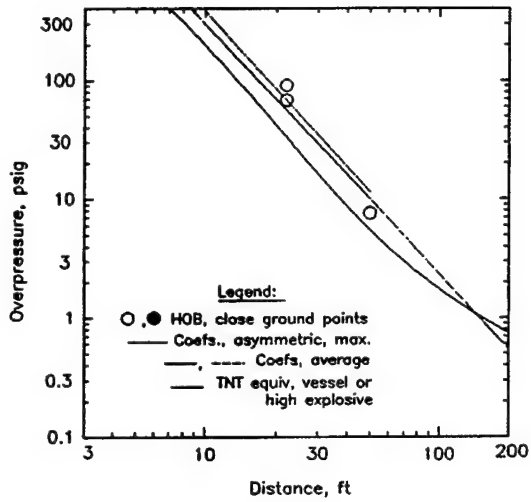
(file = P3201DTR.SPG)
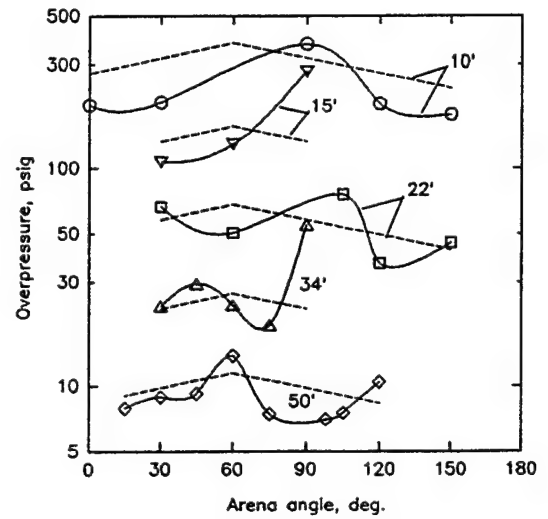
(file = P3201ATR.SPG)
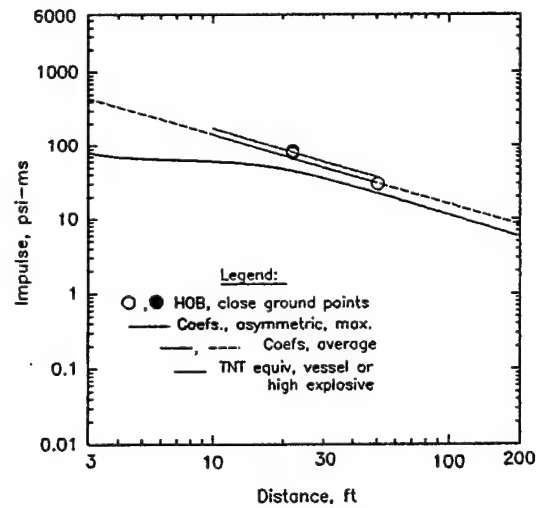
(file = I3201DTR.SPG)

Figure E.1, 65 lbs C-4 detonated at 3.5′ HOB above center of arena, 6-21-90 (PHE-2) (94.0 lbs TNT equiv.)
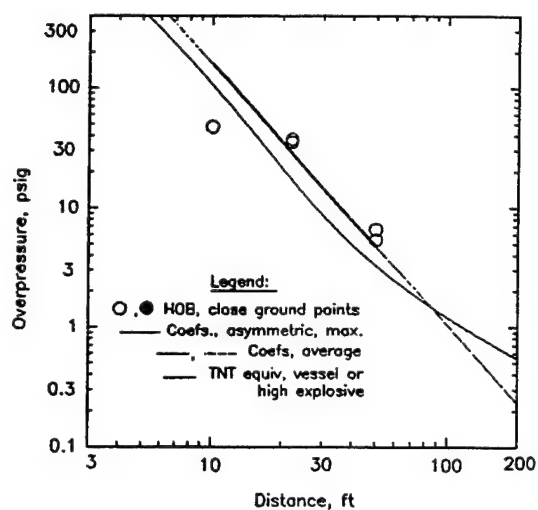
(file = P3249DTR.SPG)
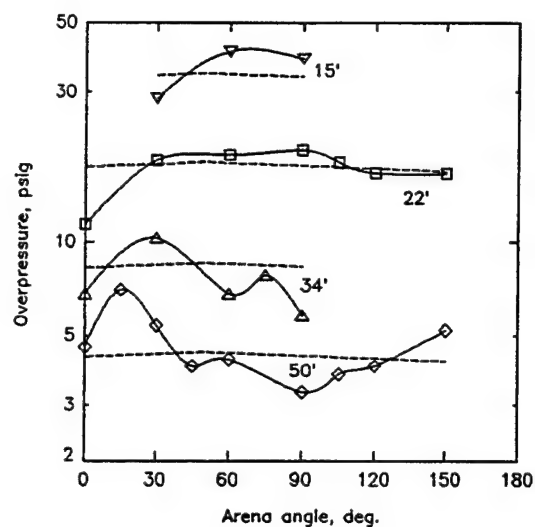
(file = P3249ATR.SPG)
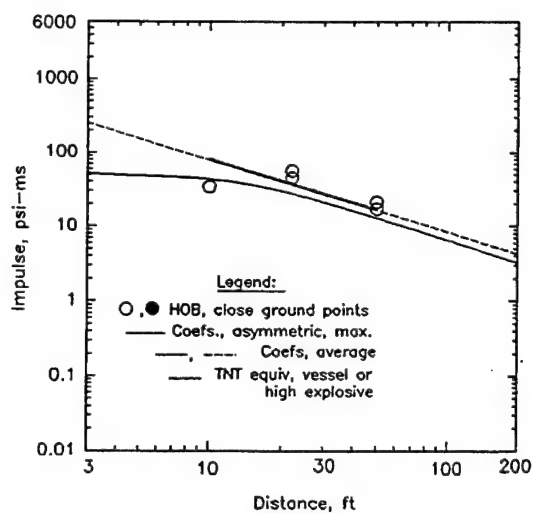
(file = I3249DTR.SPG)

Figure E.2, 33.3 lbs of composition B detonated at 3.5′ HOB above center of arena, 6-26-90 (PHE-1) (40.0 lbs TNT equiv.)
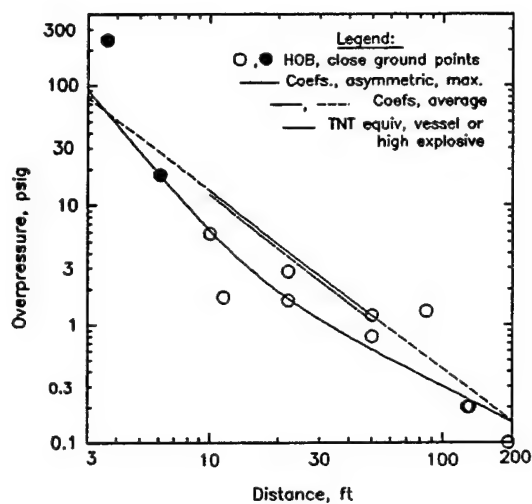
(file = P3250DTR.SPG)
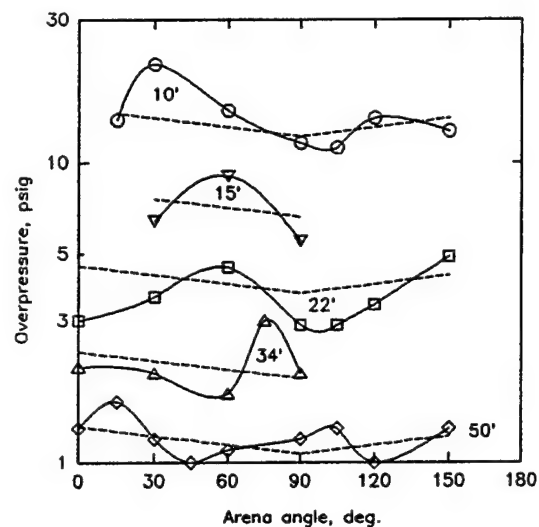
(file = P3250ATR.SPG)
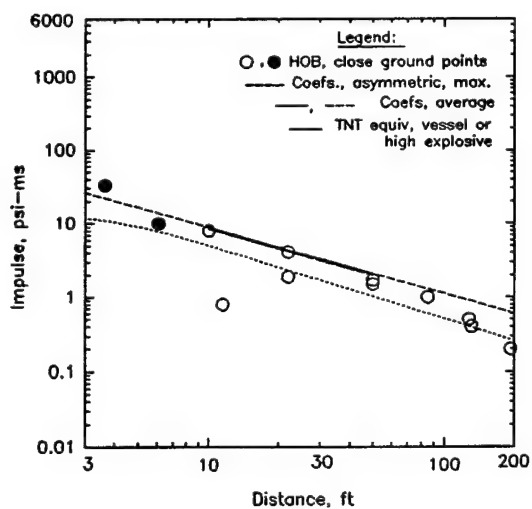
(file = I3250DTR.SPG)
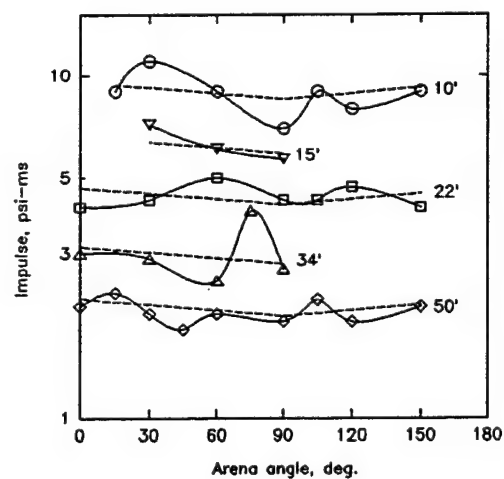
(file = I3250ATR.SPG)

Figure E.3, 0.66 lbs of pentolite detonated at 3.5' HOB above center of arena, 1-28-91 (HE 1-1) (.89 lbs TNT equiv.)
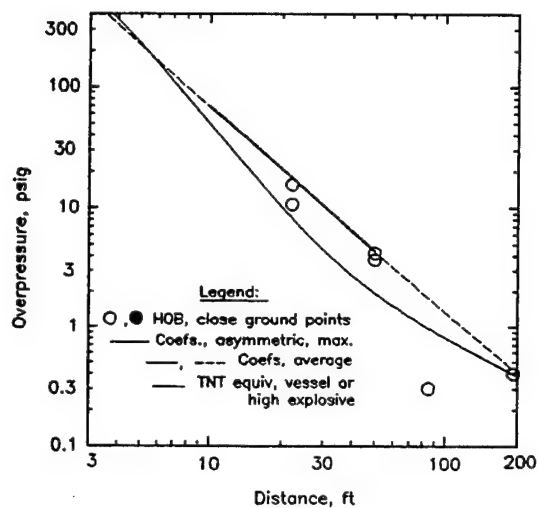
(file = P3256DTR.SPG)
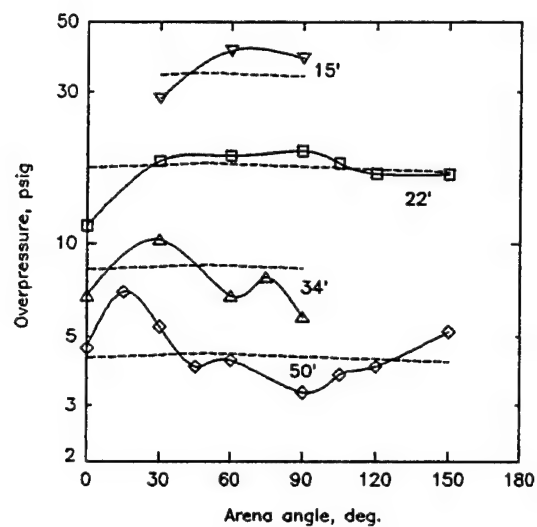
(file = P3256ATR.SPG)
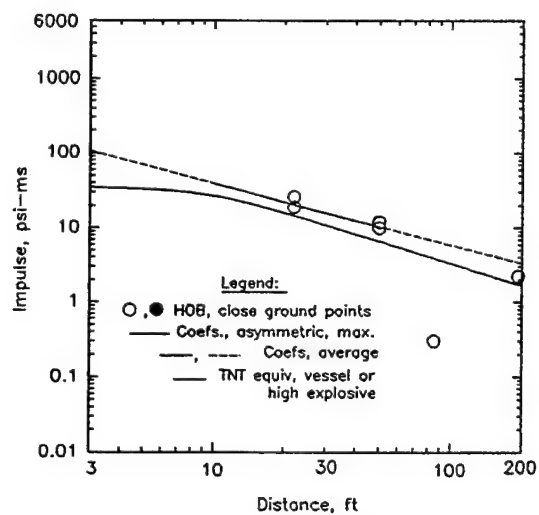
(file = I3256DTR.SPG)

Figure E.4, 9.9 lbs of pentolite detonated at 3.5′ HOB above center of arena, 1-28-91 (HE 1-2) 14.6 lbs TNT equiv.)
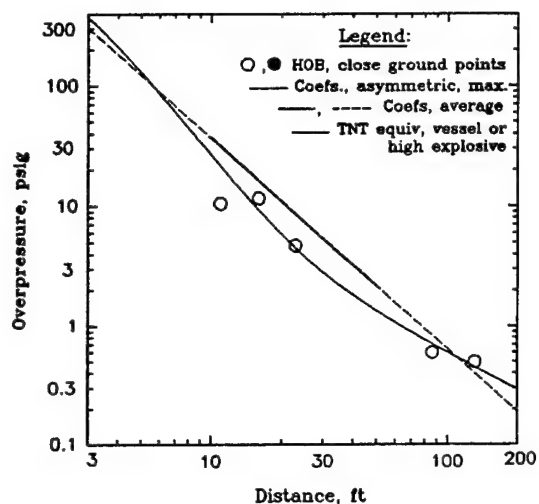
(file = P3526DTR.SPG)
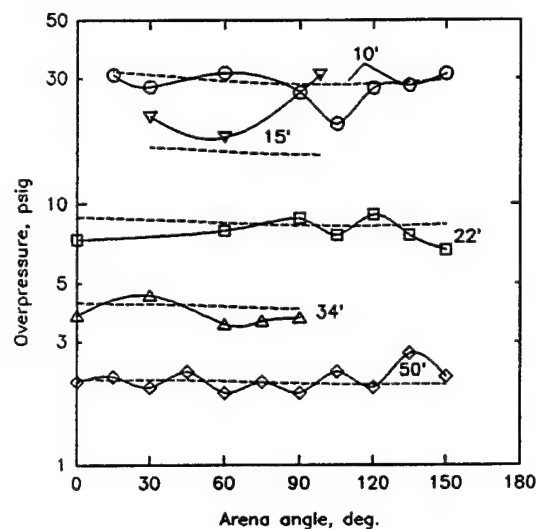
(file = P3526ATR.SPG)
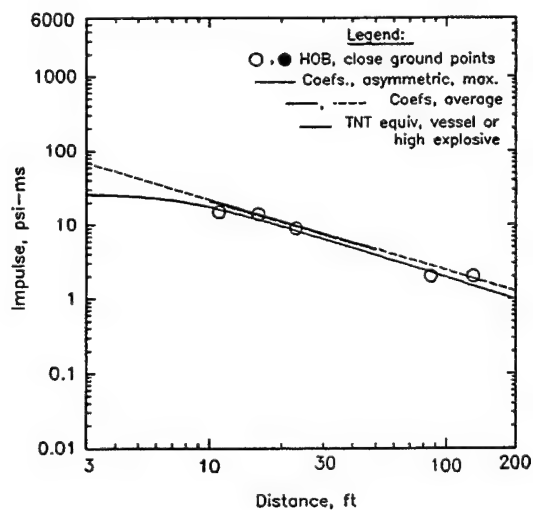
(file = I3526DTR.SPG)

**Figure E.5, 4.5 lbs of pentolite detonated at 3.5′ HOB,
above center of arena, 7-20-91 (HE 1-3) (6.6 lbs TNT equiv.)**
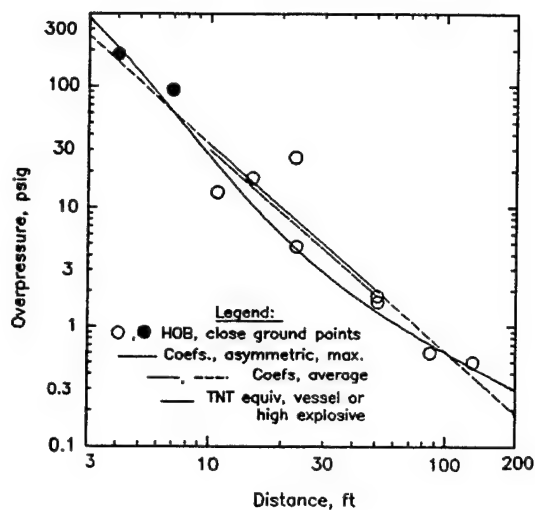
(file = P3401DTR.SPG)
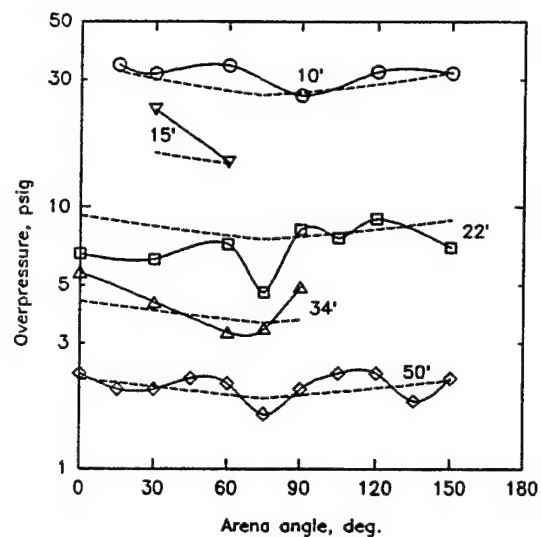
(file = P3401ATR.SPG)
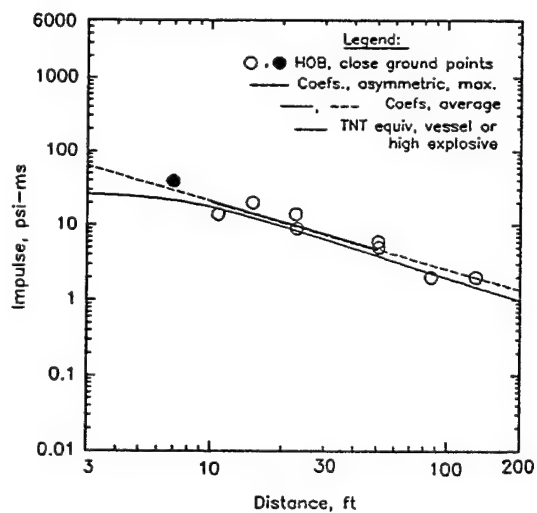
(file = I3401DTR.SPG)

**Figure E.6, 4.5 lbs of pentolite detonated at 3.5′ HOB
above center of arena, 7-18-91 (HE 2-1) (6.6 lbs TNT equiv.)**
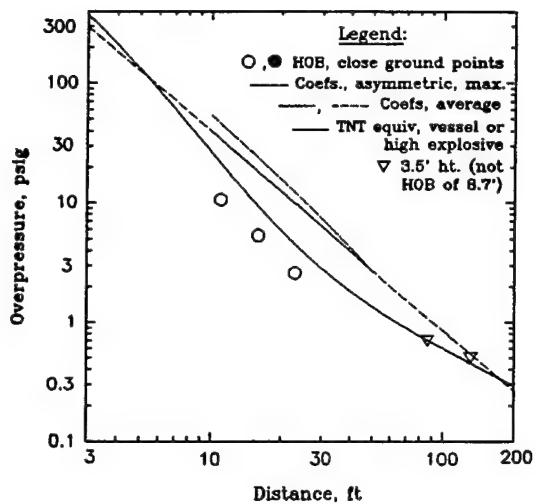
(file = P3404DTR.SPG)
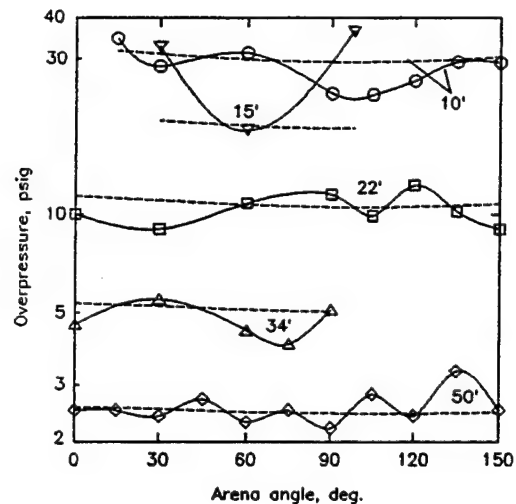
(file = P3404ATR.SPG)
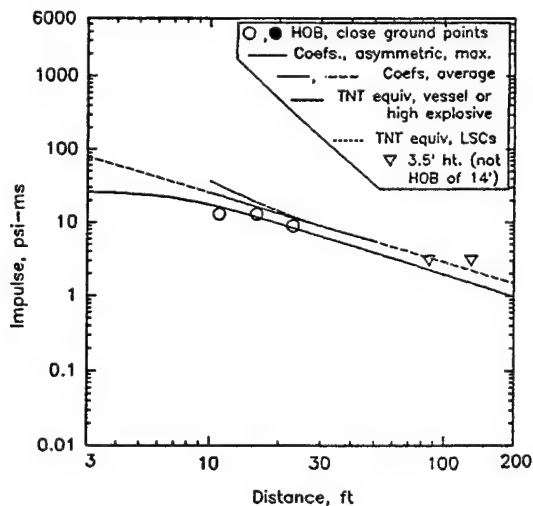
(file = I3404DTR.SPG)

Figure E.7, 4.5 lbs of pentolite detonated at 8.7′ HOB, offset 1' away from center of arena, 7-20-91 (HE 2-2) (6.6 lbs TNT equiv.)
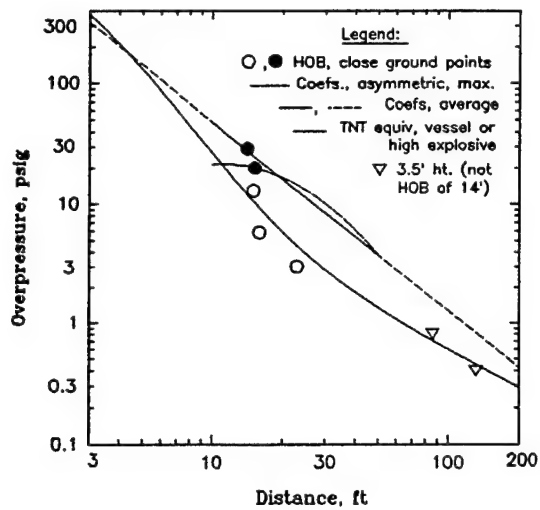
(file = P3399DTR.SPG)
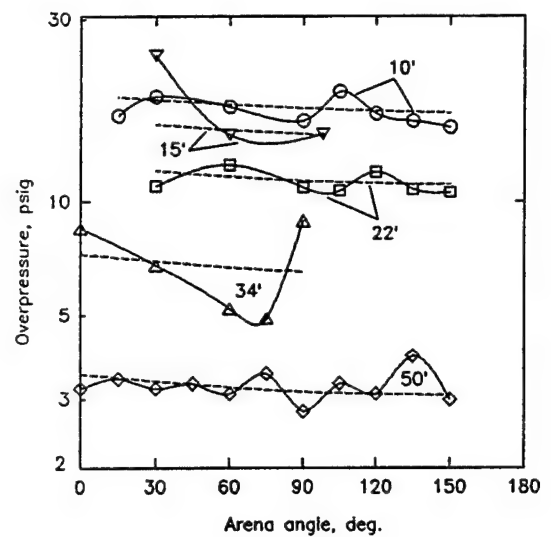
(file = P3399ATR.SPG)
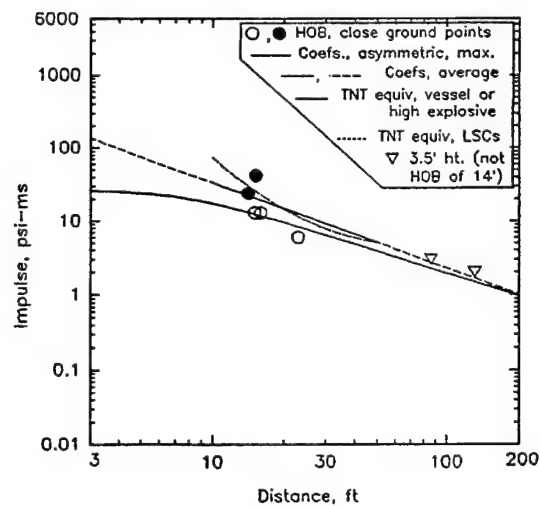
(file = I3399DTR.SPG)

Figure E.8, 4.5 lbs of pentolite detonated at 14′ HOB, offset 1′ away from center of arena, 7-16-91 (HE 2-3) (6.6 lbs TNT equiv.)
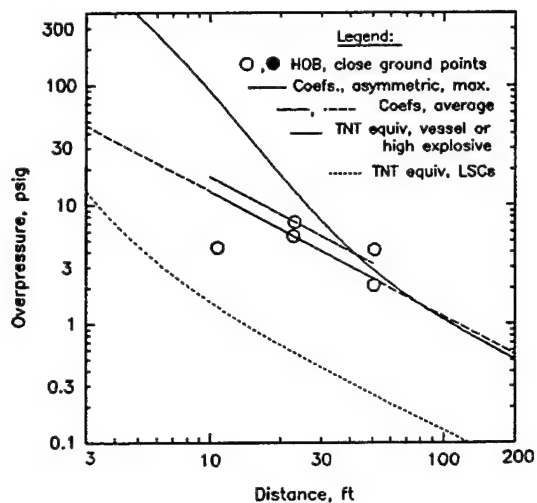
(file = P3248DTR.SPG)
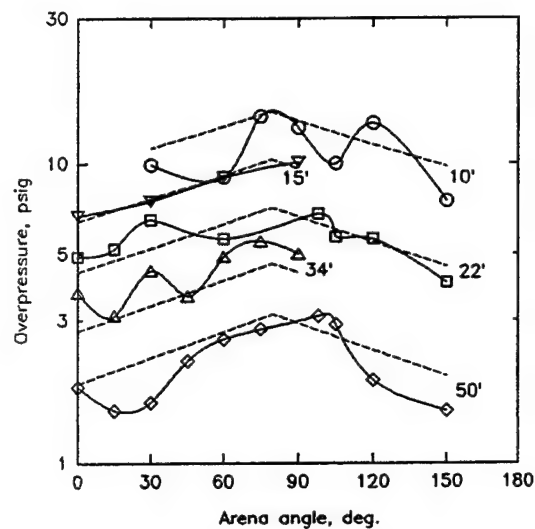
(file = P3248ATR.SPG)
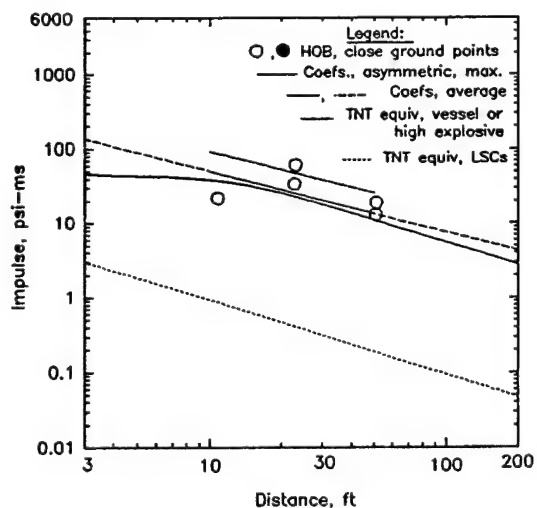
(file = I3248DTR.SPG)
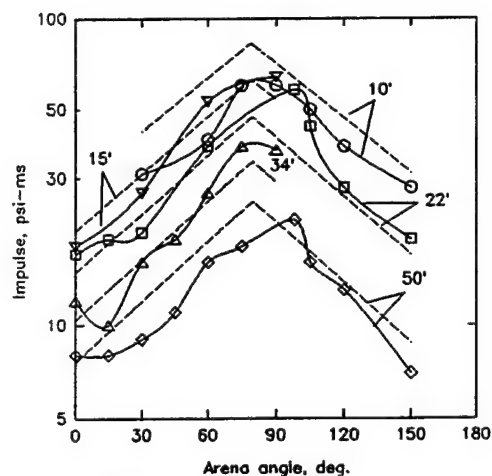
Distances per arena layout, on the ground,
not corrected for offset

(file = I3248ATR.SPG)

Figure E.9, 2′ dia. steel vessel, 53 cu. ft. volume, 3250 psi, split at near center at 3.5′ HOB, 1′ offset away from center of arena, 6-26-90 (P-1) (TNT equivs: gas = 31.7, LSC = .07)
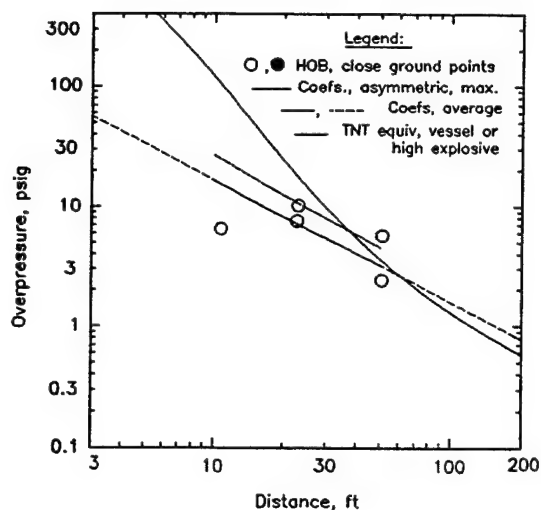
(file = P3245DTR.SPG)
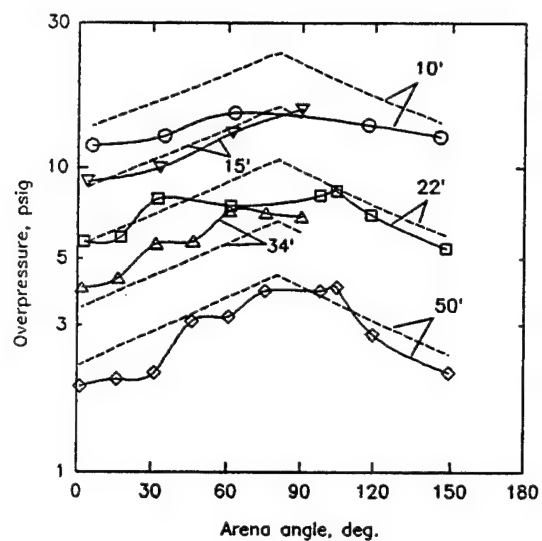
(file = P3245ATR.SPG)
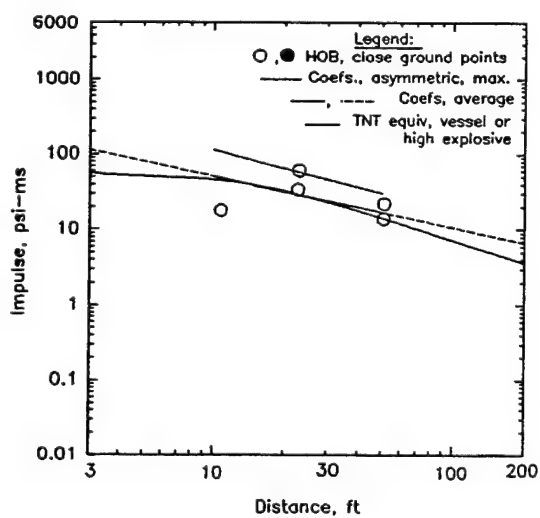
(file = I3245DTR.SPG)
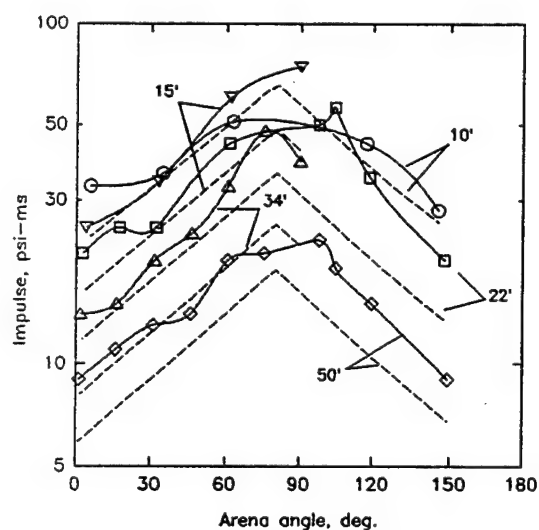
(file = I3245ATR.SPG)

Figure E.10, 2′ dia. steel vessel, 53 cu. ft. volume, 4700 psi, split at near center at 3.5′ HOB, 1′ offset away from center of arena, 6-25-90 (P-2) (TNT equivs: gas = 47.0, LSC = 0.0)
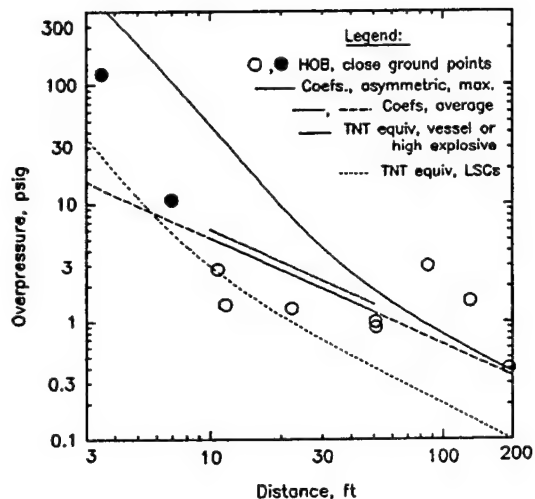
(file = P3251DTR.SPG)
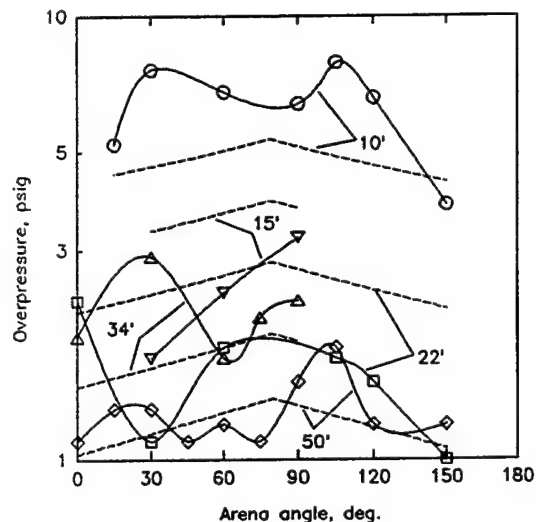
(file = P3251ATR.SPG)
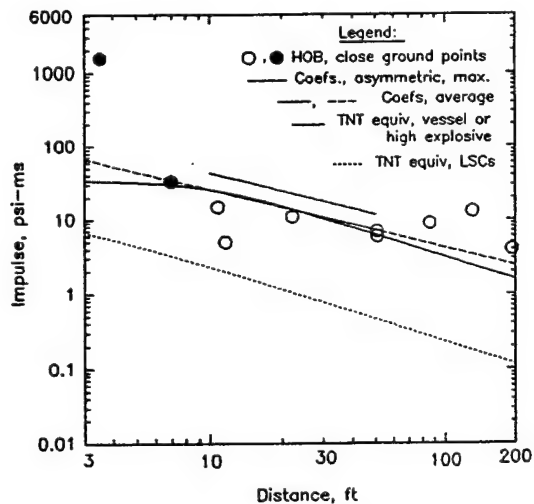
(file = I3251DTR.SPG)
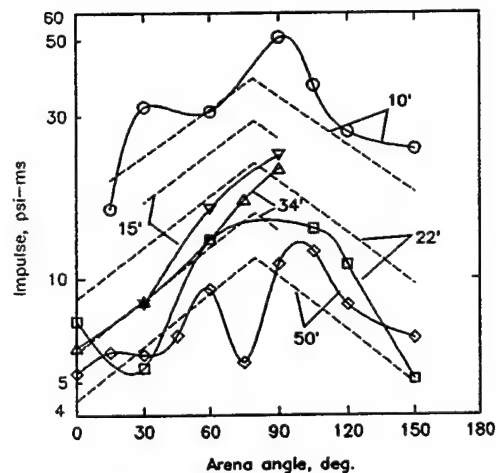
Distances per arena layout, on the ground,
not corrected for offset

(file = I3251ATR.SPG)

Figure E.11, 2′ dia. steel vessel, 53 cu. ft. volume, 1475 psi, split at center at 3.5′ HOB,
1′ offset away from center of arena, 1-25-91 (1-1) (TNT equivs: gas = 13.5, LSC = 0.27)
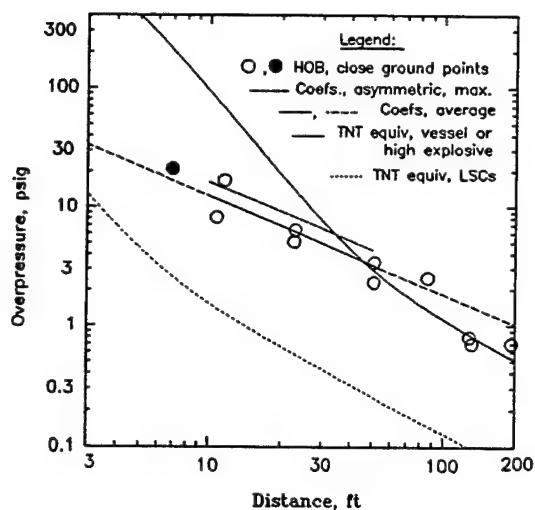
(file = P3252DTR.SPG)
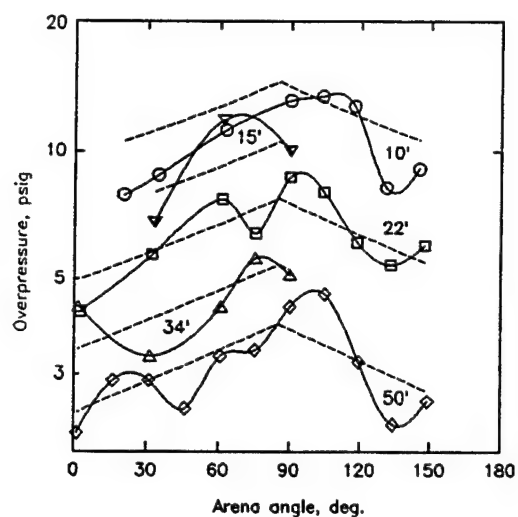
(file = P3252ATR.SPG)
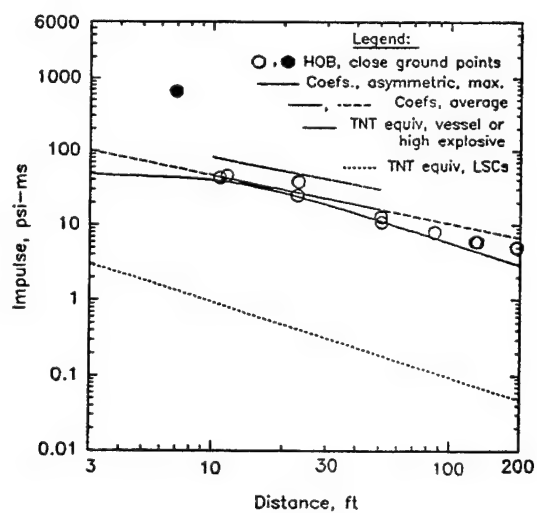
(file = I3252DTR.SPG)

Figure E.12, 2′ dia. steel vessel, 53 cu. ft. volume, 3450 psi, split at center at 3.5′ HOB, 1′ offset away from center of arena, 1-29-91 (1-2) (TNT equivs: gas = 33.8, LSC = .07)

Overpressure, psig

Distance, ft

(file = P3253DTR.SPG)

Overpressure, psig

10'

15'

22'

34'

50'

Arena angle, deg.

(file = P3253ATR.SPG)

Impulse, psi-ms

Distance, ft

(file = I3253DTR.SPG)

Legend:

O , ● HOB, close ground points
——— Coefs., asymmetric, max.
——— , ——— Coefs, average
——— TNT equiv, vessel or
              high explosive
········ TNT equiv, LSCs
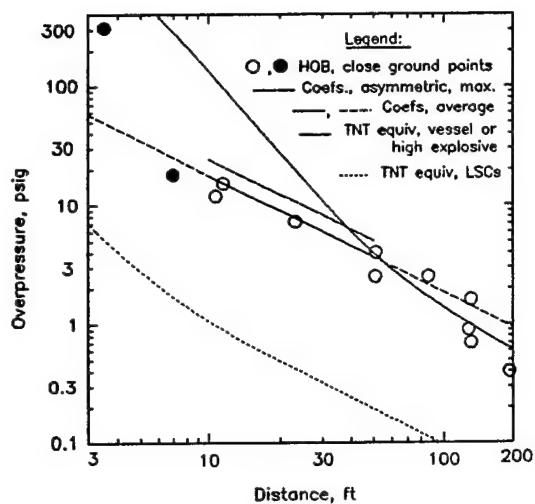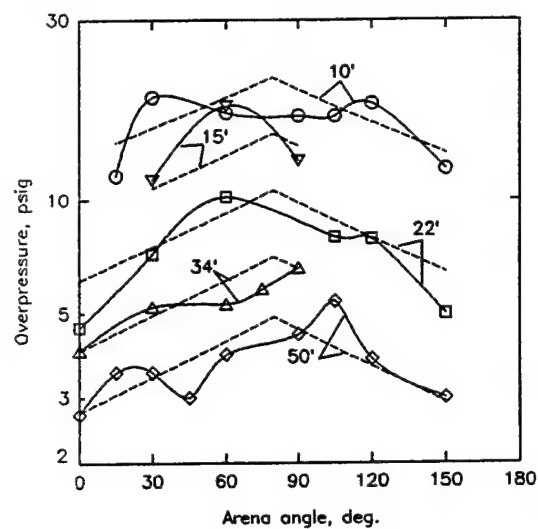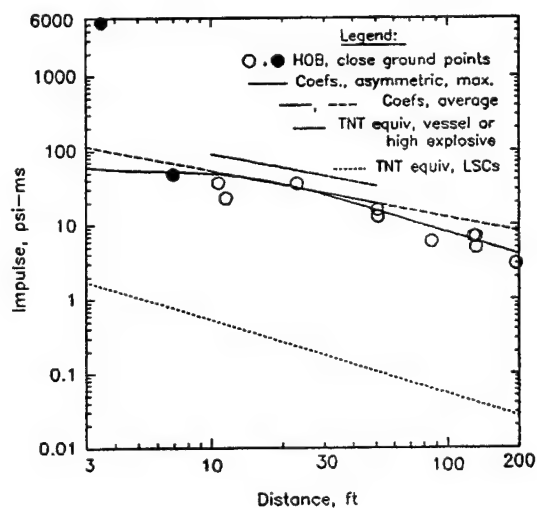
Figure E.13, 2′ dia. steel vessel, 53 cu. ft. volume, 5425 psi, split at center at 3.5′ HOB, 1′ offset away from center of arena, 1-26-91 (1-3) (TNT equivs: gas = 54.8, LSC = .03)
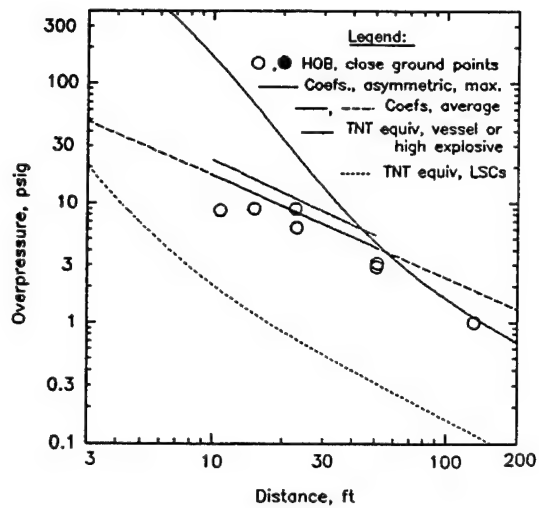
(file = P3402DTR.SPG)
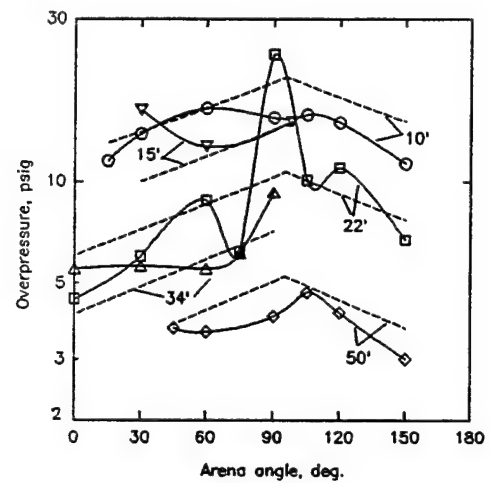
(file = P3402ATR.SPG)
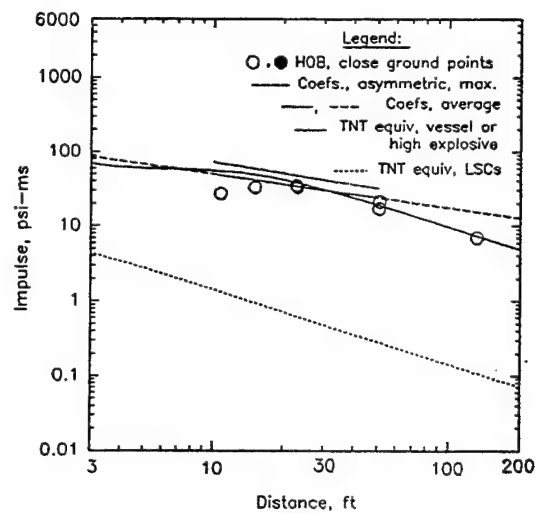
(file = I3402DTR.SPG)

Figure E.14, 2′ dia. steel vessel, 53 cu. ft. volume, 7125 psi, split at center at 3.5′ HOB, 1′ offset away from center of arena, 7-19-91 (1-4) (TNT equivs: gas = 73.4, LSC = .13)
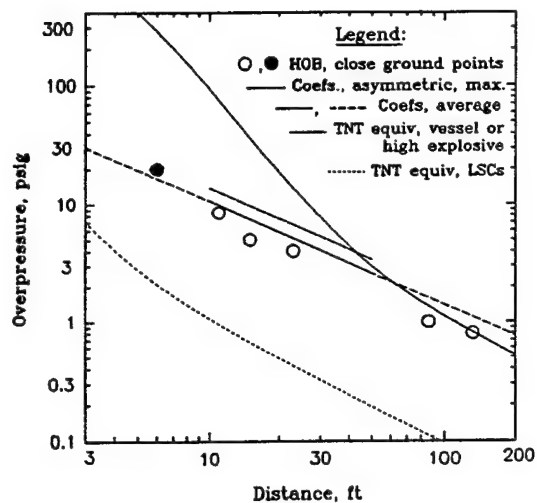
(file = P3403DTR.SPG)
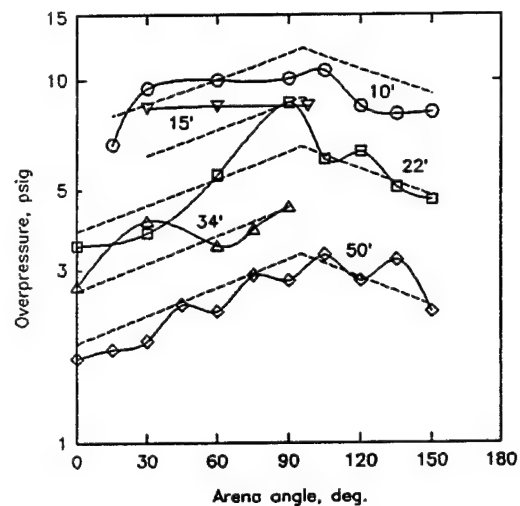
(file = P3403ATR.SPG)
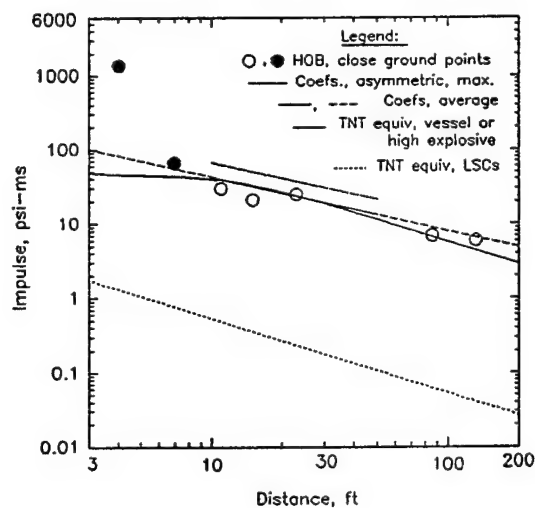
(file = I3403DTR.SPG)

Figure E.15, 2′ dia. steel vessel, 53 cu. ft. volume, 3450 psi, split at center at 3.5′ HOB, 1′ offset away from center of arena, 7-20-91 (2-1) (TNT equivs: gas = 33.8, LSC = .03)
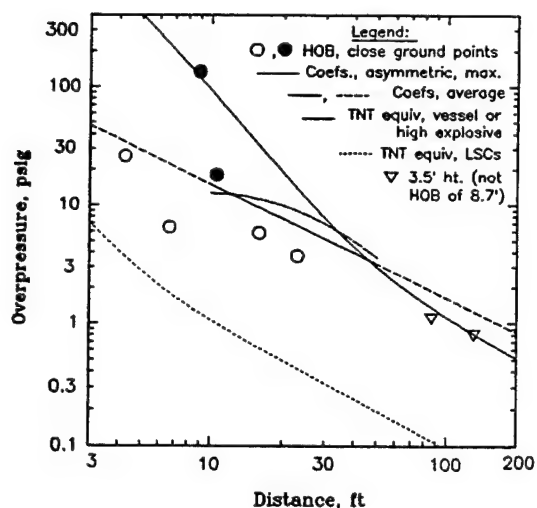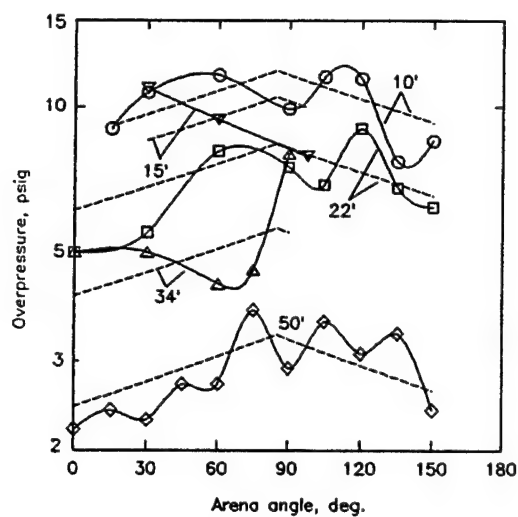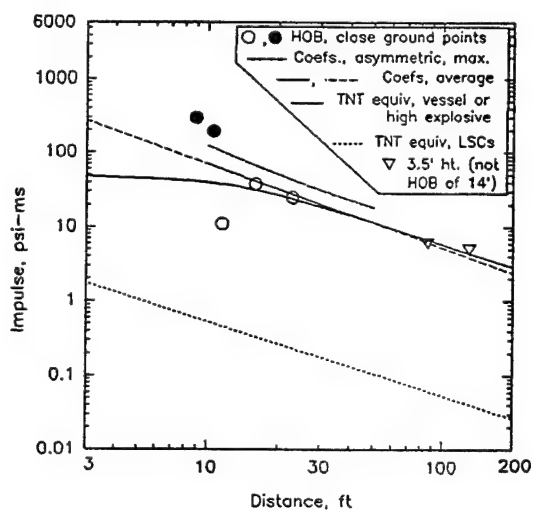
Figure E.16, 2′ dia. steel vessel, 53 cu. ft. volume, 3450 psi, split at center at 8.7′ HOB, 1′ offset away from center of arena, 7-17-91 (2-2) (TNT equivs: gas = 33.8, LSC = .03)
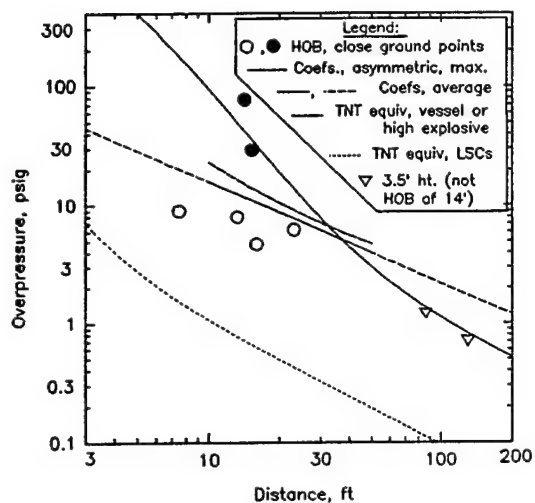
(file = P3398DTR.SPG)
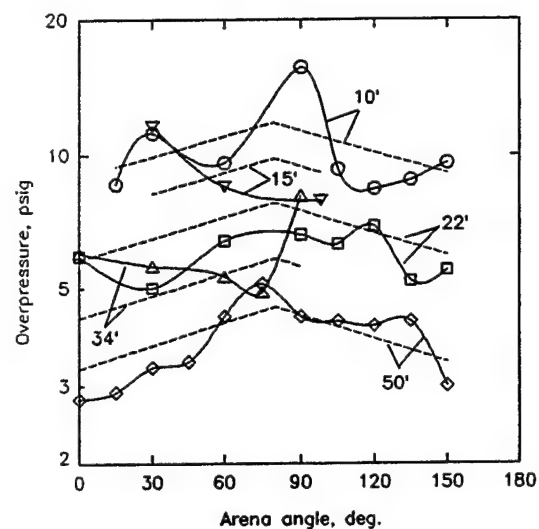
(file = P3398ATR.SPG)
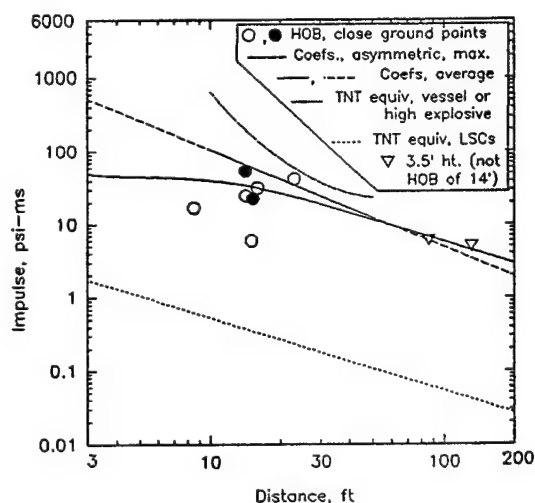
(file = I3398DTR.SPG)

Figure E.17, 2′ dia. steel vessel, 53 cu. ft. volume, 3475 psi, split at center at 14′ HOB, 1′ offset away from center of arena, 7-15-91 (2-3) (TNT equivs: gas = 34.1, LSC = .03)
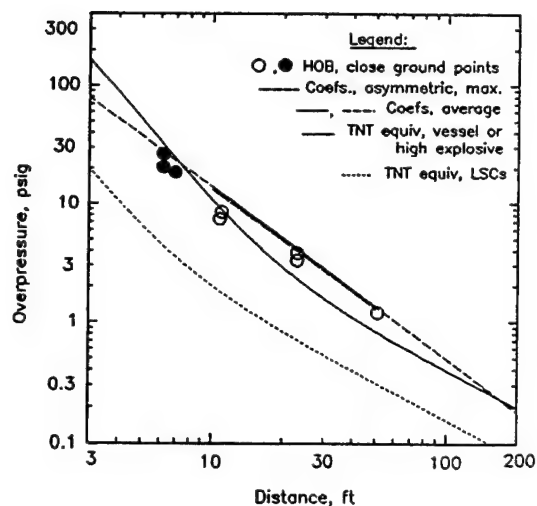
(file = P3573DTR.SPG)
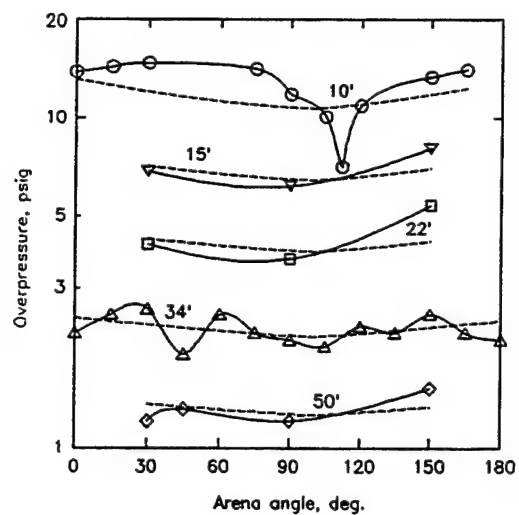

(file = P3573ATR.SPG)
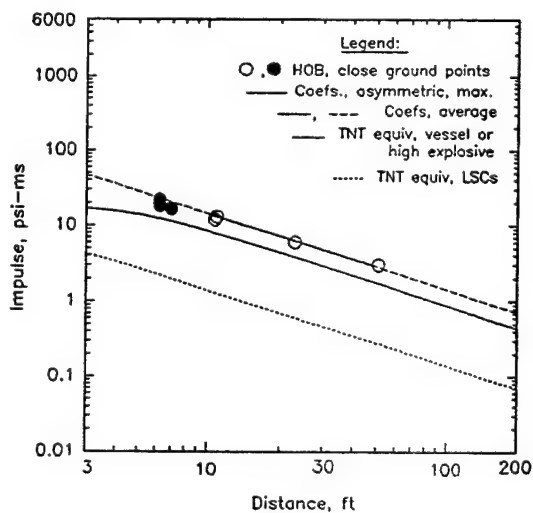
(file = I3573DTR.SPG)

Figure E.18, 1.94′ dia. composite vessel, 2.7 cu. ft. volume, 3975 psi, split at horizontal center at 3.5′ HOB, 1′ offset away from center of arena, 1-25-92 (PC) (TNT equivs: gas = 2.0, LSC = .125
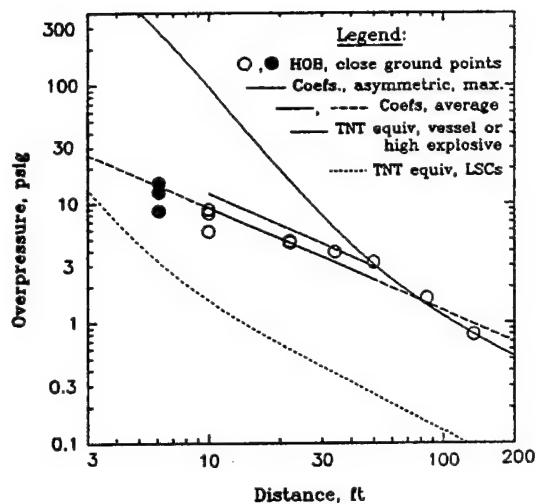
(file = P3574DTR.SPG)
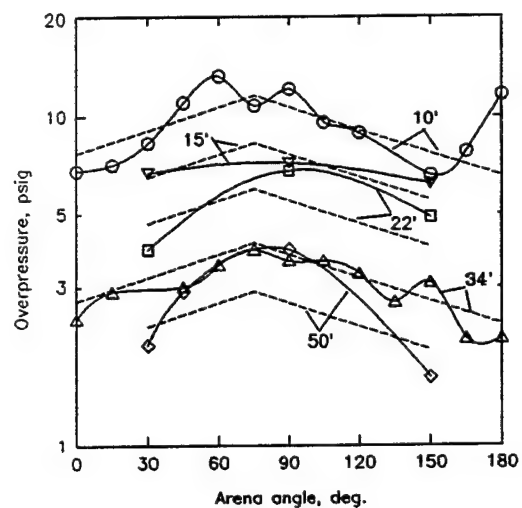
(file = P3574ATR.SPG)
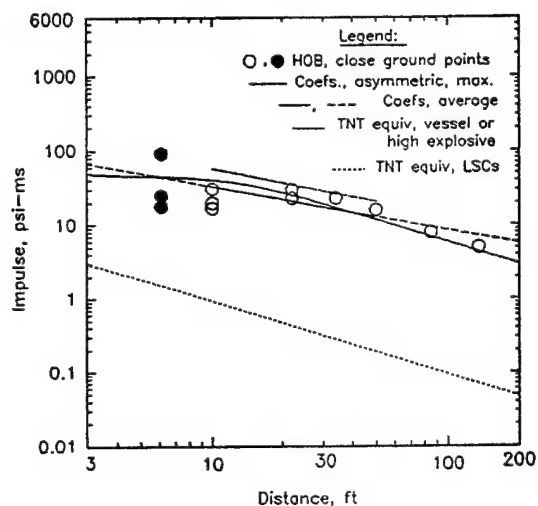
(file = I3574DTR.SPG)

Figure E.19, 2′ dia. steel vessel, 53 cu. ft. volume, 3600 psi, split at 3/4 - 1/4 length at 3.5′ HOB above center of arena, 6-16-92 (5-1) (TNT equivs: gas = 35.3, LSC = .07
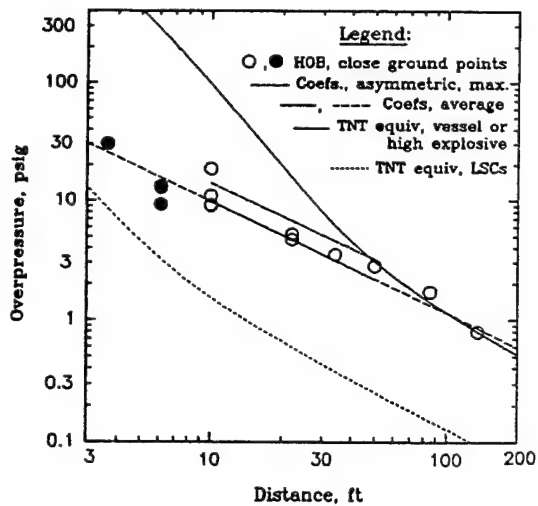
(file = P3575DTR.SPG)
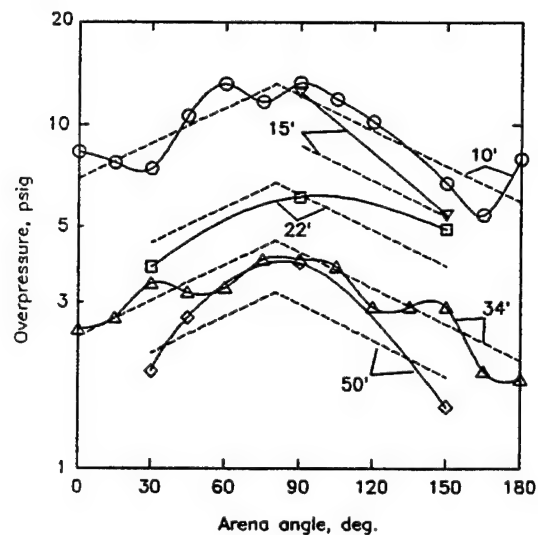
(file = P3575ATR.SPG)
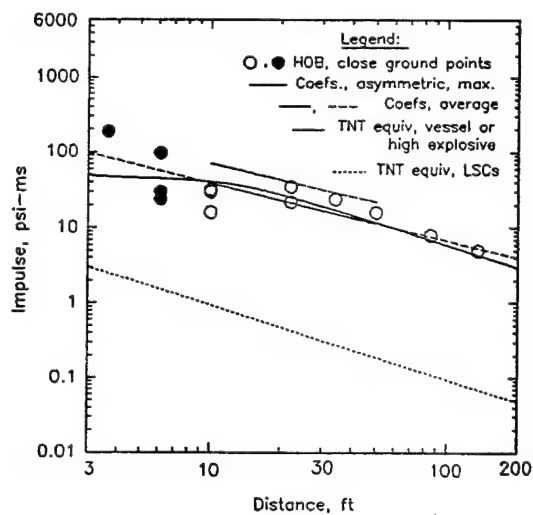
(file = I3575DTR.SPG)

Figure E.20, 2′ dia. steel vessel, 53 cu. ft. volume, 3600 psi, split at 3/4 - 1/4 length at 3.5′ HOB above center of arena, 6-17-92 (5-2) (TNT equivs: gas = 35.3, LSC = .07
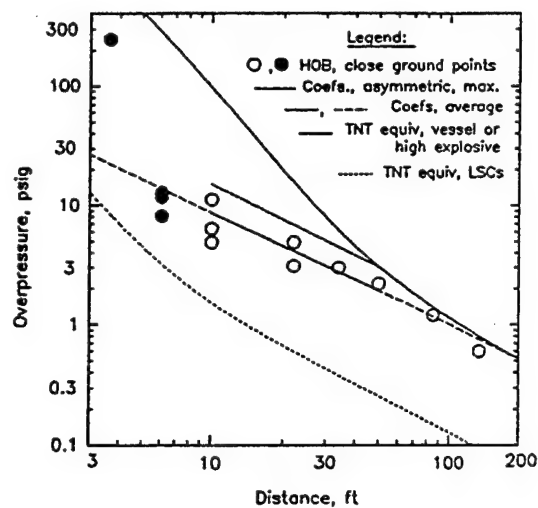
(file = P3577DTR.SPG)
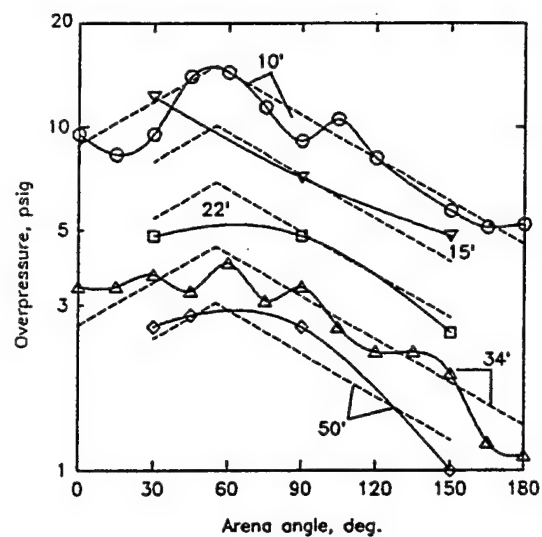
(file = P3577ATR.SPG)
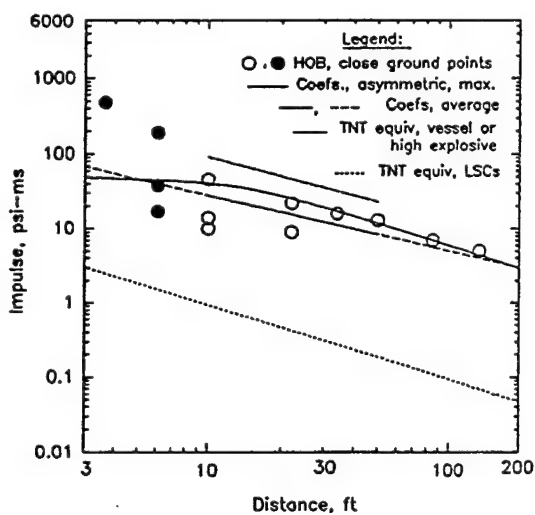
(file = I3577DTR.SPG)
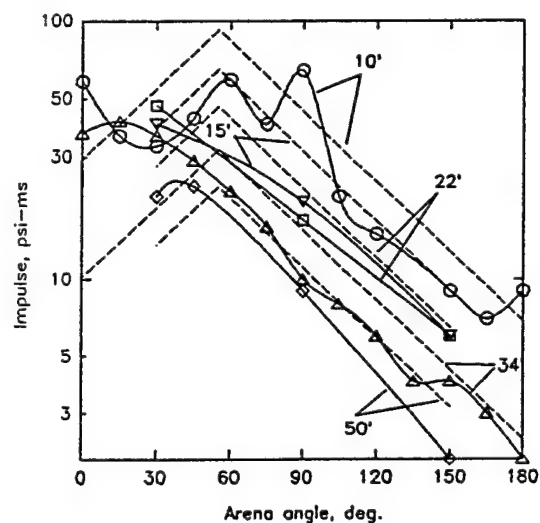
(file = I3577ATR.SPG)

Figure E.21, 2′ dia. steel vessel, 53 cu. ft. volume, 3600 psi, split at full length-endcap at 3.5′ HOB above center of arena, 6-19-92 (5-3) (TNT equivs: gas = 35.3, LSC = .07)
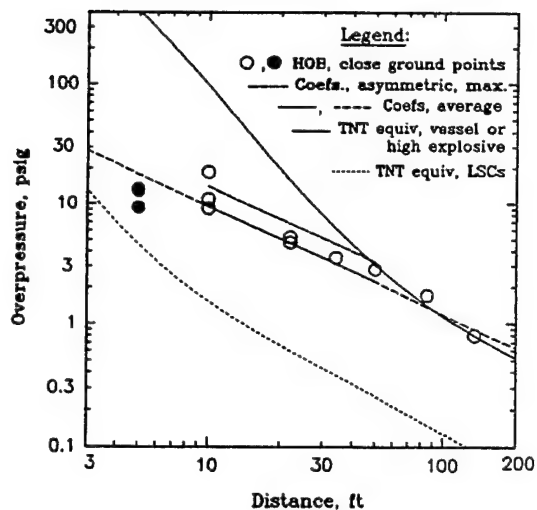
(file = P3576DTR.SPG)
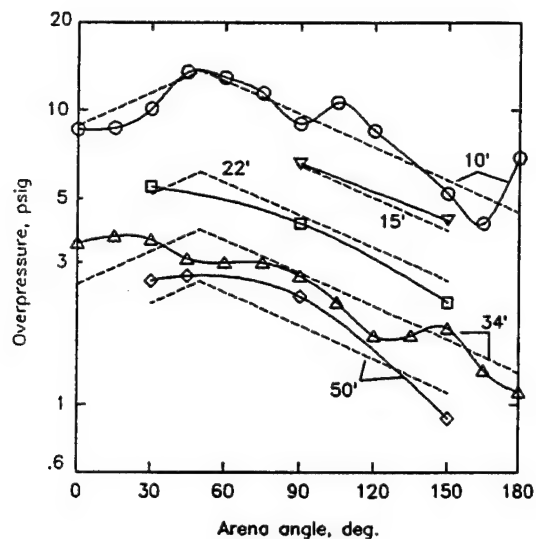
(file = P3576ATR.SPG)
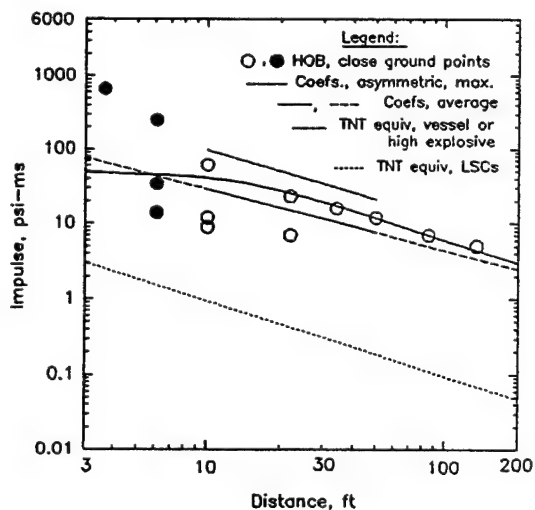
(file = I3576DTR.SPG)
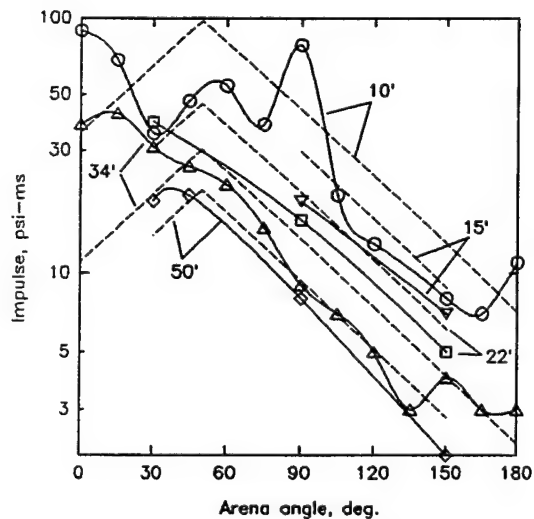
(file = I3576ATR.SPG)

Figure E.22, 2′ dia. steel vessel, 53 cu. ft. volume, 3600 psi, split at full length-endcap at 3.5′ HOB above center of arena, 6-18-92 (5-4) (TNT equivs: gas = 35.3, LSC = .07)
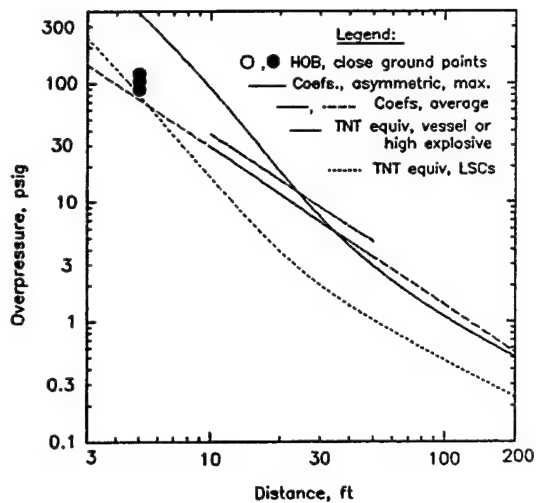
(file = P4053DTR.SPG)
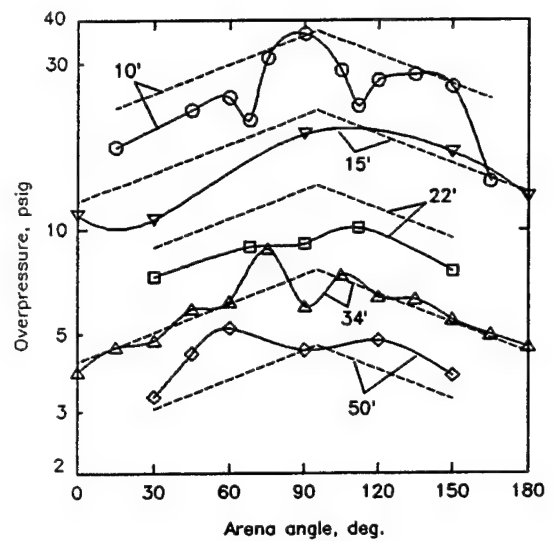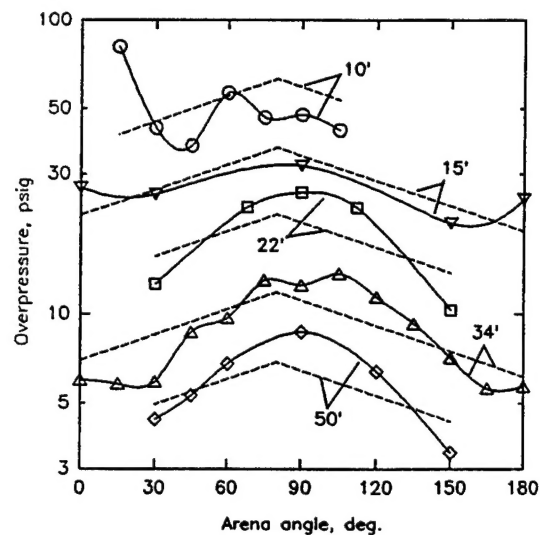

(file = P4053ATR.SPG)
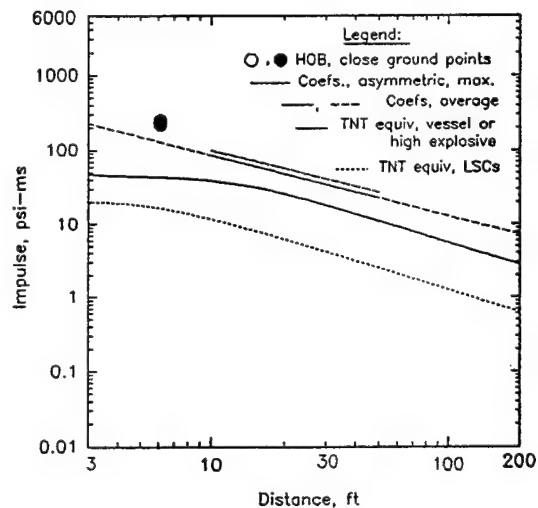
(file = I4053DTR.SPG)

Figure E.23, 3′ dia. steel vessel, 53 cu. ft. volume, 3280 psi, split into 3 fragments (2 endcaps + 1 sidewall piece) at 3.5′ HOB above center of arena, 11-2-92 (6A-1) (TNT equivs: gas = 32.2, LSC = 3.41)
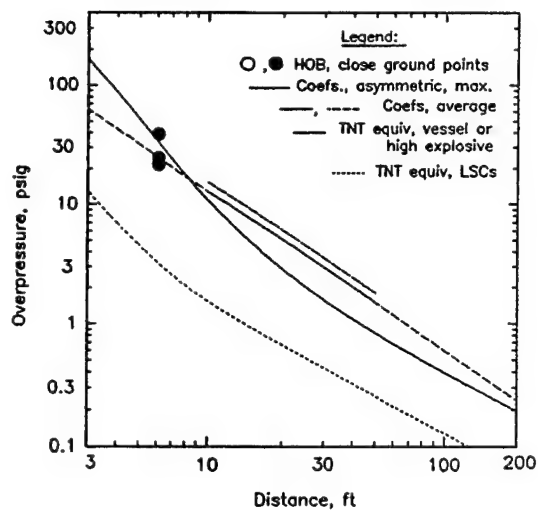
(file = P4054DTR.SPG)
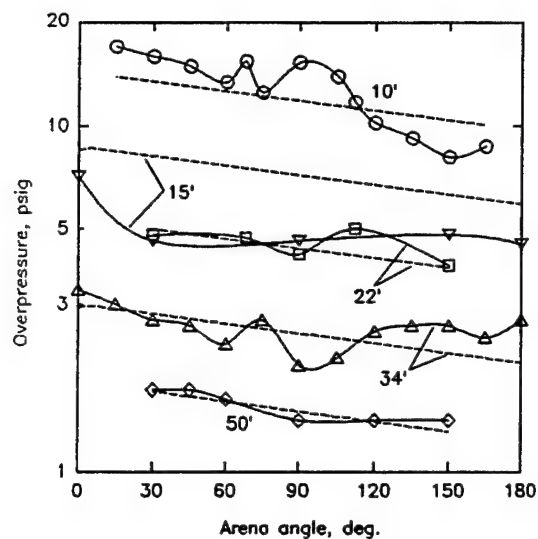
(file = P4054ATR.SPG)
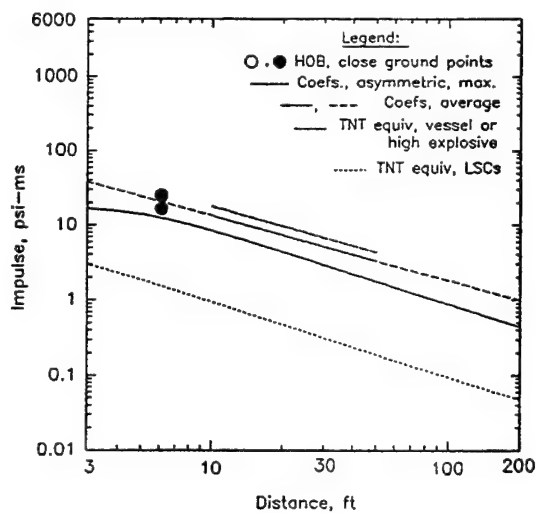
(file = I4054DTR.SPG)

Figure E.24, 1.94′ dia. composite vessel, 2.7 cu. ft. volume, 4000 psi, split at vertical center at 3.5′ HOB above center of arena, 11-3-93 (6A-2) (TNT equivs: gas = 2.0, LSC = .07)
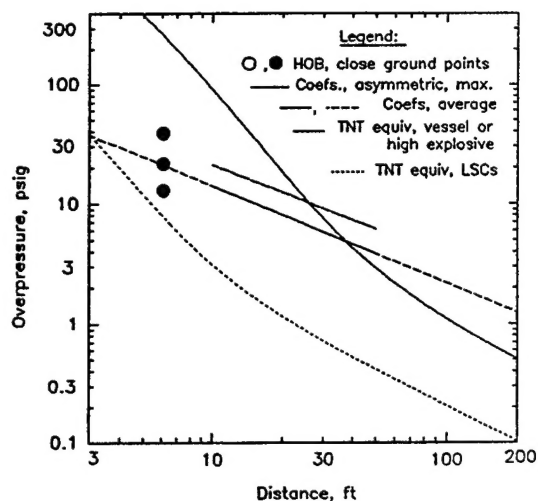
(file = P4055DTR.SPG)
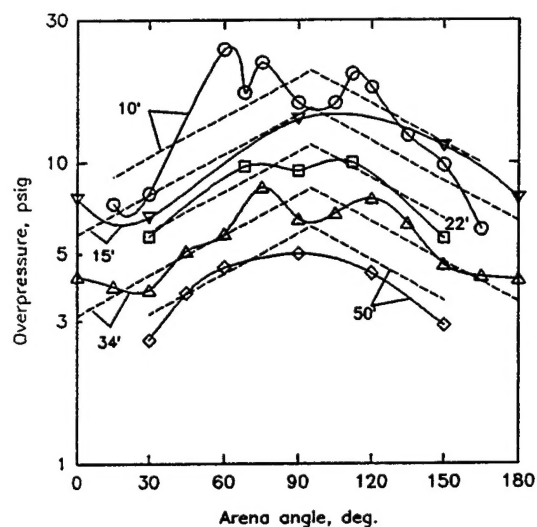
(file = P4055ATR.SPG)
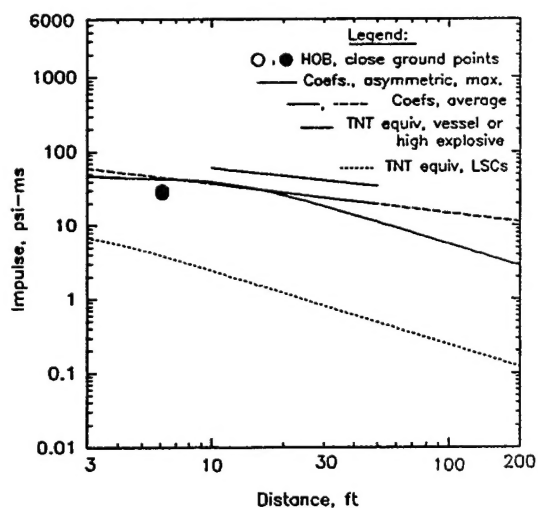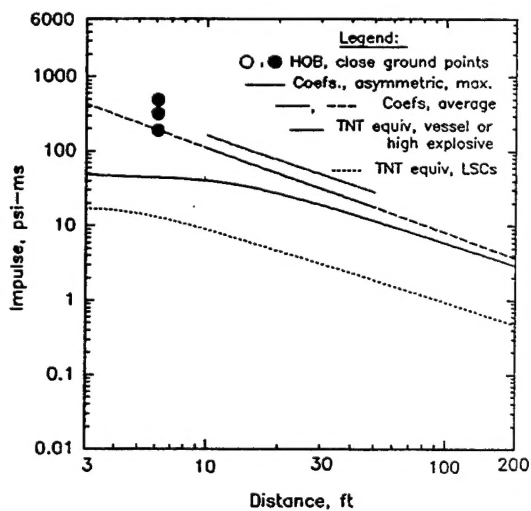

(file = I4055DTR.SPG)
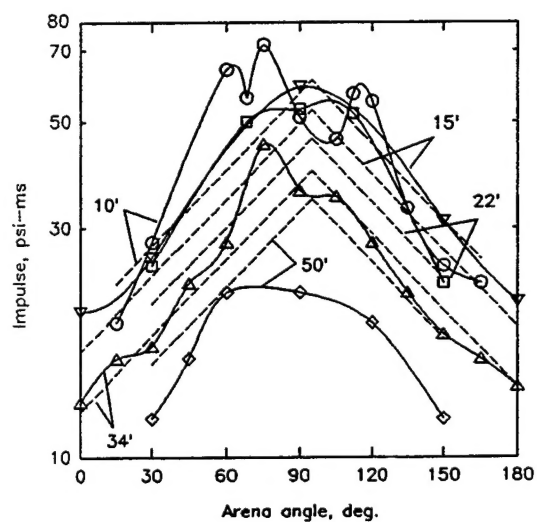
(file = I4055ATR.SPG)

Figure E.25, 3′ dia. steel vessel, 53 cu. ft. volume, 3300 psi, split at center at 3.5′ HOB above center of arena, 11-3-93 (6A-3) (TNT equivs: gas = 32.3, LSC = .29)
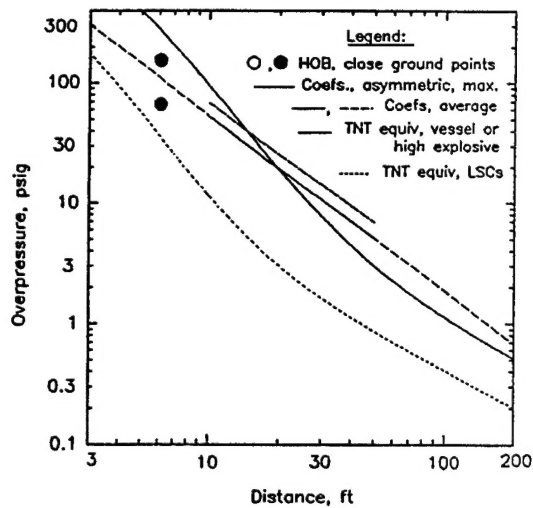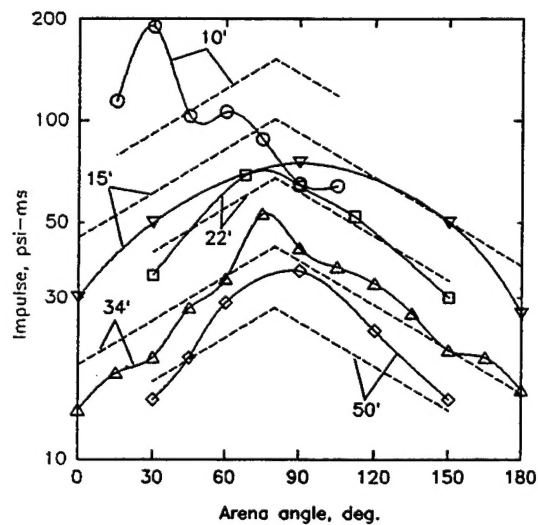
(file = P4056DTR.SPG)

(file = P4056ATR.SPG)

(file = I4056DTR.SPG)

(file = I4056ATR.SPG)

**Figure E.26, 2′ dia. steel vessel, 53 cu. ft. volume, 3500 psi,
split into 14 fragments (2 endcaps + 12 sidewall pieces) at 3.5′ HOB
above center of arena, 11-4-93 (6A-4) (TNT equivs: gas = 34.3, LSC = 2.18)**

Appendix F
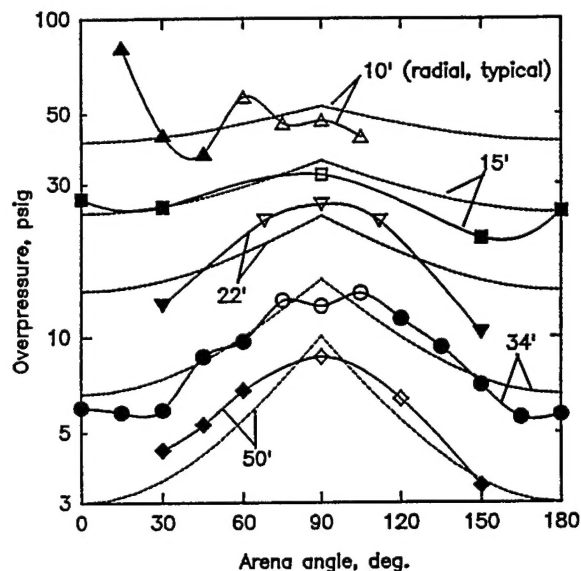## Comments on Multi-fragment Cylinder Overpressure Measurements

Figure F.1, Overpressure versus
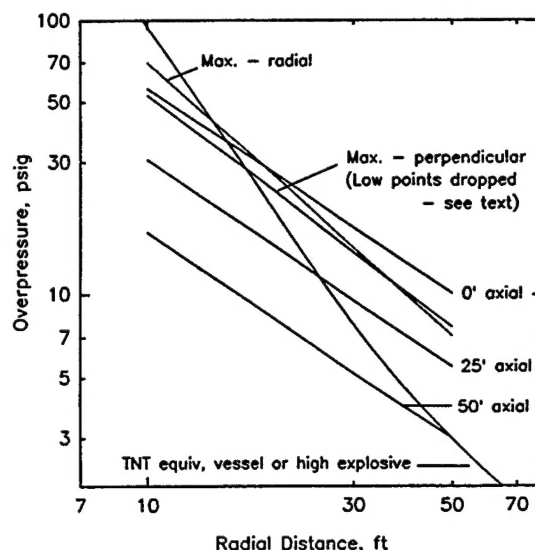Angle for Vessel Burst 6A-4

Figure F.2, Overpressure versus
Distance for Vessel Burst 6A-4

A late attempt was made to find a better analysis model to fit the overpressure and impulse data from the multi-fragment cylinder, vessel 6A-4. Ten multiple linear regressions were performed[27] using various combinations of two to four independent variables. The two best analyses, using two variables, regressed the log of overpressure versus the log of radial distance from the vessel center (as the first independent variable for both) and a second variable. The second independent variable was for 1.) the axial distance from the vessel center (18.2% error) and for 2.) the angle from the vessel center (21.8% error). Symmetry about a line perpendicular to the center of the vessel axis was assumed for all analyses and the three points at five foot distance were not used. Analysis #2 uses the independent variables typically used for the other vessels. Analysis #1 is peculiar to this vessel. The use of all three independent variables reduced the error only 0.1%. Error used is the standard deviation in percent of reading of measured overpressure.

Analysis #1 is shown in a plot of arena angle versus overpressure in Figure F.1 and in a plot of radial distance versus overpressure in Figure F.2. The lines of constant axial distance versus overpressure are curved lines in Figure F.1. The data is also plotted for comparison in Figure F.1 using both filled and open symbols and with points connected using a spline. Analysis #1 is shown by the three solid lines in Figure F.2 labeled 0', 25' and 50' axial (distance). The line labeled "Max.-radial" is equivalent to the line labeled "Coefs.,Asymmetric, max." in Figure 5.26b. The line labeled "Max -perpendicular" in Figure F.2 is the same line labeled "Max. 90° distance" in Figure 5.27. This line was found by regressing overpressure against perpendicular distance with the filled symbol points in Figure F.1 deleted but with the three points at 5' distance retained.

The equations for overpressure and impulse for analysis #1 are:

log(OP)=6.47811-1.06481*log(radial distance)-0.02419*axial distance
log(Imp.)=5.82776-0.53925*log(radial distance)-0.02700*axial distance